CONTROLLING AND VISUALIZING INTERACTIONS IN MODEL *SACCHAROMYCES CEREVISIAE* MICROBIAL COMMUNITIES: INSIGHTS ON THE EFFECT OF INVERTASE REGULATION ON COOPERATIVITY AND GROWTH DYNAMICS

By

Neydis Moreno Morales

A dissertation submitted in partial fulfillment of

the requirements for the degree of

Doctor of Philosophy

(Biophysics)

at the

UNIVERSITY OF WISCONSIN-MADISON

2023

Date of final oral examination: 05/11/2023

The dissertation is approved by the following members of the Final Oral Committee:
Megan N. McClean , Associate Professor, Biomedical Engineering
Garret Suen, Professor, Bacteriology
John Yin, Professor, Chemical and Biological Engineering
Ophelia Venturelli, Associate Professor, Biochemistry
Lindsay Kalan, Associate Professor, Medical Microbiology and Immunology

Dedication

Dedicated to Ravioli, a faithful, furry family member, my best friend and goodest boy. Our family said goodbye to him a month before my Ph.D. defense. I wish I had a little more time with him to celebrate. He never resented me for any late day in the lab. He greeted me with an enthusiastic wagging tail so forceful that the rest of him wiggled. Whether it was a bad day in the lab or a good day, he affirmed that I was always good enough, just the way I was.

Acknowledgements

If you're reading this, I did it! I would like to acknowledge all the wonderful people that contributed to my experience, professional and personal development. The Ph.D. can be at times a stressful, and long journey and these people helped me survive and sometimes thrive. Thank you to my incredibly caring, talented, and patient advisor, Megan McClean. She was supportive as I was learning and making mistakes and because of that I learned much more and became a stronger, more capable, and independent scientist. She also encouraged me to always push a little more during the week so that when she asked, "what else?" I often had one more result or question to discuss. Thank you to my committee members, who provided me with invaluable feedback and insightful questions, making my thesis work stronger.

Many thanks to the McClean lab community members. I've experienced nothing but non-selfish cooperation (inside joke for readers of this dissertation) and unity in this lab. We all contribute to making the lab environment a happy, productive one. Special thanks to Kieran Sweeney and Kevin Stindt, whose incredibly useful and easily adapted scripts saved me on multiple occasions from figuring out how to code

from scratch, and who generously helped me when I broke their code and adapted it for me. To Stephanie Geller, who became my dissertation buddy as we both trudged through final experiments, analysis, and writing. We alone could understand the exact state of mind in the days leading up to our respective defenses, thank you for cheering me on. To Lucy Jiang, who I attempted several new activities with; fishing, HIIT, and ice skating. She believed I could be successful in many things like becoming a master bread baker, despite never having made bread. Thank you for letting me believe in my full potential.

One of my closest friends, and housemate, Saurabh kept me fed and took care of the plants when I was at my busiest and most forgetful. There would have been many green casualties without you. We went on some epic road trips and hikes that punctuated my otherwise monotonous rhythm of lab, rest, repeat, many thanks to you. A big hug to my family, they may not have understood quite why I was *still* in school, but they supported me completely. Mamita, John and Gin-gin, los quiero muchísimo. Even more recognition for my dear sister, Ingrid, who always encouraged me to put self-care and the joys of life above all things, thank you. Eventually..finally! I started to listen. For those that nurtured all my growth-edges so I could overcome the many insecurities that cropped up, made even more urgent by the trials of graduate school: Molly C. (I could never thank you enough), Abby, Kendall, and Kimberly. Thanks a million! When I'm on the verge, or actively being my own worst critic, I remember you and how you might talk to me instead.

A thank you to the health care professionals (Shaina, Eliza, Tamar), who helped me realize I was neglecting my earth suit. Helping me connect with my body again when it started to malfunction and rebel from years of putting school first.

Our past scientific training has such an influence on the scientists we become, because of that a special thank you to Katy Forest, and the Forest lab members (Katiria, Jeff, Peter, Anna). A special shout-out to Anna Baker-McAllister, who was my graduate student mentor during undergrad. She continues to be my role model and a large reason for continuing to graduate school. A big thank you to the programs (PEOPLE,

McNair, SciMed) who showed me, a first-generation student, the way to college, on to graduate school and to earning my Ph.D. Lastly, as embarrassing as it might be to thank yourself in an acknowledgement section, a big thank you to myself, I really couldn't have done it without my resilience and care.

ABSTRACT

Interactions between microbes can be passive or active, inhibitory, or promotive, and act over a range of length scales including local contact-dependent interactions and longer-scale diffusion-based interactions. Interactions between microbes guide the development of microbial communities. Cooperation is a type of interaction where the product or action benefits more than one cell. I focus on an important model system, the *Saccharomyces cerevisiae public goods model for sucrose utilization.* In microbial communities, public goods are compounds produced by cooperative cells that are freely available to other cells. In this simplified community, cells expressing invertase are deemed *producers,* since invertase breaks down sucrose into glucose and fructose (the two public goods in this system). *Cheaters* are the cells that take advantage of these public goods without suffering direct fitness costs from invertase production. A major motivation for studying cooperation is to understand how cooperation is maintained in a community. It is not known how invertase is regulated in this model community. If invertase could be regulated this would affect how glucose would be available in the community. I believe that invertase regulation may be a major contributor to cooperation maintenance in a community in specific environmental conditions. In chapter 1, I introduce the *Saccharomyces cerevisiae* public goods model system which facilitates cooperative use of sucrose. I present the major contributions to our understanding of cooperation using the model system and highlight gaps in our understanding of factors that support cooperation. I conclude by explaining why regulation of invertase may be an important missing piece from our understanding of this model system. In chapter 2, I improve upon current optogenetic tools. I improved the calibration method for the LPA, a previously published optogenetic device for illuminating wells in a 24 well-plate to increase throughput and reproducibility of optogenetic experiments. In chapter 3, I present the creation of a light-inducible invertase expression in an *S. cerevisiae* strain. I characterize this strain and demonstrate spatial control of producer populations via light. Then, in chapter 4, based on the previous observation that localized

cooperators surrounded by cheaters can form bullseye patterns, particularly in nutrient-limited environments. I develop a reaction diffusion model to understand how public goods interactions and competition for resources can lead to patterning in microbial communities. The reaction-diffusion model successfully recapitulates long-range patterning in a limiting nutrient environment for the *S. cerevisiae* model community. In chapter 5, in order to measure invertase regulation I develop a method to visualize the active cooperators in a wildtype strain of S. cerevisiae. I demonstrate that *S. cerevisiae* can and does regulate the expression of invertase during growth. I use the same method to develop different strength constitutive cooperators. Finally, I compete these cooperator strategies with either cheaters or cooperators to compare the effects that invertase regulation has on cooperator and community outcomes. This work has direct implications for understanding intercellular and interspecies interactions in natural and synthetic microbial consortia containing *S. cerevisiae*. Finally, in chapter 6, I summarize the results from my thesis work. I highlight the useful tools developed to study dynamic interactions in a microbial community. I conclude by contextualizing my findings within the larger context of the public goods literature and provide future directions.

Table of Contents

Table of Figures

Table of Tables

Chapter 1: Introduction

Neydis Moreno Morales wrote this chapter.

Abstract

Interactions between microbes can take various forms, such as passive or active, inhibitory or promotive, and occur over different length scales. These interactions guide the development of microbial communities. My thesis work focuses on studying the *Saccharomyces cerevisiae* public goods model for sucrose utilization. This is a well-known model system used to study cooperation whose name: public goods stems from the fields of ecology and game theory. The system involves the production of public goods, which are compounds produced by cooperative cells that are freely available to other cells. In this chapter, I introduce this model system in more detail. I then present the contributions from past works to our understanding of cooperation, highlighting gaps in knowledge. I explain why regulation of invertase may be important to understand factors that support maintenance of cooperation and what hurdles may have prevented the study of regulation in the past. I describe my approach in investigating the role of invertase regulation on cooperation by describing my research questions and the tools I will need to answer them. I conclude with an overview of the subsequent chapters.

Introduction

Cooperation is a common behavior observed in nature [1]–[4]. For microbial communities, cooperation can make a large task more productive [5], [6] . However, cooperation appears susceptible to outside factors such as the presence of cheaters [7]–[9]. In the presence of cheaters, for example, cheaters, without any effort, could benefit from the cooperation, their fitness greater than that of the cooperators, then leading to the collapse of the community [10]–[14]. Due to pressures such as these, how cooperation persists in a population and how cooperation is affected by ecological factors is a compelling topic of research. Broadly, my dissertation work focuses on the development of tools to measure cooperation and understand the mechanisms that support cooperation in a community using the public goods model system in *Saccharomyces cerevisiae*. Specifically, I'm interested in how regulation of cooperativity in this model system affects cooperation and growth dynamics. In this model system, yeast utilize the enzyme

invertase to break down sucrose cooperatively into glucose and fructose and uptake them for growth. Model systems are useful for studying microbial communities because there are fewer variables to track and often the model system has been well-characterized, which is also true for the cooperative model system I use. Multiple model communities have been used to better understand cooperation in the microbial world, such as quorum sensing [15],siderophore production [3], [16], [17], and fruiting bodies [18]–[21]. Model systems are ever more useful if the right tools are developed to study them.

In this chapter I present an overview of the biology of the public goods community. Then, I summarize major public goods works that have contributed to our understanding of the ecology and evolution of cooperation in this system and highlight some incongruencies and gaps in the current work. I'll then focus on a crucial missing piece of this biological model, the regulation of the enzyme invertase, and the technical difficulties that may have prevented investigation of this regulation in the past. I then present my research questions and the necessary tools I will need to approach my questions. I conclude with an outline of the subsequent chapters.

The Public Goods Model system: Utilization of Sucrose by *Saccharomyces cerevisiae*

Though *Saccharomyces cerevisiae* prefers glucose, *S. cerevisiae* can use sucrose as a carbon source through the use of invertase [22], [23]. When glucose is available at a reasonable concentration, sucrose utilization pathways are repressed (as are many other alternative carbon utilization pathways) until the glucose availability falls below a threshold [23]–[25] . Once glucose is low, *S. cerevisiae* de-represses invertase expression and invertase is then secreted into the periplasmic space of the yeast wall. Invertase hydrolyzes sucrose to make two monosaccharide molecules; glucose and fructose (Figure 1). This hydrolysis occurs outside of the cell, and the cell responsible for the hydrolysis and any nearby cells then import the monosaccharides for growth. This is what makes sucrose utilization a cooperative activity.

The cooperative nature of the system, as well as the well-studied biology, makes sucrose utilization a useful model system for studying cooperation in microbes [9], [26]–[33]. In the existing literature, a typical

S. cerevisiae public goods model community is made up of two entities: the cooperators (producers of invertase) and the cheaters (non-producers of invertase). The model system was given the economics-borrowed moniker of public goods as the freed monosaccharides are considered goods made available to any public cell in the environment.

It is usual for the experimental conditions to consist of the cooperators expressing invertase using the native promoter pSUC2; cheaters are mutants who have invertase deleted (suc2Δ) (Table 1). The two individuals are combined in media with sucrose as the main carbon source (and negligible glucose). The cells, under native regulation, are presumed to highly express invertase and maintain their constitutive cooperator status throughout the experiments. It is important to highlight that this presumption may not be true, and the consequences of this presumption will be discussed further in this chapter. Nonetheless, the use of this model system has given us important insights into one of the major questions regarding cooperation—the question that motivates the work discussed in this dissertation—namely, how cooperation is maintained in a population when faced with cheaters.

Factors that may support cooperation in a mixed community and caveats

Preferential access to the public good

One important result of previous works studying cooperation in the public goods model system, is that coexistence is possible between cooperators and cheaters, while competitive exclusion is also possible [9], [27]. This result serves as good evidence that cooperation has important traits that allow it to persist in difficult environments, such as cheater presence. Teasing out what these traits is less obvious. One trait that has been discovered and which successive works have built upon, pertains to this particular form of cooperation; enzyme secretion[9], [26]–[33] . Invertase, which is retained by the producer cell imparts preferential access to the freed glucose which offsets the cost to produce invertase enough to support coexistence in a mixed community [27], [34]. It is important to point out, as mentioned earlier, that the ability to make invertase in these model systems makes this cell de facto a cooperator, which neglects the

potential that the cells capable of producing invertase are not always actively making invertase. The ability for cells to regulated invertase has likely not been studied because a tool has not been developed to visualize active cooperators in a community.

Cell density dependent growth

There is not a lot of agreement on what elements support cooperation in public goods. One might expect, for example, that high cooperator cell density would have a positive effect on the growth of the public goods community as well as the cooperator growth because that would result in more glucose being made available. However, high cooperator cell density on a public goods community appears to have a wide range of effects on the outcomes for the cooperator cells as well as the entire community's population.To begin with, the *S. cerevisiae* public goods system has demonstrated an allee effect: a positive density dependence on individual cells' fitness when cooperation is in effect [27]. This means that a community of cells (whether that be only cooperators or in coexistence with cheaters) needs enough cooperating cells to maximize benefit from the fruits of cooperation. This relationship was explored by Gore et al. using a bi-phasic logistical growth model where there is a growth rate for each, the cheater and the cooperator before the threshold number of cooperators is reached and new growth rates for each of the cell types after the threshold is met [34], [35].

It might stand to reason that higher densities of cooperator cells would be the most beneficial to both cooperators and mixed populations alike, since this would result in the most glucose becoming available. Theory predicts that it might depend, higher densities could confirm the previous statement or could benefit cheaters because they would be able to take advantage of an increase in public goods [8], [36], [37]. Gudelj is able to empirically verify both results–higher densities benefitting cheats or cooperators depending on the spatial organization [31]. However, in [34], equilibrium for mixed communities were often reached at low cooperator frequency, in this case a small proportion of cooperators were necessary to support the equilibrium population density, with cheaters benefitting the most. Cheaters also appeared

to profit the most in terms of fitness from higher cooperator densities; in [9] cheaters had a larger growth rate (1.19) relative to the producer under these conditions. In contrast, in [30], maintenance of cooperation in a mixed population required low population densities with cooperators making up a higher proportion of the total population. How cell density (both total density and cooperator density) affects cooperation and the population remains to be resolved.

The presence of cheaters supports or..., doesn't support cooperation?

Even whether cheaters are deleterious or beneficial to the maintenance of cooperation in a public goods community remains in limbo. Across other cooperative communities cheaters are often seen at conflict with the interests of maintaining cooperation and cooperative cells have developed strategies to guard against cheaters [38], [39]. However, [33] found that cheaters were actually beneficial to overall population fitness with a mixed population leading to higher total population density and higher growth rate . In [33], and [40] cooperator-only populations are posited as being potentially wasteful both in their use of available resources and their production of invertase and so mixed populations produced better outcomes for populations as a whole. Meanwhile, [34] found a neutral effect to total population growth of a community when cheaters were present but the researchers did observe a negative effect on the resilience of the community. This community did not have the ability to recover after a rapid, and extreme dilution [34]. There remains a continued need to understand how cheaters cooperate or interfere with maintenance of cooperation.

Cooperation in Spatially Organized Environments

In microbial communities the consideration of spatial organization is important as microbes live in dense potentially structured spaces, for example, in biofilms [41]. In this particular microbial community system, where cells remain stationary but several components are free to diffuse throughout space, it is evident that maintenance of cooperation, and fitness characteristics between cooperators and cheaters could differ when there is spatial structure versus growth in well-mixed environments. Several theory papers

have focused on trying to understand the effect of spatial organization on cooperation with varying results [8],[42], [43]. These are great as a starting point for insights as it can be technically complex or not possible to do these experiments empirically without the proper tools to visualize or organize cells. Often, theory when possible must be verified empirically.

When we turn to the empirical examples that utilize the public goods *S. cerevisiae* model system there are some differences in outcomes to compare from examples discussed earlier. When colonies are expanding, cooperation is maintained due to that expansion [44]. Desai et al. explains it as "survival of the fastest"; cooperator sectors have higher productivity than cheater sectors leading to positive assortment at the boundaries of a colony [44]. In contrast to previous examples [33], cooperators in higher densities fared better than cheats. In plate assays where cooperator frequency was tracked over several generations differences were observed between an average plate's landscape and smaller, local environments within the plate [40]. However, the potential effects of spatial environment and diffusion were not considered in-depth partially due to the methodology used limiting quantification [40]. The scale at which space is considered may matter as well, [29] looks at spatial structure by comparing growth outcomes in low sucrose of individual cooperator cells and clumps of about 30 cells. Clumps fared better when competing with cheaters because of the diffusion rate differences in a clump vs single cells, in other words cooperators with spatial organization could capture more of the digested sucrose. On much larger scales, previous work varied the degree of spatial organization, from well-mixed environments and on plates and found that more spatial structure favors cooperator fitness, with higher densities improving cooperator fitness relative to cheaters (maximizing both density and structure leads to cooperator relative fitness of ~1.5) [31]. Overall, these empirical examples suggest that outcomes from spatial organization can vary depending on various factors such as how the community is spatially organized, and the size of the spatial scale. More work needs to be done to fully understand the role of spatial organization on cooperation in this model system.

Experimental Variation and Technical Hurdles

The varying effects of different factors on cooperation may appear confusing or even contradictory. Despite being a well-studied model to study cooperation there appear to be complex factors whose effect on cooperation require further refinement, such as, the role of cell density, cheaters, or spatial organization. Partially, these differences could be due to methodological differences. Many variations in culturing conditions span the examples discussed here: plating, or well-mixed conditions, ranges of starting sucrose concentrations, even the way the cost of being a cooperator is determined. For instance, the frequency of a cooperator is measured by replica plating dilutions and selecting for a marker [9], at the transcriptional level via qpcr [40], and using a constitutive fluorescent reporter in the cooperator cell in a few others [29], [33], [42].

Another, equally likely probability is that we need a deeper understanding of the mechanisms driving expression at the promoter that has continued unexplored in the context of the public goods model. The promoter is driven by the environmental conditions (de-repressed and repressed in response to available monosaccharides) as much as it is impacted by the changing environment resulting from its and surrounding cells' activities (collectively all the cells consuming and freeing monosaccharides). However, there was not a tool to measure active or real-time cooperation. This is likely due to technical barriers associated with tagging a secreted protein in yeast, previous attempts had been unsuccessful [45], [46].

Throughout this section I have highlighted where there are incongruencies in our understanding of what factors support cooperation. We need new techniques to measure cooperation more directly both at the population level and at an individual level. This would be possible if we could measure real-time expression of invertase, I discuss my approach to develop such a tool further on. Furthermore, the study of cooperation would benefit from tools that would permit the direct control of cooperation in order to further study the impact of the aforementioned factors such as spatial organization.

Regulation of Invertase May Be a Missing Puzzle Piece that Supports Cooperation

The cost of cooperation

What is the cost of cooperation for a cooperator? As I mentioned earlier, literature suggests that generally a wild type cooperator cell would act as such when faced with cheater cells. Likewise, that growth in sucrose media would result in the maximal amount of invertase expression (cooperation) for the cell as had been observed under low glucose conditions [27],[33]. For the aforementioned works, the cost of cooperation has been established and treated as a constant factor within the community's framework (see Table 1). The cost is measured by comparing the growth rates for cells that are not making invertase to cells that make invertase and equating decreases in the growth rate with the cost of invertase production, or in other words, the burden of expressing invertase. However, the possibility of the cost being variable and its potential impact on the outcomes of the public goods community have been examined in the models for one of these papers [27]. The work demonstrates through their model that varying the cost would result in ratio differences at the steady state [27]. What if the wild type cooperator cell could tune their cooperation ie. the cost of their invertase expression? Afterall, the activity of the promoter is not only influenced by the surrounding environmental conditions, which cause de-repression and repression in response to available monosaccharides, but also by the continuously changing environment resulting from the metabolic activities of both the cell itself and the surrounding cells, as they collectively consume and free monosaccharides. There are studies in the realms of biofuels and metabolism that have hinted at more dynamic expression of invertase when invertase producing cells are grown in sucrose, at the population level [25], [47]. It is possible that wildtype cooperators are more strategic cooperators than has been observed before. If cooperators could tune how much invertase they made dynamically they would effectively be tuning their cooperation cost. What impact would this have on interpreting the results of previous works?

New questions surface for the public goods model system

How does a cooperator-only population regulate their cooperation? This currently is unknown, especially at the level of individual cells within a population. Would there be heterogeneity with some cells adopting a cooperator role and some invertase producing cells becoming cheaters?

Or would there be a homogeneous intermediate expression level? Is it dynamic and on what time scales? How does the regulation change when cheaters are present? There is a need for new genetic tools to probe the role that invertase regulation has on maintenance of cooperation and fitness outcomes for cooperators like fitness, frequency within a population, or total community productivity.

Overview of Chapters to Study the Role of Invertase Regulation on Cooperation

To better understand when and how regulation of invertase impacts individual and community level characteristics new genetic tools would need three characteristics: 1) the ability to control invertase regulation so that we could spatially and temporally drive cooperation in a community 2) the ability to visualize active cooperators in a wildtype cooperation to help us better understand how dynamic native regulation is and how it compares to regulation in a mixed community setting. Finally, 3) The ability to compare varying levels of constitutive invertase production to the natively regulated strategies. My work on these research questions and goals have been divided across the subsequent 5 chapters. Chapter 2 focuses on improving a calibration method for the experimental hardware necessary for the spatiotemporally control of invertase in *S. cerevisiae*. Chapter 3 focuses on the construction and validation of the spatiotemporally controlled strains of *S. cerevisiae* using optogenetics. In this chapter we also observe an interesting patterning phenomenon that seems to be affected because of the spatial organization/sequestration/segmentation of the cooperator cells and the cheater cells as well as the nutrient gradients present across an agar plate. In chapter 4, I continue to explore the bullseye pattern, I contribute to developing and validating a reaction-diffusion model that has success in recapitulating most of our experimental data. However, we also observe perplexing cases where our model fails to predict the data. This re-invigorates our pursuit to understand the role that regulation of invertase may have under

different experimental conditions. In chapter 5, we continue to develop the tools that would allow us to visualize active cooperators and compare cooperation strategies ie. regulation and production of invertase by achieving co-translational expression of a fluorescent reporter along with invertase from a single promoter of interest. Finally, I conclude by summarizing the key take-aways from my work and contextualizing my work within the larger context of the public goods in the *S. cerevisiae* field. I present suggestions for future research to target cooperative and further considerations when studying secretory systems. Appendices 1 and 2 highlight a broader application of different secretory systems; from a biomaterials engineering perspective and from another type of secreted cooperative molecule in this case aiding the survival of yeast communities when heat shocked.

References

[1] H. Celiker and J. Gore, "Cellular cooperation: insights from microbes," *Trends Cell Biol.*, vol. 23, no. 1, pp. 9–15, Jan. 2013, doi: 10.1016/j.tcb.2012.08.010.

[2] J. Cremer, A. Melbinger, K. Wienand, T. Henriquez, H. Jung, and E. Frey, "Cooperation in Microbial Populations: Theory and Experimental Model Systems," *J. Mol. Biol.*, vol. 431, no. 23, Art. no. 23, Nov. 2019, doi: 10.1016/j.jmb.2019.09.023.

[3] F. Harrison and A. Buckling, "Cooperative production of siderophores by Pseudomonas aeruginosa," *Front. Biosci. Landmark Ed.*, vol. 14, no. 11, pp. 4113–4126, Jan. 2009, doi: 10.2741/3516.

[4] X.-X. Zhang and P. B. Rainey, "Exploring the sociobiology of pyoverdin-producing Pseudomonas," *Evol. Int. J. Org. Evol.*, vol. 67, no. 11, pp. 3161–3174, Nov. 2013, doi: 10.1111/evo.12183.

[5] S. Giri, S. Waschina, C. Kaleta, and C. Kost, "Defining Division of Labor in Microbial Communities," *J. Mol. Biol.*, vol. 431, no. 23, pp. 4712–4731, Nov. 2019, doi: 10.1016/j.jmb.2019.06.023.

[6] J. Cremer, A. Melbinger, and E. Frey, "Growth dynamics and the evolution of cooperation in microbial populations," *Sci. Rep.*, vol. 2, p. 281, 2012, doi: 10.1038/srep00281.

[7] S. A. West and M. Ghoul, "Conflict within cooperation," *Curr. Biol.*, vol. 29, no. 11, pp. R425–R426, Jun. 2019, doi: 10.1016/j.cub.2019.04.028.

[8] M. Doebeli and C. Hauert, "Models of cooperation based on the Prisoner's Dilemma and the Snowdrift game," *Ecol. Lett.*, vol. 8, no. 7, pp. 748–766, 2005, doi: 10.1111/j.1461-0248.2005.00773.x.

[9] D. Greig and M. Travisano, "The Prisoner's Dilemma and polymorphism in yeast SUC genes.," *Proc. R. Soc. B Biol. Sci.*, vol. 271, no. Suppl 3, pp. S25–S26, Feb. 2004.

[10] D. R. Finn, M. App, L. Hertzog, and C. C. Tebbe, "Reconciling concepts of black queen and tragedy of the commons in simulated bulk soil and rhizosphere prokaryote communities," *Front. Microbiol.*, vol. 13, p. 969784, 2022, doi: 10.3389/fmicb.2022.969784.

[11] N. Henriksson *et al.*, "The mycorrhizal tragedy of the commons," *Ecol. Lett.*, vol. 24, no. 6, pp. 1215–1224, Jun. 2021, doi: 10.1111/ele.13737.

[12] P. D. Leenheer, M. Schuster, and H. Smith, "Strong cooperation or tragedy of the commons in the chemostat," *Math. Biosci. Eng. MBE*, vol. 16, no. 1, pp. 139–149, 11 2018, doi: 10.3934/mbe.2019007.

[13] D. J. Rankin, K. Bargum, and H. Kokko, "The tragedy of the commons in evolutionary biology," *Trends Ecol. Evol.*, vol. 22, no. 12, pp. 643–651, Dec. 2007, doi: 10.1016/j.tree.2007.07.009.

[14] Z. Sun, T. Koffel, S. M. Stump, G. M. Grimaud, and C. A. Klausmeier, “Microbial cross-feeding promotes multiple stable states and species coexistence, but also susceptibility to cheaters,” *J. Theor. Biol.*, vol. 465, pp. 63–77, Mar. 2019, doi: 10.1016/j.jtbi.2019.01.009.
[15] F. J. Romero-Campero and M. J. Pérez-Jiménez, “A model of the quorum sensing system in Vibrio fischeri using P systems,” *Artif. Life*, vol. 14, no. 1, pp. 95–109, 2008, doi: 10.1162/artl.2008.14.1.95.
[16] F. Harrison, J. Paul, R. C. Massey, and A. Buckling, “Interspecific competition and siderophore-mediated cooperation in Pseudomonas aeruginosa,” *ISME J.*, vol. 2, no. 1, pp. 49–55, Jan. 2008, doi: 10.1038/ismej.2007.96.
[17] A. Buckling *et al.*, “Siderophore-mediated cooperation and virulence in Pseudomonas aeruginosa,” *FEMS Microbiol. Ecol.*, vol. 62, no. 2, pp. 135–141, Nov. 2007, doi: 10.1111/j.1574-6941.2007.00388.x.
[18] P. Cao, A. Dey, C. N. Vassallo, and D. Wall, “How Myxobacteria Cooperate,” *J. Mol. Biol.*, vol. 427, no. 23, pp. 3709–3721, Nov. 2015, doi: 10.1016/j.jmb.2015.07.022.
[19] G. P. Sah and D. Wall, “Kin recognition and outer membrane exchange (OME) in myxobacteria,” *Curr. Opin. Microbiol.*, vol. 56, pp. 81–88, Aug. 2020, doi: 10.1016/j.mib.2020.07.003.
[20] L. J. Shimkets, “Social and developmental biology of the myxobacteria,” *Microbiol. Rev.*, vol. 54, no. 4, pp. 473–501, Dec. 1990, doi: 10.1128/mr.54.4.473-501.1990.
[21] S. Pande, P. Pérez Escriva, Y.-T. N. Yu, U. Sauer, and G. J. Velicer, “Cooperation and Cheating among Germinating Spores,” *Curr. Biol. CB*, vol. 30, no. 23, pp. 4745-4752.e4, Dec. 2020, doi: 10.1016/j.cub.2020.08.091.
[22] A. Margetić and Z. Vujčić, “Comparative study of stability of soluble and cell wall invertase from Saccharomyces cerevisiae,” *Prep. Biochem. Biotechnol.*, vol. 47, no. 3, pp. 305–311, Mar. 2017, doi: 10.1080/10826068.2016.1244683.
[23] F. Dodyk and A. Rothstein, “Factors influencing the appearance of invertase in Saccharomyces cerevisiae,” *Arch. Biochem. Biophys.*, vol. 104, no. 3, pp. 478–486, Mar. 1964, doi: 10.1016/0003-9861(64)90492-8.
[24] L. del Castillo Agudo and D. Gozalbo, “Genes involved in the regulation of invertase production in Saccharomyces cerevisiae,” *Microbiol. Madr. Spain*, vol. 10, no. 4, pp. 385–394, Dec. 1994.
[25] C. Herwig, C. Doerries, I. Marison, and U. von Stockar, “Quantitative analysis of the regulation scheme of invertase expression in Saccharomyces cerevisiae,” *Biotechnol. Bioeng.*, vol. 76, no. 3, pp. 247–258, Nov. 2001.
[26] W. L. Marques, V. Raghavendran, B. U. Stambuk, and A. K. Gombert, “Sucrose and Saccharomyces cerevisiae: a relationship most sweet,” *FEMS Yeast Res.*, vol. 16, no. 1, p. fov107, Feb. 2016, doi: 10.1093/femsyr/fov107.
[27] J. Gore, H. Youk, and A. van Oudenaarden, “Snowdrift game dynamics and facultative cheating in yeast,” *Nature*, vol. 459, no. 7244, pp. 253–256, May 2009, doi: 10.1038/nature07921.
[28] J. H. Koschwanez, K. R. Foster, and A. W. Murray, “Sucrose utilization in budding yeast as a model for the origin of undifferentiated multicellularity,” *PLoS Biol.*, vol. 9, no. 8, p. e1001122, Aug. 2011, doi: 10.1371/journal.pbio.1001122.
[29] J. H. Koschwanez, K. R. Foster, and A. W. Murray, “Improved use of a public good selects for the evolution of undifferentiated multicellularity,” *eLife*, vol. 2, p. e00367, Apr. 2013, doi: 10.7554/eLife.00367.
[30] R. C. Maclean and C. Brandon, “Stable public goods cooperation and dynamic social interactions in yeast,” *J. Evol. Biol.*, vol. 21, no. 6, pp. 1836–1843, doi: 10.1111/j.1420-9101.2008.01579.x.
[31] R. J. Lindsay, B. J. Pawlowska, and I. Gudelj, “When increasing population density can promote the evolution of metabolic cooperation,” *ISME J.*, vol. 12, no. 3, Art. no. 3, Mar. 2018, doi: 10.1038/s41396-017-0016-6.
[32] H. Celiker and J. Gore, “Competition between species can stabilize public-goods cooperation within a species,” *Mol. Syst. Biol.*, vol. 8, p. 621, Nov. 2012, doi: 10.1038/msb.2012.54.

[33] R. C. MacLean, A. Fuentes-Hernandez, D. Greig, L. D. Hurst, and I. Gudelj, “A Mixture of ‘Cheats’ and ‘Co-Operators’ Can Enable Maximal Group Benefit,” *PLOS Biol.*, vol. 8, no. 9, p. e1000486, Sep. 2010, doi: 10.1371/journal.pbio.1000486.
[34] A. Sanchez and J. Gore, “feedback between population and evolutionary dynamics determines the fate of social microbial populations,” *PLoS Biol.*, vol. 11, no. 4, p. e1001547, 2013, doi: 10.1371/journal.pbio.1001547.
[35] “Generic Indicators for Loss of Resilience Before a Tipping Point Leading to Population Collapse | Science.” https://science.sciencemag.org/content/336/6085/1175.long (accessed May 29, 2020).
[36] A. Dobay, H. C. Bagheri, A. Messina, R. Kümmerli, and D. J. Rankin, “Interaction effects of cell diffusion, cell density and public goods properties on the evolution of cooperation in digital microbes,” *J. Evol. Biol.*, vol. 27, no. 9, pp. 1869–1877, doi: 10.1111/jeb.12437.
[37] A. Ross-Gillespie, A. Gardner, A. Buckling, S. A. West, and A. S. Griffin, “Density Dependence and Cooperation: Theory and a Test with Bacteria,” *Evolution*, vol. 63, no. 9, pp. 2315–2325, 2009, doi: 10.1111/j.1558-5646.2009.00723.x.
[38] J. E. Strassmann and D. C. Queller, “Evolution of cooperation and control of cheating in a social microbe,” *Proc. Natl. Acad. Sci. U. S. A.*, vol. 108 Suppl 2, no. Suppl 2, pp. 10855–10862, Jun. 2011, doi: 10.1073/pnas.1102451108.
[39] Ö. Özkaya, R. Balbontín, I. Gordo, and K. B. Xavier, “Cheating on Cheaters Stabilizes Cooperation in Pseudomonas aeruginosa,” *Curr. Biol. CB*, vol. 28, no. 13, pp. 2070-2080.e6, Jul. 2018, doi: 10.1016/j.cub.2018.04.093.
[40] R. C. MacLean and I. Gudelj, “Resource competition and social conflict in experimental populations of yeast,” *Nature*, vol. 441, no. 7092, Art. no. 7092, May 2006, doi: 10.1038/nature04624.
[41] S. J. Kassinger and M. L. van Hoek, “Biofilm architecture: An emerging synthetic biology target,” *Synth. Syst. Biotechnol.*, vol. 5, no. 1, Art. no. 1, Mar. 2020, doi: 10.1016/j.synbio.2020.01.001.
[42] C. Hauert and M. Doebeli, “Spatial structure often inhibits the evolution of cooperation in the snowdrift game,” *Nature*, vol. 428, no. 6983, pp. 643–646, Apr. 2004, doi: 10.1038/nature02360.
[43] B. Allen, J. Gore, and M. A. Nowak, “Spatial dilemmas of diffusible public goods,” *eLife*, vol. 2, p. e01169, Dec. 2013, doi: 10.7554/eLife.01169.
[44] J. D. Van Dyken, M. J. I. Müller, K. M. L. Mack, and M. M. Desai, “Spatial Population Expansion Promotes the Evolution of Cooperation in an Experimental Prisoner’s Dilemma,” *Curr. Biol.*, vol. 23, no. 10, pp. 919–923, May 2013, doi: 10.1016/j.cub.2013.04.026.
[45] J. Li, H. Xu, W. E. Bentley, and G. Rao, “Impediments to Secretion of Green Fluorescent Protein and Its Fusion from Saccharomyces cerevisiae,” *Biotechnol. Prog.*, vol. 18, no. 4, pp. 831–838, doi: 10.1021/bp020066t.
[46] I. Kunze *et al.*, “The green fluorescent protein targets secretory proteins to the yeast vacuole,” *Biochim. Biophys. Acta BBA - Bioenerg.*, vol. 1410, no. 3, pp. 287–298, Mar. 1999, doi: 10.1016/S0005-2728(99)00006-7.
[47] M. Vitolo, M. A. Duranti, and M. B. Pellegrim, “Effect of pH, aeration and sucrose feeding on the invertase activity of intact S. cerevisiae cells grown in sugarcane blackstrap molasses,” *J. Ind. Microbiol.*, vol. 15, no. 2, pp. 75–79, Aug. 1995.

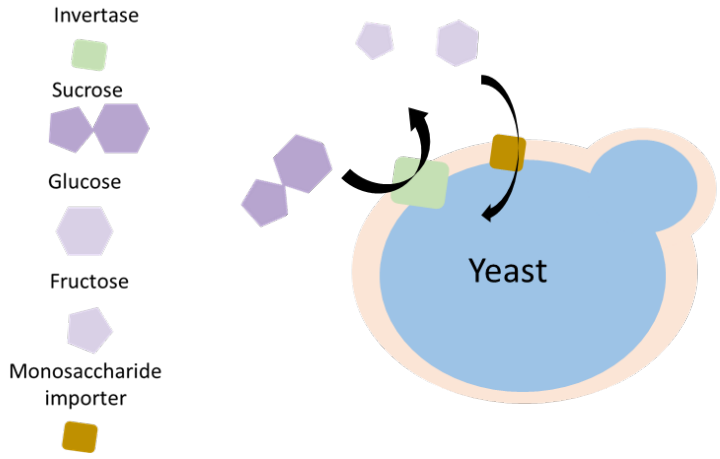

Figure 1: Diagram of a *Saccharomyces cerevisiae* invertase producer
Yeast are able to use sucrose as a carbon source through the use of the enzyme invertase. Sucrose is converted to the monosaccharides, glucose, and fructose. The yeast cell is then able to import the freed monosaccharides.

Table 1: Comparison of *Saccharomyces cerevisiae* public goods cooperation works

Reference	Methodology	Invertase regulation (Yes/No)	Cost of cooperation considered (Yes/No and details)
Gore et al., 2009 [27]	5% sucrose. Haploid cells, Cooperator has intact SUC2 gene and cheat is suc2Δ. Histidine is limited to tune the cost of cooperation. Competition in well-mixed conditions.	No	Yes. Empirically determined and tuned via experiments and modeling.
Lindsay et al., 2018 [31] (this paper treated two types of cooperation, for the purposes of this table only focused on public goods cooperation)	High (~3%), medium and low sucrose concentrations. Cooperator and cheater strains were those used in ref [27]. Competition in well-mixed conditions and on plates with increasing degrees of spatial structure.	No	Yes. Empirically determined in [33].

Gore et al., 2013 [34]	2% sucrose. Grown in a 96 well plate and diluted by a 667x factor each day. Competition in well-mixed conditions. Cooperator and cheater strains were used in ref [27].	No	Cost determined in [27]
Travisano et al., 2004 [9]	Plating on 2% sucrose plates. Intact *SUC2* diploid and diploid suc2Δ, isogenic strains. Composition information was measured by replica plating on dependent selection-dependent markers on strains.	No	No
MacLean et al., 2008 [30]	2% sucrose. Strains used in [9].Competing strains in ratios of 99%coop:1% cheater strains on plates across several cycles of re-plating. SUC2 copy number measured to get composition information.	No	No
Koschwanez et al., 2013 [29]	Several concentrations of sucrose ranging from ~3% to 0.2% .Haploid cells with intact SUC2 or with ADH1 promoter-driven expression of the fluorescent markers ymCherry (cooperators) and ymCitrine (suc2Δ).	No	Yes. Empirically determined
MacLean et al., 2010 [33]	10%,2%,0.1%, 0.01% sucrose. Intact *SUC2* diploid and suc2Δ diploid, isogenic strains. Competitions in well-mixed environments.	No	Yes. Empirically determined
Van Dyken et al., 2013 [44]	Strains used in [29], with the addition of cycloheximide resistance to the cheater. 2% sucrose. Competitions on plates. Cycloheximide is added to increase the cost for cooperators.	No	Yes. Empirically tuned by adding "cost" through addition of cycloheximide. Model incorporates game theory models of cost versus benefits

Chapter 2: Easy calibration of the Light Plate Apparatus for optogenetic experiments

This chapter was adapted and previously published here:

K. Sweeney, N. Moreno Morales, Z. Burmeister, A. J. Nimunkar, and M. N. McClean, "Easy calibration of the Light Plate Apparatus for optogenetic experiments," *MethodsX*, vol. 6, pp. 1480–1488, Jun. 2019, doi: 10.1016/j.mex.2019.06.008.

Neydis Moreno Morales and Kieran Sweeney performed the experiments. Kieran Sweeney wrote Matlab custom code. All authors contributed to discussion of the project. Zachary A. Burmeister and Amit J. Nimunkar built the LPAs. Neydis Moreno Morales, Kieran Sweeney and Megan McClean wrote the paper.

Abstract

Optogenetic systems use genetically-encoded light-sensitive proteins to control and study cellular processes. As the number and quality of these systems grows, there is an increasing need for user-friendly and flexible hardware to provide programmed illumination to cultures of cells. One platform which satisfies this need for a variety of optogenetic systems and organisms is the Light Plate Apparatus (LPA), which delivers a controlled light dose to each well of a 24-well plate. Experimental reproducibility requires appropriate calibration to produce accurate light doses within individual wells of the LPA and between LPAs. In this study, we present an easy and accurate method for calibrating the LPA. In particular, we:

- developed a 3D printed adaptor and MATLAB code to allow rapid measurement of irradiance produced by the LPA and subsequent calibration
- provide appropriate code and methodology for generating a standard curve for each LPA
- demonstrate the utility and accuracy of this method between users and LPAs

Background

Optogenetic systems provide a promising toolkit for cell biology. These systems utilize genetically-encoded light-sensitive proteins to actuate processes within the cell. The optogenetic toolkit is improving and expanding; genetically-encoded light sensitive proteins have been developed to control cellular events such as gene expression, protein localization, and phase separation [1–3]. The response of these optogenetic systems is light dose-dependent and excessive light is harmful to cells, emphasizing the importance of administering precise, quantifiable, and reproducible light doses. Until recently, the hardware necessary to administer such light doses has made the use of optogenetic tools difficult for non-specialist research groups.

The Light Plate Apparatus (LPA) is a recently-developed, flexible, and user-friendly hardware platform that promises to improve the accessibility of optogenetic technology [4]. The LPA is an open source programmable LED array that delivers controlled light doses to each well of a 24-well plate. The LPA has two LEDs (top and bottom) for each well of the 24-well plate and consists of a printed circuit board, a microcontroller, three LED drivers, and other commercially available electronic components that can be ordered and assembled within a 3D-printed enclosure. The LPA is programmed using an open-source web-based tool called Iris [5], making sophisticated illumination patterns accessible to researchers without engineering or programming experience.

A newly assembled LPA will exhibit unwanted brightness differences between wells due to inhomogeneities in the LPA and differences in LED performance. It is therefore necessary to calibrate the LPA before use so that each LED outputs the correct light intensity. The current applied to each LED can be adjusted independently by scaling a dot correction (dc) value, which ranges from 0-63. Finer adjustments to brightness can be made by pulse width modulation of the current by scaling a grayscale value (gcal), which ranges from 0-255 [6]. The dc and gcal calibration values per LED are stored as space-delimited integers in the files “dc.txt” and “gcal.txt”, which can be manually loaded onto the LPA via an SD card. Once calibrated, a user can set the LPA to administer timed light doses for each LED with the Iris webtool, which outputs “Iris” values that control the intensity of each LED. The Iris values further scale the pulse width modulation of the current, such that the current supplied to each LED is ultimately pulse width modulated by (Iris×gcal)/255. With dc, gcal, and Iris set to their maximum values a current of 17.8 mA can be supplied to each LED in the array simultaneously. On a calibrated LPA, two LEDs assigned the same Iris value should output the same light dose. These Iris values (and other light program properties) are saved to the file “program.lpf” (which is loaded onto the LPA via the SD card) and range between 0 (no LED output) and 4095 (100% LED output).

The published LPA documentation included two methods for calibrating an LPA. Both methods generally involve tuning the dc and gcal values such that the brightest LEDs are dimmed to match the brightness of the dimmest LEDs. In the first method, a MATLAB script is used to calculate tuned gcal values based on relative LED intensity measurements extracted from digital photos of the LPA. In the second approach, each LED is manually measured with a probe spectrometer and the gcal value for each LED is scaled to produce a desired intensity reading. Both methods produce more uniform LED output after successive rounds of calibration.

We have developed a third method for calibrating the LEDs based on absolute irradiance measurements acquired using a standard photodiode optical power sensor. A power meter with an optical power sensor represents the minimal equipment for any lab interested in performing quantitative optogenetic experiments. A 3D-printed adapter that interfaces with the 24-well plate and appropriate MATLAB code allow a single user to quickly measure absolute irradiance per well and perform subsequent calibration. We extend our methodology to calculate a standard curve for each LPA, allowing Iris values to be chosen such that a desired irradiance can be attained per well. This allows us to utilize multiple LPAs simultaneously to administer equivalent light doses, dramatically increasing experimental throughput.

Materials and equipment

- Light Plate Apparatus [4]
- Iris webtool [5]
- SanDisk card and reader
- Flat polystyrene bottom 24-well plate with opaque well walls (Arctic White LLC, AWLS-303008)
- Diffuser sheets (Rosco, #3008)
- Power sensor adaptor (See supplementary materials)
- Photodiode power sensor (ThorLabs, #S120VC [7])

- Power meter (ThorLabs, #PM100D)
- Thorlabs Optical Power Monitor (OPM) Version 1.1 software (www.thorlabs.com)
- LPA_calibration.m and LPA_standardCurve.m MATLAB scripts

Calibration Procedure

In our protocol (**Fig. 1A**), the user measures the irradiance of each well of the LPA in order, generating an irradiance signal which resembles a series of 24 repeated square waves. The included MATLAB script "LPA_calibration.m" then identifies the wells from the signal (**Fig. 1B**), measures the mean irradiance value per well, and calculates the calibration values needed for uniform LED output across the LPA (**Fig. 1C**). The detailed steps involved in calibration are as follows:

1. Two text files ("gcal.txt" and "dc.txt") are used to specify the appropriate dc and gcal calibration value for each LED. Set all gcal values in "gcal.txt" to 255 and all dc values in "dc.txt" to 63 using a text editor, then load the text files onto the SD card. We start with these maximum calibration values to achieve the highest irradiance output from the LPA. As the LPA undergoes multiple rounds of calibration, these calibration values will be scaled downwards such that each LED is tuned to match the irradiance output of the dimmest LED of the LPA. This procedure measures the top and bottom LED sets independently but calculates calibration values for all 48 LEDs together.

2. Using the Iris webtool, create a steady-state light program in which all of the top LEDs are set to the same Iris value (we used 2000) and all of the bottom LEDs are set to zero. Download and unzip the resulting "program.lpf" file and transfer it onto the SD card. Load the SD card into the LPA and turn it on. Place a 24-well plate on the LPA, which should be fitted with three diffuser sheets over the LEDs as described by Gerhardt *et al*., 2016. Use a plate with a flat transparent bottom and opaque well walls to prevent light transmission between neighboring wells.

3. To assemble the equipment needed for calibration **(Fig. S1)**, plug the optical power sensor into the optical power meter (OPM), which should be connected to a computer running the Thorlabs OPM software. Set the OPM software to record irradiance measurements (in $\mu W/cm^2$) at the appropriate wavelength to a log file. We measured the blue LEDs of our LPA at 470 nm at a sampling rate of 1 Hz. Fit the power sensor adaptor over the power sensor. The adaptor slots into the wells of the 24-well plate and aligns the active sensor area to the center of each well so that each measurement is taken from a consistent location between the top and bottom LEDs. We measure the LPA through the 24-well plate like this because 1) it allows us to acquire quick and consistent light measurements that are proportional to the light dose received by cells grown in the well and 2) it allows one to make intermittent irradiance measurements while cells are growing in the plate and estimate changes in irradiance due to cell growth. Neither measurement noise **(Fig. S2A)** nor light bleeding between wells (Fig. S2B) has a substantial effect on these measurements.

4. With the power sensor pressed flat against an opaque surface, start recording irradiance measurements in the OPM software. Move the sensor into well 1 of the 24-well plate to record light measurements, then press the sensor back against the opaque surface to record dark measurements. Continue this process for the remaining wells, measuring left to right across each row before moving down to the next row and pressing the sensor against the flat surface between each well measurement. We typically measure each well for 5 seconds and against the flat surface for 3 second intervals. Sampling at 1 Hz, this typically results in five measurements per well, which are averaged to give an irradiance measurement for each LED. Stop recording irradiance measurements in the OPM software when all wells are measured. The recorded waveform should resemble a series of 24 repeated square pulses with each peak corresponding to an LED measurement (**Fig. 1B**).

5. Repeat steps 2-4, but with a new “program.lpf” file loaded onto the LPA such that all the bottom LEDs are set to the same Iris value (e.g., 2000 again) and all the top LEDs are set to zero.

6. Run the MATLAB script “LPA_calibration.m”. At the first prompt select “grayscale” as the calibration value to be tuned and at the next prompt set the calibration round to 1. Load the recorded measurements for the top LED set (“channel 1 data”) and bottom LED set (“channel 2 data”) and set an output folder for saving measured LED irradiances and calculated calibration values in the subsequent prompts. After running, the script displays the mean, standard deviation, and coefficient of variation (CV) of the irradiances of all LEDs on the LPA in the command window and outputs two graphs. One graph shows the recorded waveform and to which well each peak is mapped (**Fig. 1B**). From this graph it is easy to determine if the script is correctly identifying the wells. If it is not, try changing the segmentation parameters in the script, starting with “ampthresh,” which sets the irradiance threshold above which samples are considered potential well measurements. The other graph (**Fig. 1C**) shows a heatmap with the mean irradiance of each LED and another heatmap with newly calculated gcal values. The calculated gcal values and measured irradiances from this first round of calibration are saved in the designated output folder as “gcal_round_1.csv” and “meanIntensities_round_ 1.csv”.

7. Copy the calculated gcal values from “gcal_round_*.csv” into “gcal.txt” where “*” indicates the current calibration round. Transfer the updated file to the LPA via the SD card. Repeat steps 1-6 to calculate the next round of calibration values. The displayed CV value should decrease as the irradiance outputs of all LEDs across the LPA converge.

8. Repeat steps 1-7 as needed for additional rounds until the LPA is calibrated. We continue until the CV of all LEDs is below 1%. The script will output new files “meanIntensities_round_*.csv” and “gcal_round_*.csv” for each round, where “*” indicates the current calibration round.

Note that the above steps describe the calibration of the LPA by calculating gcal values that provide uniform LED irradiances across the LPA. For coarser adjustments to light output, one can tune the dc values via an equivalent process by selecting “dot correction” as the calibration value to be tuned at the prompt in “LPA_calibration.m” and updating the values in “dc.txt” with each round of calibration. We

typically did not find this necessary; just tuning the gcal values was usually sufficient to calibrate an LPA within three rounds.

Standard Curve Procedure

Once calibrated, the LPA delivers a uniform light dose across all the wells of the LPA. At this stage, it is useful to generate an equation relating the Iris values set when designing a light program to the light output of each well. This allows a user to predict the Iris values necessary to achieve a desired light dose and enables higher-throughput experiments by allowing multiple LPAs to deliver equivalent light doses. In general, this is done by measuring the light output of the LPA at a given light dose and solving for the equation relating light dose to Iris value. This can be done with measurements made at a single Iris value, though here we do this over a wide range of Iris values to demonstrate that our script can accept measurements made over an arbitrary number of Iris values in order to make accurate predictions and to show that the relationship between Iris and light dose is linear.

1. Assemble the calibrated LPA, 24-well plate, and optical power meter components as described in the *Calibration Procedure* of the LPA. Using the Iris webtool, set all LEDs of the LPA to output an equal light dose by setting their Iris values to an equal number. We start by setting all Iris values to 250.

2. Record the irradiance output across the LPA as described in step 4 of the *Calibration Procedure*. For calculating the standard curve, it is not necessary to measure the irradiance output of every well. We measured only eight randomly selected wells. When saving the log files for these measurements in the OPM software, include the Iris value in the filename. Do not include any other numbers in the filename. For example, we saved our first set of irradiance measurements as “Iris250.csv”. The MATLAB script for calculating the standard curve extracts the Iris value associated with a given set of measurements from the filename.

3. Repeat step two with all the LEDs set to a different Iris value. Do this until you have covered the full range of Iris values you intend to use. The script accepts measurements made at an arbitrary number of

Iris values so long as the files are named correctly. We repeated step two until we had light output measurements for Iris values equal to 250, 500, 1000, 2000, and 4000.

4. Run the "LPA_standardCurve.m" script. At the first prompt, import all of the measurements you made in the previous steps. At the next prompt, enter the number of wells you measured per Iris value. The script outputs two graphs (**Fig. S3**). As before, the first graph (**Fig. S3A**) shows how peaks in the recorded irradiance values are mapped to each well. The second graph (**Fig. S3B**) shows a standard curve relating light output (in $\mu W/cm^2$) to Iris value and includes the linear equation describing this relationship. One can determine the Iris values needed to achieve specified light doses directly from the graph using MATLAB's data cursor tool. One can also specify the desired light outputs in the vector "targetLightOutput" and the script will return the corresponding Iris values in the command line. In either case, the returned value should be assigned to both LEDs in a given well to provide the desired light dose in that well.

Method Validation

To confirm that our LPA calibration process leads to the convergence of LED irradiances across the LPA, we tracked the irradiance of each LED as we performed three successive rounds of calibration with a fixed Iris value of 2000 on a representative LPA (**Fig. 2, Fig. S7**). Before the first round of calibration, the mean irradiance of all LEDs was 109.6 $\mu W/cm^2$ with a coefficient of variation of 12.6% (**Fig. 2A**). After the third round of calibration, the brightest LEDs were dimmed to match the irradiance of the dimmest LED, such that the mean irradiance of all LEDs was 83.5 $\mu W/cm^2$ with a coefficient of variation (CV) of 0.82%. We consider LPAs with a CV lower than 1% to be calibrated.

We next generated a standard curve relating Iris value to LED irradiance for the calibrated LPA by measuring the light output of the LPA over a range of Iris values and using the "LPA_standardCurve.m" script as described previously (**Fig. 3A**). The script generates an equation for the line that best fits the measurements (blue triangles). The equation takes the form Intensity = a×Iris (where *a* is the fitted

parameter) and represents the relationship between Iris value and irradiance and can be used to estimate the Iris value for both the top and bottom LEDs in a given well needed to achieve a specified light dose. We predicted the Iris values needed to achieve irradiances of 25, 50, 100, 200, and 300 μW/cm^2 and measured the light output of the LPA using these predicted Iris values. In all cases, the measured values (blue circles) were within 4% of the target value. The utility of the standard curve is contingent upon having a well-calibrated LPA (**Fig. S8**).

One LPA provides 24 wells in which to culture cells and expose them to appropriate light doses. Increasing throughput requires multiple LPAs calibrated such that they can administer the same light doses. By calibrating our LPAs and relating Iris values to light dose using an absolute irradiance measurement, we can easily configure multiple LPAs to produce the same light output (**Fig. 3B**). We predicted Iris values needed to produce light outputs of 25, 50, 100, 200, and 300 μW/cm^2 for three LPAs. Though the LPAs had different standard curves, and thus require different Iris values to generate a given light dose, we were able to achieve irradiances within 3% of the targeted irradiance for all LPAs. This enables us to consistently and quantitatively use multiple LPAs simultaneously for higher throughput experiments.

To further demonstrate reduced light dose variation following calibration we set all the LEDs of an uncalibrated LPA to a constant Iris value and measured the irradiance of each well. We then calibrated the LPA, and assigned all wells a constant Iris value such that the mean irradiance output by the calibrated LPA approximately matched that of the uncalibrated LPA (**Fig. 4**). We did this at three light doses and each time observed significantly reduced irradiance variation.

To determine how LPA calibration effects an *in vivo* optogenetic system, we measured the light-induced expression of the red fluorescent protein mRuby in the yeast *Saccharomyces cerevisiae.* The expression of mRuby is driven by a CRY2-CIB1 split transcription factor gene induction system [8,9] that is activated by blue light (470 nm). We aliquoted yeast at mid-log phase into 24-well plates over a calibrated and uncalibrated LPA mounted in a shaking incubator and set to output a range of blue light doses. The

calibrated LPA was configured as described in the *Calibration Procedure* and set to deliver target light doses of 0, 10, 25, 50, 75, and 100 μW/cm^2, in order, to columns 1-6 of the 24-well plates (resulting in four replicates per light dose). We assigned the same Iris values to the uncalibrated LPA, which showed more variation in irradiance between wells and consistently exceeded the target light doses (**Fig. 5A**). We incubated the yeast at 30°C under these lighting conditions for four hours and measured the resulting mRuby expression by flow cytometry (**Fig. 5B**). Though biological variability dominates the effect of light dose variability in this case, mRuby expression is consistently higher for the uncalibrated LPA, which is expected due to its higher light doses.

Conclusions

Our method allows the quick calibration of an LPA using an optical power meter and the creation of a standard curve relating light dose to Iris value. Our method makes it easy to administer controlled and consistent light doses across the wells of a single LPA and between multiple LPAs.

Acknowledgements and funding
The authors would like to thank S. Geller, K. Lauterjung, M. An-adirekkun, T. Scott, and F. Gambacorta for assistance in testing the protocol and comments on the manuscript. This work was supported by the University of Wisconsin Carbone Cancer Center Support Grant (P30 CA014520) and the National Institutes of Health (Grant 1R35GM128873). Kieran Sweeney is supported by a Genomic Sciences Training Program NHGRI Training Grant (5T32HG002760). Neydis Moreno Morales is supported by the Science and Medicine Graduate Research Scholars (SciMed GRS) program at the University of Wisconsin-Madison. Megan Nicole McClean, Ph.D., holds a Career Award at the Scientific Interface from the Burroughs Wellcome Fund.

References

[1] K. Kolar, W. Weber, Synthetic biological approaches to optogenetically control cell signaling, Curr. Opin. Biotechnol. 47 (2017) 112–119. doi:10.1016/j.copbio.2017.06.010.

[2] K. Kolar, C. Knobloch, H. Stork, M. Žnidarič, W. Weber, OptoBase: A Web Platform for Molecular Optogenetics, ACS Synth. Biol. 7 (2018) 1825–1828. doi:10.1021/acssynbio.8b00120.

[3] L.J. Bugaj, G.P. O'Donoghue, W.A. Lim, Interrogating cellular perception and decision making with optogenetic tools., J. Cell Biol. 216 (2017) 25–28. doi:10.1083/jcb.201612094.

[4] K.P. Gerhardt, E.J. Olson, S.M. Castillo-Hair, L.A. Hartsough, B.P. Landry, F. Ekness, R. Yokoo, E.J. Gomez, P. Ramakrishnan, J. Suh, D.F. Savage, J.J. Tabor, An open-hardware platform for optogenetics and photobiology, Sci. Rep. 6 (2016) 1–13. doi:10.1038/srep35363.

[5] Iris, (2016). taborlab.github.io/Iris/.

[6] TLC5941 Datasheet, (2008). www.ti.com/lit/ds/symlink/tlc5941.pdf.

[7] Thorlabs S120VC Spec Sheet, (2016). www.thorlabs.com/drawings/bb6cf240bbf37a61-82F257AF-BE33-702C-6D399BD79993219C/S120VC-SpecSheet.pdf.

[8] C.J. Stewart, M.N. Mcclean, Design and Implementation of an Automated Illuminating, Culturing, and Sampling System for Microbial Optogenetic Applications, J. Vis. Exp. (2017) 54894. doi:10.3791/54894.

[9] J. Melendez, M. Patel, B.L. Oakes, P. Xu, P. Morton, M.N. McClean, Real-time optogenetic control of intracellular protein concentration in microbial cell cultures, Integr. Biol. (United Kingdom). 6 (2014) 366–372. doi:10.1039/c3ib40102b.

[10] M.A. Sheff, K.S. Thorn, Optimized cassettes for fluorescent protein tagging in *Saccharomyces cerevisiae*, Yeast. 21 (2004) 661–670. doi:10.1002/yea.1130.

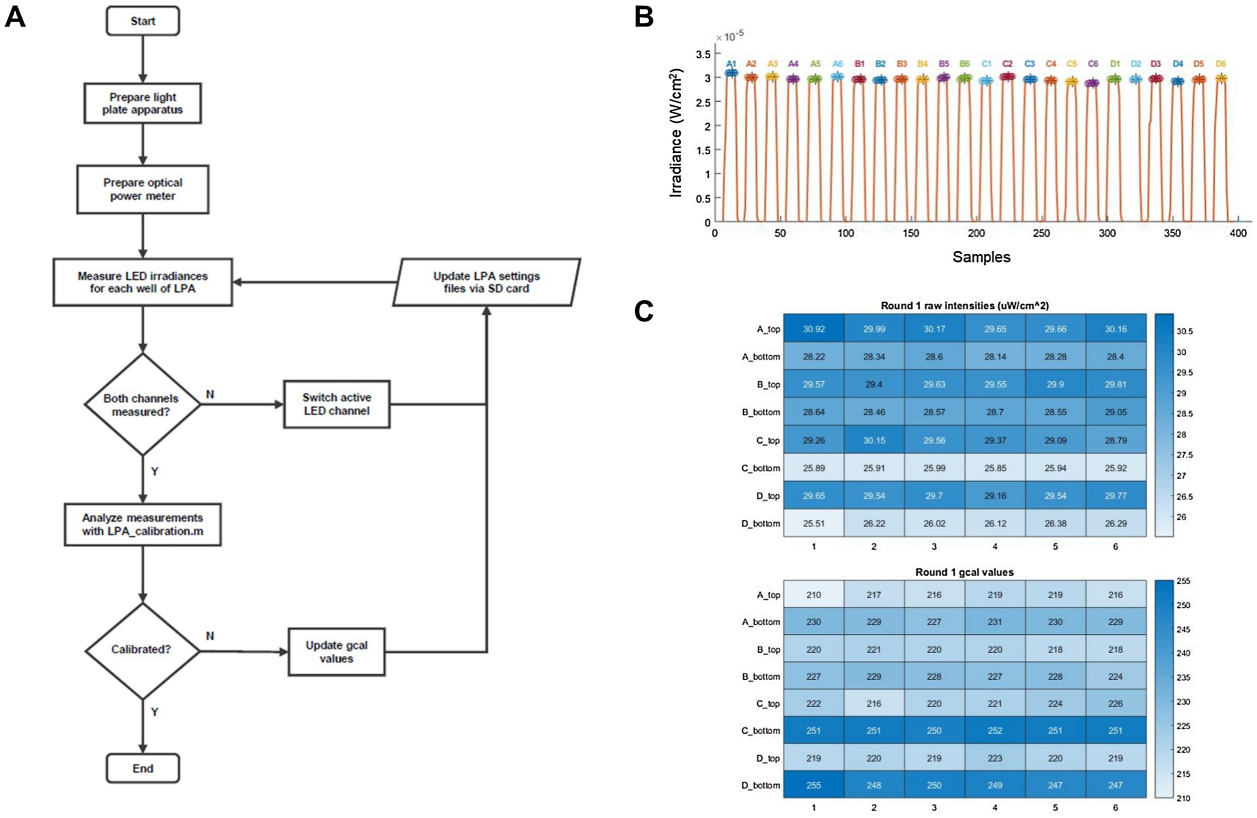

Figure 1. Calibration process for an LPA fitted with two blue LEDs per well.

(A) A flow chart detailing the steps of the calibration process. (B) Representative image of well irradiance measurements acquired in series as identified by "LPA_calibration.m". Well identifiers (*e.g. "A1")* are indicated. Each well was covered by on average 5 samples. We sampled at a rate of 1Hz so there is 1 second between each sample. The entire plate was measured in less than 400 seconds. (C) Representative well irradiance measurements and tuned gcal values per LED as calculated by "LPA_calibration.m".

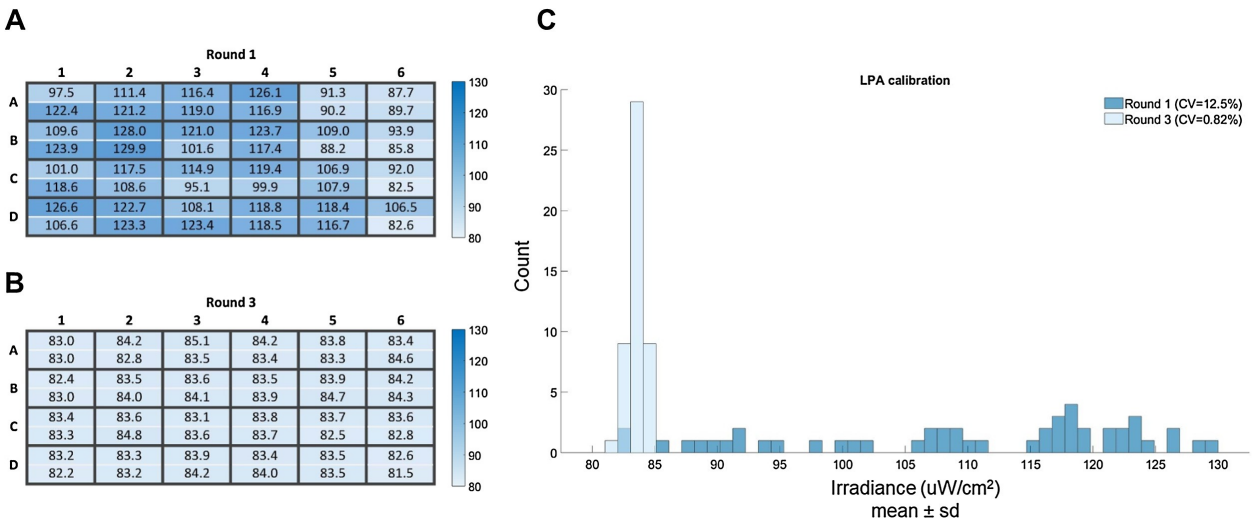

Figure 2. Representative results of an LPA calibration. Each well has two blue LEDs.

(A) Heatmap of the irradiance measurements for each LED prior to round one of calibration showing the uneven distributions of LED irradiances in an uncalibrated LPA. The CV of the LED irradiances is 12.5% before calibration. (B) Heatmap of the irradiance measurements for each LED on the same LPA after three rounds of calibration. The CV of the LED irradiances is 0.82% after calibration. (C) Histogram depicting the data represented in the heatmaps of this figure. The values across the calibrated LPA have converged to the dimmest LED.

Figure 3

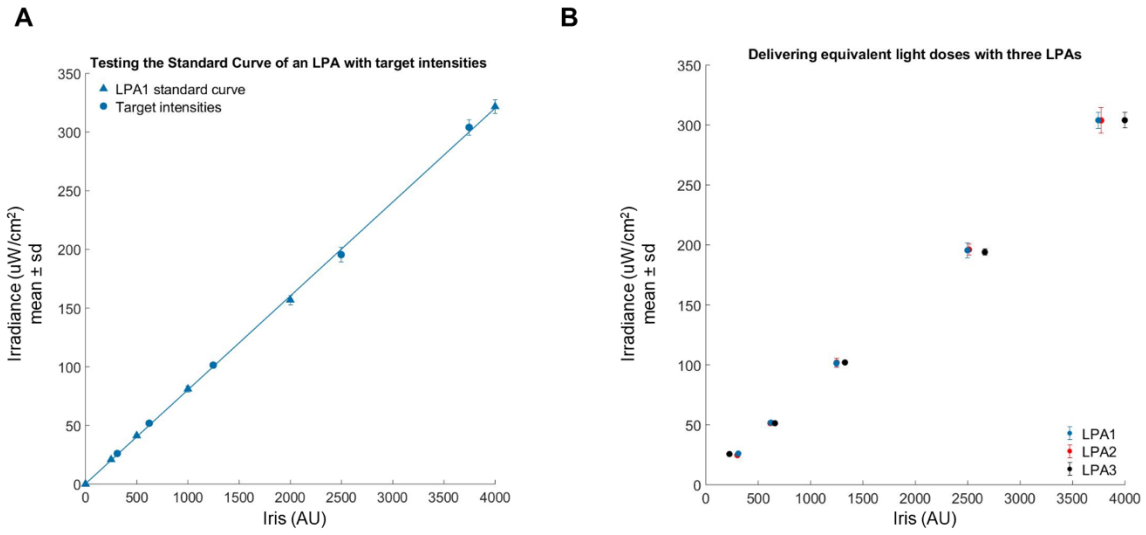

Figure 3. A standard curve and measurements relating Iris values to irradiance.

All plot markers represent the mean and standard deviation of a set of eight measurements. (A) A standard curve generated from a set of measurements across the programmable range of Iris values (triangular markers). Predicted Iris values for specific target irradiances were then programmed and the actual irradiance measured (circular markers). (B) Target irradiances for three different LPAs are shown (circular markers). The measurements between LPAs at the target irradiances all cluster closely and are within 3% of their respective targets.

Figure 4

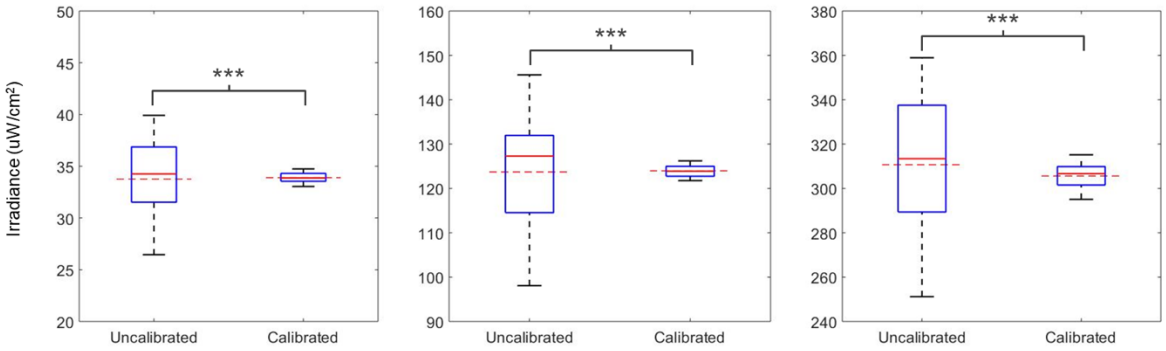

Figure 4.Irradiance measurements from an LPA before and after calibration.

We set all the LEDs of an uncalibrated LPA to a constant Iris value and measured the irradiance of each well. We then calibrated the LPA and assigned all wells a constant Iris value such that the mean irradiance output by the calibrated LPA approximately matched that of the uncalibrated LPA (Fig. 4A) and measured the irradiance of each well. We did this at three light doses and each time observed significantly reduced irradiance variability (asterisks indicate $p<0.001$ as calculated by Levene's test for equality of variances). The dashed red lines depict the average irradiance across the whole LPA for each condition.

Figure 5

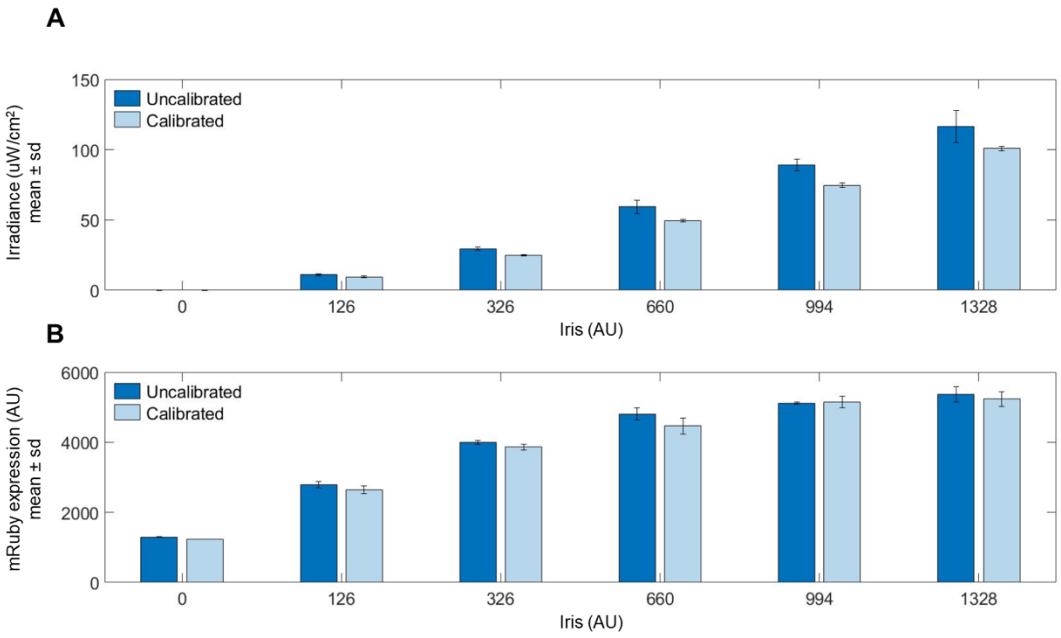

Figure 5. Light-induced mRuby expression.

Light-induced mRuby expression in yeast grown on a calibrated and uncalibrated LPA set to deliver a range of light doses. Each bar represents the mean of four replicates. The Iris values listed denote the Iris value used for both the top and bottom LED of each well for each plate column. (A) Mean irradiance for each column of the uncalibrated and calibrated LPA plates. Irradiance is consistently higher and more variable for the uncalibrated LPA (B) Reporter gene expression is consistently higher on the uncalibrated LPA.

Chapter 3: Optogenetic tools for public goods control in *Saccharomyces cerevisiae*

This chapter was previously published here:

N. Moreno Morales, M. T. Patel, C. J. Stewart, K. Sweeney, and M. N. McClean, "Optogenetic Tools for Control of Public Goods in Saccharomyces cerevisiae," *mSphere*, vol. 6, no. 4, pp. e00581-21, doi: 10.1128/mSphere.00581-21.

N.M.M., C.S., and M. P. designed experiments and performed experiments. N.M.M., C.S., and M.P. performed molecular cloning and strain construction. K.S. wrote image analysis software. N.M.M. and M.N.M. analyzed data and wrote the paper. N.M.M., C.S., M.P., K.S. and M.N.M. edited and approved the manuscript. M.N.M. supervised the project.

Abstract

Microorganisms live in dense and diverse communities, with interactions between cells guiding community development and phenotype. The ability to perturb specific intercellular interactions in space and time provides a powerful route to determining the critical interactions and design rules for microbial communities. Approaches using optogenetic tools to modulate these interactions offer promise, as light can be exquisitely controlled in space and time. We report new plasmids for rapid integration of an optogenetic system into *Saccharomyces cerevisiae* to engineer light-control of expression of a gene of interest. In a proof-of-principle study, we demonstrate the ability to control a model cooperative interaction, namely the expression of the enzyme invertase (SUC2) which allows *S. cerevisiae* to hydrolyze sucrose and utilize it as a carbon source. We demonstrate that the strength of this cooperative interaction can be tuned in space and time by modulating light intensity and through spatial control of illumination. Spatial control of light allows cooperators and cheaters to be spatially segregated, and we show that the interplay between cooperative and inhibitory interactions in space can lead to pattern formation. Our strategy can be applied to achieve spatiotemporal control of expression of a gene of interest in *Saccharomyces cerevisiae* to perturb both intercellular and interspecies interactions.

Importance

Recent advances in microbial ecology have highlighted the importance of intercellular interactions in controlling the development, composition and resilience of microbial communities. In order to better understand the role of these interactions in governing community development it is critical to be able to alter them in a controlled manner. Optogenetically-controlled interactions offer advantages over static perturbations or chemically-controlled interactions as light can be manipulated in space and time and doesn't require the addition of nutrients or antibiotics. Here we report a system for rapidly achieving light-control of a gene of interest in the important model organism *Saccharomyces cerevisiae* and demonstrate

that by controlling expression of the enzyme invertase we can control cooperative interactions. This approach will be useful for understanding intercellular and interspecies interactions in natural and synthetic microbial consortia containing *Saccharomyces cerevisiae* and serves as a proof-of-principle for implementing this approach in other consortia.

Introduction

Interactions between individual cells and species dictate the development and phenotype of microbial communities[1]–[3]. These interactions are regulated in time and space, and often arise due to the different metabolic capabilities of specific cells and species [4], [5]. Cooperative interactions are common, and cooperativity is often characterized by the presence of a shared public good which is produced by cooperative cells (producers) and freely available to other cells [3], [6], [7]. Production of the public good is often costly, and cooperative interactions are susceptible to the presence of "cheaters", cells which exploit the public good without providing any contribution of their own[8].

The budding yeast *Saccharomyces cerevisiae* engages in a cooperative interaction by secreting invertase, an enzyme which catalyzes the hydrolysis of sucrose into glucose and fructose. Due to its long domestication history and early enzymatic research on invertase [9]–[11], invertase secretion by *S. cerevisiae* has long been used as a model system for studying public goods interactions and the emergence of cooperation in microbial communities. The *S. cerevisiae* genome contains several unlinked loci encoding invertase (SUC1-SUC8) [12], [13] but all except SUC2 are located within telomere sequences [14]. The strain used in this study (S288C) encodes only one functional invertase enzyme, SUC2 [12], [15]. There is a constitutively expressed intracellular form of invertase, but the secreted, glycosylated form which is regulated by glucose repression and important for cooperativity is secreted into the periplasmic space [16]. Most invertase (95%) remains in the cell wall; nevertheless, yeast capture only a small fraction of the sugars that sucrose hydrolysis releases with most of the glucose and fructose diffusing away to be

utilized by other cells [17]–[19]. Hence the sugars produced from sucrose hydrolysis represent a "public good". Invertase is costly to produce, and producing populations are susceptible to invasion by cheaters [17], [20].

There is growing evidence from both experiments and simulations that when and where a public good is produced within a microbial community can have dramatic consequences for community stability and the maintenance of cooperativity [21]–[27]. The spatial arrangement of genotypes within microbial communities can influence whether or not producers sufficiently benefit from the production of public goods, or whether cheaters are able to invade and take-over the community [3], [26], [28–30]. Indeed, efficient use of public goods has been identified as a possible driver for the evolution of multicellularity [31]. Furthermore, the dynamic control of public goods in both space and time could be used to manipulate synthetic consortia for applications in bioproduction and biotechnology [32], [33]. Yet few tools exist for spatiotemporal control of specific community interactions.

Optogenetic tools offer the potential to overcome this limitation by utilizing genetically encoded light-sensitive proteins to actuate processes within the cell in a light-dependent manner. Light is a powerful actuator as it is inexpensive, easily controlled in time and space, and *S. cerevisiae* contains no known native photoreceptors [34]. Light can be rapidly added and removed from cell cultures or spatially targeted [35–38], meaning it can be used to study how regulation of microbial interactions determines microbial community development [39–41]. We report here the development of an optogenetic tool that allows the expression of a specific metabolic enzyme of interest to be put under light control in *S. cerevisiae*. Using this system, we demonstrate that we can use light to control when and where invertase is expressed within well-mixed and spatially organized populations of *S. cerevisiae.* Light control of this cooperative interaction shows that invertase expression in a community of yeast has important effects on overall community growth and spatial structure. Our results suggest that optogenetic control of microbial interactions is an important new approach to understanding and engineering microbial communities.

Results

Plasmid Design and System Overview

To enable light-based control of cooperativity we first developed constructs that, when integrated into yeast, allow us to make expression of a specific gene light-inducible. We generated an integrable cassette containing the essential components of a blue-light reconstituted transcription factor. We chose to use a split transcription factor consisting of a DNA-binding domain fused to the naturally occurring *Arabidopsis* cryptochrome CRY2 photolyase domain (DBD-CRY2PHR) and the CIB1 protein fused to the VP16 activation domain (VP16-CIB1). In response to blue-light CRY2 undergoes a conformational change that allows it to bind CIB1, which recruits the VP16 activation domain to a promoter of interest containing binding sites for the selected DNA-binding domain (DBD) driving gene expression. We chose the DNA-binding domain of the Zif268 transcription factor (ZDBD), which is known to bind a 9-bp site (GCGTGGGCG) that has only 11 predicted binding sites in the *S. cerevisiae* genome [42]. Studies using the ZDBD on an estradiol inducible transcription factor have shown that artificial transcriptional activators using this DNA-binding domain in *S. cerevisiae* generate very little off-target gene expression activity [42,43]. When the Zif268 DNA-binding domain is fused to CRY2PHR, the resulting ZDBD-CRY2PHR/VP16-CIB1 transcription factor controls the expression of yeast genes under a pZF(BS) promoter containing GCGTGGGCG binding sites (BS) in a blue-light dependent manner [43].

Stable integration of the ZDBD-CRY2PHR/VP16-CIB1 transcription factor is a more promising approach than maintenance of the optogenetic components on episomal plasmids, as expression from plasmids is known to be noisy and requires constant selection [44]. In order to integrate the ZDBD-CRY2PHR/VP16-CIB1 optogenetic machinery without loss of a marker, we used the heterologous URA3 from *Kluyveromyces lactis* (KlURA3) flanked by two direct repeats of the loxP sequence to allow for Cre recombinase mediated marker excision [45]. The components were cloned as indicated in **Figure 1A** using

standard cloning techniques as described in the Methods. Homology arms on either side of the cassette allow for rapid integration at the HO locus, which is not required for growth and does not have an effect on growth rate [46], [47]. We also included spacer DNA of approximately the same length (1.4 kb) as KIURA3 (1.5 kb) as indicated in **Figure 1A** based on initial tests of the scheme which indicated that the spacing between the two open reading frames encoding the split transcription factor is important for optimal function of the optogenetic system (**Supplemental Figure 1**).

Integration of the ZDBD-CRY2PHR/VP16-CIB1 machinery at HO enables light dependent expression from the pZF(3BS) promoter in cultures grown in liquid and on solid media (**Figure 1B, Supplemental Figure 2**). Excision of the KIURA3 marker still results in some attenuation of gene expression in the marker-recycled strain (**Figure 1B**). We hypothesize that this is due to repression of ZDBD-CRY2PHR expression by the strongly expressed upstream VP16-CIB1 gene (**Figure 1A**). This could be due to terminator-promoter interactions as previously reported [48], [49]. Previous work has shown that the ratio of CRY2PHR to CIB1 in the split transcription factor is important for maximal gene expression [43] and it is possible that removing the KlURA3 marker changes the ratio to be slightly less favorable. We note that using higher light intensities (**Supplemental Figure 3A**) increases gene expression and that significant expression does not require a multi-copy reporter plasmid (**Supplemental Figure 3B**). In subsequent experiments, the reduced expression due to excision of the KIURA3 marker did not cause difficulties but we note that if maximal gene expression is required, constructs designed to optimize the dosage of VP16-CIB1 and ZDBD-CRY2PHR have been described [43].

To allow specific genes in the yeast genome to be optogenetically controlled, we designed a cassette containing a pZF(BS) promoter (5'->3') and the KanMX cassette (3'->5') (**Supplemental Figure 4A**), which confers resistance to the antibiotic G418 [50]. Replacing an endogenous promoter with this cassette in a strain containing the ZDBD-CRY2PHR/VP16-CIB1 split transcription factor puts expression of the gene of interest under blue-light control. We verified that in the dark, replacement of the native promoter with

pZF(BS) effectively generates a deletion. Replacement of the HIS3 promoter with this cassette generates a histidine auxotroph (*his3*-) in the dark and the ability to grow without histidine is recovered when grown in blue light in the presence of the ZDBD-CRY2PHR/VP16-CIB1 split transcription factor (**Supplemental Figure 5A**). Gene expression from this promoter is rapid (7-fold gene expression in 2 hours) as assessed by pZF(BS)-yEVENUS (**Supplemental Figure 4B**). In combination, the cassettes containing an integrable light-responsive split transcription factor (ZDBD-CRY2PHR/VP16-CIB1) and a drug-selectable promoter cassette (KanMX4-pZF(BS)) allow expression of a gene of interest to be put under light control in a variety of *S. cerevisiae* strains.

Creation of a Light-inducible Invertase *S. cerevisiae* Strain

We decided to take advantage of the well-understood invertase public goods system in budding yeast to generate yeast strains where cooperative intercellular interactions could be controlled by light (**Figure 2A**). In a yeast strain with the ZDBD-CRY2PHR/VP16-CIB1 optogenetic system stably integrated at HO we replaced the SUC2 promoter with pZF(3BS) (using the KanMX-pZF(3BS) cassette). Lawns of strains plated on YP-Sucrose were able to grow in blue-light, but not in the dark (**Supplemental Figure 5B**) indicating that these strains induced SUC2 in a light-dependent manner, allowing the cells to produce invertase and utilize sucrose.

We further tested the ability of this strain to recover growth on YP-Sucrose in liquid cultures exposed to blue-light. We grew cultures over a range of light intensities (0 $\mu W/cm^2$-14 X 10^2 $\mu W/cm^2$) and measured optical density after 24 and 48 hours of growth (**Figure 2B,C**) . The parent strain (SUC2) quickly saturated at both 24 and 48 hours. In contrast, the pZF-SUC2 strain showed very little growth after both 24 and 48 hours of growth in the dark. Increasing intensity of blue light led to saturating optical densities at both 24 and 48 hours. Interestingly, at high light intensities (>4 $\mu W/cm^2$) we reproducibly observed that pZF-SUC2

cultures reached a higher density than the wild-type pSUC2-SUC2 parent strain (yMM1146). It is possible that by decoupling production of invertase from the native regulation, the light-inducible strains overproduced invertase and are hence able to access more carbon from the sucrose. At low intensities of light (**Figure 2B,** 0.110 μW/cm^2 and 0.680 μW/cm^2) the culture did not show significant growth at 24 hours but by 48 hours was able to reach a wild-type level of saturation. This could be due to the known Allee effect [51], [52], [52]–[54] (density-dependent growth) caused by the cooperative metabolism of sucrose by secreted invertase. At low intensities of light, low invertase production and secretion slows sucrose hydrolysis and population growth, delaying the point (relative to higher light intensity cultures) at which the population reaches a density that supports maximal growth rate.

We further tested the induction dynamics of our light-inducible strain over a several day growth experiment (**Figure 3**). The wild-type SUC2 strain quickly saturated after 20 hours of growth while the pZF-SUC2 strain had a delayed lag period, relative to the wild-type strain, which we interpret in light of the data in **Figure 2B** as needed time to accumulate invertase and glucose in the media after light induction. Subsequent to initiation of growth, the pZF-SUC2 strain showed very similar growth kinetics to the wild-type strain and quickly reached saturation. Again, the pZF-SUC2 reached a higher density than the wild-type strain at saturation, as we previously observed (**Figure 3**). Interestingly, the pZF-SUC2 strain also showed some growth in the dark, albeit after an extremely delayed lag period. We know from previous studies [43] that the pZF promoter is not absolutely silent, and therefore we interpret this growth as being due to an extremely slow accumulation of functional invertase and hexose due to leakiness from the pZF promoter. We confirmed that our sampling method did not inadvertently expose cultures to unwanted light by demonstrating that the final densities of our time course samples did not show any significant difference relative to untouched endpoint samples (**Supplemental Figure 6**).

Light Patterning Allows for Spatial Control of Producer Populations

The experiments described above demonstrate that we can control invertase production, and therefore cooperativity, with blue light. However, these experiments were all done in well mixed populations, while microbial communities are generally highly structured 2D- or 3D-environments. Therefore, we wanted to test our ability to spatially control cooperativity in populations of *S. cerevisiae*.

Localized illumination of a regular grid of pZF-SUC2 strains arrayed onto an agar pad demonstrated that a small, spatially localized group of cooperators (**Supplemental Figure 7A**) can support growth of a much larger number of cheaters in two-dimensional environments. This is expected due to diffusion of hexose. While the invertase enzyme is anchored to the plasma membrane, the fructose and glucose converted by the enzyme is free to diffuse and a relatively small fraction is captured by the cell that makes it[17]. To further validate this technique, we generated plates containing a lawn of pZF-SUC2 cells and illuminated a spot through a 6 mm pinhole (**Figure 4A)**. We found that after 4 days, the growth of very few cheaters was supported, with the majority of growth visible within the illuminated region. However, after 7 days of illumination, the cooperating cells supported a large growth of cheaters presumably because they were continuing to produce invertase and hydrolyze sucrose to hexose and the majority of hexose diffuses away from the illuminated cells (*i.e.* the producers).

Spatial Patterning Due to Spatial Segregation of Cooperators and Nutrient Competition

In our pinhole experiment, we noticed a subtle ring effect (**Figure 4B,** Day 7), where the illuminated cooperators (at the center) grew well, surrounded by a ring of lesser growth, and finally more dense growth of cheaters at the periphery of the entire colony. This kind of ring-like pattern formation is predicted in reaction-diffusion systems where an activator and an inhibitor diffuse from a central source on different timescales[55–58]. In our system, the central cooperators are activating the growth of cheaters by producing hexose while simultaneously inhibiting the growth of cheaters by serving as a sink for other

limiting growth factors (*i.e.,* nutrients) [55]–[57]. Cheaters growing near the initially faster growing cooperators have access to hexose but are deprived of other nutrients, while cheaters at the periphery have more access to the limiting nutrient in the plate and eventually have access to hexose diffusing from the central cooperators, and therefore grow to a higher density.

In order to explore this observation more fully, we used auxotrophic strains to allow control of a limiting nutrient on the plates. Our wild-type pSUC2-SUC2 and opto-control pZF-SUC2 strains are leu2 auxotrophs allowing us to control leucine amino acid concentration in the plates to limit a nutrient. As a control, we generated a constitutive suc2Δ leu2Δ cheater strain. We spotted suc2Δ leu2Δ cheaters, pZF-SUC2, or pSUC2-SUC2 cells onto lawns of suc2Δ leu2Δ cheaters. Leucine concentrations in the plates were chosen to be 100% (0.1 mg/ml) or 50% (0.05 mg/ml) of the amount used in standard synthetic media [59]. As expected, spotting suc2Δ leu2Δ cheaters onto a lawn of suc2Δ leu2Δ cheaters does not allow for any growth in either light or dark **(Figure 5A)**. In contrast, both pZF-SUC2 or wild-type pSUC2-SUC2 cells spotted onto cheaters and grown in blue light allows for clear growth of the cooperators (either pZF-SUC2 or wild-type) surrounded by a zone where growth of the suc2Δ leu2Δ cheaters is inhibited and a larger ring of dense cheater growth **(Figure 5A, B)**. The growth inhibition zone is larger for wild-type cooperators than pZF-SUC2 cooperators **(Figure 5B, Supplemental Figure 7B, 8)**. We interpret this to be due to more rapid induction of invertase and glucose production in the wild-type strains which allows the wild-type strain to more quickly reach a high density of cooperators allowing further cooperator growth (as also seen in **Figure 3**), and greater utilization and depletion of leucine. That leucine is the limiting nutrient is evidenced by lesser growth in both the wild-type and pZF-SUC2 strains at 50% leucine than at 100% leucine **(Supplemental Figure 7B, 8)**.

Discussion

This study develops and demonstrates the use of an optogenetic tool to control cooperation in a yeast microbial community. By making expression of invertase (encoded by the SUC2 gene) light-controllable we demonstrate temporal and spatial control of public goods production. We show that the timing of invertase expression is important, and delays in expression can significantly slow community growth. In addition, we show that localized cooperation can generate distinct patterning of cooperators and cheaters. Despite frequent investigation of *S. cerevisiae* invertase secretion as a model cooperative community, most models approximate invertase production as constant in time and space despite known native regulation in response to external factors such as nutrient concentration [60], [61]. Optogenetic control of invertase will allow for further dissection of how regulation of this enzyme in space and time allows cooperators to coexist and compete with cheaters. While we have focused on the control of an intercellular interaction, the optogenetic constructs and strains generated in this study can be immediately used by other researchers to put any gene of interest under the control of blue light in *Saccharomyces cerevisiae.* The optogenetic system is orthogonal to native regulatory systems [43] and could be easily modified to utilize additional markers or CRISPR technology for integration into a variety of yeast strains or species.

More generally, this study suggests that optogenetics will be a powerful tool for understanding how spatiotemporal regulation of cooperation, and other interactions, control microbial community structure and phenotype. Interactions in microbial communities are mediated by diffusible compounds, and numerous studies indicate that short-range interactions on the micron to millimeter scale are important for controlling community structure and phenotype [62]–[64]. Yet controlling the spatial arrangement of microbes on these length scales can be challenging. Microfluidic devices allow spatial segregation of microbes at different length scales but require sophisticated engineering and specialized equipment [65]–[68]. In addition, it is more challenging to define three-dimensional structure using a microfluidic device

and collection of the community for subsequent downstream analysis (*e.g.,* gene expression) can be difficult. Bioprinting is a burgeoning technique which holds promise for building complex, three-dimensional microbial communities with defined spatial structure [65], [69]–[71]. However, bioprinting does not easily allow intercellular and interspecies interactions to be modulated in time. Optogenetics has the potential to be integrated with or to supersede these existing technologies for fine spatiotemporal control of community interactions. Scanning and parallel light-targeting methods can be combined with one and multi-photon excitation to precisely localize light in both two and three dimensions as well as in time. In addition, existing illumination techniques can be combined with amenable animal models, such as *C. elegans* [72], to allow unprecedented *in vivo* dissection of the importance of intercellular interactions and their regulation in the establishment and phenotype of microbial communities. To extend the techniques described in this article to mixed-kingdom communities, optogenetic systems developed for bacteria [80], [81] could be utilized. Indeed, in *Sinorhizobium meliloti*, a nitrogen fixing soil bacterium, the blue-light sensitive transcription factor EL222 was recently used to control production of the public good exopolysaccharide enabling manipulation of biofilm formation [41]. Hybrid optochemical approaches also hold promise for repurposing existing inducible systems, as a recent study showed that photocaged IPTG could be used to control coculture interactions in the bacterium *Corynebacterium glutamicum* [39].

Finally, in addition to providing a path towards understanding how intercellular interactions regulate naturally occurring microbial communities, optogenetic tools have important implications for engineering synthetic microbial consortia. Engineered consortia are of great interest in biotechnology because they can perform more complicated functions than single-species or single-strain communities [73]. However, maintaining the appropriate ratio of different consortia members represents a challenge and would benefit from dynamic control modalities. Control mechanisms for cocultures via interspecies interactions (such as quorum sensing and metabolite exchange) have been described [74]–[76] and dynamic control of these interactions using optogenetics and predictive control strategies [36], [77] could enable

community maintenance and optimization. Similar optogenetic approaches in monocultures have already enabled significant gains in bioproduction [35], [78], [79]. In addition, the spatial control provided by light could allow the formation of sophisticated living biomaterials. Co-cultures of *Saccharomyces cerevisiae* and the cellulose-producing *Komagataeibacter rhaeticus* bacteria are mediated by yeast invertase production and capable of producing functionalized cellulose biomaterials. Optogenetic control of *Saccharomyces cerevisiae* invertase production could allow for sophisticated control of these living materials as well as patterning, as demonstrated in this work for the simple case of localized producers. In addition, as demonstrated by the grid experiment (**Supplemental Figure 77A**) a small number of producers can support a much larger population, indicating that in living materials it may be possible to have a relatively small population responsible for the metabolic burden of consortia growth while other members can focus on additional functionality.

Materials and Methods

Yeast Strains and Culture Methods

Yeast strains used in this study are shown in **Supplemental Table S1**. Yeast transformation was accomplished using standard lithium-acetate transformation [82]. For integrating plasmids, the integration was validated using either colony PCR or, when colony PCR proved difficult, by PCR of genomic DNA. Genomic DNA was extracted using the Bust n' Grab protocol [83]. Primers used for validating integrations are listed in **Supplemental Table 2**. All transformants were checked for the petite phenotype by growth on YEP-glycerol (1% w/v Bacto-yeast extract-BD Biosciences 212750, 2% w/v Bacto-peptone-BD Biosciences 211677, 3% [v/v] glycerol-Fisher Bioreagents BP229-1, 2% w/v Bacto-agar-BD Biosciences #214030)[22]. Only strains deemed respiration competent by growth on YEP-glycerol were used for subsequent analysis. Details of individual strain construction are described in the **Supplemental Material**.

Yeast cultures were grown in either yeast peptone (YP) media (10 g/L Bacto yeast extract, 20g/L Bacto peptone for solid media + 20g/L of Bacto agar) or Synthetic Complete (SC) media (6.7 g/L Yeast Nitrogen Base without amino acids-DOT Scientific, 1% v/v KS amino acid supplement without appropriate amino acids). The carbon source supplied was either dextrose (D) or sucrose (SUC) at 2% v/v concentration. As needed, episomal plasmids were maintained by growing yeast in SC media lacking the appropriate amino acids required for plasmid selection. For light induction experiments followed by fluorescence assays (flow cytometry or microscopy) yeast were always grown in Synthetic Complete media [59].

Bacterial strains and growth media

Escherichia coli (E. coli) strain DH5α was used for all transformation and plasmid maintenance in this study. *E. coli* were made chemically competent following either the Inoue method [84] or using the Zymo Research Mix & Go! Protocol (Zymo Research T3002). *E. coli* were grown on LB agar (10% w/v Bacto-Tryptone, 5% w/v Bacto Yeast Extract, 5% w/v NaCl, 15% w/v Bacto Agar) or LB liquid media (10% w/v Bacto-Tryptone, 5% w/v Bacto Yeast Extract, 5% w/v NaCl). Appropriate antibiotics were used to select for and maintain plasmids. Antibiotic concentrations used in this study were as follows: LB+CARB agar 100 µg/mL carbenicillin, LB+CARB liquid media 50 µg/mL carbenicillin, 25 µg/ml chloramphenicol, 50µg/ml kanamycin. Plasmids were prepared using the Qiagen bacterial miniprep kit (Qiagen #27104).

Plasmid Construction

Construction of plasmids used throughout this study was accomplished using a combination of methods including Yeast Recombinational Cloning [85] and standard restriction enzyme based cloning. Details of individual plasmid construction are described in the **Supplemental Materials.**

Generation of optogenetic invertase strain

In order to make an integrable version of the SV40NLS-VP16-CIB1 loxP-KlURA3-loxP SV40NLS-ZIF268DBDCRY2PHR cassette, this cassette was cut from pMM364 using XbaI/PacI and ligated into

pMM327. This plasmid was linearized using AatII and transformed into yMM1146 (Matα trp1Δ63 leu2Δ1 ura3-52) to generate yMM1367 (Matα trp1Δ63 leu2Δ1 ura3-52 HO::SV40NLS-VP16-CIB1 loxP-KlURA3-loxP SV40NLS-Zif268DBD-CRY2PHR). The KIURA3 marker was excised from this strain using Cre-mediated recombination as described below to generate yMM1390 (Matα trp1Δ63 leu2Δ1 ura3-52 HO::SV40NLS-VP16-CIB1 loxP SV40NLS-Zif268DBD-CRY2PHR). In order to make the expression of invertase light-inducible, the pZF(3BS) promoter replaced the native pSUC2 promoter by amplifying KanMX-rev-pZF(3BS) with oMM768/769 from pMM353, transforming yMM1390 and selecting for G418 resistant colonies. These colonies were further checked by colony PCR and sequencing and for the inability to grow on YP-Sucrose in the dark and became strain yMM1406.

Recycling of loxP-flanked markers

The Cre-loxP system was used to recycle the KIURA3 marker flanked by loxP recombination sites (loxP-KIURA3-loxP). Cre-mediated recombination was accomplished by adapting the CRE recombinase-mediated excision protocol from Carter and Delneri (2010) [86]. The strain yMM1367 (Matα trp1Δ63 leu2Δ1 ura3-52 HO::SV40NLS-VP16-CIB1 loxP-KlURA3-loxP SV40NLS-Zif268DBD-CRY2PHR) was transformed with 0.25-0.5µg of pMM296 (pSH65, pGAL1-CRE $Bleo^R$). These transformants were plated onto YPD and then replica plated onto selective media (YPD +10µg/ml phleomycin (InvivoGen)) after overnight growth. To express CRE and induce recombination phleomycin resistant colonies were selected and grown overnight in 3ml of YP-Raffinose (1% w/v yeast extract (BD Biosciences), 2% w/v Bacto-peptone (BD Biosciences), and 2% w/v raffinose (Becton Dickinson 217410)). The following day, cells were harvested by centrifuging at 3750 rpm for 5 minutes, washed in sterile miliQ water, and resuspended in 10ml of YP-Galactose (1% w/v yeast extract (BD Biosciences), 2% w/v Bacto-peptone (BD Biosciences), 2% w/v galactose (BD Biosciences 216310)) at an OD_{600} of 0.3. These cultures were incubated at 30°C with shaking for 2-3 hours. This culture was then diluted and plated on YPD and then replica plated onto SC-

5FOA (25% w/v g Bacto-Agar, 6.72% w/v YNB, 1% v/v mL 20x KS supplement without URA, 2% v/v glucose, 10 mL 5-Fluoroorotic Acid (Zymo Research), 50 mg uracil (MP Biomedicals 103204). 5FOA resistant colonies were checked for excision of the KIURA3 marker using colony PCR. Transformants with KlURA3 excised were grown in liquid YPD to saturation twice and then plated on YPD for ~100 colonies per plate. These were replica plated onto YPD + 10µg/ml phleomycin. Phleomycin sensitive colonies (colonies that had lost the plasmid pMM296) were reconfirmed by colony PCR to have loxed out KlURA3. This generated yMM1390 (Matα trp1Δ63 leu2Δ1 ura3-52 HO::SV40NLS-VP16-CIB1 loxP SV40NLS-Zif268DBD-CRY2PHR).

Blue light induction of yeast cultures in liquid media

For blue light induction experiments in liquid media light was applied in one of three ways: 1) Peripheral Illumination: Cultures were grown in glass culture tubes on the outside lane of a roller drum at room temperature. Control (dark) samples were put in test tubes wrapped in foil on the inner lane of the roller drum. Three LEDs outputting 460nm blue light (Sparkfun #COM-08718) were placed at the three, nine, and twelve o'clock positions of the roller drum and turned on at T=0 (~3000 µW/cm^2 at the LED; ~25 μW/cm^2 at the sample) as described previously [35], [43]. 2) Bottom Illumination: Cultures growing in glass tubes in a roller drum were directly illuminated from the bottom of the glass culture tube by LEDs mounted into the roller drum. The circuit was composed of three LEDs per tube (Sparkfun, #COM-09662), resistors of varying strength (Sparkfun, #COM-10969) and a 12 V power supply (LED supply, #12V-WM-xxA). 3) Light Plate Apparatus: Cultures were grown in 24 well plates (Arctic White, #AWLS-303008) and placed on a Light Plate Apparatus (LPA) [87]. The Light Plate Apparatus (LPA) is a published optogenetic tool which provides programmed illumination to each well of a 24-well plate. We assembled our LPA as described in [87] and calibrated as previously described [88], [89].

For all illumination methods, response was assessed by flow (traditional or imaging) cytometry as described below or measurement of optical density. The light output of all light sources was measured

and validated with a standard photodiode power sensor (Thorlabs, #S120VC) and power meter (Thorlabs, #PM100D) as previously described [43], [88], [89].

Blue light induction of drug resistance or restoration of histidine auxotrophy

To assess blue-light induction of drug resistance from a pZF(3BS)-NatMX plasmid, strain yMM1355 (Matα trp1Δ63 leu2Δ1 ura3-52 HO::GAL4AD-CIB1 loxP-KLURA3-loxP FLAG(3X)-SV40NLS- Zif268DBD -CRYPHR) was transformed with the pZF(3BS)-NatMX plasmid (pMM369) or an empty vector control (pMM6). Growth was assessed in the presence of clonNat (nourseothricin, 50μg/ml, YPD plates) in either 450nm blue light (50 µW/cm^2) or the dark by frogging saturated cultures at 1:10 dilution series onto the appropriate plates and growing for 2 days at 30°C in either light or dark. To assess recovery of histidine auxotrophy, strain yMM1295 was transformed with appropriate combinations of pMM284 (ZDBD-CRY2), pMM159 (GAL4AD-CIB1), pMM6 (ø), and pMM7 (ø) and saturated overnight cultures were frogged at 1:10 dilutions onto either SC or SC-Leu-Trp-His. Plates were grown at 30°C under 460 nm blue light or in total darkness. All strains grew on fully supplemented SC in either the light or dark (data not shown). Results for SC-Leu-Trp-His with and without light are shown in **Supplemental Figure 5A.**

Growth in sucrose media at different blue light intensities

Biological replicates were picked from a single colony on a YPD plate and transferred to a glass culture tube containing 5 mls of YPD media and grown to saturation overnight in the dark. The saturated culture (1.5ml) was pelleted by centrifuge (Eppendorf, #EP5401000137), washed twice with sterile water and resuspended in sterile MilliQ water to wash out residual media. These concentrated cells were then diluted at 1:100 into 5mls of SC-Sucrose to OD_{600}~0.16 and placed in a roller drum with the corresponding light dose or wrapped in aluminum foil for the no light control. The cultures were allowed to grow for a

total of 48 hours with 100uL of sample taken every 24 hours in order to measure the OD600 of the culture using a spectrophotometer (Fisher Scientific,#14-385-445).

Time course of growth with light induction in sucrose media

A single yeast colony of yMM1406 and yMM1146 were inoculated into 5mls of YPD and grown overnight to saturation. Of these cultures, 1ml was pelleted and the pellet was washed three times with sterile water to wash out residual media. These cultures were then resuspended and diluted in SC-Sucrose media to an OD_{600} of 0.05. Each culture was divided into 12 wells of a 24-well plate (2ml of the diluted cultures) with a glass bead (Fisher Scientific, #11- 312B 4mm) to increase aeration and the plates were covered with a breathable sealing membrane (USA Scientific #9123-6100) to reduce evaporation. Three light doses were programmed into the LPA with the arbitrary IRIS units of 0, 250, and 500. These correspond to 0 $\mu W/cm^2$, 2.32 $\mu W/cm^2$, and 5.01 $\mu W/cm^2$, respectively. This resulted in a set of four wells for each strain at each light condition. Two of these wells were sampled at each timepoint, while two were left untouched until the final endpoint measurement to verify that intermediate manipulation of the plate did not inadvertently expose cultures to light. At each time point 100 µL of the culture was removed to measure the optical density of the culture, the sealing membrane was replaced, and the plate was returned to the incubator. Optical densities outside of the previously determined linear range of our spectrophotometer were diluted to be in the linear rang at a ratio of 1:10 or 1:100 as needed. The experiment runtime was 54 hours.

Blue light patterning

Patterning of yeast plates with blue light

Yeast strain yMM1406 (optogenetic producer) was inoculated into a 5mL test tube of YPD and grown overnight to saturation. The next day the culture was pelleted by microcentrifuge (Eppendorf,

#EP5401000137) at 3000G for 2 minutes, resuspended in sterile water to wash out residual media from the cell pellet, this process was repeated twice. The final OD600 of the yeast cells was measured at 0.119 using a spectrophotometer (Fisher Scientific, #14-385-445). 200 µL of the cell suspension was plated on YP-Sucrose plates and spread throughout the plate using glass beads (Fisher Scientific, #11- 312B 4mm). The plates were wrapped in sterile, construction paper photomasks with one, 6 mm hole placed at the center of the plate and aluminum foil backing to prevent light contamination and control plates of no photomask (full-light at ~57 µW/cm^2) or complete photomask (no-light). The plates were placed under a blue light LED array and allowed to grow at room temperature for a week (until growth appeared to stagnate). Pictures of the plates were taken on day 4 and day 7 with a 28mm, 12 megapixel camera (iPhone 7).

Frogger plate patterning

Yeast strain yMM1406 (optogenetic producer) was inoculated into a 5mL test tube of YP-D to grow overnight, the culture was set back to an OD600 of OD 0.219 and grown for a few hours until an OD600 of 0.538 was reached. The culture was pelleted in a microcentrifuge (Eppendorf, #EP5401000137) at 3000G for 2 minutes and washed 3x with sterile water to wash away residual media. The culture was diluted to an OD600 of 0.079 measured with a spectrophotometer (Fisher Scientific, #14-385-445) and a frogger tool (Dan-Kar corp, #MC48) was used to stamp a large culture plate (Corning, #431111) of YP-D agar, a photomask was placed over the bottom of the plate and only a small section of the plate (2 cm^2) was exposed to light at an intensity ~145 µW/cm^2 under a blue light LED array (HQRP New Square 12-inch Grow Light Blue LED 14W). The light source, and plate were placed in 30°C incubator. A lightbox (Amazon, #ME456 A4 LED Light Box) was used to illuminate the plate from the bottom and camera (gel box camera and hood) was used to image the plate on day 4.

Spot assay with blue light

Yeast strains yMM1146 (wildtype producer), yMM1456 (non-producer) and yMM1406 (optogenetic producer) were inoculated into a 5mL test tube of YP-D to grow overnight. Cells were pelleted using a microcentrifuge (Eppendorf, #EP5401000137) at 3000G for 2 minutes and washed with YP-Sucrose to remove residual media containing dextrose, this was repeated 3 times. All cultures were diluted to an OD600 of 0.04 measured with a spectrophotometer (Fisher Scientific,#14-385-445) before plating onto solid YP-Sucrose plates (Fisher Scientific, #BP94S01). Onto the lawns of suc2Δ leu2Δ cheaters growing on either 0.1mg/mL or 0.05mg/mL leucine we spotted 5µL of either suc2Δ leu2Δ cheaters, pZF-SUC2, or wild-type cells. Plates contained leucine concentrations of either 100% (0.1 mg/ml) or 50% (0.05 mg/ml) of the amount used in standard synthetic complete media [59]. All plates were spread with 150µL of the yMM1456 (suc2Δ leu2Δ) strain with glass beads (Fisher Scientific, #11- 312B 4mm), the beads were removed, and the plate allowed to dry for 10 minutes. Then, a 5µL drop of either yMM1146,1406, or 1456 was applied to the center of a petri dish and left face-up to dry for another 10 minutes. The plates were then placed upside down in a 30°C incubator in a single layer under a blue LED light source at an intensity 145 µW/cm^2 (HQRP New Square 12-inch Grow Light Blue LED 14W) for 7 days. On the seventh day the pictures were imaged with ChemiDoc imaging system (BioRad, #12003154) an exposure of 0.06 seconds in the brightfield setting and analyzed using an ImageJ plug-in Clockscan [90].

Quantification of Plate Growth

Radial intensity traces of patterned plates using Clockscan

The patterned plates were analyzed using a published ImageJ plug-in, Clock Scan [90] which outputs averaged radial intensity values for the image.

Identifying pattern features using custom MATLAB Script

We quantify the growth of yeast on a plate from images using a custom MATLAB script that examines intensity versus radius along angular slices through the center of the plate and identifies the bounds of

features such as valleys and rings. Because it's hard to accurately identify these features from individual angular slices or the single, composite intensity profile given by a clockscan [90], we use a bootstrap-based approach to repeatedly identify potential features from randomly selected sets of angular slices and select the most frequently identified potential features as true features.

This starts by roughly identifying the central yeast spot using MATLAB's circle finder and cropping the image around this spot. A polar transformation is then applied to the cropped image to create a polar image where each column of pixels corresponds to an angular slice through the plate. These angular slices are then sampled with replacement to construct a composite image. An intensity profile is generated from each composite image by taking the median intensity value at each radius. The intensity profile is filtered to remove noise and features are identified from the resulting signal. For example, potential valley bounds are identified as the locations where the derivative of the filtered intensity profile is at its maximum and minimum. This process is repeated for hundreds of composite images to create distributions of potential features. True features are then selected as the mode of these distributions. Using MATLAB's circle find to identify the outer edges of the plate, which we know to be 100 mm across, we then convert the feature measurements to physical units. Code is available upon request.

Flow Cytometry

Gene expression in response to blue light was assayed using fluorescent reporters and either traditional or imaging flow cytometry. Traditional flow cytometry was performed on a BD Biosciences LSR II Flow Cytometer (488nm laser and 505LP dichroic filter). The flow cytometry data was then analyzed using custom Matlab scripts. Imaging cytometry was done with the ImageStream MarkII and analysis completed using the IDEAS software or custom Matlab/ImageJ scripts modified from those described in [29].

All samples from culture tubes were prepared by diluting yeast cell culture (250-500µl) into 800µl of ice-cold PBS + 0.1% Tween-20. Samples were kept on ice or at 4°C until being analyzed. Samples from the Light Plate Apparatus (LPA) were taken by transferring 50µl of culture from each well of the LPA to a well a 96-well plate containing 150 µL of PBS+0.1% Tween-20. Samples run on the LPA were measured without sonication. Samples grown in glass culture tubes were sonicated with 10 bursts of 0.5 seconds each once diluted in PBS and prior to flow cytometry.

Acknowledgements

This work was financially supported by the National Institutes of Health [R35GM128873], the National Science Foundation [2045494] and a Lewis-Sigler Fellowship from Princeton University (M.N.M.). Flow cytometry was enabled by the University of Wisconsin Carbone Cancer Center Support Grant P30 CA014520 as well as the Princeton Flow Cytometry Resource Facility. Megan Nicole McClean, Ph.D holds a Career Award at the Scientific Interface from the Burroughs Wellcome Fund. Neydis Moreno Morales was supported by a short-term Genomic Sciences Training Program NHGRI Training Grant (5T32HG002760) and the Science and Medicine Graduate Research Scholars (SciMed GRS) program at the University of Wisconsin-Madison.

References

[1] R. M. Stubbendieck, C. Vargas-Bautista, and P. D. Straight, “Bacterial Communities: Interactions to Scale,” *Front. Microbiol.*, vol. 7, Aug. 2016, doi: 10.3389/fmicb.2016.01234.

[2] O. Ponomarova and K. R. Patil, “Metabolic interactions in microbial communities: untangling the Gordian knot,” *Curr. Opin. Microbiol.*, vol. 27, pp. 37–44, Oct. 2015, doi: 10.1016/j.mib.2015.06.014.

[3] C. D. Nadell, K. Drescher, and K. R. Foster, “Spatial structure, cooperation and competition in biofilms,” *Nat. Rev. Microbiol.*, vol. 14, no. 9, pp. 589–600, Sep. 2016, doi: 10.1038/nrmicro.2016.84.

[4] M. Gralka, R. Szabo, R. Stocker, and O. X. Cordero, “Trophic Interactions and the Drivers of Microbial Community Assembly,” *Curr. Biol. CB*, vol. 30, no. 19, pp. R1176–R1188, Oct. 2020, doi: 10.1016/j.cub.2020.08.007.

[5] J. Friedman and J. Gore, “Ecological systems biology: The dynamics of interacting populations,” *Curr. Opin. Syst. Biol.*, vol. 1, pp. 114–121, Feb. 2017, doi: 10.1016/j.coisb.2016.12.001.
[6] S. Germerodt *et al.*, “Pervasive Selection for Cooperative Cross-Feeding in Bacterial Communities,” *PLoS Comput. Biol.*, vol. 12, no. 6, p. e1004986, Jun. 2016, doi: 10.1371/journal.pcbi.1004986.
[7] S. Mitri and K. R. Foster, “The genotypic view of social interactions in microbial communities,” *Annu. Rev. Genet.*, vol. 47, pp. 247–273, 2013, doi: 10.1146/annurev-genet-111212-133307.
[8] P. Smith and M. Schuster, “Public goods and cheating in microbes,” *Curr. Biol. CB*, vol. 29, no. 11, pp. R442–R447, Jun. 2019, doi: 10.1016/j.cub.2019.03.001.
[9] J. A. Barnett, “A history of research on yeasts 2: Louis Pasteur and his contemporaries, 1850-1880,” *Yeast Chichester Engl.*, vol. 16, no. 8, pp. 755–771, Jun. 2000, doi: 10.1002/1097-0061(20000615)16:8<755::AID-YEA587>3.0.CO;2-4.
[10] A. J. Brown, “XXXVI.—Enzyme action,” *J. Chem. Soc. Trans.*, vol. 81, no. 0, pp. 373–388, Jan. 1902, doi: 10.1039/CT9028100373.
[11] L. Michaelis, M. L. Menten, K. A. Johnson, and R. S. Goody, “The original Michaelis constant: translation of the 1913 Michaelis-Menten paper,” *Biochemistry*, vol. 50, no. 39, pp. 8264–8269, Oct. 2011, doi: 10.1021/bi201284u.
[12] M. Carlson and D. Botstein, “Organization of the SUC gene family in Saccharomyces.,” *Mol. Cell. Biol.*, vol. 3, no. 3, pp. 351–359, Mar. 1983.
[13] G. I. Naumov and E. S. Naumova, “Comparative genetics of yeasts: A novel β-fructosidase gene SUC8 in Saccharomyces cerevisiae,” *Russ. J. Genet.*, vol. 46, no. 3, pp. 323–330, Mar. 2010, doi: 10.1134/S1022795410030099.
[14] M. Carlson, J. L. Celenza, and F. J. Eng, “Evolution of the dispersed SUC gene family of Saccharomyces by rearrangements of chromosome telomeres.,” *Mol. Cell. Biol.*, vol. 5, no. 11, pp. 2894–2902, Nov. 1985.
[15] M. Carlson, B. C. Osmond, and D. Botstein, “Mutants of yeast defective in sucrose utilization,” *Genetics*, vol. 98, no. 1, pp. 25–40, May 1981, doi: 10.1093/genetics/98.1.25.
[16] M. Carlson and D. Botstein, “Two differentially regulated mRNAs with different 5′ ends encode secreted and intracellular forms of yeast invertase,” *Cell*, vol. 28, no. 1, pp. 145–154, Jan. 1982, doi: 10.1016/0092-8674(82)90384-1.
[17] J. Gore, H. Youk, and A. van Oudenaarden, “Snowdrift game dynamics and facultative cheating in yeast,” *Nature*, vol. 459, no. 7244, Art. no. 7244, May 2009, doi: 10.1038/nature07921.
[18] P. C. Esmon, B. E. Esmon, I. E. Schauer, A. Taylor, and R. Schekman, “Structure, assembly, and secretion of octameric invertase,” *J. Biol. Chem.*, vol. 262, no. 9, pp. 4387–4394, Mar. 1987.
[19] M. Tammi, L. Ballou, A. Taylor, and C. E. Ballou, “Effect of glycosylation on yeast invertase oligomer stability,” *J. Biol. Chem.*, vol. 262, no. 9, pp. 4395–4401, Mar. 1987.
[20] D. Greig and M. Travisano, “The Prisoner’s Dilemma and polymorphism in yeast SUC genes.,” *Proc. R. Soc. B Biol. Sci.*, vol. 271, no. Suppl 3, pp. S25–S26, Feb. 2004.
[21] D. Misevic, A. Frénoy, D. Parsons, and F. Taddei, “Effects of public good properties on the evolution of cooperation,” presented at the Artificial Life, Jul. 2012, pp. 218–225. doi: 10.7551/978-0-262-31050-5-ch030.
[22] S. D. Allison, “Cheaters, diffusion and nutrients constrain decomposition by microbial enzymes in spatially structured environments,” *Ecol. Lett.*, vol. 8, no. 6, pp. 626–635, 2005, doi: 10.1111/j.1461-0248.2005.00756.x.
[23] R. Kümmerli, K. T. Schiessl, T. Waldvogel, K. McNeill, and M. Ackermann, “Habitat structure and the evolution of diffusible siderophores in bacteria,” *Ecol. Lett.*, vol. 17, no. 12, pp. 1536–1544, Dec. 2014, doi: 10.1111/ele.12371.

[24] R. Kümmerli, A. S. Griffin, S. A. West, A. Buckling, and F. Harrison, “Viscous medium promotes cooperation in the pathogenic bacterium Pseudomonas aeruginosa,” *Proc. R. Soc. B Biol. Sci.*, vol. 276, no. 1672, pp. 3531–3538, Oct. 2009, doi: 10.1098/rspb.2009.0861.
[25] T. Julou *et al.*, “Cell–cell contacts confine public goods diffusion inside Pseudomonas aeruginosa clonal microcolonies,” *Proc. Natl. Acad. Sci.*, vol. 110, no. 31, pp. 12577–12582, Jul. 2013, doi: 10.1073/pnas.1301428110.
[26] B. Momeni, A. J. Waite, and W. Shou, “Spatial self-organization favors heterotypic cooperation over cheating,” *eLife*, vol. 2, p. e00960, Nov. 2013, doi: 10.7554/eLife.00960.
[27] R. J. Lindsay, B. J. Pawlowska, and I. Gudelj, “When increasing population density can promote the evolution of metabolic cooperation,” *ISME J.*, vol. 12, no. 3, pp. 849–859, Mar. 2018, doi: 10.1038/s41396-017-0016-6.
[28] C. D. Nadell, K. R. Foster, and J. B. Xavier, “Emergence of Spatial Structure in Cell Groups and the Evolution of Cooperation,” *PLOS Comput. Biol.*, vol. 6, no. 3, p. e1000716, Mar. 2010, doi: 10.1371/journal.pcbi.1000716.
[29] Q. Su, A. Li, and L. Wang, “Spatial structure favors cooperative behavior in the snowdrift game with multiple interactive dynamics,” *Phys. Stat. Mech. Its Appl.*, vol. 468, no. C, pp. 299–306, 2017.
[30] H. J. Kim, J. Q. Boedicker, J. W. Choi, and R. F. Ismagilov, “Defined spatial structure stabilizes a synthetic multispecies bacterial community,” *Proc. Natl. Acad. Sci. U. S. A.*, vol. 105, no. 47, pp. 18188–18193, Nov. 2008, doi: 10.1073/pnas.0807935105.
[31] J. H. Koschwanez, K. R. Foster, and A. W. Murray, “Improved use of a public good selects for the evolution of undifferentiated multicellularity,” *eLife*, vol. 2, p. e00367, Apr. 2013, doi: 10.7554/eLife.00367.
[32] M. Cavaliere, S. Feng, O. S. Soyer, and J. I. Jiménez, “Cooperation in microbial communities and their biotechnological applications,” *Environ. Microbiol.*, vol. 19, no. 8, pp. 2949–2963, Aug. 2017, doi: 10.1111/1462-2920.13767.
[33] D. Rodríguez Amor and M. Dal Bello, “Bottom-Up Approaches to Synthetic Cooperation in Microbial Communities,” *Life Basel Switz.*, vol. 9, no. 1, p. 22, Feb. 2019, doi: 10.3390/life9010022.
[34] F. Salinas, V. Rojas, V. Delgado, E. Agosin, and L. F. Larrondo, “Optogenetic switches for light-controlled gene expression in yeast,” *Appl. Microbiol. Biotechnol.*, vol. 101, no. 7, pp. 2629–2640, Apr. 2017, doi: 10.1007/s00253-017-8178-8.
[35] J. Melendez, M. Patel, B. L. Oakes, P. Xu, P. Morton, and M. N. McClean, “Real-time optogenetic control of intracellular protein concentration in microbial cell cultures,” *Integr. Biol. Quant. Biosci. Nano Macro*, vol. 6, no. 3, pp. 366–372, Mar. 2014, doi: 10.1039/c3ib40102b.
[36] C. Carrasco-López, S. A. García-Echauri, T. Kichuk, and J. L. Avalos, “Optogenetics and biosensors set the stage for metabolic cybergenetics,” *Curr. Opin. Biotechnol.*, vol. 65, pp. 296–309, Oct. 2020, doi: 10.1016/j.copbio.2020.07.012.
[37] A. Milias-Argeitis *et al.*, “In silico feedback for in vivo regulation of a gene expression circuit,” *Nat. Biotechnol.*, vol. 29, no. 12, pp. 1114–1116, Nov. 2011, doi: 10.1038/nbt.2018.
[38] D. Figueroa, V. Rojas, A. Romero, L. F. Larrondo, and F. Salinas, “The rise and shine of yeast optogenetics,” *Yeast Chichester Engl.*, vol. 38, no. 2, pp. 131–146, Feb. 2021, doi: 10.1002/yea.3529.
[39] A. Burmeister *et al.*, “(Optochemical) Control of Synthetic Microbial Coculture Interactions on a Microcolony Level,” *ACS Synth. Biol.*, vol. 10, no. 6, pp. 1308–1319, Jun. 2021, doi: 10.1021/acssynbio.0c00382.
[40] Y. Huang, A. Xia, G. Yang, and F. Jin, “Bioprinting Living Biofilms through Optogenetic Manipulation,” *ACS Synth. Biol.*, vol. 7, no. 5, pp. 1195–1200, May 2018, doi: 10.1021/acssynbio.8b00003.

[41] A. Pirhanov *et al.*, “Optogenetics in Sinorhizobium meliloti Enables Spatial Control of Exopolysaccharide Production and Biofilm Structure,” *ACS Synth. Biol.*, vol. 10, no. 2, pp. 345–356, Feb. 2021, doi: 10.1021/acssynbio.0c00498.

[42] R. S. McIsaac, B. L. Oakes, X. Wang, K. A. Dummit, D. Botstein, and M. B. Noyes, “Synthetic gene expression perturbation systems with rapid, tunable, single-gene specificity in yeast,” *Nucleic Acids Res.*, vol. 41, no. 4, p. e57, Feb. 2013, doi: 10.1093/nar/gks1313.

[43] J. M. An-Adirekkun *et al.*, “A yeast optogenetic toolkit (yOTK) for gene expression control in Saccharomyces cerevisiae,” *Biotechnol. Bioeng.*, vol. 117, no. 3, pp. 886–893, Mar. 2020, doi: 10.1002/bit.27234.

[44] M. E. Lee, W. C. DeLoache, B. Cervantes, and J. E. Dueber, “A Highly Characterized Yeast Toolkit for Modular, Multipart Assembly,” *ACS Synth. Biol.*, vol. 4, no. 9, pp. 975–986, Sep. 2015, doi: 10.1021/sb500366v.

[45] U. Gueldener, J. Heinisch, G. J. Koehler, D. Voss, and J. H. Hegemann, “A second set of loxP marker cassettes for Cre-mediated multiple gene knockouts in budding yeast,” *Nucleic Acids Res.*, vol. 30, no. 6, p. e23, Mar. 2002.

[46] W. P. Voth, J. D. Richards, J. M. Shaw, and D. J. Stillman, “Yeast vectors for integration at the HO locus,” *Nucleic Acids Res.*, vol. 29, no. 12, pp. E59-59, Jun. 2001, doi: 10.1093/nar/29.12.e59.

[47] F. Baganz, A. Hayes, D. Marren, D. C. Gardner, and S. G. Oliver, “Suitability of replacement markers for functional analysis studies in Saccharomyces cerevisiae,” *Yeast Chichester Engl.*, vol. 13, no. 16, pp. 1563–1573, Dec. 1997, doi: 10.1002/(SICI)1097-0061(199712)13:16<1563::AID-YEA240>3.0.CO;2-6.

[48] H. Redden, N. Morse, and H. S. Alper, “The synthetic biology toolbox for tuning gene expression in yeast,” *FEMS Yeast Res.*, vol. 15, no. 1, pp. 1–10, Feb. 2015, doi: 10.1111/1567-1364.12188.

[49] I. H. Greger and N. J. Proudfoot, “Poly(A) signals control both transcriptional termination and initiation between the tandem GAL10 and GAL7 genes of Saccharomyces cerevisiae.,” *EMBO J.*, vol. 17, no. 16, pp. 4771–4779, Aug. 1998, doi: 10.1093/emboj/17.16.4771.

[50] A. Wach, A. Brachat, R. Pöhlmann, and P. Philippsen, “New heterologous modules for classical or PCR-based gene disruptions in Saccharomyces cerevisiae,” *Yeast Chichester Engl.*, vol. 10, no. 13, pp. 1793–1808, Dec. 1994, doi: 10.1002/yea.320101310.

[51] “Principles of Animal Ecology by Allee, W.C., Park, Orlando, Emerson, Alfred E, Park, Thomas, Schmidt, Karl P.: Good Hard Cover (1967) | ‘Pursuit of Happiness’ Books.” https://www.abebooks.com/Principles-Animal-Ecology-Allee-W.C-Park/201587764/bd (accessed Apr. 30, 2023).

[52] L. Dai, D. Vorselen, K. S. Korolev, and J. Gore, “Generic indicators for loss of resilience before a tipping point leading to population collapse,” *Science*, vol. 336, no. 6085, pp. 1175–1177, Jun. 2012, doi: 10.1126/science.1219805.

[53] A. Sanchez and J. Gore, “Feedback between Population and Evolutionary Dynamics Determines the Fate of Social Microbial Populations,” *PLOS Biol.*, vol. 11, no. 4, p. e1001547, Apr. 2013, doi: 10.1371/journal.pbio.1001547.

[54] K. R. Lauterjung, N. M. Morales, and M. N. McClean, “Secrete to beat the heat,” *Nat. Microbiol.*, vol. 5, no. 7, pp. 883–884, Jul. 2020, doi: 10.1038/s41564-020-0748-3.

[55] S. Basu, Y. Gerchman, C. H. Collins, F. H. Arnold, and R. Weiss, “A synthetic multicellular system for programmed pattern formation,” *Nature*, vol. 434, no. 7037, Art. no. 7037, Apr. 2005, doi: 10.1038/nature03461.

[56] J. D. Murray, Ed., *Mathematical Biology: II: Spatial Models and Biomedical Applications*, vol. 18. in Interdisciplinary Applied Mathematics, vol. 18. New York, NY: Springer, 2003. doi: 10.1007/b98869.

[57] W. Kong, A. E. Blanchard, C. Liao, and T. Lu, “Engineering robust and tunable spatial structures with synthetic gene circuits,” *Nucleic Acids Res.*, vol. 45, no. 2, pp. 1005–1014, Jan. 2017, doi: 10.1093/nar/gkw1045.
[58] J. J. Tabor *et al.*, “A Synthetic Genetic Edge Detection Program,” *Cell*, vol. 137, no. 7, pp. 1272–1281, Jun. 2009, doi: 10.1016/j.cell.2009.04.048.
[59] “Synthetic Complete (SC) Medium,” *Cold Spring Harb. Protoc.*, vol. 2016, no. 11, p. pdb.rec090589, Nov. 2016, doi: 10.1101/pdb.rec090589.
[60] L. Sarokin and M. Carlson, “Upstream region of the SUC2 gene confers regulated expression to a heterologous gene in Saccharomyces cerevisiae.,” *Mol. Cell. Biol.*, vol. 5, no. 10, pp. 2521–2526, Oct. 1985.
[61] L. Neigeborn and M. Carlson, “Genes affecting the regulation of SUC2 gene expression by glucose repression in Saccharomyces cerevisiae,” *Genetics*, vol. 108, no. 4, pp. 845–858, Dec. 1984, doi: 10.1093/genetics/108.4.845.
[62] O. X. Cordero and M. S. Datta, “Microbial interactions and community assembly at microscales,” *Curr. Opin. Microbiol.*, vol. 31, pp. 227–234, Jun. 2016, doi: 10.1016/j.mib.2016.03.015.
[63] A. Dal Co, S. van Vliet, D. J. Kiviet, S. Schlegel, and M. Ackermann, “Short-range interactions govern the dynamics and functions of microbial communities,” *Nat. Ecol. Evol.*, vol. 4, no. 3, pp. 366–375, Mar. 2020, doi: 10.1038/s41559-019-1080-2.
[64] G. P. Donaldson, S. M. Lee, and S. K. Mazmanian, “Gut biogeography of the bacterial microbiota,” *Nat. Rev. Microbiol.*, vol. 14, no. 1, pp. 20–32, Jan. 2016, doi: 10.1038/nrmicro3552.
[65] S. Gupta, T. D. Ross, M. M. Gomez, J. L. Grant, P. A. Romero, and O. S. Venturelli, “Investigating the dynamics of microbial consortia in spatially structured environments,” *Nat. Commun.*, vol. 11, no. 1, Art. no. 1, May 2020, doi: 10.1038/s41467-020-16200-0.
[66] R. N. Alnahhas *et al.*, “Spatiotemporal Dynamics of Synthetic Microbial Consortia in Microfluidic Devices,” *ACS Synth. Biol.*, vol. 8, no. 9, pp. 2051–2058, Sep. 2019, doi: 10.1021/acssynbio.9b00146.
[67] A. Burmeister and A. Grünberger, “Microfluidic cultivation and analysis tools for interaction studies of microbial co-cultures,” *Curr. Opin. Biotechnol.*, vol. 62, pp. 106–115, Apr. 2020, doi: 10.1016/j.copbio.2019.09.001.
[68] A. Burmeister *et al.*, “A microfluidic co-cultivation platform to investigate microbial interactions at defined microenvironments,” *Lab. Chip*, vol. 19, no. 1, pp. 98–110, Dec. 2018, doi: 10.1039/C8LC00977E.
[69] A. Saha *et al.*, “Additive Manufacturing of Catalytically Active Living Materials,” *ACS Appl. Mater. Interfaces*, vol. 10, no. 16, pp. 13373–13380, Apr. 2018, doi: 10.1021/acsami.8b02719.
[70] W. F. Hynes, J. Chacón, D. Segrè, C. J. Marx, N. C. Cady, and W. R. Harcombe, “Bioprinting microbial communities to examine interspecies interactions in time and space,” *Biomed. Phys. Eng. Express*, vol. 4, no. 5, Art. no. LLNL-JRNL-754585, Aug. 2018, doi: 10.1088/2057-1976/aad544.
[71] J. Merrin, S. Leibler, and J. S. Chuang, “Printing Multistrain Bacterial Patterns with a Piezoelectric Inkjet Printer,” *PLOS ONE*, vol. 2, no. 7, p. e663, Jul. 2007, doi: 10.1371/journal.pone.0000663.
[72] L. A. Hartsough *et al.*, “Optogenetic control of gut bacterial metabolism to promote longevity,” *eLife*, vol. 9, p. e56849, Dec. 2020, doi: 10.7554/eLife.56849.
[73] R. Ohlendorf, R. R. Vidavski, A. Eldar, K. Moffat, and A. Möglich, “From dusk till dawn: one-plasmid systems for light-regulated gene expression,” *J. Mol. Biol.*, vol. 416, no. 4, pp. 534–542, Mar. 2012, doi: 10.1016/j.jmb.2012.01.001.
[74] A. Levskaya *et al.*, “Engineering Escherichia coli to see light,” *Nature*, vol. 438, no. 7067, Art. no. 7067, Nov. 2005, doi: 10.1038/nature04405.

[75] K. Brenner, L. You, and F. H. Arnold, “Engineering microbial consortia: a new frontier in synthetic biology,” *Trends Biotechnol.*, vol. 26, no. 9, pp. 483–489, Sep. 2008, doi: 10.1016/j.tibtech.2008.05.004.

[76] Y. Chen, J. K. Kim, A. J. Hirning, K. Josić, and M. R. Bennett, “Emergent genetic oscillations in a synthetic microbial consortium,” *Science*, vol. 349, no. 6251, pp. 986–989, Aug. 2015, doi: 10.1126/science.aaa3794.

[77] N. Marchand and C. H. Collins, “Peptide-based communication system enables Escherichia coli to Bacillus megaterium interspecies signaling,” *Biotechnol. Bioeng.*, vol. 110, no. 11, pp. 3003–3012, Nov. 2013, doi: 10.1002/bit.24975.

[78] T. Kouya, Y. Ishiyama, T. Tanaka, and M. Taniguchi, “Evaluation of positive interaction for cell growth between Bifidobacterium adolescentis and Propionibacterium freudenreichii using a co-cultivation system with two microfiltration modules,” *J. Biosci. Bioeng.*, vol. 115, no. 2, pp. 189–192, Feb. 2013, doi: 10.1016/j.jbiosc.2012.09.005.

[79] R. J. Lovelett, E. M. Zhao, M. A. Lalwani, J. E. Toettcher, I. G. Kevrekidis, and J. L Avalos, “Dynamical Modeling of Optogenetic Circuits in Yeast for Metabolic Engineering Applications,” *ACS Synth. Biol.*, vol. 10, no. 2, pp. 219–227, Feb. 2021, doi: 10.1021/acssynbio.0c00372.

[80] S. Pouzet, A. Banderas, M. Le Bec, T. Lautier, G. Truan, and P. Hersen, “The Promise of Optogenetics for Bioproduction: Dynamic Control Strategies and Scale-Up Instruments,” *Bioeng. Basel Switz.*, vol. 7, no. 4, p. 151, Nov. 2020, doi: 10.3390/bioengineering7040151.

[81] E. M. Zhao *et al.*, “Optogenetic regulation of engineered cellular metabolism for microbial chemical production,” *Nature*, vol. 555, no. 7698, pp. 683–687, Mar. 2018, doi: 10.1038/nature26141.

[82] R. D. Gietz and R. H. Schiestl, “High-efficiency yeast transformation using the LiAc/SS carrier DNA/PEG method,” *Nat. Protoc.*, vol. 2, no. 1, Art. no. 1, Jan. 2007, doi: 10.1038/nprot.2007.13.

[83] S. Harju, H. Fedosyuk, and K. R. Peterson, “Rapid isolation of yeast genomic DNA: Bust n’ Grab,” *BMC Biotechnol.*, vol. 4, no. 1, p. 8, Apr. 2004, doi: 10.1186/1472-6750-4-8.

[84] J. Sambrook and D. W. Russell, “The Inoue Method for Preparation and Transformation of Competent E. Coli: ‘Ultra-Competent’ Cells,” *Cold Spring Harb. Protoc.*, vol. 2006, no. 1, p. pdb.prot3944, Jun. 2006, doi: 10.1101/pdb.prot3944.

[85] E. C. Andersen, “PCR-directed in vivo plasmid construction using homologous recombination in baker’s yeast,” *Methods Mol. Biol. Clifton NJ*, vol. 772, pp. 409–421, 2011, doi: 10.1007/978-1-61779-228-1_24.

[86] Z. Carter and D. Delneri, “New generation of loxP-mutated deletion cassettes for the genetic manipulation of yeast natural isolates,” *Yeast Chichester Engl.*, vol. 27, no. 9, pp. 765–775, Sep. 2010, doi: 10.1002/yea.1774.

[87] K. P. Gerhardt *et al.*, “An open-hardware platform for optogenetics and photobiology,” *Sci. Rep.*, vol. 6, no. 1, Art. no. 1, Nov. 2016, doi: 10.1038/srep35363.

[88] E. O. Grødem, K. Sweeney, and M. N. McClean, “Automated calibration of optoPlate LEDs to reduce light dose variation in optogenetic experiments,” *BioTechniques*, vol. 69, no. 4, pp. 313–316, Oct. 2020, doi: 10.2144/btn-2020-0077.

[89] K. Sweeney, N. Moreno Morales, Z. Burmeister, A. J. Nimunkar, and M. N. McClean, “Easy calibration of the Light Plate Apparatus for optogenetic experiments,” *MethodsX*, vol. 6, pp. 1480–1488, 2019, doi: 10.1016/j.mex.2019.06.008.

[90] M. Dobretsov, G. Petkau, A. Hayar, and E. Petkau, “Clock Scan Protocol for Image Analysis: ImageJ Plugins,” *JoVE J. Vis. Exp.*, no. 124, p. e55819, Jun. 2017, doi: 10.3791/55819.

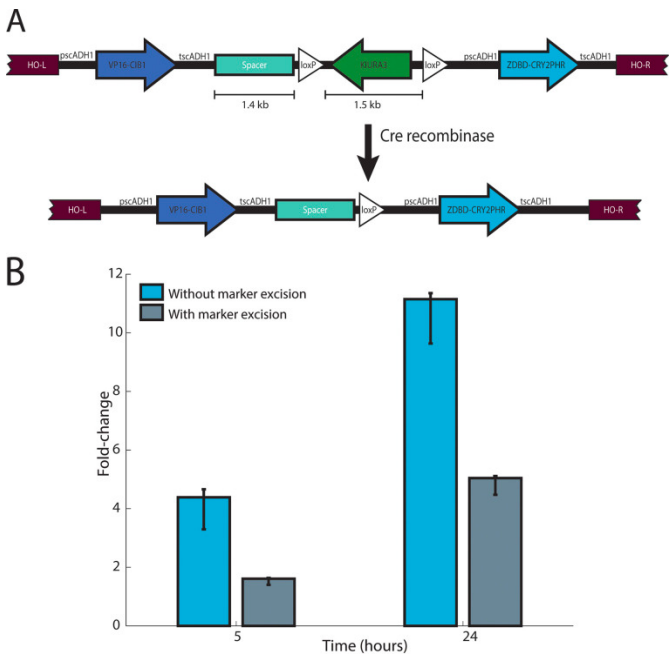

Figure 1. Characterization of vectors to integrate the blue light inducible split transcription factor (ZDBD-CRY2PHR/CIB1-VP16) into yeast with marker recovery.

(A) The split TF vector inserts ZDBD-CRY2PHR and VP16-CIB1 at the HO locus under the expression of constitutive (pADH1) promoters with KIURA3 selection. Expression of Cre-recombinase and recombination of the loxP sites removes the KIURA3 marker, leaving it available for future strain manipulation. (B) Illumination of strains with ZDBD-CRY2PHR/CIB1-VP16 and a pZF(3BS)-yEVENUS reporter at 460nm (50 μW/cm^2) demonstrates that the ZDBD-CRY2PHR/CIB1-VP16 transcription factor drives gene expression from the pZF promoter in strains with or without recycling of the KIURA3 marker. However, removal of the KIURA3 marker does reduce expression from the pZF promoter approximately two-fold. Expression of yEVENUS was measured using imaging cytometry. Error bars are bootstrapped 95% confidence intervals for the mean expression level.

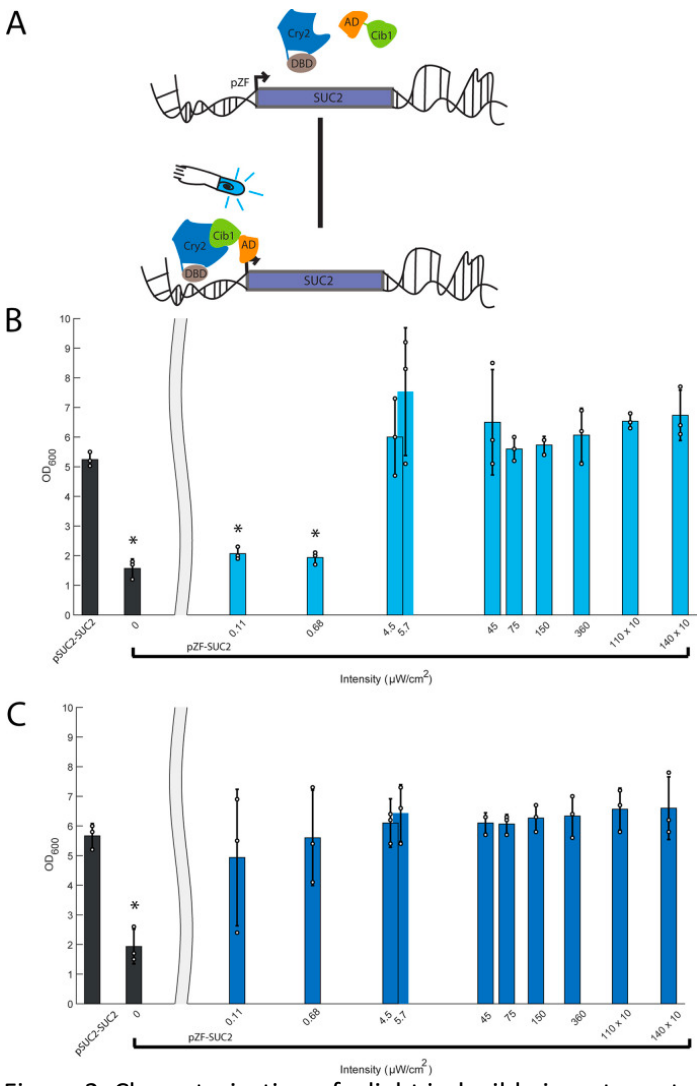

Figure 2. Characterization of a light inducible invertase strain.

(A) In a yeast strain containing the ZDBD-CRY2PHR/VP16-CIB1 gene cassette the invertase endogenous promoter (pSUC2) was substituted with the orthogonal light inducible promoter (pZF) using the KanMX-pZF(3BS) cassette. In the dark, chimeric proteins ZDBD-CRY2PHR and VP16-CIB1 remain unbound and are inactive. Upon the addition of light CRY2 undergoes a conformational change that allows binding to CIB1 and recruits VP16-CIB1 to the promoter to drive transcription. The optogenetic strain pZF-SUC2 was exposed to a range of light intensities (0 μW/cm^2-14 X 10^2 μW/cm^2) in YP-Sucrose media. (B) At 24 hours the wild-type strain (pSUC2-SUC2) shows robust growth, while the control (pZF-SUC2, 0 μW/cm^2) does not. When provided a sufficient light dose, the pZF-SUC2 strain is able to recover wild-type growth in 24 hours (intensities >4 μW/cm^2) (C) After 48 hours, all pZF-SUC2 strains exposed to light catch up to the wild-

type (pSUC2-SUC2) strain. Each bar represents three biological replicates and the individual data points are shown. (* denotes p<0.05, two-way ANOVA)

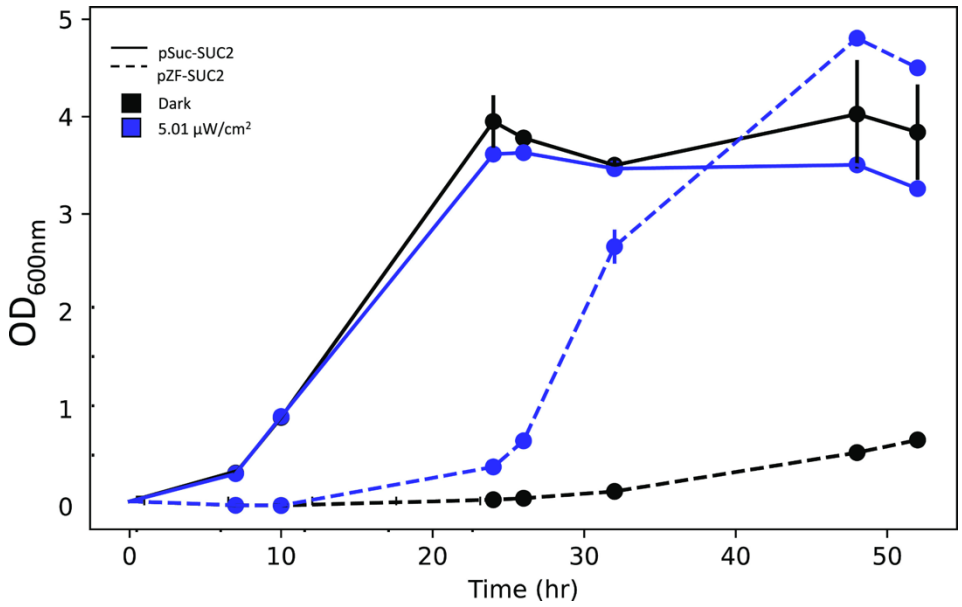

Figure 3.Light induction time course of light inducible strain (pZF-SUC2, dashed line) and wildtype strain (pSUC2-SUC2, solid line).

Light intensities are 5.01 µW/cm^2 (blue) and 0 µW/cm^2 light (black) (n=2). Error bars are standard deviation. Error bars not visible are smaller than the marker. The optogenetically controlled strain displays a long lag in growth, which may be due to the time needed to accumulate invertase and break down sucrose to support growth after light induction.

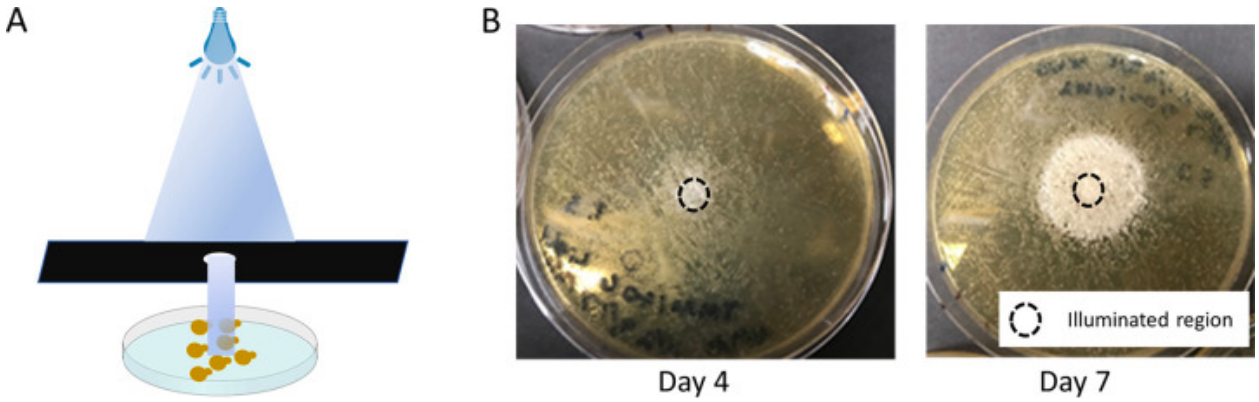

Figure 4: Controlled light results in patterned growth of a synthetic public goods community.
(A) Spatial patterning of our public goods communities can be achieved by optogenetically controlling invertase expression in an illuminated area. A photomask limits the illuminated area on a petri plate resulting in patterned growth. (B) A representative image of the public goods community patterned on a standard petri plate. The black circle denotes the illuminated area of the plate. Growth was imaged on Day 4 and Day 7.

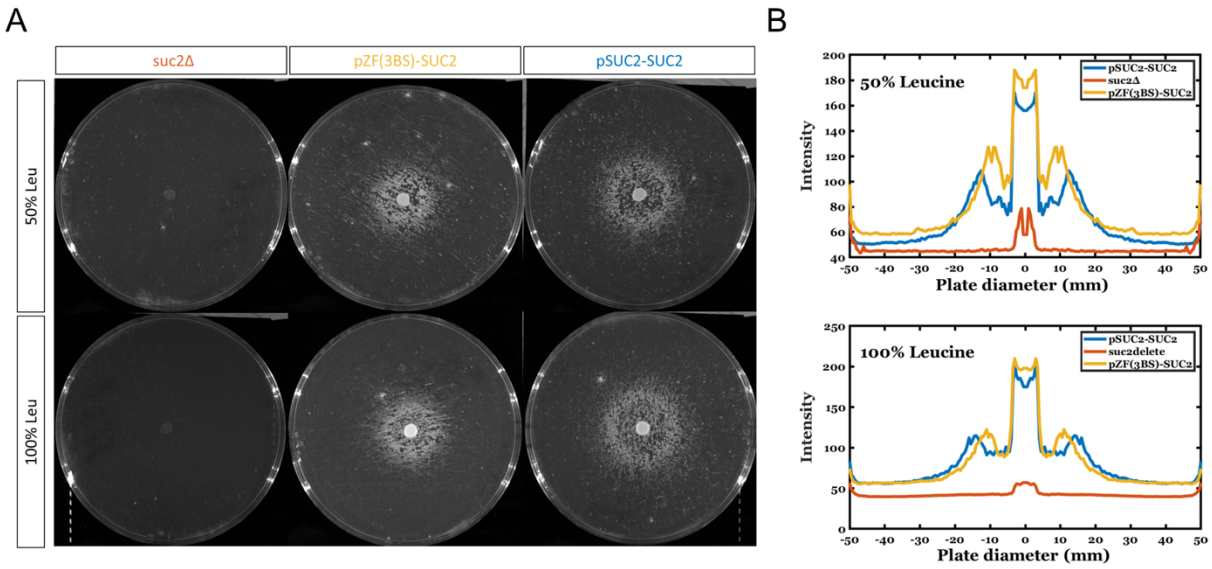

Figure 5: Spot patterning assay on nutrient limited SC-Sucrose plates.
(A) Representative images of spot assay plates. The top row is composed of 50% leucine plates while the bottom row shows the 100% leucine condition. All plates were spread with the constitutive cheater strain, suc2Δ leu2Δ. From left to right the spotted strains are: suc2Δ leu2Δ, pZF-SUC2 and pSUC2-SUC2. (B) Plots showing an averaged radial intensity profile of the spotted plates across the diameter of the plate. At both concentrations of leucine, the pSUC2-SUC2 strain (blue) shows a larger inhibition of growth zone than the pZF-SUC2 (yellow) strain. In all cases, there is no growth of the suc2Δ leu2Δ(orange) strain.

Chapter 4: Interactions between cooperators and cheaters in nutrient-limiting environments generate long-range patterning effects

This chapter is in preparation for submission.

Neydis Moreno Morales constructed strains, performed experiments, and analyzed data. Anik Chaturbedi developed the partial differential equation model in consultation with Neydis Moreno Morales, performed calculations, and Anik Chaturbedi and Neydis Moreno Morales interpreted model results. Neydis Moreno Morales, Anik Chaturbedi, and Megan McClean wrote the paper.

Abstract

The structure and function of microbial communities is regulated, in part, by metabolic interactions between species within the community. A common interaction is cooperation, specifically the production of public goods, where some cells, termed cooperators, will produce a compound that benefits all microbes in the community. This includes benefitting cheaters, microbes that do not participate in producing the beneficial compound and therefore do not accrue any of the production cost. The production by the budding yeast *Saccharomyces cerevisiae* of invertase, which converts non-metabolizable sucrose into the metabolizable sugars glucose and fructose is a model public goods interaction. We discovered that in structured, two-dimensional environments localized invertase-producing yeast cells surrounded by cheaters (which cannot produce invertase) produce bullseye growth patterns with the centralized cooperators growing but also supporting growth at a distance of a ring of cheater cells. We discovered that this pattern develops in a stereotypical way over the course of days, with the cooperators growing first, followed by later evolution of the cheater ring, and that this pattern is regulated by the concentration of the limiting nutrient. We developed a partial differential equation model that accounts for sucrose conversion, hexose and leucine consumption, nutrient diffusion, and both cheater and cooperator growth. This model is capable of producing bullseye patterns and agrees well with our original experimental results. We find that both experimentally and as predicted by the model, initial cell density and the initial ratio of cooperators to cheaters does not significantly affect patterning. We use the model to predict how nutrients, population composition, and biochemical patterns affect relative growth of cooperators and cheaters. Finally, we find that the model cannot fit experimental data from varied sucrose concentrations which leads us to hypothesize that some factor, for instance regulation of invertase production, could be necessary to explain patterning under these conditions.

Introduction

Microorganisms live in dense and diverse communities[1], [2]. These communities are critical for global and human health, as they regulate a variety of processes including biogeochemical cycling and the functioning of the microbiota of multicellular organisms[3]–[5]. These communities can also wreak havoc, for instance by causing treatment-resistant biofilm infections or by invading and destroying surfaces and flow systems in industrial settings. Microbes within these communities do not exist in isolation, instead they must contend with the existence of their neighbors which means dealing with limited resources, chemical warfare, and other sophisticated interactions. Interactions between microbes can be passive or active, inhibitory or promotive, and act over a range of length-scales including local contact-dependent interactions and longer-scale diffusion-based interactions[6]–[8]. The interaction dynamics between individual microbes and species guide the development and persistence of these complex communities. Studies of naturally occurring microbial communities, as well as synthetic biology studies utilizing simplified communities, indicate that intra- and interspecies interactions are crucial to regulating overall community productivity and biomass, as well as the spatial structure of populations residing within the community.

Cooperation, where one microbial species benefits another, is common in microbial communities[1], [9], [10]. Public goods interactions are a common type of cooperation, where a resource produced by cooperative cells (cooperators) is freely available to other cells in the community. This includes “cheaters”, cells which exploit public goods without incurring any of the production cost nor providing any known contribution of their own[9]. The budding yeast *Saccharomyces cerevisiae* engages in a cooperative interaction by secreting invertase, an enzyme that catalyzes hydrolysis of sucrose into glucose and fructose (Figure 1). The free hexose is available to all cells in the community, and therefore represents a public good. While naturally occurring microbial communities are complex, with many players and

sometimes unknown interactions, invertase secretion in *S. cerevisiae* represents a relatively simple and controllable interaction in a model organism that can be used in studying public goods interactions and their role in microbial community structure and function. Though model communities do not perfectly capture all of the complexity of natural environments, such simplified models have proven useful for understanding the basic phenomena and principles governing community formation and function in time and space [11]–[13].

In another study, we fortuitously discovered that in mixed communities of invertase producing and cheating yeast growing on agar plates with sucrose as the carbon source, localized cooperators surrounded by cheaters produce bullseye patterns [14](Also see, Chapter 3). The localized cooperators grow, while creating an immediate zone of inhibition where cheaters do not grow well, followed by an outer ring of robust cheater growth. This is particularly true when other nutrients in the growth media, for example amino acids, are limited. This simple community and the associated bullseye phenomena provides an opportunity to model and understand how public goods interactions combined with competition for resources can lead to spatial structure and patterning in microbial communities. Furthermore, the length scale of interactions that we see in the bullseye patterns is on the order of several millimeters. While short range interactions, on the order of subcell lengths (~100 μm) [6], [15], [16] are well known to play a role in microbial communities, the role of longer scale interactions is less well understood. Finally, while public goods interactions have been extensively studied, we still don't understand how cooperators prevent and withstand cheating and how this varies in well-mixed versus structured spatial environments. The bullseye model provides an opportunity to understand how localized cooperators might be able to pioneer a new environment, by taking advantage of an otherwise inaccessible nutrient, and the consequences this has for relative cooperator and cheater fitness.

In this chapter we further elucidate how population and environmental factors, especially nutrient availability, affect the bullseye pattern formation. We develop a partial differential equation model which can reproduce the patterning by accounting for hexose production, nutrient utilization, and cooperator and cheater growth. We use the model to explore how environmental and cellular factors could modulate the patterning. Finally, we explore where our model cannot fit experimental data well, and what they might mean for additional factors that may impact patterning. We conclude by proposing a factor that could be responsible, in this case regulation of cooperation.

Results

Cooperators Surrounded by Cheaters in Two Dimensional Spatial Environments Generate Distinct Bullseye Patterns in Community Growth

In previous work [14] (also described in Chapter 3) we observed that spatial segregation of invertase-producing cooperators within two-dimensional microbial communities leads to millimeter scale patterning on agar plates. Specifically, on agar plates containing sucrose as the sole carbon source a spot of cooperators (d~5mm) on top of a lawn of cheater cells (incapable of producing invertase) leads to bullseye patterning. The cooperator spot grows well, surrounded by a ring of lesser growth, and finally a more dense growth of cheaters at the periphery (Figure 2A).

To understand how this pattern evolves over time, we seeded a spot of a spot of invertase-producing yeast (pSUC2-SUC2) onto a lawn of suc2Δ cheater cells on plates containing sucrose as the sole carbon source (20 mg/ml sucrose). We imaged plates daily, and observed that the bullseye pattern evolves over time with the central spot of cooperators growing first, followed by some modest growth of cheaters in the immediate vicinity of the cooperators, and eventually formation of a ring of cheaters on the periphery

(Figure 2B). As in our previous work[14], we could quantify the patterning by imaging the plates and measuring the average radial intensity using Clockscan. This quantification confirmed the pattern progression visible by eye over the course of 7 days, with the initial cooperator spot first growing, followed by cheater growth in the immediate vicinity, and much stronger cheater growth emerging at the periphery starting at Day 4 to generate the bullseye pattern (**Figure 2C**).

The Bullseye Pattern is Regulated by the Amount of Limiting Nutrient

A potential explanation for the patterning is that the initial cooperator spot, by virtue of having immediate access to hexose through invertase production and hydrolysis of sucrose, is able to grow sooner and deplete the local area of necessary additional nutrients needed for growth. Thus the initial cooperators serve as both a source of hexose, which eventually diffuses out to allow cheater growth, but also a sink for other nutrients. In our previous work [14] (**Chapter 3, Figure 5**) we showed that by generating cooperators auxotrophic for leucine (leu2Δ) we created bullseye patterns with much clearer inhibition zones between the cooperator spot and the ring of cheater growth(**Chapter 3, Figure 5**).

To more carefully explore this effect, we plated a spot of cooperators on plates containing varying concentrations of leucine ranging from 0% to 100% (0.1 mg/ml). (**Figure 3A**). We observed that leucine concentration affects overall growth of both cooperators and cheaters, as would be expected, while minimally affecting where the peak cheater ring occurs relative to the central cooperator spot. This was verified by quantifying the plate images using Clockscan (**Figure 3B**). To ensure that patterning was indeed due to the interplay between cooperators and cheaters, and not simply due to differences in density between the central cooperator spot and the lawn of cheaters, we repeated this experiment by spotting cooperators onto a lawn of cooperators. This does not result in bullseye patterns at any concentration of leucine (Supplemental Figure 1). We also found that increasing the amount of leucine (0.5g/ml or 1g/ml)

destroyed the bullseye patterns, instead resulting in cooperators surrounded by a uniform disk of cheater growth (**Supplemental Figure 2**).

Development of a Reaction-Diffusion Model Incorporating Hexose Production and Leucine Depletion

In order to better understand the patterning and test our hypothesis that patterning could be generated by the interplay between production of hexose by the interior cooperator spot, and depletion of other limiting nutrients by the same cooperators, we developed a reaction diffusion equation describing these processes. In a well mixed system, such as a culture flask, it is possible to capture the dynamics of such a process using a system of mutually dependent ordinary differential equations to simulate changes in nutrients and cell density. However, in this system, spatial differences in the concentration of nutrients or cell density are clearly important, therefore we utilized a system of partial differential equations. We took advantage of symmetry in our experimental setup, and modeled the system as a 1-dimensional radially symmetric system. That is, variations in the azimuthal and polar angles are ignored and nutrient concentrations and cell densities are assumed to vary only along the radial direction in time.

The sole carbon source in our experimental system is sucrose, which can only be consumed by hydrolysis into fructose and glucose by invertase. We describe diffusion and hydrolysis of sucrose in our system as follows:

$$\frac{\partial c_{sucrose}(r,t)}{\partial t} = D_{sucrose}\frac{1}{r^2}\frac{\partial}{\partial r}(r^2\frac{\partial c_{sucrose}(r,t)}{\partial r}) - R_{sucrose_{depletion}}(r,t) \quad 4.1$$

where $c_{sucrose}$ is the local concentration of sucrose and $D_{sucrose}$ is the diffusion constant of sucrose in the medium.

The total rate of depletion of sucrose $R_{sucrose_{depletion}}$ is dependent on the rate at which sucrose is converted to hexose by the invertase produced by a single cooperator cell, $r_{sucrose \rightarrow hexose}$ and the density of cooperators at a particular location, $d_{producers}$ such that we have:

$$R_{sucrose_{depletion}}(r,t) = r_{sucrose \rightarrow hexose}(r,t) \times d_{producer}(r,t) \quad 4.2$$

We treat glucose and fructose similarly, and lump them both into hexose, as they are similar molecules, both can be metabolized by both cooperators and cheaters, and they are produced at the same rate upon sucrose conversion. This is keeping with prior modeling efforts in the literature[7], [17], [18].

$$r_{sucrose \rightarrow hexose}(r,t) = k_{invertase} \frac{c_{sucrose}(r,t)}{k_{m_{invertase}} + c_{sucrose}(r,t)} \quad 4.3$$

In this model, the rate constant $k_{invertase}$ is a combined factor representing the concentration of the available invertase and the actual rate of the invertase mediated conversion of sucrose to hexose. In our model, all cooperator cells are assumed to produce invertase and convert sucrose to hexose at an equal rate.

Hexose is produced by the hydrolysis of sucrose, and it is consumed by both cooperator and cheater cells. Therefore, hexose concentration changes due to diffusion, conversion of sucrose to hexose, and consumption by growing cells:

$$\frac{\partial c_{hexose}(r,t)}{\partial t} = D_{hexose} \frac{1}{r^2} \frac{\partial}{\partial r} (r^2 \frac{\partial c_{hexose}(r,t)}{\partial r}) + R_{hexose_{production}}(r,t) - R_{hexose_{consumption}} \quad 4.4$$

The variables c_{hexose} and D_{hexose} are, respectively, the total local concentration of glucose and fructose and the diffusion coefficient of glucose. We assumed that glucose and fructose diffuse at the same rate since both molecules share similar physical and chemical characteristics. The net rate of hexose production due to a conversion of sucrose is modeled similarly to the rate of sucrose depletion, $R_{sucrose_{depletion}}$. On a mass basis, the rate of hexose production is 1.05 times that of the sucrose depletion rate since during the hydrolysis of sucrose into hexose the mass of water being consumed needs to be taken into account.

$$R_{hexose_{production}}(r,t) = 1.05 \times R_{sucrose_{depletion}}(r,t) \quad 4.5$$

The total rate of hexose consumption is proportional to the rate at which hexose is consumed by either cooperator or cheater cells, both of which consume hexose at the same rate, and the total cell density at a given location:

$$R_{hexose_{consumption}}(r,t) = r_{hexose_{consumption}}(r,t) \times (d_{producer}(r,t) + d_{cheater}(r,t)) \quad 4.6$$

To account for the consumption of a limiting nutrient, we include equations describing the consumption of leucine and its diffusion, as leucine is the nutrient that we experimentally control in our system to produce limitation. The availability of leucine is dependent on the consumption of leucine by both

cooperator and cheater cells, as well as diffusion. The rate of change of leucine concentration over time along the radial direction can therefore be modeled using the following equation:

$$\frac{\partial c_{leucine}(r,t)}{\partial t} = D_{leucine}\frac{1}{r^2}\frac{\partial}{\partial r}(r^2\frac{\partial c_{leucine}(r,t)}{\partial r}) - R_{leucine_{consumption}}(r,t) \quad 4.7$$

where $c_{leucine}$ and $D_{leucine}$ are respectively the local concentration and diffusion coefficient of leucine. The rate of total leucine concentration is modeled similarly to the rate of total hexose consumption since leucine is consumed by both cell types equally. Similar to the case of hexose, we also assume that both types of cells depend on leucine consumption for their ability to grow, and the dependence on leucine is identical for both cooperator and cheater cells. For our experimental system, where both cooperators and cheaters are leu2Δ this makes sense. The rate of leucine consumption is therefore proportional to the concentration of both cooperators and cheaters:

$$R_{leucine_{consumption}}(r,t) = r_{leucine_{consumption}}(r,t)\times(d_{producer}(r,t)+d_{cheater}(r,t)) \quad 4.8$$

The bullseye patterns are caused by differential growth of cooperators and cheaters in different areas of the agar plate. The growth of cooperators and cheater, $d_{producer}$ and $d_{cheater}$ are described by the following equations:

$$\frac{\partial d_{producer}(r,t)}{\partial t} = D_{producer}\frac{1}{r^2}\frac{\partial}{\partial r}(r^2\frac{\partial d_{producer}(r,t)}{\partial r}) + R_{producer_{growth}}(r,t) \quad 4.9$$

$$\frac{\partial d_{cheater}(r,t)}{\partial t} = D_{cheater}\frac{1}{r^2}\frac{\partial}{\partial r}(r^2\frac{\partial d_{cheater}(r,t)}{\partial r}) + R_{cheater_{growth}}(r,t) \quad 4.10$$

As *Saccharomyces cerevisiae* cells are immotile, they undergo growth based on consumption of local hexose and leucine, but do not diffuse and therefore the $D_{producer}$ and $D_{cheater}$ diffusion coefficients are set to 0. The total growth rate of cooperators $R_{producer_{growth}}$ and cheaters, $R_{cheater_{growth}}$ are dependent on the growth rate of individual cooperator and cheaters cells, $r_{producer_{growth}}$ and $r_{cheater_{growth}}$ and the density of cooperator and cheater cells at that location and are modeled as follows:

$$R_{producer_{growth}}(r,t) = r_{producer_{growth}}(r,t) \times d_{producer}(r,t) \quad 4.11$$

$$R_{cheater_{growth}}(r,t) = r_{cheater_{growth}}(r,t) \times d_{cheater}(r,t) \qquad 4.12$$

In our model, the growth rates of individual cooperators and cheaters are dependent on the rate at which cells consume the essential nutrients hexose and leucine. The effect of all other essential nutrients on growth is lumped into the growth rate constant, $k_{cell\ growth}$ as we assume that all nutrients besides hexose and leucine are in excess in the system. The key difference between the growth rates of cooperators and cheaters is the cost of invertase production, k_{cost} which results in slower growth rate of the cooperators as compared to the cheaters due to them having to spend resources in producing the invertase[17]. This is in addition to the hexose and leucine consumption rates that are dependent on the local nutrient concentration and vary throughout the plate. It is important to note that the cost of invertase production is assumed to be constant for all cooperator cells, with the assumption that all cooperator cells produce invertase at the same rate. This is a common assumption in models of cooperative phenomena[7], [17]–[19].

$$r_{producer_{growth}}(r,t) = k_{cost} \times k_{cell\ growth} \times r_{hexose_{consumption}}(r,t) \times r_{leucine_{consumption}}(r,t) \qquad 4.13$$

$$r_{cheater_{growth}}(r,t) = k_{cell\ \ growth} \times r_{hexose_{consumption}}(r,t) \times r_{leucine_{consumption}}(r,t) \quad 4.14$$

We assume that the rate of consumption of hexose or leucine by a cell is dependent on the concentration of the corresponding nutrient through Michaelis-Menten kinetics of the following form:

$$r_{hexose_{consumption}}(r,t) = k_{hexose_{consumption}} \frac{c_{hexose}(r,t)}{k_{m_{hexose_{consumption}}} + c_{hexose}(r,t)} \quad 4.15$$

$$r_{leucine_{consumption}}(r,t) = k_{leucine_{consumption}} \frac{c_{leucine}(r,t)}{k_{m_{leucine_{consumption}}} + c_{leucine}(r,t)} \quad 4.16$$

A Reaction-Diffusion Model Incorporating Hexose Production and Leucine Depletion Reproduces the Bullseye Patterning

With our partial differential equations in hand, we set about seeing if our system of equations could reproduce the observed bullseye patterning. Based on experimental conditions we set the initial concentration of all nutrients as well as cooperators and cheater cells. We based diffusion constants for

hexose on that of glucose, and took diffusion coefficients for glucose, sucrose, and leucine from literature measurements[20].

Table 4.1:Fixed parameters for partial differential equation model

Name	**Initial Concentration**	**Unit**	**Diffusion Coefficient (m2/h)**	**Weight for growth function**
Glucose	0.00E+00	g/m^3	2.41E-06	0.5
Sucrose	2.00E+0.4	g/m^3	1.87E-06	0
Leucine	1.00E+02	g/m^3	2.63E-06	0.5
cooperators	1.66E+10	# $cells/m^3$	0	N/A
Cheaters	3.18E+09	# $cells/m^3$	0	N/A
Radius cooperator area	0.004	m	N/A	N/A

To obtain the parameters that can reproduce the trend observed in the specific experiments chosen for the calibration of the model, namely the evolution of the bullseye pattern over 7 days at 100% leucine (**Figure 2C**) as well as the leucine dosage experiment (**Figure 3B**), first the parameters were varied both individually and simultaneously at different levels over a wide range to mimic a global optimization process. The parameter set representing the best fit was then selected, based on a visual predictive check of similarity of both cases mentioned above to their experimental counterparts. Then the parameters were fine tuned manually to improve the fitting further. The fitted parameters are provided in Table 4.2.

Table 4.2: Fit parameters in the model and their values

Parameter	**Value**	**Unit**
KInvertase	1 107	g/(#*hr)
KmInvertase	2 103	g/m^3
KGlucoseConsumption	5 10-8	g/(#*hr)
KmGlucoseConsumtion	3 102	g/m^3

KLeucineConsumption	2.5 10-8	g/(#*hr)
KmLeucineConsumption	1 104	g/m^3
kCellGrowth	3 1015	$1/(hr*(g/(\#*hr))^2$
kCost	0.7	N/A

Importantly, the model produces bullseye patterns, indicating that the interplay between a central source of hexose production and consumption of a limiting nutrient, in this case leucine, is sufficient to reproduce the observed patterns. The model agrees well with both the evolution of bullseye patterning over time (**Figure 4A,B**) as well as the changes in patterning as a function of leucine limitation (**Figure 4C, D**). In the evolution over time experiment (**Figure 4A**) the model (**Figure 4B**) is able to recapitulate the evolution of the outer ring by Day 7. In the leucine limitation experiment (**Figure 4C**), the model reproduces the trend of the outer cheater ring increasing in density as the concentration of leucine increases (**Figure 4D**).

In addition, the model provides clues as to how the concentration of resources evolves within the plate to generate patterning. At steady state, sucrose and leucine are both largely depleted at the center of the plate, presumably stopping cooperator growth. However, diffusion leads to a peak of hexose at a distance from the central cooperator spot, which when combined with remaining leucine, allows cheaters to grow in the ring producing a bullseye pattern (**Figure 5**).

A Reaction-Diffusion Model Predicts That Patterning is Not Dependent on the Initial Density of Cheaters or the Total Plating Density

The model confirms that patterning occurs because the initial cooperator population is able to produce invertase and convert sucrose to hexose, thus allowing growth while depleting the surrounding area of essential nutrients (in our experiments, leucine). Once the cooperator population inhibits its own growth through nutrient depletion, an outer ring of cheaters is able to grow due to accumulation of hexose and remaining leucine. One might then predict that where the cheater ring occurs should not depend

dramatically on the initial number of cheaters, as their growth is controlled by the initial cooperator population. This is indeed the model's prediction. Keeping the initial number of cooperators constant within the central spot, and *in silico* varying the initial density of cheaters from 10-100% of the initial experiment ($3.18X10^8$- $3.18x10^9$ cells/m^3) does not dramatically affect either the location or density of the ring. We verified this experimentally, by plating an initial cooperator spot on varying densities of cheaters. The experimental results agree well with the model's predictions (**Figure 6A,B**).

We also hypothesized that the total plating density, keeping the initial ratio of cooperators and cheaters constant, would not significantly affect the bullseye pattern. Again, the initial cooperator growth should set both the availability of hexose at a distance from the cooperators as well as the depletion of essential nutrients, and we find *in silico* that while higher density platings result in both more cooperators and cheaters, the patterning is not significantly affected. This was confirmed experimentally, where we see that the density of both the central cooperator spot as well as the ring is affected by the initial plating density but the location of the ring does not change significantly (**Figure 6 C,D**).

It is worth noting that at low densities, growth of cells on the plate is not uniform, but is stochastic due to local changes in plating density and the presence or absence of cheaters in some locations on the plate. This leads to a lack of continuity in cheater density experimentally at lower plating densities. As this stochasticity is not implemented in our model, which assumes a continuous density of cells, this likely leads to some of the discrepancies seen between the model and experiment in Figure 6 for both the ratio and total density experiments.

In addition to asking how the initial ratio of cooperators to cheaters as well as the initial cell density affects patterning and the relative fitness of cooperators to cheaters, we also asked how the initial coverage of the cooperators affects their ability to grow in the presence of cheaters, as well as affects to the patterning. We explored this question using the model and found that larger cooperator regions (seeded at the same density) allow less cheater growth. The model predicts that a larger area of cooperators will

grow to a lower density, presumably due to limited nutrients, but these larger cooperator areas also capture more nutrients and thus allow less relative cheater growth (**Figure 7**). This is consistent with the known Allee effect for cooperators, where there is a density-dependent positive effect on growth and fitness [21]. Future work can combine the model and experiments to better understand how the initial distribution of cooperators and cheaters controls patterning and relative fitness.

Model Allows Exploration of Parameters That Affect Relative Fitness of Cooperators And Cheaters

We next used the model to explore how different parameters affect the growth of cooperators relative to cheaters. First, we examined *in silico* how levels of sucrose and leucine affected the relative growth of cooperators and cheaters (**Figure 8**). From the simulations it is clear, as is also evident in the experimental data, that more nutrients (either sucrose or leucine) leads to greater growth of cooperators and cheaters, and greater growth of all cells overall. However, interestingly, at the highest levels of sucrose, there is a non-monotonic relationship between leucine concentration and the relative growth of cheaters to cooperators. For example, at 20 mg/ml sucrose, the highest concentration used in our experiments, the lowest relative growth of cheaters happens at intermediate concentrations of leucine (20-40%; 0.02-0.04 mg/ml). This non-monotonic effect of nutrients is interesting, and suggests that at intermediate concentrations of leucine, cooperators might actually be able to capture relatively more of the limited nutrients. We would like to verify these computational predictions experimentally in the future.

With the model in hand we could also ask how the initial community composition, that is concentration of cells overall, as well as the initial ratio of cheaters to cooperators affects the relative growth of cheaters and cooperators (**Figure 9**). As expected, one can see by comparing any column in **Figure 9** that starting with a smaller community, i.e. with lower densities, leads to more relative growth with respect to the starting point, as expected. This can be explained simply through the competition for essential nutrients

between fewer cells in the case of starting with a smaller community. It is also evident that limiting the presence of cheaters (i.e. lower cheater to cooperator ratio, or CPR) leads to more growth for cooperators as well as cheaters, and consequently a total (or combined) growth of the overall population. This can again be explained by the fact that more cheaters at the beginning leads to more competition for shared nutrients between cells and therefore less growth at the individual cell level. As evident in **Figure 9**, the relative cooperator fitness is maximized when the starting community size and starting cheater-to-cooperator ratio (CPR) is highest, which also represents an initial community with the highest number of total cells. The presence of more total cells at the start leading to the lowest final CPR can probably be explained by the fact that more cells also mean the presence of more cooperators which translates to more sucrose converted to hexose and consumed by cooperators and therefore leading to more cooperator growth and as a consequence less leucine for cheaters and therefore a lower final CPR. It is perhaps simpler to understand the community moving towards a lower final CPR with more cheaters at the start since this means the same amount of hexose that is not consumed by the cooperators is shared among more cheaters. Overall, these trends combined together show that relative cooperator fitness is maximized when the community is largest at the start and therefore the competition for resources is strongest.

One advantage of the model is that we can ask how parameters that are not easy to modify experimentally, such as growth rate and the sucrose to hexose conversion rate affect the relative fitness of cooperators. Perhaps unsurprisingly, **Figure 10** shows us that increasing the rate at which sucrose is converted to hexose benefits cheaters, presumably because cooperators are unable to capture as much of this resource as it is produced more quickly. We also find that the cooperator fitness is non-monotonic in growth rate. Intermediate growth rates (compare rows in **Figure 10**), are preferred for cooperators. At these intermediate growth rates, the relative growth of cheaters to cooperators over the course of the experiment is minimized.

Model Does Not Predict Patterning When Varying Sucrose Concentrations, Perhaps Due to the Assumption of Constitutive Invertase Expression

In our initial experiments and modeling, we kept the sucrose concentration at 20 mg/ml. We interrogated the model to determine how decreasing sucrose concentrations would affect the patterning. The model predicts that lowering sucrose decreases growth of both cooperators and cheaters (**Figure 11A**) but does not significantly affect the formation of the bullseye, with the location of the ring shifting inwards slightly and the density decreasing as sucrose concentration decreases.

However, when we tested these model predictions experimentally (**Figure 11B**) we found a tremendous amount of difference between the model and the experiments. Specifically, at lower concentrations of sucrose 10-20% of our original concentration (2mg/ml and 4mg/ml) we find that there is no depletion zone and therefore no visible bullseye pattern in the experimental data. Additionally, the density of the ring is not monotonic in sucrose concentration, but is rather maximal for 40% sucrose (8mg/ml).

There are several possible explanations for the discrepancy between our model trends and trends in the experiments. For example, it is possible that our experiments had not quite reached steady state at 7 days, due to the lack of sucrose (and therefore glucose) and subsequent slow growth, and that observing the experiments for longer would have allowed for bullseye patterns to appear. This is also tricky to determine experimentally, as other factors (for example, drying of the agar plate) start to change the experimental environment as the experiment progresses. Another very interesting possibility is that ignoring invertase regulation in our model leads to inaccurate predictions.

Discussion

This study identifies patterning in cooperator-cheater populations when cooperator *S. cerevisiae* yeast are surrounded by cheaters which cannot convert sucrose into metabolizable sugars. Specifically, we find that bullseye pattern formation, where central cooperator cells deplete cheater growth nearby but allow

a ring of cheater growth at a distance, producing bullseyes. We experimentally measure how this pattern evolves over time and how nutrients available to both cooperators and cheaters affect the patterning. To better understand regulation of this pattern, we develop a partial differential equation model which can reproduce the patterning by accounting for hexose production by cooperators and nutrient depletion by cooperator and cheater growth. The model allows us to explore how nutrients, initial population composition, and parameters which are difficult to vary experimentally, such as the sucrose conversion rate and cellular growth rate, affect the relative fitness of cooperators and cheaters. Finally, we show that the model does a poor job of predicting pattern formation on different concentrations of sucrose.

Interactions between microbes within microbial communities are known to be important for community development and structure[22]–[24]. However, most studies have focused on short-range interactions between species including contact-dependent interactions and metabolic interactions acting at very short distances. In fact, some studies have suggested that metabolic exchange can happen only within a few cell lengths[6]. In our patterning, central cooperators are able to metabolically interact with cheaters tens of millimeters away to produce the bullseye pattern, which is on the order of thousands of cell lengths. Thus our experimental observations and modeling hint that while local interactions are important for microbial community development and function, at least under certain conditions, long-range metabolic interactions are also possible with implications for community outcomes, including in our case the relative fitness of cooperators and cheaters. This may be important for understanding community structure in larger scale environments, including the gastrointestinal tract and biofilms on medical devices, and even common experimental platforms, such as the agar plates used in this study.

This work also has implications for bioengineering consortia and microbial communities. Engineered microbial consortia, consisting of different microbial strains or species, provide an opportunity to expand the capabilities of engineered organisms by increasing the number of genes and metabolic capabilities available to perform the desired task. However, understanding the “design rules” for combining organisms

and maintaining stability to create productive synthetic consortia remain elusive[25]–[27]. In addition, many applications for the use of engineered microbial communities will require self-organization and patterning [28], including applications to produce living, self-healing materials which I discuss in Appendix 1. It is possible that principles similar to those uncovered in this chapter, where the interplay between production and nutrient utilization generates patterning, could be used to self-organize or spatially structure engineered communities. Indeed, many microbes, including the cellulose-producing bacteria *Komagataeibacter rhaeticus*, are unable to metabolize sucrose. As *K. rhaeticus* already co-exists with *S. cerevisiae* in natural communities, such as kombucha fermentation [29], this raises the possibility of using *S. cerevisiae* cooperator conversion of sucrose and appropriate nutrient limitations to generate pattern formation in *K. rhaeticus* and cellulose production. Optogenetic control of cooperator status, as described in **Chapter 3**, could further be used to generate more complex spatial patterning.

Finally, while our model was able to generate bullseye patterning, it was not able to fit patterning data from sucrose limitation experiments. We found experimentally that at low concentrations of sucrose no distinguishable bullseye pattern is produced. As will be discussed in Chapter 5, production of invertase is regulated, presumably based on glucose concentration, which is not accounted for in our model. Therefore, it is possible that at low concentrations of sucrose, where the production of glucose will also be limited, cooperators produce less invertase and therefore "hoard" hexose locally inhibiting growth of the outer cheater ring. It remains to be seen if the addition of invertase regulation into our model would explain the patterning we discovered experimentally. In Chapter 5 we experimentally explore invertase regulation and its potential consequences for cooperator fitness relative to cheaters.

Methods

Yeast Strains and Culture Methods

Yeast strains used in this study are shown in **Supplemental Table S1**. Yeast transformation was accomplished using standard lithium-acetate transformation. For integrating plasmids, the integration was validated using either colony PCR or, when colony PCR proved difficult, by PCR of genomic DNA. Genomic DNA was extracted using the Bust n' Grab protocol. Primers used for validating integrations are listed in **Supplemental Table 2**. All transformants were checked for the petite phenotype by growth on YEP-glycerol (1% w/v Bacto-yeast extract-BD Biosciences 212750, 2% w/v Bacto-peptone-BD Biosciences 211677, 3% [v/v] glycerol-Fisher Bioreagents BP229-1, 2% w/v Bacto-agar-BD Biosciences #214030)[22]. Only strains deemed respiration competent by growth on YEP-glycerol were used for subsequent analysis. Details of individual strain construction are described in the **Supplemental Material**.

Yeast cultures were grown in either yeast peptone (YP) media (10 g/L Bacto yeast extract, 20g/L Bacto peptone for solid media + 20g/L of Bacto agar) or Synthetic Complete (SC) media (6.7 g/L Yeast Nitrogen Base without amino acids-DOT Scientific, 1% v/v KS amino acid supplement without appropriate amino acids).The carbon source supplied was either dextrose (D) or sucrose (SUC) at 2% v/v concentration. As needed, episomal plasmids were maintained by growing yeast in SC media lacking the appropriate amino acids required for plasmid selection.

Patterning

Spot assay

Yeast strains yMM1146(wildtype cooperator) and yMM1456 (non-cooperator) were inoculated into a 5mL test tube of YP-D to grow overnight. Cells were pelleted using a microcentrifuge (Eppendorf, #EP5401000137) at 3000G for 2 minutes and washed with YP-SUC to remove residual media containing dextrose, this was repeated 3 times. To create lawns the desired strains were diluted to an OD600nm of 0.04 measured with a spectrophotometer (Fisher Scientific,#14-385-445) before plating onto solid SC-SUC plates (Fisher Scientific, #BP94S01) and 150uL of the cultures spread with glass beads ((Fisher Scientific, #11- 312B 4mm). The beads were removed and the plate allowed to dry for 10 minutes. Onto

the lawns of either suc2Δ leu2Δ cheaters or wildtype cooperators a 5uL drop of either yMM1146, or 1456 was applied to the center of a petri dish and left face-up to dry for another 10 minutes. The plates were then placed upside down in a 30°C/room temperature incubator in a single layer for 7 days. At the desired time frames the plates were imaged with a ChemiDoc imaging system (BioRad, #12003154) with an exposure of 0.06 seconds in the brightfield setting and analyzed using an ImageJ plug-in Clockscan (reference).

Leucine concentrations: Plates contained leucine concentrations between 0% (0 mg/ml) and 100% (0.1 mg/ml), for example, a plate at 50% leu contains 0.05 mg/ml of the amount used in standard synthetic complete media.

Sucrose concentrations: Plates contained sucrose concentrations between 0% (0 mg/ml) and 100% (20 mg/ml), for example, a plate at 50% leu contains 10 mg/ml of the amount used in standard synthetic complete media.

Density and ratio variation: Plates were seeded with cell cultures that were diluted to an OD600nm between 0.004 (10%) and 0.04 (100%)

Quantification of Plate Growth

Radial intensity traces of patterned plates using custom MATLAB Script

We quantify the growth of yeast on a plate from images using a custom MATLAB script that examines intensity versus radius along angular slices through the center of the plate and identifies the bounds of features such as valleys and rings. Because it's hard to accurately identify these features from individual angular slices or the single, composite intensity profile given by a clockscan[30], we use a bootstrap-based approach to repeatedly identify potential features from randomly selected sets of angular slices and select the most frequently identified potential features as true features.

This starts by roughly identifying the central yeast spot using MATLAB's circle finder and cropping the image around this spot. A polar transformation is then applied to the cropped image to create a polar

image where each column of pixels corresponds to an angular slice through the plate. These angular slices are then sampled with replacement to construct a composite image. An intensity profile is generated from each composite image by taking the median intensity value at each radius. The intensity profile is filtered to remove noise and features are identified from the resulting signal. For example, potential valley bounds are identified as the locations where the derivative of the filtered intensity profile is at its maximum and minimum. This process is repeated for hundreds of composite images to create distributions of potential features. True features are then selected as the mode of these distributions. Using MATLAB's circle find to identify the outer edges of the plate, which we know to be 100 mm across, we then convert the feature measurements to physical units. Code is available upon request.

Model Implementation and Fitting

The model was implemented in the MATLAB release R2020b. The system of 1-dimensional partial differential equations along the outward radial direction were solved using the inbuilt algorithm *pdepe* which uses another matlab solver *ode15s* to solve the equations. This algorithm as described in MATLAB literature is a "a variable-step, variable-order (VSVO) solver based on the numerical differentiation formulas (NDFs) of orders 1 to 5." The initial conditions of the system were defined based on the experimental system and are outlined in **Table 4.1**. The boundary conditions were assumed to be no flux at the outer boundaries of the plate. The radial length of the system was discretized in 500 grids (also known as cells), each spanning 0.1 mm. The system of PDEs was simulated for either 7 days (or 168 hours) for the cases where the simulated outcome was compared with the state of the plate after 7 days and for the rest of the predictive cases simulated with the model, the system was simulated up to 'steady state' where that was defined as the state where either leucine or both sucrose and glucose are almost completely depleted (sum of concentration at all grid points throughout the entire radial distance is less than 1 gm3 or 10-6gcc) .

To obtain the parameters that can reproduce the trend observed in the specific experiments chosen for the calibration of the model, namely the evolution of the bullseye pattern over 7 days at 100% leucine (**Figure 2C**) as well as the leucine dosage experiment (**Figure 3B**), first the parameters were varied both individually and simultaneously at different levels over a wide range to mimic a global optimization process. The parameter set representing the best fit was then selected, based on a visual predictive check of similarity of both cases mentioned above to their experimental counterparts. Then the parameters were fine tuned manually to improve the fitting further, thus mimicking a further local optimization step. The fitted parameters are provided in **Table 4.2.** Code for simulating the model and for the manual sensitivity analysis to identify appropriate parameters is available upon request and will be made publicly available on Github upon publication.

References

[1] C. D. Nadell, K. Drescher, and K. R. Foster, "Spatial structure, cooperation and competition in biofilms," *Nat. Rev. Microbiol.*, vol. 14, no. 9, pp. 589–600, Sep. 2016, doi: 10.1038/nrmicro.2016.84.

[2] R. L. Bier *et al.*, "Linking microbial community structure and microbial processes: an empirical and conceptual overview," *FEMS Microbiol. Ecol.*, vol. 91, no. 10, p. fiv113, Oct. 2015, doi: 10.1093/femsec/fiv113.

[3] S. Macfarlane, B. Bahrami, and G. T. Macfarlane, "Mucosal biofilm communities in the human intestinal tract," *Adv. Appl. Microbiol.*, vol. 75, pp. 111–143, 2011, doi: 10.1016/B978-0-12-387046-9.00005-0.

[4] T. J. Battin, L. A. Kaplan, J. Denis Newbold, and C. M. E. Hansen, "Contributions of microbial biofilms to ecosystem processes in stream mesocosms," *Nature*, vol. 426, no. 6965, pp. 439–442, Nov. 2003, doi: 10.1038/nature02152.

[5] C. Arnosti, "Microbial Extracellular Enzymes and the Marine Carbon Cycle," *Annu. Rev. Mar. Sci.*, vol. 3, no. 1, pp. 401–425, 2011, doi: 10.1146/annurev-marine-120709-142731.

[6] A. Dal Co, S. van Vliet, D. J. Kiviet, S. Schlegel, and M. Ackermann, "Short-range interactions govern the dynamics and functions of microbial communities," *Nat. Ecol. Evol.*, vol. 4, no. 3, Art. no. 3, Mar. 2020, doi: 10.1038/s41559-019-1080-2.

[7] R. J. Lindsay, B. J. Pawlowska, and I. Gudelj, "When increasing population density can promote the evolution of metabolic cooperation," *ISME J.*, vol. 12, no. 3, Art. no. 3, Mar. 2018, doi: 10.1038/s41396-017-0016-6.

[8] N. Weiland-Bräuer, "Friends or Foes—Microbial Interactions in Nature," *Biology*, vol. 10, no. 6, p. 496, Jun. 2021, doi: 10.3390/biology10060496.

[9] S. Mitri and K. Richard Foster, "The Genotypic View of Social Interactions in Microbial Communities," *Annu. Rev. Genet.*, vol. 47, no. 1, pp. 247–273, 2013, doi: 10.1146/annurev-genet-111212-133307.

[10] S. Germerodt *et al.*, “Pervasive Selection for Cooperative Cross-Feeding in Bacterial Communities,” *PLOS Comput. Biol.*, vol. 12, no. 6, p. e1004986, Jun. 2016, doi: 10.1371/journal.pcbi.1004986.
[11] G. L. Lozano *et al.*, “Introducing THOR, a Model Microbiome for Genetic Dissection of Community Behavior,” *mBio*, vol. 10, no. 2, pp. e02846-18, Mar. 2019, doi: 10.1128/mBio.02846-18.
[12] J. Bengtsson-Palme, “Microbial model communities: To understand complexity, harness the power of simplicity,” *Comput. Struct. Biotechnol. J.*, vol. 18, pp. 3987–4001, Jan. 2020, doi: 10.1016/j.csbj.2020.11.043.
[13] C. M. Jessup *et al.*, “Big questions, small worlds: microbial model systems in ecology,” *Trends Ecol. Evol.*, vol. 19, no. 4, pp. 189–197, Apr. 2004, doi: 10.1016/j.tree.2004.01.008.
[14] N. Moreno Morales, M. T. Patel, C. J. Stewart, K. Sweeney, and M. N. McClean, “Optogenetic Tools for Control of Public Goods in Saccharomyces cerevisiae,” *mSphere*, vol. 6, no. 4, pp. e00581-21, Aug. 2021, doi: 10.1128/mSphere.00581-21.
[15] M. J. I. Müller, B. I. Neugeboren, D. R. Nelson, and A. W. Murray, “Genetic drift opposes mutualism during spatial population expansion,” *Proc. Natl. Acad. Sci.*, vol. 111, no. 3, pp. 1037–1042, Jan. 2014, doi: 10.1073/pnas.1313285111.
[16] B. Momeni, A. J. Waite, and W. Shou, “Spatial self-organization favors heterotypic cooperation over cheating,” *eLife*, vol. 2, p. e00960, Nov. 2013, doi: 10.7554/eLife.00960.
[17] R. C. MacLean, A. Fuentes-Hernandez, D. Greig, L. D. Hurst, and I. Gudelj, “A Mixture of ‘Cheats’ and ‘Co-Operators’ Can Enable Maximal Group Benefit,” *PLOS Biol.*, vol. 8, no. 9, p. e1000486, Sep. 2010, doi: 10.1371/journal.pbio.1000486.
[18] R. J. Lindsay, M. J. Kershaw, B. J. Pawlowska, N. J. Talbot, and I. Gudelj, “Harbouring public good mutants within a pathogen population can increase both fitness and virulence,” *eLife*, vol. 5, p. e18678, Dec. 2016, doi: 10.7554/eLife.18678.
[19] J. Gore, H. Youk, and A. van Oudenaarden, “Snowdrift game dynamics and facultative cheating in yeast,” *Nature*, vol. 459, no. 7244, Art. no. 7244, May 2009, doi: 10.1038/nature07921.
[20] P. S. Stewart, “Diffusion in Biofilms,” *J. Bacteriol.*, vol. 185, no. 5, pp. 1485–1491, Mar. 2003, doi: 10.1128/JB.185.5.1485-1491.2003.
[21] W. C. Allee, A. E. Emerson, O. Park, T. Park, and K. P. Schmidt, *Principles of Animal Ecology*. W.B.Saunders, 1949.
[22] N. A. Abreu and M. E. Taga, “Decoding molecular interactions in microbial communities,” *FEMS Microbiol. Rev.*, vol. 40, no. 5, pp. 648–663, Sep. 2016, doi: 10.1093/femsre/fuw019.
[23] S. R. Proulx, D. E. L. Promislow, and P. C. Phillips, “Network thinking in ecology and evolution,” *Trends Ecol. Evol.*, vol. 20, no. 6, pp. 345–353, Jun. 2005, doi: 10.1016/j.tree.2005.04.004.
[24] S. T. Pickett and M. L. Cadenasso, “Landscape ecology: spatial heterogeneity in ecological systems,” *Science*, vol. 269, no. 5222, pp. 331–334, Jul. 1995, doi: 10.1126/science.269.5222.331.
[25] K. E. Duncker, Z. A. Holmes, and L. You, “Engineered microbial consortia: strategies and applications,” *Microb. Cell Factories*, vol. 20, no. 1, p. 211, Nov. 2021, doi: 10.1186/s12934-021-01699-9.
[26] O. S. Venturelli *et al.*, “What is the key challenge in engineering microbiomes?,” *Cell Syst.*, vol. 14, no. 2, pp. 85–90, Feb. 2023, doi: 10.1016/j.cels.2023.01.002.
[27] C. E. Lawson, “Retooling Microbiome Engineering for a Sustainable Future,” *mSystems*, vol. 6, no. 4, pp. e00925-21, Aug. 2021, doi: 10.1128/mSystems.00925-21.
[28] J. Lu, E. Şimşek, A. Silver, and L. You, “Advances and challenges in programming pattern formation using living cells,” *Curr. Opin. Chem. Biol.*, vol. 68, p. 102147, Jun. 2022, doi: 10.1016/j.cbpa.2022.102147.

[29] C. Gilbert *et al.*, “Living materials with programmable functionalities grown from engineered microbial co-cultures,” *Nat. Mater.*, vol. 20, no. 5, pp. 691–700, May 2021, doi: 10.1038/s41563-020-00857-5.
[30] M. Dobretsov, G. Petkau, A. Hayar, and E. Petkau, “Clock Scan Protocol for Image Analysis: ImageJ Plugins,” *JoVE J. Vis. Exp.*, no. 124, p. e55819, Jun. 2017, doi: 10.3791/55819.

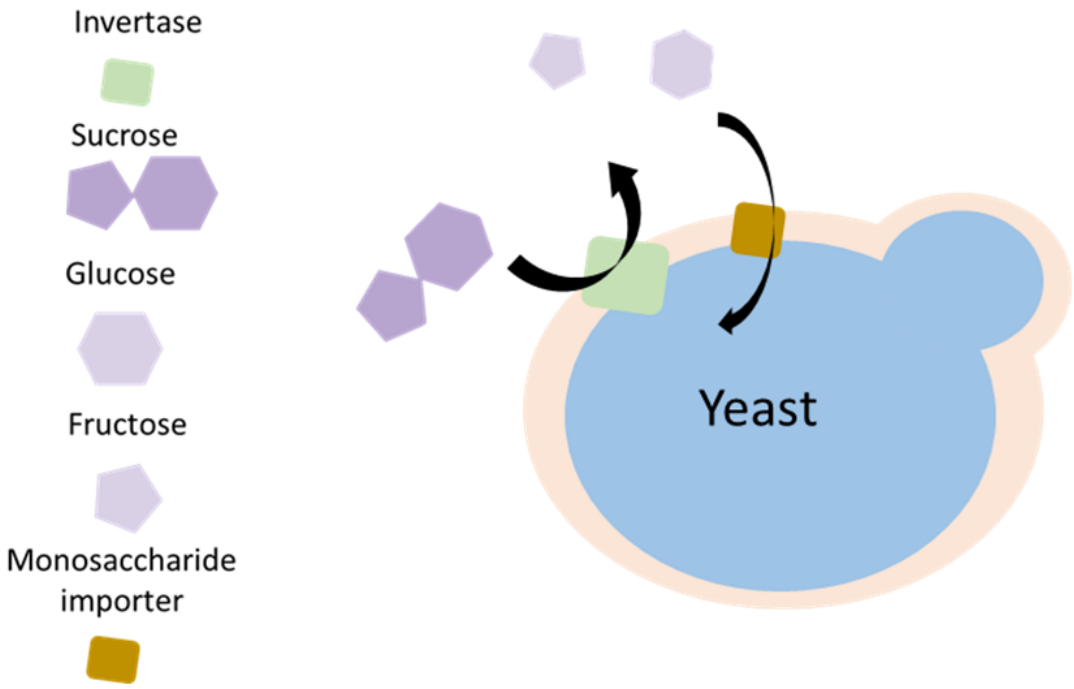

Figure 1. Sucrose utilization in Saccharomyces cerevisiae

Wild-type *Saccharomyces cerevisiae* yeast produce invertase which hydrolyzes the disaccharide sucrose into monosaccharides glucose and fructose. While sucrose is not directly metabolizable by many microbes, including budding yeast, both fructose and glucose readily are. Because the invertase enzyme is located in the periplasmic space, ~99% of the liberated hexose diffuses away before it can be imported[19], making invertase production and secretion a cooperative behavior.

Figure 2

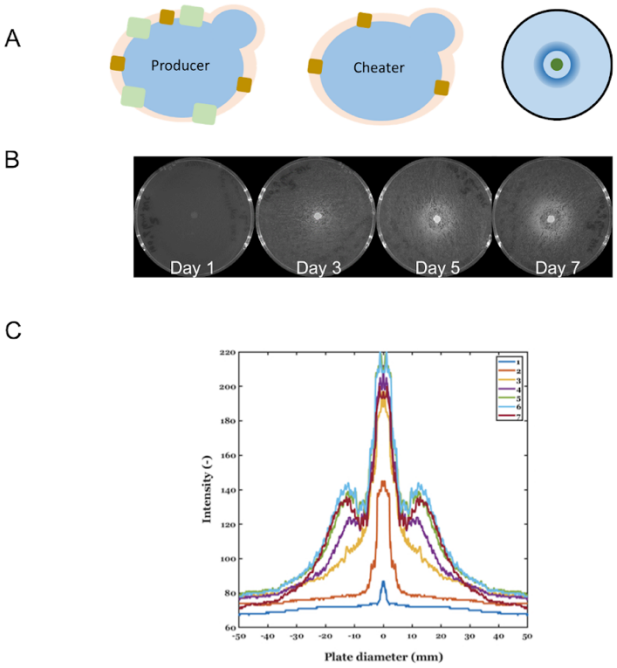

Figure 2. Bullseye pattern formation over 7 days.

(A) Cooperator yeast cells capable of producing hexose from sucrose through invertase (green squares) and importing hexose through transports (brow squares) are spotted in the center of a petri dish containing 2% sucrose as the carbon source (green circle) and seeded with a lawn of cheaters. After 7 days a ring of cheaters develops surrounding the initial cooperator spot. (B) Growth progresses over the course of days, with growth of initial cooperator spot being evident first followed by development of the ring of cheaters, forming a bullseye pattern. (C) Quantification of plate images taken daily over the course of the experiment shows the evolution of the patterning. The figure legend indicates the experimental day.

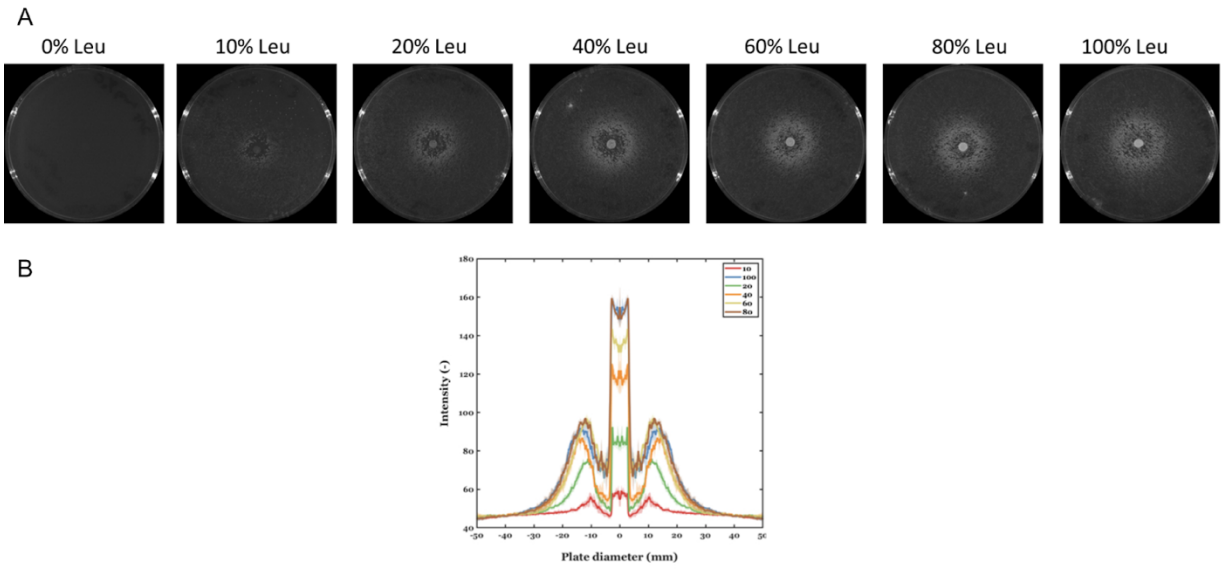

Figure 3. Pattern development on limiting leucine.

(A) Cooperator yeast cells are spotted in the center of a petri dish seeded with cheaters and containing varying concentrations of leucine. The bullseye pattern develops similarly, but to different densities, on different concentrations of leucine ranging from 0%-100% (0-0.1 mg/ml). **(B)** Quantification of the plate images show that the bullseye pattern remains relatively constant for different concentrations of leucine, but the density changes with increasing leucine. The figure legend indicates percentage leucine in the plate.

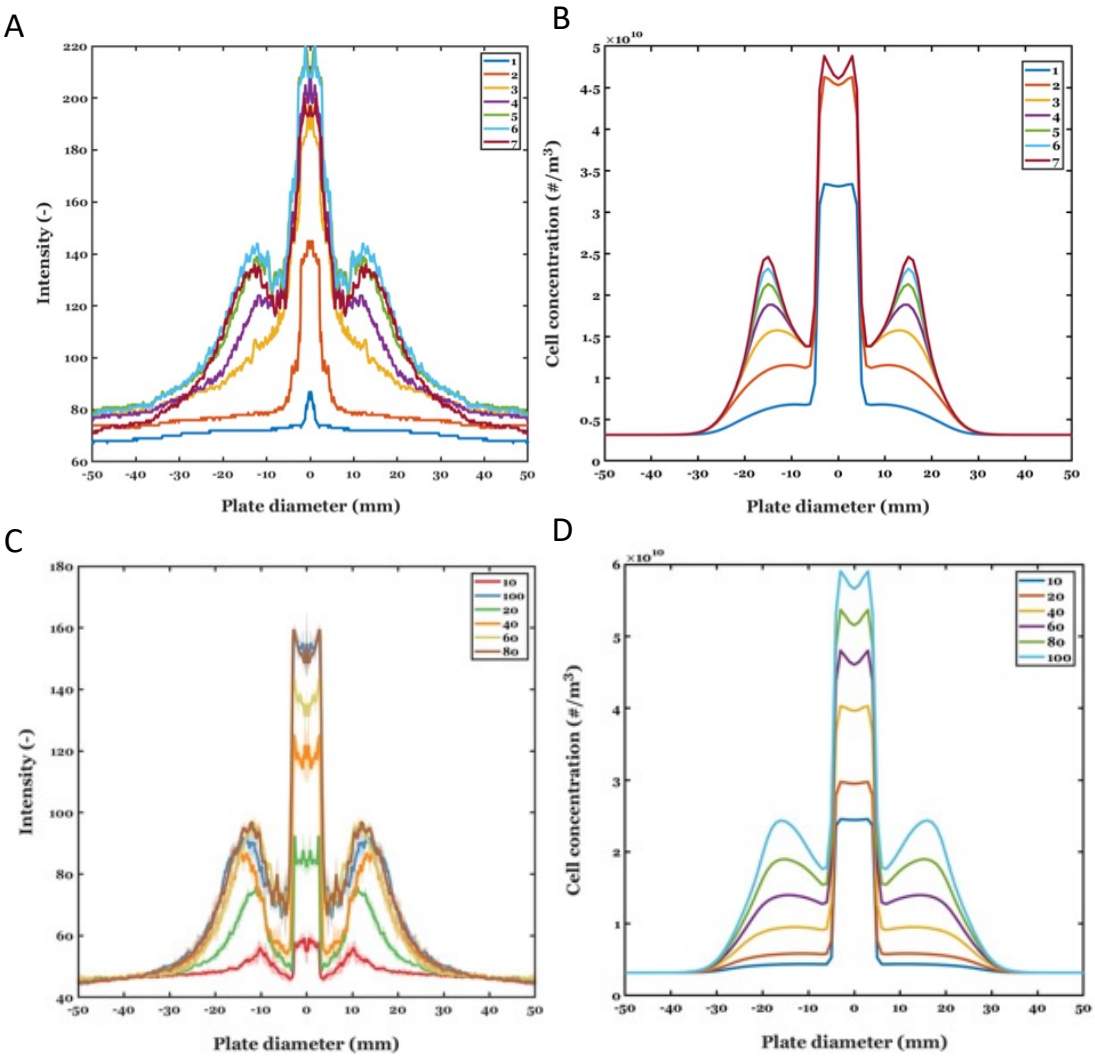

Figure 4. Model is able to recapitulate experimental conditions

A. Cooperator yeast cells are spotted in the center of a petri dish seeded with cheaters and imaged everyday for seven days. Quantification of the plate images show the evolution of the bullseye pattern. Growth is concentrated from the spot and radiates out, by day four one can begin to distinguish the distinct features of the bullseye pattern. The figure legend indicates the day of imaging. B. Model agrees well with the evolution of the bullseye pattern over seven days. The figure legend indicates the day. C. Cooperator yeast cells are spotted in the center of a petri dish seeded with cheaters and containing varying concentrations of leucine. Quantification of the plate images show that the bullseye pattern remains relatively constant for different concentrations of leucine, but the density changes with

increasing leucine. The figure legend indicates percentage leucine in the plate. D. Model reproduces the trends of growth in different concentrations of leucine. The figure legend indicates percentage leucine in the plate.

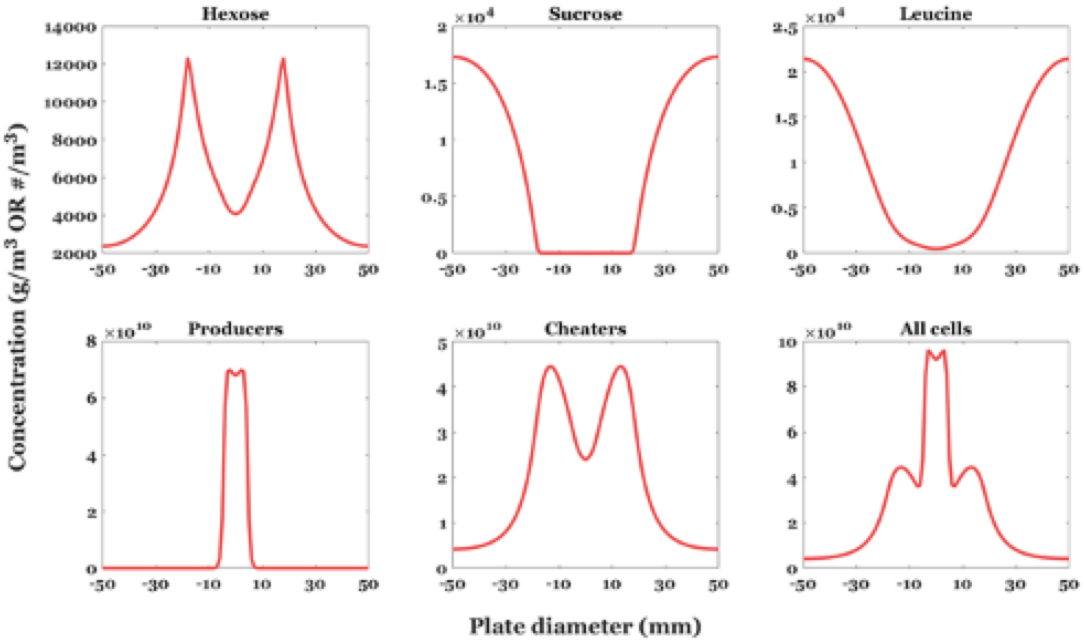

Figure 5. Steady state concentrations of limiting nutrients and cell growth predicted with the model

The model is able to inform our understanding of the evolution of nutrients and the generation of patterning. At steady state there appears to be a peak of hexose at a distance from the cooperator spot making it available to cheater cells. This is paired with a depletion of sucrose and leucine at the center that stops cooperator growth.

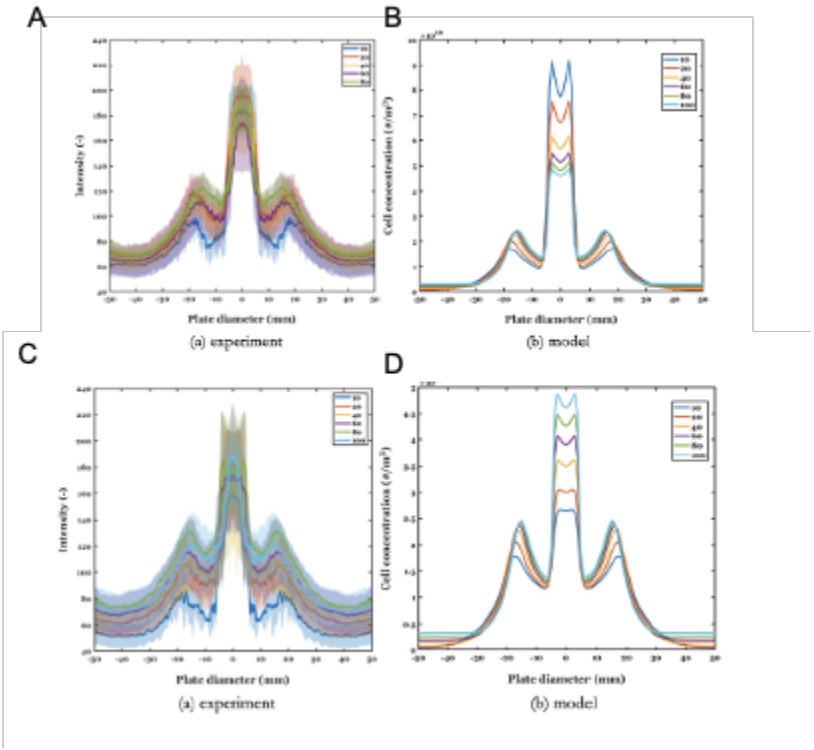

Figure 6. No observable effect due to varying initial cheater-to-cooperator ratio or total plating density on patterning

A. Cooperator yeast cells are spotted in the center of a petri dish seeded with cheaters at varying concentrations. Quantification of the plate images show that the evolution of the bullseye pattern is not dependent on the initial cheater density. Figure legend indicates the initial cheater density at the start of the experiment. B. Model is able to predict that the initial cheater density will not affect evolution of the patterning. Figure legend indicates the initial cheater density of the community at the start of the simulation. C. Cooperator yeast cells are spotted in the center of a petri dish seeded with cheaters at varying concentrations of total initial density. Quantification of the plate images show that the evolution of the bullseye pattern is not dependent on the initial density. Figure legend indicates the initial density at the start of the experiment. D. Model correctly predicts that the initial density will not affect evolution of the patterning. Figure legend indicates the initial density of the community at the start of the experiment.

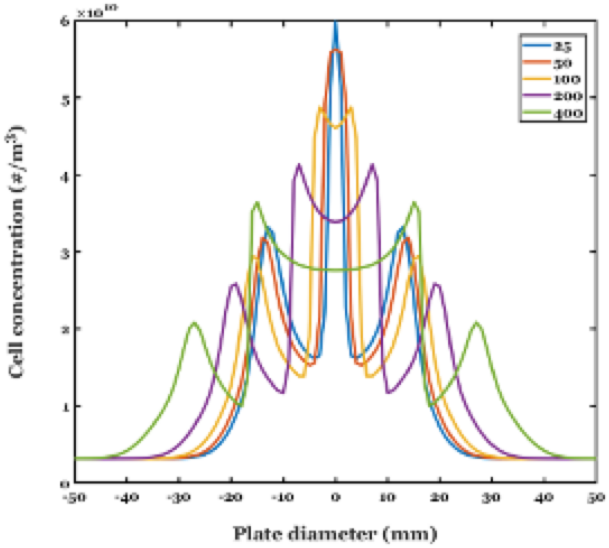

Figure 7. Effect of initial size of cooperator community on cell growth and relative fitness

Simulation of the model predicts that changes in the initial coverage of area by cooperators results in less cheater growth. Varying the initial coverage of area by the cooperators also results in a larger, but lower density area of cooperator growth. Figure legend displays the initial coverage area of cooperators in percent of the original coverage area (100 is the original coverage area used in experiments).

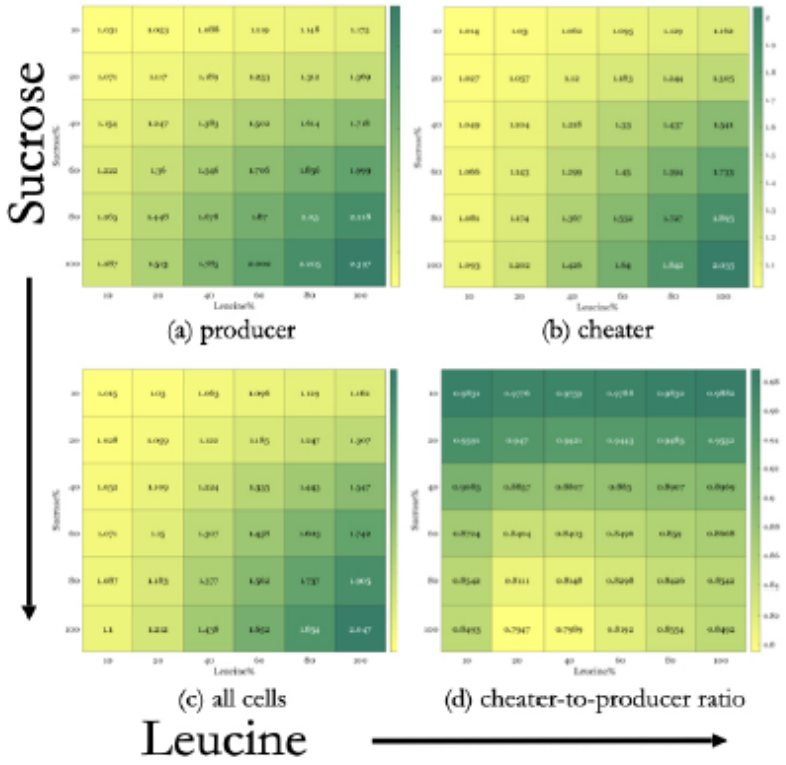

Figure 8. Effect of nutrient availability on community growth and relative fitness of cells

Experiments *in silico* reveal the effects of nutrient availability on: A. Cooperator growth. Increasing leucine and sucrose availability lead to greater cooperator growth. B. Cheater growth. Increasing leucine and sucrose availability lead to greater cheater growth. C. All cells. Increasing leucine and sucrose availability, unsurprisingly, lead to greater growth of all cells. D. Cheater-to-producer ratio. A non-monotonic effect on the relative growth of cheaters-to-cooperators is observed. Relative cheater growth is lowest at low sucrose concentrations paired with intermediate leucine availability.

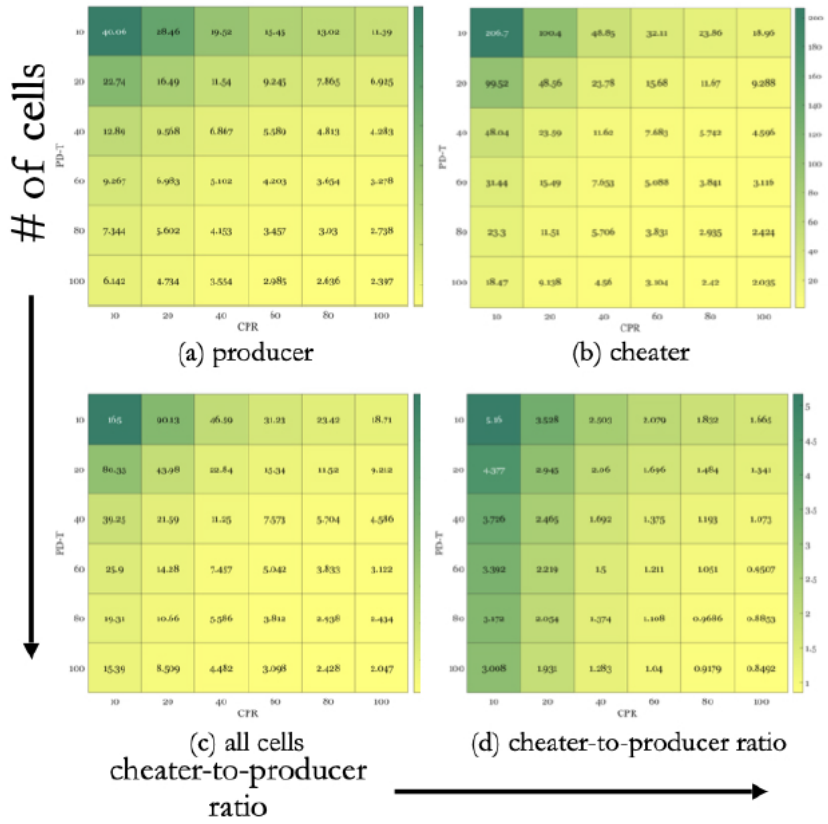

Figure 9. Effect of initial community composition on community growth and relative fitness of cells

The model simulations indicate that beginning with a smaller community (featuring lower densities) leads to a higher level of relative growth from the initial point, as anticipated. Additionally, the simulations predicted that limiting the presence of cheaters (i.e. lower cheater to cooperator ratio) leads to more growth for cooperators as well as cheaters, and consequently total growth of the overall population. According to simulations, the maximum relative fitness of cooperators occurs when the community size and the initial cheater-to-cooperator ratio (CPR) are both at their highest

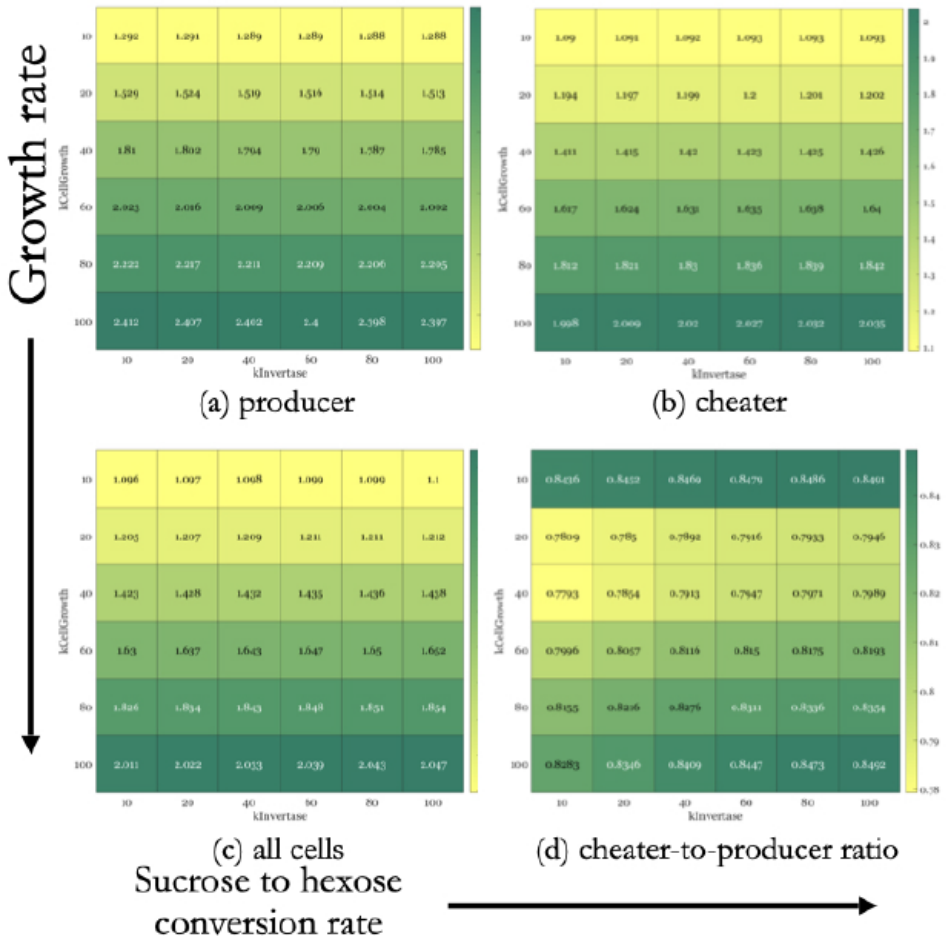

Figure 10. Effect of growth and sucrose conversion rate modulation on community growth and cooperator fitness

Simulations predict that increasing the conversion rate of sucrose to hexose appears to favor cheaters perhaps due to cooperators limited ability to capture a sufficient amount of glucose due to its rapid production. The model also predicts that cooperator fitness demonstrates a non-monotonic relationship with growth rate, indicating that intermediate growth rates are more favorable for cooperators.

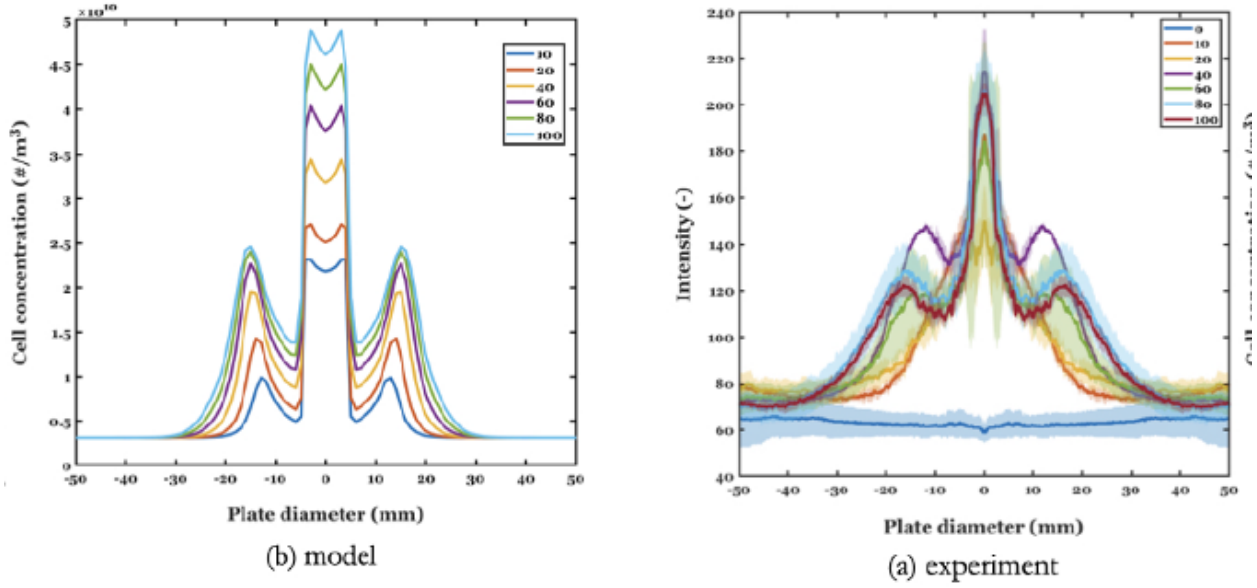

Figure 11. Effect of varying sucrose availability on community growth

A. The model predicts that reducing the amount of sucrose will lead to a decline in growth for both cooperators and cheaters, but a minimal impact on the formation of the bullseye pattern. Figure legend indicates the starting sucrose concentration for the simulation. B.The experimental results deviate significantly from the model predictions. When sucrose concentration is lowered to 10-20% of the original concentration, no depletion zone or visible bullseye pattern is observed in the experimental data. Furthermore, the density of the ring does not follow a monotonic trend with respect to sucrose concentration, and instead, reaches a maximum at 40% sucrose. Figure legend indicates the starting sucrose concentration for the experiment.

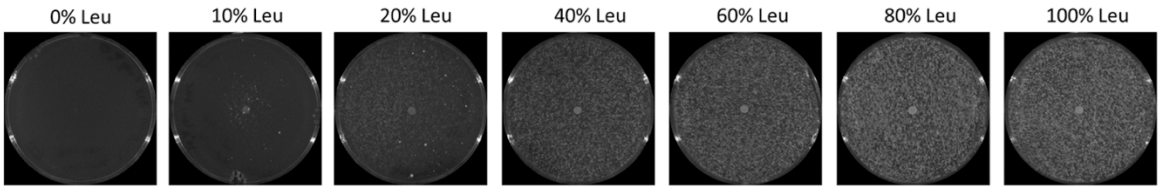

Supplemental Figure 1. Simple density differences do not explain the patterning.
On varying concentrations of leucine, cooperators were spotted onto a lawn of cooperators at the same density as cheaters in **Figure 3**. In this case, both dense cooperators and more dilute cooperators can produce invertase and convert sucrose to hexose, and no patterning is observed.

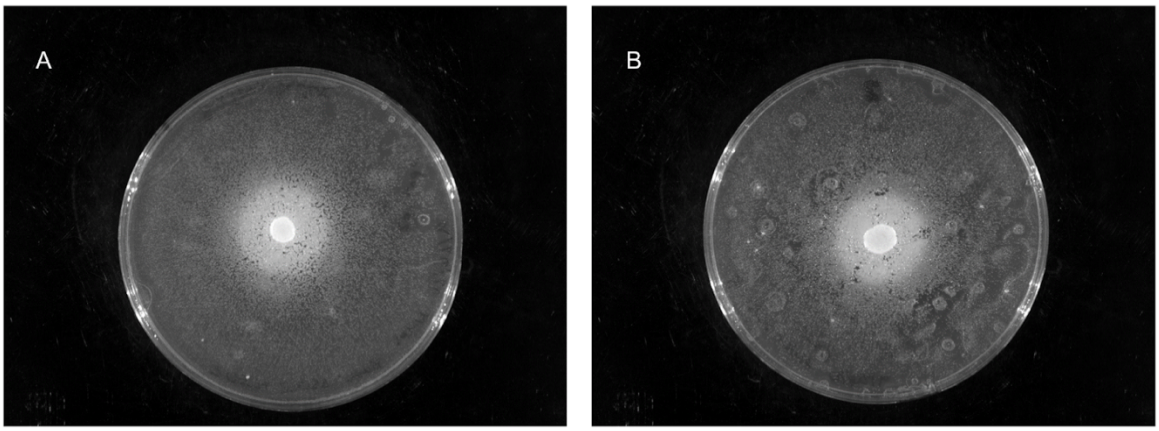

Supplemental Figure 2. Leucine limitation is important to generation of a bullseye pattern.
Increasing the concentration of leucine in the petri dishes to 0.5 mg/ml or 1 mg/ml (5x and 10x the maximal concentration in the experiments in **Figure 2**, **Figure 3**) removes the bullseye patterning, indicating that deprivation of leucine is important in generating the bullseye pattern.

Chapter 5: Regulation of invertase expression by *Saccharomyces cerevisiae* can limit cheater growth in spatially organized microbial communities

This chapter was written by Neydis Moreno Morales. Megan N. McClean provided incredibly helpful feedback. All data was collected and analyzed by Neydis Moreno Morales. Kieran Sweeney adapted the custom MATLAB script for improved image analysis used in the spot assay and provided a custom MATLAB script for parsing data from the Fluent. Kevin Stindt adapted a custom matlab script for the colony count analysis in Figure 13.

Abstract

The cooperative use of sucrose by the yeast, *Saccharomyces cerevisiae* is a popular model system to understand persistent questions about cooperativity in the microbial ecology field. Some of these questions are: How is cooperation maintained in a population? What mechanisms protect cooperation maintenance in a mixed community of cooperators and cheaters (cells which do not make invertase). Despite extensive work on this model there are still important characteristics about this model system that have not been explored in-depth. We still do not know if a population of producer cells regulate their expression during growth in sucrose media. This would be a major shift in our understanding of the popular model system, usually a cell with the ability to cooperate is assumed to cooperate constitutively when growing in sucrose. The ability to regulate invertase could be an important mechanism that supports the maintenance of cooperation in a population. An ideal tool would allow for the identification of cell genotypes (cooperator or cheater) and cell phenotypes (*active* invertase expression vs *inactive*). This would permit for the quantification of population ratios in, as well as a method for distinguishing the level of cooperation by invertase producers. This would also permit the identification of cell types in space on plates. In this chapter I present a method to visualize the *active* cooperators in a wildtype strain of S. cerevisiae using 2a peptides to achieve co-translational production of invertase and a fluorescent reporter from the respective promoter. I demonstrate that S. cerevisiae can and does regulate the expression of invertase during growth. I switch the promoters in the invertase-2A-reporter constructs to develop constitutive cooperators with different strength constitutive promoters (pREV and pPGK1). Finally, I compete these cooperator strategies with either cheaters or other cooperator types to compare the effects that invertase regulation has on cooperator and community outcomes. The results presented in this chapter suggest that the regulation of invertase expression by the wildtype cooperator cells in sucrose may have a significant impact on limiting growth of a cheater when compared to other cooperation strategies in spatially structured environments.

Introduction

Chapter 4 delved into the patterning phenomenon observed in [1] (also described in Chapter 3), where a distinct density difference appeared in the growth of co-localized cooperators (invertase driven by the wildtype pSUC2 promoter) and cheaters on a lawn, creating a "bullseye" effect (**refer to Chapter 3, Figure 5**). The model took into account the growth rates of cooperators and cheaters, as well as the production and diffusion rates of molecules that were hypothesized to be limiting nutrients, specifically sucrose, monosaccharides (glucose and fructose), and the amino acid leucine.

However, there were significant disparities between the model's predictions and the experimental results in one case. Specifically, the model failed to accurately predict how varying sucrose concentrations would affect the pattern. The model predicted that a similar "bullseye" pattern would emerge. This discrepancy was intriguing because, up until this point, the model appeared to include enough information to capture and predict growth patterns. The model had not accounted for invertase regulation; instead, much like the standard-setting work of Gore et al., cooperators were assumed to cooperate at a consistent level [2]. I wanted to revisit the possibility that wildtype cooperators may be able to regulate invertase production during growth in sucrose. Specifically, is invertase regulated in strains using the wildtype promoter (pSUC2)? How does regulation affect fitness in those strains? And when is regulation beneficial?

Previous works measured the cost to produce invertase in similar ways and concluded that the cost was constant

Gore's work was one of the earliest public goods cooperation related work that quantified biological characteristics of the system such as the glucose capture efficiency of cooperators, density-dependent fitness decreases in sucrose, and the fitness cost of producing invertase. Their subsequent works [3]–[5] all use their previous findings to develop models or interpret results.

The cost of invertase production across the public goods literature is calculated in a similar method in several works [2], [6], [7]. This is calculated by comparing the growth rates of cooperator and cheater cells in media that does not induce invertase expression for the cooperator, to growth rates in glucose concentrations that would force invertase expression in a cooperator (very low concentrations of glucose) and calculating the fitness deficit for the invertase producer (the cooperator). The costs in the previously mentioned works do vary a bit, in [2]a 2.5% growth deficit is calculated, in [6] a 4% cost is measured, and in [7] a 0.35% cost is measured, this could be due to strain differences or different concentrations of glucose being used. However, this method for calculating cost of invertase does not seem to accurately represent the reality of an invertase producing cell as it likely oversimplifies the interactions between environmental factors and biology that occur when growth occurs in sucrose. An invertase producing cell likely drives the changes of sugars in the environment as well as responds to their production when growing in sucrose. A cell with invertase regulation, in theory, could be continuously recalibrating invertase expression from changes in available glucose. A community of cooperators with the ability to regulate invertase may not be a homogeneous population of invertase expressors, rather some may cooperate and some may cheat. How regulation might affect growth dynamics has two main parts to explore. Is invertase regulation occurring? How does regulation affect community growth dynamics and composition of a cooperator-cheater community?

Invertase regulation needs to be characterized

The conflicting results between my model and the growth patterning I found in changing sucrose concentrations from chapter 4, as well as the realization that invertase regulation had been presumed to be constant in the public goods works that incorporated a model [1]-[8] caused me to ask new questions about invertase regulation. We still do not know how a population of natively-regulated invertase producing cells might distribute the labor of invertase expression in sucrose media–are all cells producing invertase at a homogenous constitutive level or could there be some heterogeneity? Perhaps some cells

take on the role of an *active* cooperator, constantly producing invertase, and a majority of cells remain *inactive*, despite genotypically being able to express invertase. There is some preliminary support from literature that invertase expression may be regulated. This literature focuses on utilizing industrial strains for invertase production in the production of biofuel relevant molecules. Nonetheless, their work suggests that regulation of invertase is taking place as the invertase activity of a culture grown in sucrose varies over time [9], [10].

Investigating the effect of invertase regulation necessitates a tool to measure active cooperators in wildtype yeast strains

In part, it is possible that regulation of invertase expression has been understudied due to a lack of tools for measuring cooperation.I did not have the tools to assess if invertase regulation is taking place and what the impact of that regulation might have on fitness and interpreting results from competition with a cheater. An ideal tool would allow for the identification of cell genotypes (cooperator or cheater) and cell phenotypes (*active* vs *inactive*). This would permit for the quantification of population ratios, as well as a method for distinguishing the level of cooperation by invertase producers.

Past public goods work has attempted to differentiate between cooperators and cheaters through the use of constitutively expressed fluorescent markers [1]-[4],[6],[7]. However, this does not give us phenotypic resolution of the invertase expression level of wildtype cooperators (expression from the pSUC2 native promoter). It is likely that a tool for measuring invertase expression from individual cells had not been developed previously due to the hurdles of tagging a secreted protein; Previous attempts to tag invertase had failed [11]–[13]. It is also the case that previous work was not interested in the effect of regulation, as discussed previously, it was treated more like a switch, expressed in the absence of glucose [1]-[7]. The methods in [8], [9], can only capture bulk, population level information and does not distinguish between the variation in *active* (cells producing invertase) that may be present within the population.

I want to show that wildtype strains are able to regulate invertase expression. I then would like to understand the role of invertase regulation in well-mixed and spatial environments. In this chapter, I first focus on the creation of essential tools that would allow me to characterize invertase regulation. I then demonstrate that invertase regulation is occurring in strains that use the native promoter pSUC2, which includes the strains that I and my colleagues in [1]-[7] use in our work. I then compare how regulation affects the growth rates in glucose and sucrose by comparing the growth rates in strains that constitutively express invertase (pSUC2 promoter swapped with pREV or pPGK1). Finally, I demonstrate that regulation may not affect growth rates in sucrose media when cheaters are present in liquid cultures. However, regulation is important in spatially organized environments. Using the spot assay from Chapter 4 we see that regulated strains (pSUC2) are able to limit cheater growth and the region where growth is limited is larger when compared to the constitutively expressing strains pREV and pPGK1.

Results

Use of 2A Peptides Allows Generation of an Invertase Expression Reporter

As mentioned previously, there are technical hurdles to creating a fluorescent reporter of invertase activity due to secretion mechanisms[11], [13]. To create a tool that can monitor the expression of invertase from individual cells without interfering with the secretion mechanism, I use 2A peptides to achieve bi-cistronic expression from one promoter. 2A peptides are short, virally derived sequences that interfere with ribosomal function. The 2A peptides contain a sequence motif of EXNPGP which causes a "stop-carry on" process at the sequence [14]. At the "G-P" junction of the PGP motif the ribosome stalls, fails to make a peptide bond, releases the upstream peptide, and continues translation resulting in the production of two functional proteins [15]. The virally-derived 2A peptides have been successfully used in yeast for metabolic engineering [16] and some efforts have been made to characterize different 2A

peptide sequences [15], [17]. There are a few reasons that 2A peptide cleavage efficiency might vary, like sequence and length [15]. Three 2A peptide sequences that were previously used in yeast [16], [17], were chosen for incorporation in the development of the bi-cistronic constructs.

The 2A peptides are referred to throughout this chapter as ERBV1, PTV, and TAV. As a control, I also made a non-functional 2A peptide; ERBV1FAIL. This peptide lacked the PGP sequence of the "EXNPGP" motif, which should result in a non-functional fusion protein. The constructs consist of one promoter (pSUC2 or pZIF), the invertase gene (SUC2) at the 5' end, followed by the 2a peptide sequence, then the fluorescent reporter (mCherry) (**Figure 1**). This organization was chosen to avoid interfering with secretory pathways as the secretion sequences are located on the 5' end of the open reading frame [18]–[20].

I measured the cleavage efficiencies via western blot to probe for cleaved (27 kDA) and uncleaved mCherry product (88 kDA) (**Figure 2**) from the pZif-SUC2-2A-mCherry construct grown in the light (expression expected) and the dark (no expression expected). The ratio of cleaved mCherry over total cleaved and uncleaved product for the three peptides were compared, and, although a one-way anova failed to reject the null hypothesis (no significant difference between means of different 2A peptide cleavage efficiencies), the ERBV1 peptide was selected for continued use because it had the highest cleavage efficiency of the three (**Figure 3**). The constructs were validated to be functional via fluorescence microscopy (**Figure 4A**) and the ability for the pSUC2 strain to express mCherry in a carbon source concentration dependent manner as would be expected (**Figure 4B**). The bi-cistronic constructs from here on will be referred to by the promoter names for ease of legibility, ie. "pSUC2".

Invertase Expression is Regulated in Media Containing Sucrose as the Sole Carbon Source

The bi-cistronic constructs with the pSUC2 was grown in 2% glucose and 2% sucrose and the resulting mCherry fluorescence was measured throughout a 40 hour time course (**Figure 5**). The expression profile over time for the pSUC2 promoter was different depending on the carbon source of the media. In glucose

media expression seemed to be constant and lower when compared to similar time point measurements in sucrose media (**Figure 5**). For comparison, a pPGK1 time course does not display regulation in a carbon source dependent manner (**Supplemental Figure 1**). In sucrose media the mCherry expression varied over time, reaching a peak around hour 12, and then decreasing. This is promising evidence that cooperator cells with pSUC2 as a promoter can and do regulate their expression throughout growth. Cells may be accumulating enough freed glucose in the media to repress some invertase expression and prevent excess, wasteful invertase. Although yeast cannot sense available sucrose [21], [22] to tune invertase expression, the responsiveness of the pSUC2 promoter to the glucose concentration in the environment could serve as a useful mechanism for cells to tune their investment of invertase production in a dynamic manner.

In order to measure how sucrose regulation affects growth dynamics such as growth rates, lag times and saturation I needed to make constitutive strains for comparison and be able to identify cooperators and cheaters.

Growth Assays Demonstrate That Constitutive Strains Have No Significant Growth Defects

I wanted to compare how the different cooperation strategies (regulated and low/high constitutive) would impact growth dynamics in glucose and whether there would be any growth defects. The cooperator strains (pSUC2, pREV, pPGK1) and the cheater strain (suc2Δ) were each subjected to a growth course over 40 hours in 2% glucose. The growth curves were plotted and fitted using the four parameter Gompertz equation (**Figure 6A**):

$$y = A \times \exp\left[-\exp\left(\frac{\mu \times \exp(1)}{A}(\lambda - x) + 1\right)\right] + N_0 \quad (1)$$

The Gompertz equation is a commonly used sigmoid curve , used to fit and describe growth data [23], [24]. Modifications to the general form have been used to describe growth phases in microbial systems

[25]–[27]. From the fitted data, model parameters were extracted including: growth rate (μ), max amplitude (A), and lag time (λ).

The growth rates in glucose of pSUC2, pREV, pPGK1, and suc2Δ were not significantly different from each other. There did not appear to be significant growth defects from invertase expression or constitutively producing invertase as the growth rates and lag times are comparable for all strains (**Figure 6B**).

Multicolor Strains Allow Distinct Cell Populations to be Identified

Additional bi-cistronic constructs were created with promoters characterized to give constitutive expression (pREV and pPGK1). These promoters were selected based on the reported level of their expression, low and high, respectively [28]. A fluorescent cheater cell (suc2Δ) lacking the invertase gene was created by incorporating an mTurquoise fluorophore. These constructs were transformed into the LEU2 locus on Chromosome III of yNM72 (table) and yNM73 via homologous recombination. yNM72 and yNM73 (Table 1), but differ in an additional constitutive fluorescent marker (mVenus). These cells could now be combined to make communities consisting of pSUC2 and constitutive invertase expression (pREV or pPGK1), or a cooperator (one of pSUC, pREV, or pPGK1) and suc2Δ (cheater)(**Figure 7**). This was possible because different combinations of fluorescent markers could be used to distinguish between cooperator types and between cooperators and cheaters (**Figure 7B-D**). I would be able to use the fluorescent reporters to collect information about the composition of the community (cooperators versus cheaters) as well as measure how the distribution of expression from the invertase reporters might vary via flow cytometry.

Regulated Strain pSUC2 Exhibits Differences in Growth Dynamics During Growth in Sucrose Compared to the Constitutive Cooperators

As described in detail in the introduction, [2] was a standard setting paper for the study of public goods. The methodology used to determine cost of invertase expression and other parameters has been adopted by subsequent works related to public goods in yeast [7], [8]. The cost of invertase expression is determined by comparing growth rates of a cheater strain in low glucose concentrations to the growth rate of a cooperator strain and the differences of growth rates in these two conditions is attributed to the burden of expressing invertase on growth rate for those individuals. This does not seem to accurately represent the environments where invertase expression would be beneficial and relevant for the pSUC2 strain. In order to compare how regulation affects growth dynamics in sucrose we repeated the growth curves for each of our cooperator and cheater strains this time in sucrose which should also allow invertase producing yeast to benefit from their expression and reflect more accurately how invertase expression affects growth in sucrose (**Figure 8**).

Growth rates in sucrose were lower than the growth rates in glucose for each respective strain (**Figure 6B**). This is to be expected, likely caused by a slow-down of growth due to the delay of converting sucrose into the necessary monosaccharides for growth. The growth rates in sucrose of pSUC2 decreased significantly and the lag times increased when compared to growth rates in glucose which might demonstrate the additional burden that the pSUC strain has when tasked with making invertase. Another interesting observation is the growth dynamics in sucrose of the constitutive cooperator strain pPGK1 (**Figure 8 A-B**). The growth rate for this strain is significantly lower in sucrose. It is possible that, while the strain benefitted from a smaller lag in growth due to high constitutive expression of invertase, that same high expression was burdensome to the cells. Invertase expression perhaps has a saturating effect, where more invertase does not result in faster conversion of sucrose into monosaccharides, and so does not contribute to increasing the growth rate. However, constitutive high expression permitted this strain to

begin growth sooner, likely due to higher total invertase activity from the same number of cells. Although the growth rate and lag times for the suc2Δ strain are not accurately captured by the Gompertz equation (**Supplemental Figure 15**) it is worth noting that the suc2Δ strain eventually experienced growth in sucrose, which we did not expect, (after a lag of ~ 20 hours). It is possible that the suc2Δ strain was able to use much less efficient metabolic pathways. Some yeast strains have demonstrated the ability to import sucrose and utilize maltase internally [29], [30]. It is also possible that other chemical processes occurred in the media at the time due to the heat and time, resulting in the breakdown of sucrose into necessary monosaccharides which could be tested in future experiments.I do not suspect contamination as the mTurquoise in those wells corresponded well to the growth observed in those wells which indicates the growth observed in those wells is due to suc2Δ.

Growth Assays Demonstrate That Regulated Invertase Expression Allows Yeast to Follow A Cost-Conscious Strategy When Competing with Cheaters

Next, I wondered how invertase regulation might impact the growth dynamics of strains when growing in competition with cheaters (suc2Δ). In a similar manner as the previously described growth assays a cooperator (either pSUC2, pREV or pPGK1) and a suc2Δ cheater were combined at equal starting ratios and allowed to grow for over 40 hours in either 2% glucose or 5% sucrose. The growth curves were then plotted and fitted using the four parameter Gompertz equation.

It appears that pSUC2 is able to pick their investment based on glucose availability in response to glucose availability which is expected (**Figure 9**). This is observed with a difference between the glucose growth rate of the pSUC2 strain in competition when compared to the other cooperator-cheater pairs (**Figure 8A**). The growth rate for that community was more comparable to the growth rate of individual strains grown in glucose and was significantly different from cooperator-cheater pairs grown in sucrose (**Figure 8A**). This data suggests that the ability of pSUC2 to tune invertase expression in response to their

environment (glucose concentration) is favorable to constitutive expression when competing with cheaters. This seems to be due to the burden experienced by the constitutive strains to make unnecessary invertase.

Co-cultures in sucrose had longer lag times when compared to individual strains, which might be explained by a slowdown of growth due to competition for limiting monosaccharides caused by cheater presence (**Figure 8B**). An alternative explanation may be that there are similar total number of cells in these instances but a smaller proportion of cooperators resulting in less glucose produced in the same time period, which then affects when these cultures can grow. This can also help to explain the longer lag time and higher variability observed in the pSUC2 cooperator-cheater cultures because of the delay due to the time for pSUC2 to begin expressing invertase and accumulate sufficient glucose for growth.

Weeklong Competitions Between Cooperator-Cheater Communities Reveal That Communities with Regulated pSUC2 Cooperators Reach Similar Community Compositions to Communities with Constitutive pREV Cooperators

The work in [2] was also one of the first to demonstrate that the *Saccharomyces cerevisiae* public goods model system could follow snowdrift game rules, as opposed to prisoner's dilemma. In a snowdrift game, cooperation can be maintained at some frequency within the population. I wanted to compare how regulation affects the equilibrium composition of cooperator-cheater communities. [2] previously demonstrated that cheaters reached a steady state by the fifth day of competition following a ~23 hour growth-dilution cycles. These competitions found that the pSUC2-cheater composition had reached a majority of cheater cells (0.7) and that a relatively small fraction of pSUC2 cooperators (0.3) were necessary to maintain the population at steady-state. I repeated their experiments with my pSUC2 and constitutive strains expecting to see similar proportions for the pSUC2 co-culture and to compare the results to the composition of the low/high constitutive cooperator-cheater cultures. The proportions in

the competition experiments after 7 days of growth and dilution were the opposite of my expectations for the wildtype strain (pSUC2). I did not observe a steady-state equilibrium even after seven days. In addition the cooperators were a majority of the population (~0.67) and cheaters were a minority (~0.33) (**Figure 10**). Although, [2] and I did not use the exact same strains, my results were unexpected. The constitutive strains followed the same trends as pSUC2 with cooperators in the majority. pREV was more comparable to the fractions reached by pSUC2 (~0.69), which was expected based on their comparable levels of mCherry expression (**Figure 7D**) and similar lag times (**Figure 8**). pPGK1 had the highest ratios (~0.77) which leads me to wonder if other factors may be at play that make pPGK1 a competitive strain despite a perceived burden from high expression of invertase. If cells are able to break down more sucrose locally (due to more invertase per cell), perhaps other characteristics such as glucose capture efficiencies would be affected and would need to be measured.

The Ratio Reached by Regulated Strain pSUC2 in Weeklong Competitions Between Cooperators Depends on the Cooperator Pairing

In the growth assays of cooperator-cheater pairs I demonstrated that regulated invertase expression allows yeast to follow a cost-conscious strategy when competing with cheaters. Specifically, that regulation allowed pSUC2 to not express invertase unnecessarily when growing with cheaters in glucose which resulted in higher growth rates for these cultures. I wanted to compare how the composition of communities for competing cooperators might be affected by the ability of pSUC2 to regulate expression in response to glucose. I expected that a pSUC2 strain might be able to take the "rare strategy" in competition and in the presence of obligate cooperators would be able to cheat like an obligate cheater (suc2Δ). This expectation is based on previous theories that the *Saccharomyces cerevisiae* public goods cooperation follows snowdrift game rules [2] although, it has not been demonstrated experimentally. In this case, I expected to see the pSUC2 strain able to reach proportions that the suc2Δ reached in the

previous set of experiments (**Figure 10A**). This seemed to be the case. When the high constitutive cooperator (pPGK1) was present in competition with the regulated pSUC2, the "cooperator" pPGK1 was in the majority after a week of growth (~0.67). As was the case in the previous section, the pSUC2 and pREV cooperators seem to be fairly comparable to each other. Their competition reached an equilibrium ratio closer to that of the starting ratio (50:50), with pSUC2 having a slightly higher proportion (~0.54) (**Figure 10B**). This increase when compared to the ratio of the suc2Δ strain in the pREV-suc2Δ community could be explained with it being beneficial for pSUC2 to be a cooperator with the benefit of pREV providing constitutive (but low) cooperativity from expression of invertase.

Interestingly, pPGK1 was also a better performer (~0.69) when competing with the other constitutive cooperator pREV. This may be further support that higher expression of invertase resulted in an unexpected trait improvement, such as, preferential glucose access.

Invertase Regulation Limits Cheater Growth in Spatially Organized Environments

Previously, we described the spot assay, this was a method to compete cooperators and cheaters (suc2Δ) in a spatially structured way [1](also see,chapter 3). The growth of the cells would result in a characteristic bullseye pattern with variations in the density and distances of the regions (**refer to Figure 5 in chapter 3**). These regions were: "spot", where cooperators were placed on the plate, a "ring" of more dense growth located at a distance from the spot, and a "valley" which described the region in-between the spot and the ring, with less dense growth (**Figure 11**). I wanted to repeat these experiments with the addition of the constitutive cooperators. How would the absence of regulation impact the pattern's features? I wondered if the ability to regulate invertase by pSUC2 would be a beneficial trait when the environment for competition was spatially structured since pSUC2 may be able to concentrate local glucose concentrations and limit nearby cheater growth.

Qualitatively there are some clear differences in the bullseye pattern and density of growth in those regions between each of the cooperators (**Figure 11A**). I used an improved version of the custom matlab script to analyze the images and identify the regions on the plate (**Figure 11 B-C**). The average lengths of these features (measured from the center of the plate) as well as the intensities were quantified (**Figure 12**).

There does appear to be a benefit to regulation of invertase in spatially structured environments. However, it is necessary to compare both the distances of the features as well as the densities of those regions together to form a complete picture. The growth inhibition zone [1] (ie. valley) was affected by the type and levels of cooperation in a cooperator dependent manner. It would appear that pPGK1 is able to have a larger growth inhibition zone and may be better in limiting cheater growth followed by pSUC2 then pREV (**Figure 12 A**). This is not the case, when the intensity information is incorporated into the interpretation of this data. The regulated cooperator pSUC2 had less dense growth in both the ring and valley region than pPGK1 and pREV (**Figure 12 B**). pSUC2 also had a longer valley region than pREV. Combining the information from these measurements (length and density) supports my original hypothesis that regulation of invertase is advantageous when competing in a spatially structured environments. The regulation of invertase may allow pSUC2 strains to create an environment where nearby cheater growth is limited, in addition to limiting total cheater growth. In spatially structured environments due to the differences in diffusion and segregation of the cells, regulation may result in higher local concentrations of glucose, which in response would result in reduced expression of invertase. This would limit the rate of sucrose conversion and the availability of glucose for nearby cheater cells. The co-localization of regulated cooperators at the spot would provide preferential access to glucose and other limiting nutrients, as was discussed in chapter 4, as it would for the other cooperators. A preliminary experiment where the method for spatial organization of cooperators and cheaters resulted in individual colonies serves as additional support for this hypothesis. The distances between cooperator colonies and

cheater (suc2Δ) colonies were slightly longer when compared to pPGK1 (**Figure 13**), although more validation and replicates are necessary for this experiment.

In addition, the pSUC2 benefits from the ability to regulate in response to environmental glucose potentially explaining the differences we see with the constitutive cooperator strains as they are not able to pause or reduce their cooperativity (in other words their invertase expression). pPGK1 for example, is able to grow without much of a lag on sucrose media (**Figure 8B**). The high constitutive expression paired with the short lag is likely able to support faster growth of nearby cheaters and results in more total growth of cheaters and support cheater growth at larger distances. pREV supports more growth than the pSUC2 and pPGK1 and at shorter distances. I believe pREV has two hindrances in a spatial environment, it grows slower (**Figure 8B**) when transferred to sucrose, so it does not use limiting resources quickly, and it also provides glucose constantly rather than in a regulated manner. In conclusion, it appears to be beneficial to regulate expression of invertase in a spatially structured environment when compared to constitutive expression.

Discussion

I demonstrated that the wildtype promoter, pSUC2, results in regulation of invertase expression during growth in sucrose (**Figure 5**). This was possible because our invertase reporter allowed us to identify *active* cooperators in a population by measuring mCherry fluorescence. This is an exciting result as previous public goods work had not considered regulation as a property that cooperators could tune during growth or competition. Rather the cost of producing invertase was represented as a constant property when competing with cheaters [2], [6], [7], [31] (also see Chapter 1, Table 1). I was also able to visualize invertase expression more quickly and more directly than measuring the invertase activity of a population as previous works had done [9], [10] .

When is regulation beneficial? One clear advantage to invertase regulation was observed in the spot assay competitions (**Figure 11A, 12**). pSUC2 fared better in terms of creating a clearance zone, where less cheat growth was supported, and in terms of supporting less cheat growth throughout the plate. Regulation is likely to benefit from the spatial environment because cooperators are able to benefit from co-localization, this has been observed in a previous work where clumps of cooperators were able to outcompete cheaters in well-mixed environments [7]. In addition, the unique properties of a spatial environment might favor regulation such as differences in diffusion, organization of cells and the ability to tune invertase expression in response to local glucose concentrations. The properties of a spatial environment and their effects on microbial communities are explored in chapter 4 and across several works involving experimental systems and theory [8], [31]–[36]. There is a small caveat to consider when interpreting the results from the plate images. Intensity is not a direct proxy for growth, it is more of an approximation. In the future it may be necessary to develop more quantitative methods if warranted (absolute cell counts, for example). It might also be interesting to incorporate invertase regulation into the model described in chapter 4 and see how the results align with the experimental conditions tested here, but this was outside the scope of the questions we seeked to answer in this chapter.

Regulation had some small effects on growth dynamics. In alignment with our expectations, being able to "turn off" the burden of invertase expression in glucose media when co-cultured with cheaters was advantageous for the growth rates of the population (**Figure 9A**). The growth rate in this co-culture case was remarkably similar to individual strains grown in glucose (**Figure 6B**). Besides the longer lag observed in the sucrose competition assay (**Figure 9B**), due to the delay in expression and accumulation of invertase, regulation did not appear to have any discernible advantages or disadvantages in well-mixed environments. It would be interesting for future work to explore how the growth dynamics of these competitions would change for the regulated strain when being transferred directly from growth in

sucrose or other glucose poor conditions. I might expect that this would affect the ability of the population to begin growth sooner.

I was able to explore how community composition might be affected by regulation (**Figure 10**). My approach to identifying cooperators and differentiating between cooperator types and cheaters made that possible (**Figure 7**). Although the composition of my communities after seven days did not agree with past works [2], [3] I did observe some interesting trends. The composition of the regulated communities seemed more comparable to the fractions reached by the pREV cooperator and suc2Δ when competing with the pPGK1 cooperator. This was in agreement with my expectations that pREV and pSUC2 exhibited similar mCherry expression levels, and that pSUC2 may behave more like a cheater when co-cultured with another cooperator. Additionally, when pREV and pSUC2 were in competition they were able maintain a more even composition.

I did not expect the high constitutive cooperator (pPGK1) to fare as well as it did. In well-mixed conditions it seemed to have an advantage over other cooperation styles, both when competing with cheaters and other cooperators (**Figure 10**). One possibility, is that high expression of invertase improved the ability of pPGK1 to capture more released glucose, and grow better. [37] hypothesized that to utilize a scarce public good this might be a strategy that yeast would evolve. This was one of the strategies that was evolved, other strategies included increased expression of hexose importer proteins, or became clumpier [37]. Future work would benefit from measuring the properties of the three cooperator strains, that being invertase activity, glucose capture efficiencies to understand why increased invertase expression seemed so beneficial to the cooperator in well-mixed conditions. The invertase activity could be measured through the use of commercially available kits to measure invertase activity (Abcam cat# 197005). Glucose capture efficiencies for each cooperator could be measured using methods like the one used here [2].

The work presented here gives us a small sampling of the ways that invertase regulation might affect cooperativity in different environments. More work is needed to understand when regulation is beneficial,

here pSUC2 strains were growing in glucose before transferring in sucrose. It is possible that the outcomes in population would have looked different if the population of cooperators-cheaters had *active* cooperators when the competition began. The methods developed here would allow for a deeper investigation on other properties of invertase regulation like the ability to form a nutrient memory. The galactose pathway is another regulated system for the use of alternative carbon sources (galactose). Previous work has demonstrated interesting behavior in this pathway's ability to anticipate nutrient changes in the environment [38], [39]. Interesting questions abound regarding the effects and mechanisms of invertase regulation. It is exciting to think about the works to come.

Methods

Yeast Strains and Culture Methods

Yeast strains used in this study are shown in **Table 1**. Yeast transformation was accomplished using standard lithium-acetate transformation. For integrating plasmids, the integration was validated using either colony PCR or, when colony PCR proved difficult, by PCR of genomic DNA. Genomic DNA was extracted using the Bust n' Grab protocol. Primers used for constructing the 2A peptide sequences are listed in **Table 2**. All transformants were checked for the petite phenotype by growth on YEP-glycerol (1% w/v Bacto-yeast extract-BD Biosciences 212750, 2% w/v Bacto-peptone-BD Biosciences 211677, 3% [v/v] glycerol-Fisher Bioreagents BP229-1, 2% w/v Bacto-agar-BD Biosciences #214030)[22]. Only strains deemed respiration competent by growth on YEP-glycerol were used for subsequent analysis.

Yeast cultures were grown in Synthetic Complete (SC) media (6.7 g/L Yeast Nitrogen Base without amino acids-DOT Scientific, 1% v/v KS amino acid supplement without appropriate amino acids).The carbon source supplied was either dextrose (D) at 2% v/v (unless otherwise indicated) or sucrose (SUC) at 2%, or 5% v/v concentration (unless otherwise indicated).

Blue light induction of yeast cultures in liquid media

For blue light induction experiments were grown in 24 well plates (Arctic White, #AWLS-303008) and placed on a light plate apparatus (LPA) [40]. The light output of all light sources was measured and validated with a standard photodiode power sensor (Thorlabs, #S120VC) and power meter (Thorlabs, #PM100D). All cultures were grown in a 30° incubator with agitation. Biological replicates were picked from a single colony on a YPD plate and transferred to YPD media. The cells were grown to saturation in the dark. 1.5 mL of the saturated cultures were pelleted by centrifuge (Eppendorf, #EP5401000137), washed twice and resuspended in sterile MilliQ water to wash out residual media. The yeast cultures were diluted to an OD600 of 0.05 in SC-SUC and divided into 12 wells of a 24 well plate for a total culture volume of 2mL. A glass bead (Fisher Scientific, #11- 312B 4mm) was placed in each well to increase aeration and a breathable sealing membrane was used to cover the top of the plate (USA Scientific ,#9123-6100).

Western Blots

A standard western blot protocol was followed, with details following closely to the protocol located here [41]. Preparation of protein extract followed standard NaOH protocols. Whole cell lysate samples were thawed on ice then spun down at 1320 RPM for 5 minutes. The samples were loaded on a 4-12% Bis-tris gel and run for about an hour, until the dye front began to run out. The gel was transferred onto a PDMS blot. The iBlot2 Dry blotting system was used to transfer on the blot. *Probe:* Anti-mcherry antibody ab167453 (Abcam). *Imaging:* Diluted imaging substrate by 1:10, incubated blot for 5 minutes before imaging. Blot was stored on TBST o/n then stripped before blocking and probing for loading controls, beta-actin.Whole cell lysate samples were thawed on ice then spun down at 1320 RPM for 5 minutes. The samples were loaded on a 4-12% Bis-tris gel and run for about an hour, just until the dye front began to run out. To transfer the gel onto a PDMS blot the iBlot2 Dry blotting system was used. Antibodies were saved with 1% sodium azide and for re-use. Diluted imaging substrate by 1:10, incubated blot for 5

minutes before imaging. Blot was stored on TBST overnight and stripped before blocking and probing for loading controls, beta-actin.

Flow cytometry

All mCherry fluorescence data shown was acquired with an Attune NxT flow cytometer. Calibration of voltages was done using BD Sphero Rainbow beads (Thermofischer cat #556286) The mCherry data was acquired using a 620/15 nm filter and excitation at 561 nm. The mTurq data was acquired using a 440/50 nm filter and excitation at 405 nm.The mVenus data was acquired using a 590/40 nm filter and excitation at 488 nm. All yeast samples were prepared for flow cytometry by adding 50 uL yeast culture to 150 uL PBS + 0.1% Tween over ice. All flow cytometry acquisitions included at least 20,000 initial events that were gated to remove debris and isolate single cells. Median mCherry, mTurq and mVenus fluorescence for each gated sample was calculated in FlowJo.

Growth curves

Yeast strains used in the growth curve experiments can be found in Table 1. A single colony was picked from a plate and inoculated into a culture tube with 5mL of YPD media. The cell was cultured overnight in a rotating drum at 30℃. To remove any residual glucose 1mL of the yeast strain was pelleted, and washed three times in Synthetic media without carbon or amino acids added. The yeast culture was then diluted to an OD600 concentration of 0.003 in either 5% sucrose or 2% glucose. 200 µL of yeast culture was transferred into a 96-well plate, in triplicate. To avoid edge-effects the 36 perimeter wells were filled with water or media blanks. The plate was transferred to the Fluent for growth. The Fluent consists of a Bioshakes component that regulates temperature and shakes to provide a well-mixed environment. A plate reader for Optical density measurements and fluorescent readings, and the robotic components and software to move the plate between different elements of the fluent. A custom fluent script was used to measure the OD600 and fluorescent channels (mCherry, mTurquoise, mVenus) every 30 minutes for the duration of the experiment. A custom matlab script is then used to parse out the data for

quantification. Competition growth curves were performed in almost an identical manner, with the addition of combination of the respective strains in a 50:50 ratio by first diluting each individual culture to an OD600 value of 0.5 combining in equal volumes and then proceeding to dilute to the starting OD600 of 0.003.

Competition experiments (composition at 7 days)

The work by [2] informed our experimental design as I wanted to be able to compare my results to this work, and gain new insights into invertase regulation by comparing the differences in equilibrium compositions with the equilibrium composition reached when the cooperation was constitutive. Yeast strains (can be found in Table 1) were picked from a single colony and allowed to grow in YPD overnight. To remove residual glucose 1mL of culture was pelleted and washed as described in the preceeding section. Cheater and cooperators (or cooperator and cooperator) were then combined in a 50:50 ratio (using OD600 measurements) and diluted to a seeding density of 0.003. These competition experiments were carried out in 5mL culture tubes in 5% sucrose in triplicate. A 50 µL sample was taken and diluted into PBS as described in the flow cytometry section. Serial dilutions of the cultures were carried out by diluting to the starting density of 0.003 with new media. This process was repeated over seven days.

Spot assay Patterning

The spot assay was performed as previously described in chapter 3 and 4, and [1] with the corresponding cooperator and cheater strains listed within the chapter and listed in Table 1.

Quantification of Plate Growth

Radial intensity traces of patterned plates were calculated using a custom MATLAB Script, previously described in chapter 3, and 4. Improvements were made in the algorithm to center the image on the central spot which improves the measurements from the clockscan function. The spot start, ring peak and ring trough are found as previously described. The valley trough is a new feature which is defined as the point located midway between the valley trough and the ring peak height, this results in better feature

detection. Lastly, a greatly improved feature is the ability to use the features to measure the intensities directly from the images.

Colony count assays

Strains used in the colony count assay (pPGK1 & pSUC2, Figure 13) were grown overnight, washed, pelleted and resuspended in sucrose media as described in Growth assays section. The strains were diluted to an OD600 of 0.003 and plated onto SC-Suc agar plates. They were incubated at room temperature for four days and imaged on a Zeiss Axio Zoom stereoscope at the Newcomb imaging center. A custom matlab script was adapted and used to segment individual cells and then cells were identified by their fluorescent channels. Cheaters would be present in the mTurquoise image, all cells would be mVenus fluorescent, the corresponding absence of mTurquoise could be used to identify cooperators. pSUC2 mCherry fluorescence was dim, and hard to capture by the imaging modality. pPGK1 did have enough signal to identify cooperators by mCherry fluorescence, but in order to maintain consistency, cells were identified in the former way.

References

[1] N. Moreno Morales, M. T. Patel, C. J. Stewart, K. Sweeney, and M. N. McClean, “Optogenetic Tools for Control of Public Goods in Saccharomyces cerevisiae,” *mSphere*, vol. 6, no. 4, p. e0058121, Aug. 2021, doi: 10.1128/mSphere.00581-21.

[2] J. Gore, H. Youk, and A. van Oudenaarden, “Snowdrift game dynamics and facultative cheating in yeast,” *Nature*, vol. 459, no. 7244, pp. 253–256, May 2009, doi: 10.1038/nature07921.

[3] A. Sanchez and J. Gore, “Feedback between Population and Evolutionary Dynamics Determines the Fate of Social Microbial Populations,” *PLOS Biol.*, vol. 11, no. 4, p. e1001547, Apr. 2013, doi: 10.1371/journal.pbio.1001547.

[4] “Generic Indicators for Loss of Resilience Before a Tipping Point Leading to Population Collapse | Science.” https://science.sciencemag.org/content/336/6085/1175.long (accessed May 29, 2020).

[5] H. Celiker and J. Gore, “Competition between species can stabilize public-goods cooperation within a species,” *Mol. Syst. Biol.*, vol. 8, p. 621, Nov. 2012, doi: 10.1038/msb.2012.54.

[6] R. C. MacLean, A. Fuentes-Hernandez, D. Greig, L. D. Hurst, and I. Gudelj, “A Mixture of ‘Cheats’ and ‘Co-Operators’ Can Enable Maximal Group Benefit,” *PLOS Biol.*, vol. 8, no. 9, p. e1000486, Sep. 2010, doi: 10.1371/journal.pbio.1000486.

[7] J. H. Koschwanez, K. R. Foster, and A. W. Murray, “Sucrose utilization in budding yeast as a model for the origin of undifferentiated multicellularity,” *PLoS Biol.*, vol. 9, no. 8, p. e1001122, Aug. 2011, doi: 10.1371/journal.pbio.1001122.

[8] R. J. Lindsay, B. J. Pawlowska, and I. Gudelj, “When increasing population density can promote the evolution of metabolic cooperation,” *ISME J.*, vol. 12, no. 3, Art. no. 3, Mar. 2018, doi: 10.1038/s41396-017-0016-6.

[9] C. I. S. Rodrigues, A. Wahl, and A. K. Gombert, “Aerobic growth physiology of Saccharomyces cerevisiae on sucrose is strain-dependent,” *FEMS Yeast Res.*, vol. 21, no. 3, p. foab021, Apr. 2021, doi: 10.1093/femsyr/foab021.

[10] C. Herwig, C. Doerries, I. Marison, and U. von Stockar, “Quantitative analysis of the regulation scheme of invertase expression in Saccharomyces cerevisiae,” *Biotechnol. Bioeng.*, vol. 76, no. 3, pp. 247–258, Nov. 2001.

[11] J. Li, H. Xu, W. E. Bentley, and G. Rao, “Impediments to Secretion of Green Fluorescent Protein and Its Fusion from Saccharomyces cerevisiae,” *Biotechnol. Prog.*, vol. 18, no. 4, pp. 831–838, doi: 10.1021/bp020066t.

[12] S. Gal and N. V. Raikhel, “A carboxy-terminal plant vacuolar targeting signal is not recognized by yeast,” *Plant J.*, vol. 6, no. 2, pp. 235–240, 1994, doi: 10.1046/j.1365-313X.1994.6020235.x.

[13] I. Kunze *et al.*, “The green fluorescent protein targets secretory proteins to the yeast vacuole,” *Biochim. Biophys. Acta BBA - Bioenerg.*, vol. 1410, no. 3, pp. 287–298, Mar. 1999, doi: 10.1016/S0005-2728(99)00006-7.

[14] P. Sharma, F. Yan, V. A. Doronina, H. Escuin-Ordinas, M. D. Ryan, and J. D. Brown, “2A peptides provide distinct solutions to driving stop-carry on translational recoding,” *Nucleic Acids Res.*, vol. 40, no. 7, pp. 3143–3151, Apr. 2012, doi: 10.1093/nar/gkr1176.

[15] Z. Liu *et al.*, “Systematic comparison of 2A peptides for cloning multi-genes in a polycistronic vector,” *Sci. Rep.*, vol. 7, no. 1, p. 2193, May 2017, doi: 10.1038/s41598-017-02460-2.

[16] J. Beekwilder *et al.*, “Polycistronic expression of a β-carotene biosynthetic pathway in Saccharomyces cerevisiae coupled to β-ionone production,” *J. Biotechnol.*, vol. 192, pp. 383–392, Dec. 2014, doi: 10.1016/j.jbiotec.2013.12.016.

[17] T. M. Souza-Moreira *et al.*, “Screening of 2A peptides for polycistronic gene expression in yeast,” *FEMS Yeast Res.*, vol. 18, no. 5, Aug. 2018, doi: 10.1093/femsyr/foy036.

[18] R. Taussig and M. Carlson, “Nucleotide sequence of the yeast SUC2 gene for invertase,” *Nucleic Acids Res.*, vol. 11, no. 6, pp. 1943–1954, Mar. 1983, doi: 10.1093/nar/11.6.1943.

[19] D. Perlman, P. Raney, and H. O. Halvorson, “Mutations affecting the signal sequence alter synthesis and secretion of yeast invertase,” *Proc. Natl. Acad. Sci. U. S. A.*, vol. 83, no. 14, pp. 5033–5037, Jul. 1986, doi: 10.1073/pnas.83.14.5033.

[20] C. A. Kaiser and D. Botstein, “Secretion-defective mutations in the signal sequence for Saccharomyces cerevisiae invertase,” *Mol. Cell. Biol.*, vol. 6, no. 7, pp. 2382–2391, Jul. 1986, doi: 10.1128/mcb.6.7.2382-2391.1986.

[21] L. Neigeborn and M. Carlson, “Genes Affecting the Regulation of SUC2 Gene Expression by Glucose Repression in SACCHAROMYCES CEREVISIAE,” *Genetics*, vol. 108, no. 4, Art. no. 4, Dec. 1984.

[22] Ö. Kayikci and J. Nielsen, “Glucose repression in Saccharomyces cerevisiae,” *FEMS Yeast Res.*, vol. 15, no. 6, p. fov068, Sep. 2015, doi: 10.1093/femsyr/fov068.

[23] K. M. C. Tjørve and E. Tjørve, “The use of Gompertz models in growth analyses, and new Gompertz-model approach: An addition to the Unified-Richards family,” *PLOS ONE*, vol. 12, no. 6, p. e0178691, Jun. 2017, doi: 10.1371/journal.pone.0178691.

[24] C. P. Winsor, “The Gompertz Curve as a Growth Curve,” *Proc. Natl. Acad. Sci. U. S. A.*, vol. 18, no. 1, pp. 1–8, Jan. 1932.

[25] A. M. Gibson, N. Bratchell, and T. A. Roberts, “Predicting microbial growth: growth responses of salmonellae in a laboratory medium as affected by pH, sodium chloride and storage temperature,” *Int. J. Food Microbiol.*, vol. 6, no. 2, pp. 155–178, Mar. 1988, doi: 10.1016/0168-1605(88)90051-7.

[26] R. L. Buchanan, “Using Spreadsheet Software for Predictive Microbiology Applications,” *J. Food Saf.*, vol. 11, no. 2, pp. 123–134, 1990, doi: 10.1111/j.1745-4565.1990.tb00045.x.
[27] R. L. Buchanan, R. C. Whiting, and W. C. Damert, “When is simple good enough: a comparison of the Gompertz, Baranyi, and three-phase linear models for fitting bacterial growth curves,” *Food Microbiol.*, vol. 14, no. 4, pp. 313–326, Aug. 1997, doi: 10.1006/fmic.1997.0125.
[28] M. E. Lee, W. C. DeLoache, B. Cervantes, and J. E. Dueber, “A Highly Characterized Yeast Toolkit for Modular, Multipart Assembly,” *ACS Synth. Biol.*, vol. 4, no. 9, pp. 975–986, Sep. 2015, doi: 10.1021/sb500366v.
[29] C. Gonçalves, M. Marques, and P. Gonçalves, “Contrasting Strategies for Sucrose Utilization in a Floral Yeast Clade,” *mSphere*, vol. 7, no. 2, p. e0003522, Apr. 2022, doi: 10.1128/msphere.00035-22.
[30] A. Geber, P. R. Williamson, J. H. Rex, E. C. Sweeney, and J. E. Bennett, “Cloning and characterization of a Candida albicans maltase gene involved in sucrose utilization,” *J. Bacteriol.*, vol. 174, no. 21, pp. 6992–6996, Nov. 1992, doi: 10.1128/jb.174.21.6992-6996.1992.
[31] J. D. Van Dyken, M. J. I. Müller, K. M. L. Mack, and M. M. Desai, “Spatial Population Expansion Promotes the Evolution of Cooperation in an Experimental Prisoner’s Dilemma,” *Curr. Biol.*, vol. 23, no. 10, pp. 919–923, May 2013, doi: 10.1016/j.cub.2013.04.026.
[32] S. D. Allison, “Cheaters, diffusion and nutrients constrain decomposition by microbial enzymes in spatially structured environments,” *Ecol. Lett.*, vol. 8, no. 6, pp. 626–635, 2005, doi: 10.1111/j.1461-0248.2005.00756.x.
[33] B. Allen, J. Gore, and M. A. Nowak, “Spatial dilemmas of diffusible public goods,” *eLife*, vol. 2, p. e01169, Dec. 2013, doi: 10.7554/eLife.01169.
[34] A. E. Blanchard and T. Lu, “Bacterial social interactions drive the emergence of differential spatial colony structures,” *BMC Syst. Biol.*, vol. 9, no. 1, p. 59, Sep. 2015, doi: 10.1186/s12918-015-0188-5.
[35] P. Breugelmans, K. B. Barken, T. Tolker-Nielsen, J. Hofkens, W. Dejonghe, and D. Springael, “Architecture and spatial organization in a triple-species bacterial biofilm synergistically degrading the phenylurea herbicide linuron,” *FEMS Microbiol. Ecol.*, vol. 64, no. 2, pp. 271–282, May 2008, doi: 10.1111/j.1574-6941.2008.00470.x.
[36] J. M. Chacón, W. Möbius, and W. R. Harcombe, “The spatial and metabolic basis of colony size variation,” *ISME J.*, vol. 12, no. 3, Art. no. 3, Mar. 2018, doi: 10.1038/s41396-017-0038-0.
[37] J. H. Koschwanez, K. R. Foster, and A. W. Murray, “Improved use of a public good selects for the evolution of undifferentiated multicellularity,” *eLife*, vol. 2, p. e00367, Apr. 2013, doi: 10.7554/eLife.00367.
[38] O. S. Venturelli, I. Zuleta, R. M. Murray, and H. El-Samad, “Population Diversification in a Yeast Metabolic Program Promotes Anticipation of Environmental Shifts,” *PLOS Biol.*, vol. 13, no. 1, p. e1002042, Jan. 2015, doi: 10.1371/journal.pbio.1002042.
[39] S. R. Stockwell, C. R. Landry, and S. A. Rifkin, “The yeast galactose network as a quantitative model for cellular memory,” *Mol. Biosyst.*, vol. 11, no. 1, pp. 28–37, Jan. 2015, doi: 10.1039/c4mb00448e.
[40] K. P. Gerhardt *et al.*, “An open-hardware platform for optogenetics and photobiology,” *Sci. Rep.*, vol. 6, p. 35363, Nov. 2016, doi: 10.1038/srep35363.
[41] J. P. Dexter, P. Xu, J. Gunawardena, and M. N. McClean, “Robust network structure of the Sln1-Ypd1-Ssk1 three-component phospho-relay prevents unintended activation of the HOG MAPK pathway in Saccharomyces cerevisiae,” *BMC Syst. Biol.*, vol. 9, no. 1, p. 17, Mar. 2015, doi: 10.1186/s12918-015-0158-y.
[42] “Part:BBa K2110012 - parts.igem.org.” http://parts.igem.org/Part:BBa_K2110012 (accessed Apr. 30, 2023).
[43] S. Partow, V. Siewers, S. Bjørn, J. Nielsen, and J. Maury, “Characterization of different promoters for designing a new expression vector in Saccharomyces cerevisiae,” *Yeast*, vol. 27, no. 11, pp. 955–964, 2010, doi: 10.1002/yea.1806.

[44] L. Xiong, Y. Zeng, R.-Q. Tang, H. S. Alper, F.-W. Bai, and X.-Q. Zhao, “Condition-specific promoter activities in Saccharomyces cerevisiae,” *Microb. Cell Factories*, vol. 17, no. 1, p. 58, Apr. 2018, doi: 10.1186/s12934-018-0899-6.

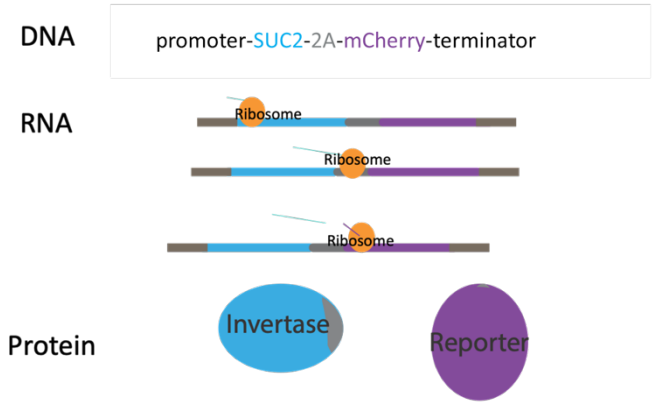

Figure 1. Bi-cistronic expression through the use of a 2A peptide

Graphic represents the bi-cistronic expression process using a 2A peptide to create an invertase reporter

The DNA construct includes the desired promoter followed by the invertase gene (SUC2), the 2A peptide and mCherry (reporter of invertase). During translation the ribosome is demonstrated moving along the DNA sequence, upon reaching the 2A peptide the upstream sequence is released by the ribosome and translation continues. This results in the production of 2 function proteins from one promoter.

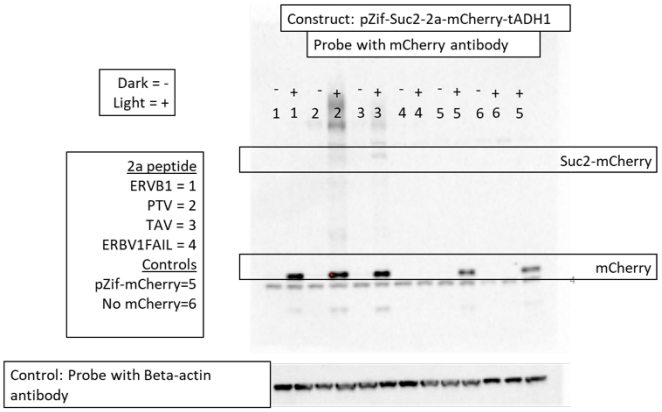

Figure 2. Probing for cleaved mCherry on a Western blot can be used to quantify cleavage efficiencies

Cleavage efficiencies of 2A peptides are measured by probing for mCherry via western blot

The construct pZIF-SUC2-2A-mCherry-tADH1 was made with the 2A peptide being: ERBV1, TAV, and, PTV.Cells were induced with constant light, or darkness. Whole cell lysates were probed for mCherry and β-actin as a control. There is significant expression from the functional 2A peptides and controls in the light conditions.

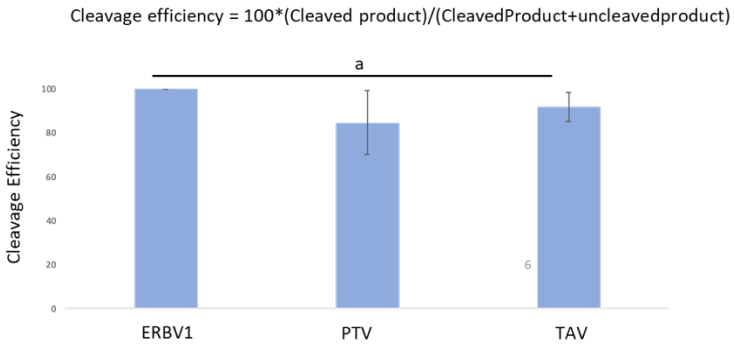

Figure 3. Cleavage efficiencies for three 2A peptides
The 2A peptide ERBV1 had the highest cleavage efficiency

Westerns were imaged and quantified via densitometry. The bar graph represents the mean cleavage efficiency of three biological replicates and the standard deviation. No significant differences in the means were detected using a one-way ANOVA. ERBV1 was the selected 2A peptide due to higher cleavage efficiencies of the three.

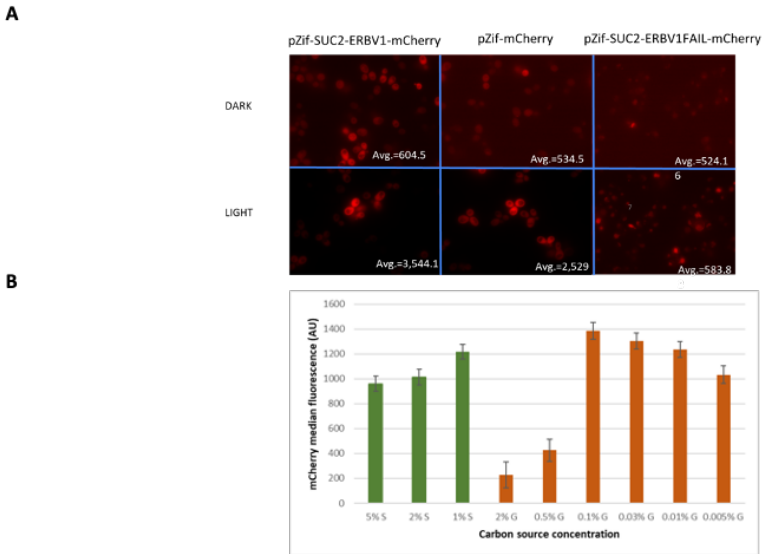

Figure 4. The ERBV1 2A peptide retains expected functions

A.The pZIF construct was grown in the light and dark to test for light-dependent expression of mCherry. The fluorescence microscopy images demonstrate similar fluorescent levels to a construct that does not incorporate the 2A peptide. The ERBV1FAIL peptide is not functional and the low fluorescence detectable seems to be compartmentalized within the cell. B. The pSUC2 strain demonstrates responsive expression levels in different concentrations of media, which would be expected from a regulated strain.

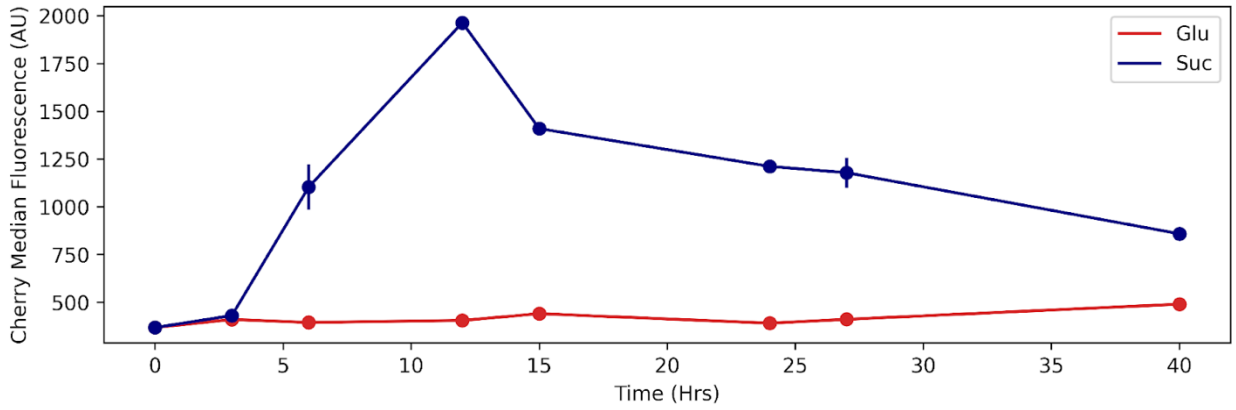

Figure 5. pSUC2 yeast regulates invertase during growth in sucrose

The median mCherry fluorescence serves as a reporter of regulation at the pSUC2 promoter in response to the breakdown of sucrose into glucose and fructose. The mCherry expression does not change dramatically over time in the glucose condition. In contrast, mCherry expression displays a peak, and then a decrease. The starting time point (Time = 0 hrs) is a sample of the overnight culture. Data points represent 3 replicates and the error bars represent the coefficient of variation (CV).

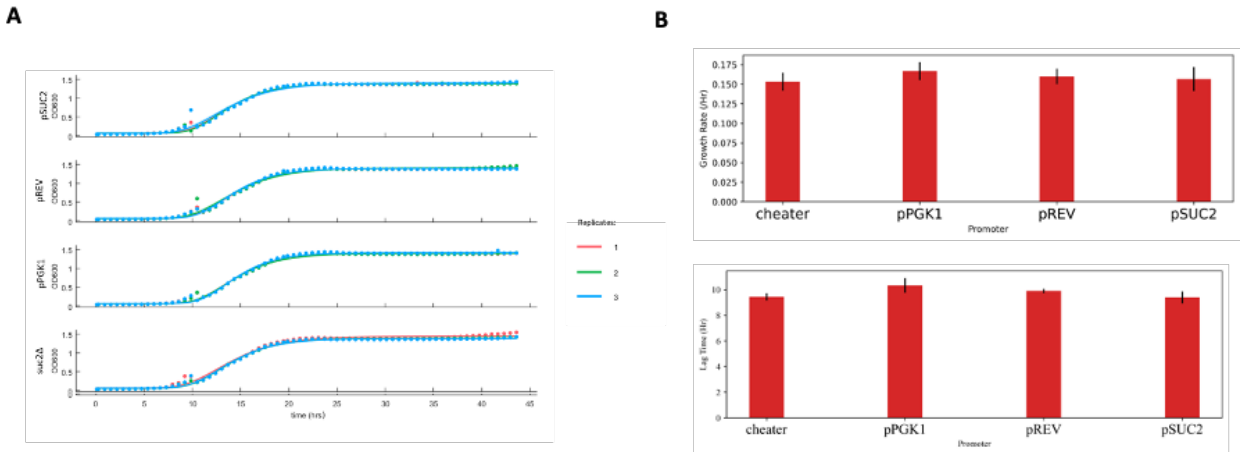

Figure 6. Strains expressing constitutive invertase do not display growth defects during growth in glucose

A. Each strain was grown in glucose for over 40 hours with OD600 measurements every half hour. The growth dynamics are similar to each other. The data points represent three replicates for each strain with the Gompertz curve overlaid for each replicate. B. Growth rates and lag times are not significantly different between the regulated pSUC2 promoter, the suc2Δ, and the two constitutive promoters pREV and pPGK1. A one-way analysis of variance failed to reject the null hypothesis.

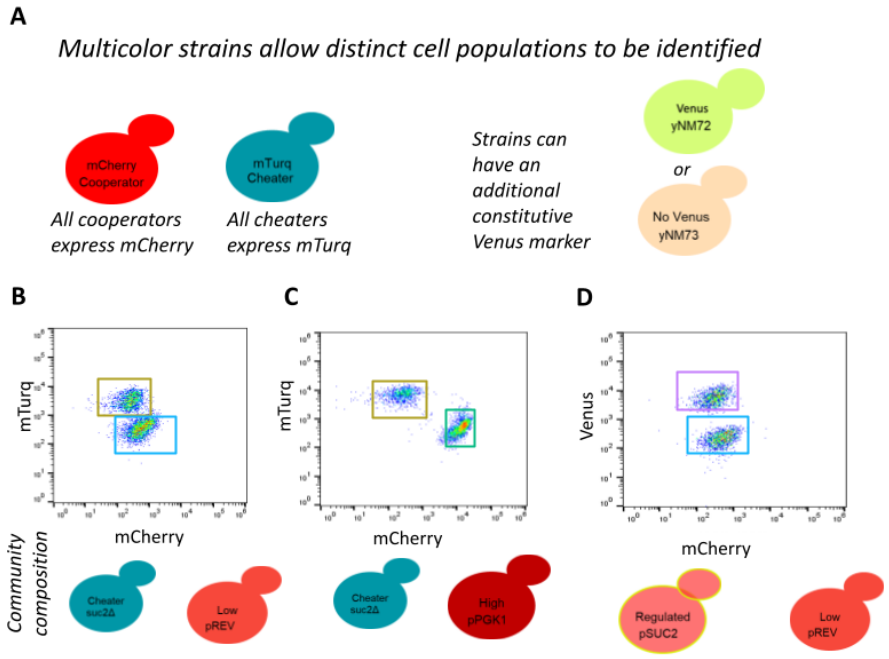

Figure 7. Multicolor strains allow cell populations to be distinguished from one another in a community A. Diagram of the available fluorescent reporter combinations for the cooperator and cheaters. Cheaters can be distinguished by a constitutively expressed mTurquoise marker. *Active* cooperators can be identified through expression of an mCherry reporter. Each of these options could have an additional constitutive venus reporter. Allowing us to distinguish between cooperator types as well. B. Representative gating to identify a community composed of a cheater (suc2Δ) and a low constitutive cooperator (pREV). C. Representative gating to identify a community composed of a cheater (suc2Δ) and a strong constitutive cooperator (pPGK1). D. Representative gating to identify a community composed of a regulated cooperator (pSUC2) and a low constitutive cooperator (pREV) through an additional mVenus reporter.

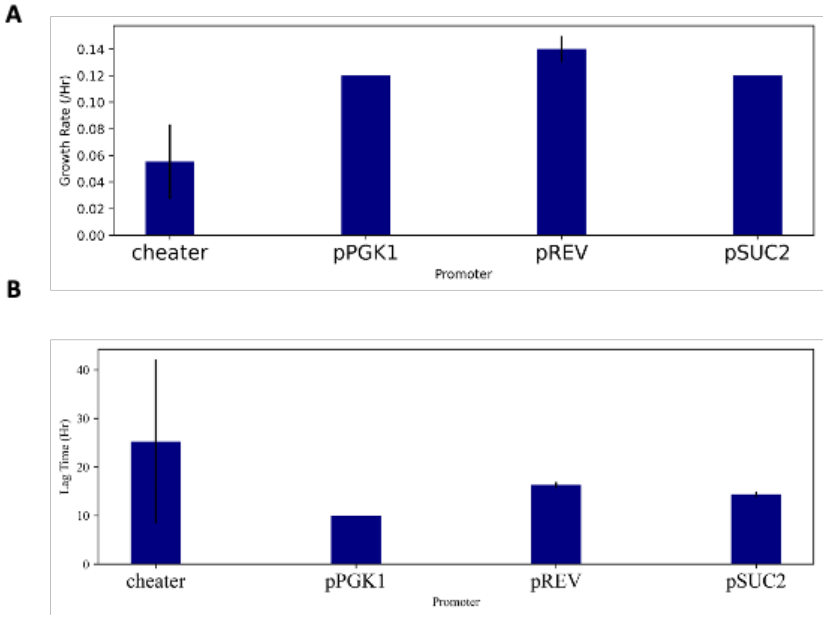

Figure 8.

Growth dynamics of cooperators and cheaters differ in sucrose

A. pREV had the highest growth rate in sucrose of the cooperators. Statistically these differences were not identified as significant as a one-way analysis of variance failed to reject the null hypothesis. The cheater grew in sucrose after a long time but the Gompertz fitted equation was not able to fit the growth dynamics of the cheater well, see supplemental figure 2. B. pPGK1 had a shorter lag time when grown in sucrose presumably because expressing invertase strongly helped this strain grow immediately upon transfer. The pREV strain demonstrated the longest lag times, followed by pSUC2. A one way analysis of variance (ANOVA) failed to reject the null hypothesis when comparing lag times in sucrose between cooperators. Cheater (suc2Δ) growth was not able to be captured by the Gompertz equation.

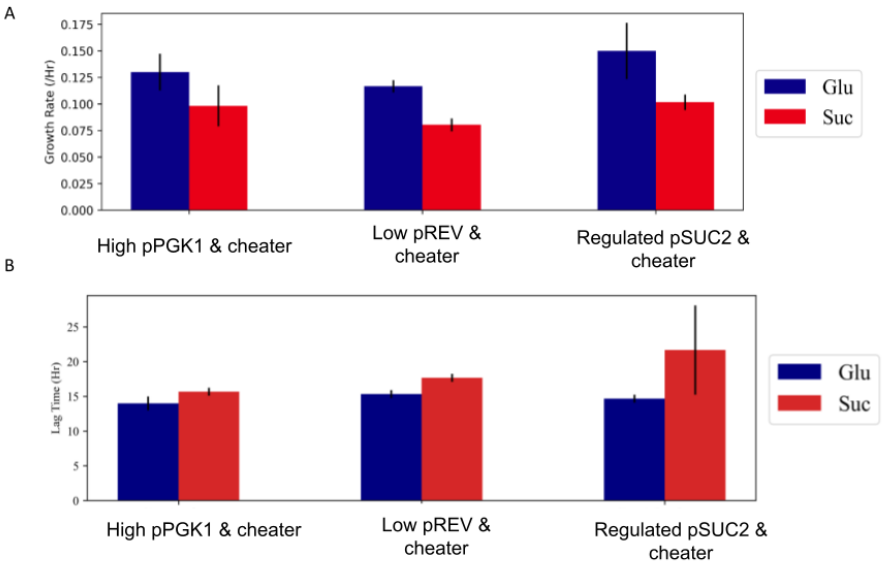

Figure 9. Regulation of invertase allows pSUC2 to pick and tune their investment based on glucose availability

A. The growth rates in competition experiments for growth in glucose and sucrose demonstrate that the population with pSUC2 is able to maintain a higher growth rate due to pSUC2 not investing in the production of invertase. When invertase is expressed by pSUC2 (growing in sucrose) the population has a similar growth rate to the population with pPGK1 as the cooperator. Bars represent the average of three replicates and error bars are standard deviation. B. Populations with regulated invertase (pSUC2) experienced longer lag times and more variation between replicates. Bars represent the average of three replicates and error bars represent the standard deviation.

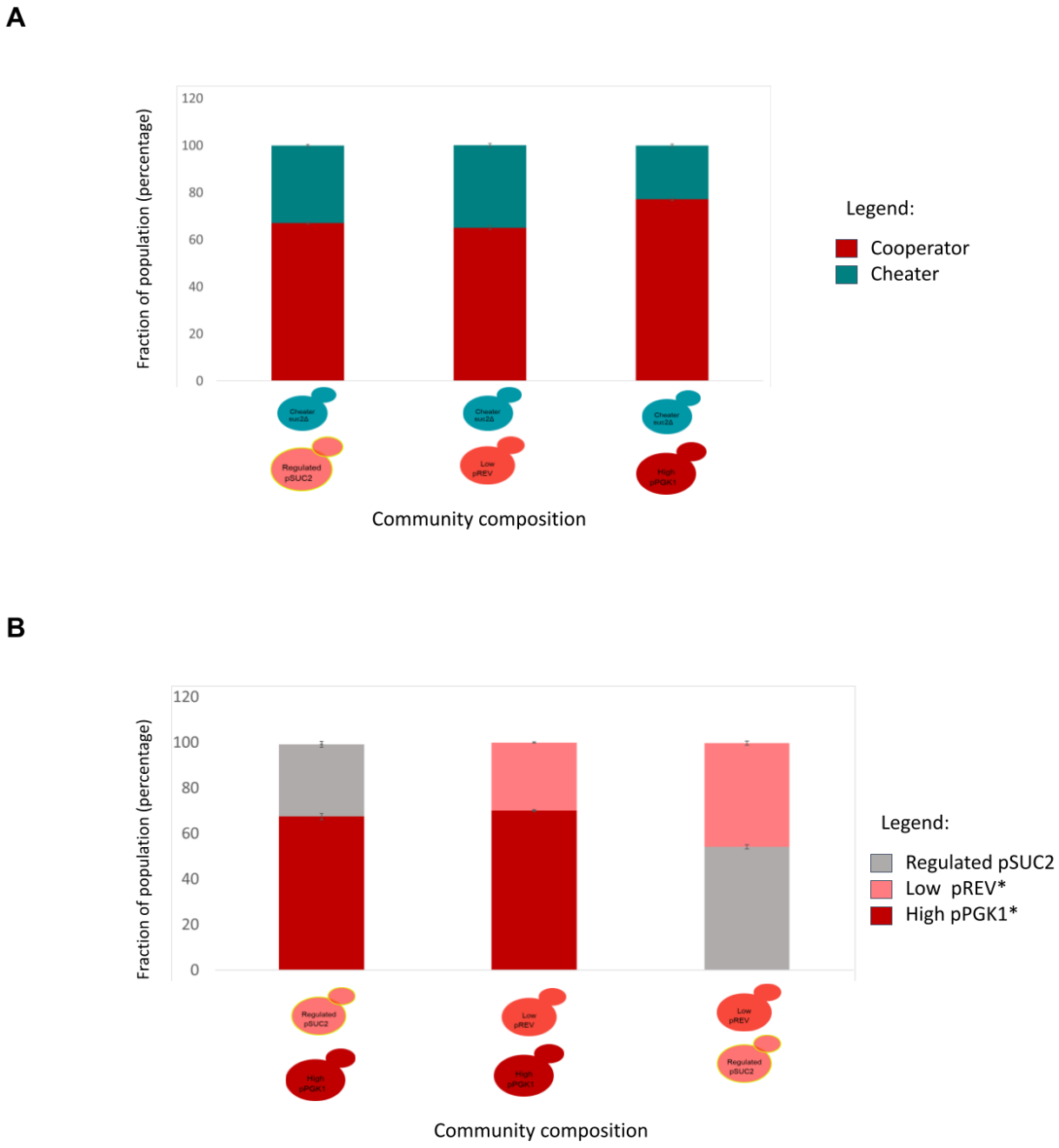

Figure 10.

Communities with regulated invertase (pSUC2) reached similar compositions to communities with low constitutive cooperators (pREV)

A. Composition of cooperator-cheater communities after seven days of competition. Cooperators were the majority. Communities with the high constitutive cooperator pPGK1 were composed of a large fraction (0.77) of cooperators, pPGK1 outperformed the other cooperators in competition. Communities with

pREV and pSUC2 reached similar fractions (~0.69 and 0.67 respectively). Bars represent the average of three replicates and error bars represent the coefficient of variation (CV).

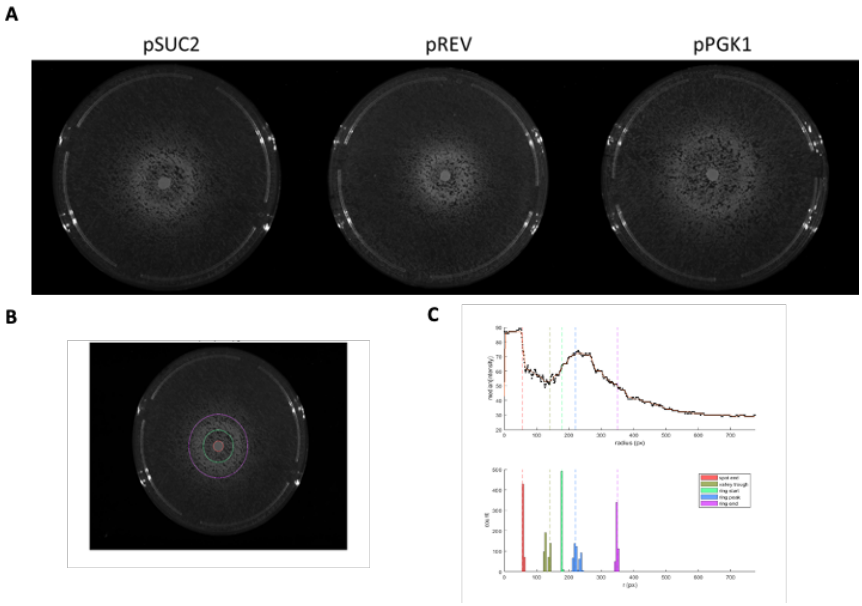

Figure 11.
Bullseye patterning of spatially structured communities and feature detection

A. Representative images of the bullseye patterning for each of the cooperator types spotted in the middle and the cheater (suc2Δ) spread as a lawn. Feature differences are noticeable between cooperators. The ring is largest on pPGK1, followed by pSUC2 and pREV. Some density differences are detectable by eye as well. B. Feature identification is overlaid on the plate. The red circle is the spot feature. The green line is the ring start (also valley end). The magenta line is the ring end. B. The custom MATLAB script performs a clockscan of the image and is used to identify features. The output of this analysis is displayed.

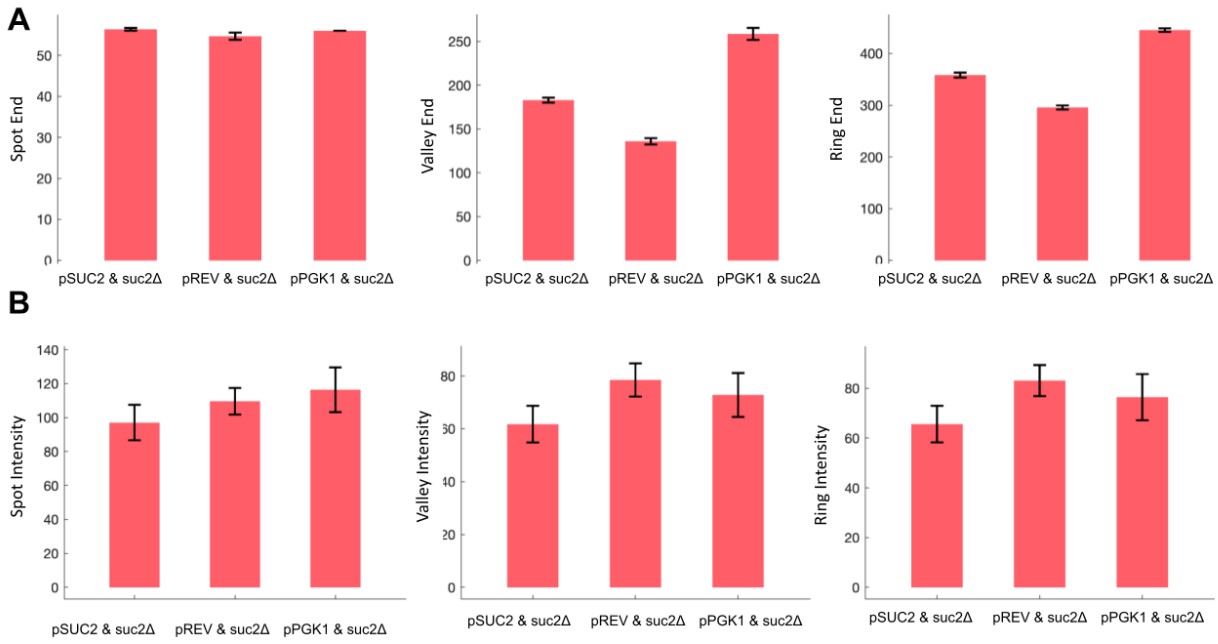

Figure 12.

Comparison of feature lengths and intensities between regulated and constitutive cooperators

A. Lengths of plate features are displayed for each cooperator-cheater pair. Lengths are measured from the center of the plate to the corresponding feature. The lengths of the valley (ring start) and length of the ring in increasing order for the cooperators is pREV, pSUC2, then pPGK1. Bars represent the average of three replicates and error bars represent the standard deviation. B. Intensities for plate features are directly calculated from the images. Notably the regulated cooperator (pSUC2) had lower intensities in the valley and ring features than the constitutive cooperators correlating with limiting cheater growth. Bars represent the average of three replicates and error bars represent the standard deviation.

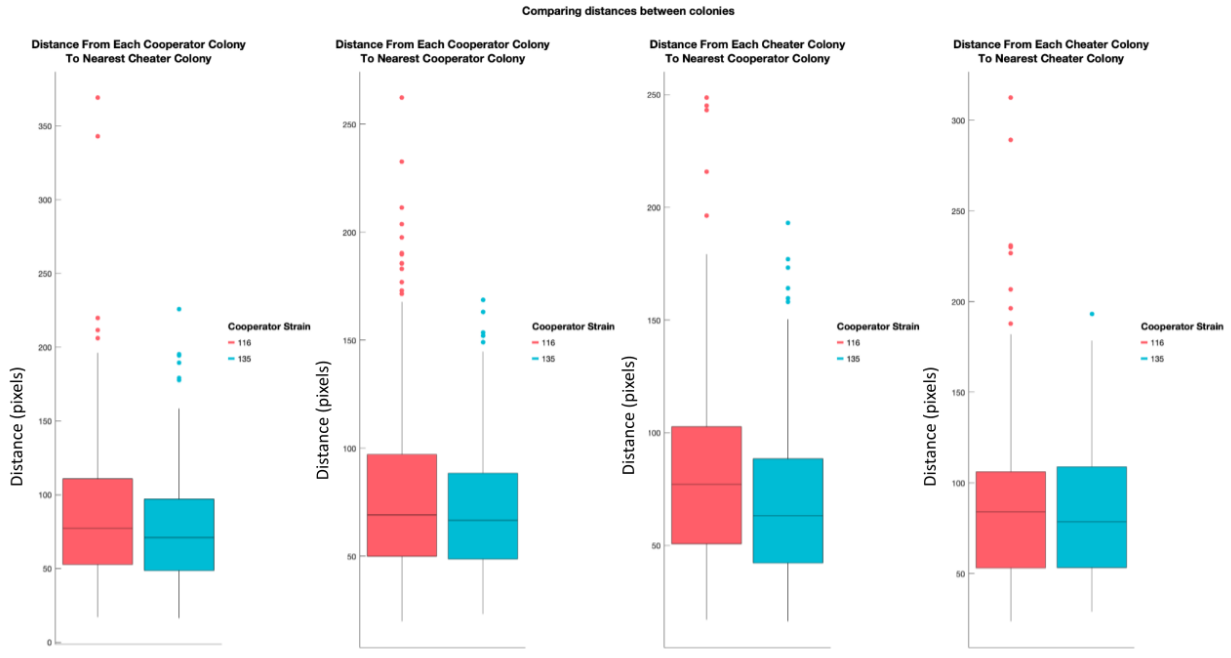

Figure 13. Preliminary colony count experiment supports spot assay finding that regulation of cooperation can limit cheater growth in spatially organized environments

Distances from cooperator colony to the nearest neighbor were measured and averaged. Overall, regulated strains (pSUC2) appeared to have larger distances to their nearest neighbor be that cheater or cooperator. Box plot demonstrates the interquartile range and outliers of four images of regions within a plate.

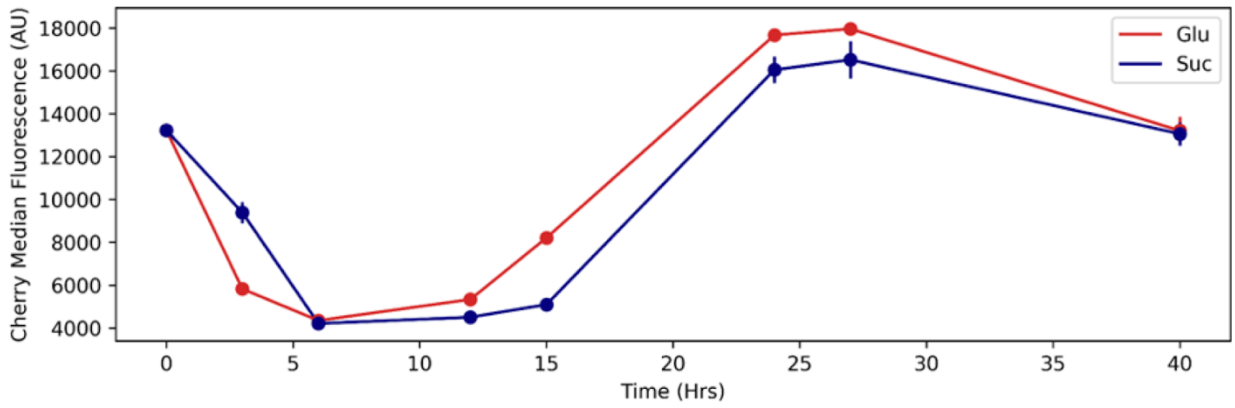

Supplemental Figure 1.

Expression from pPGK1 did not display regulation in sucrose

Expression from the constitutive promoter pPGK1 was strong, as expected, and did not have significantly increased expression profiles when comparing similar time points for growth in sucrose (Figure 5). The expression for pPGK1 at hours 24,27,and 40 were significantly higher from the expression at earlier time points. Additionally, the expression from pPGK1 was slightly higher in glucose than sucrose. Although [28] found consistent expression from pPGK1 from two fluorescent markers, it is possible that pPGK1 is not entirely a consistently consititutive promoter. Data [42] shows an increase in expression over 24 hours with each time point (6,12,24 hours) showing significant increases in expression over growth to reach maximum expression. Other works also show that pPGK1 expression can be affected by different media conditions or could be affected by different stressors [43], [44].

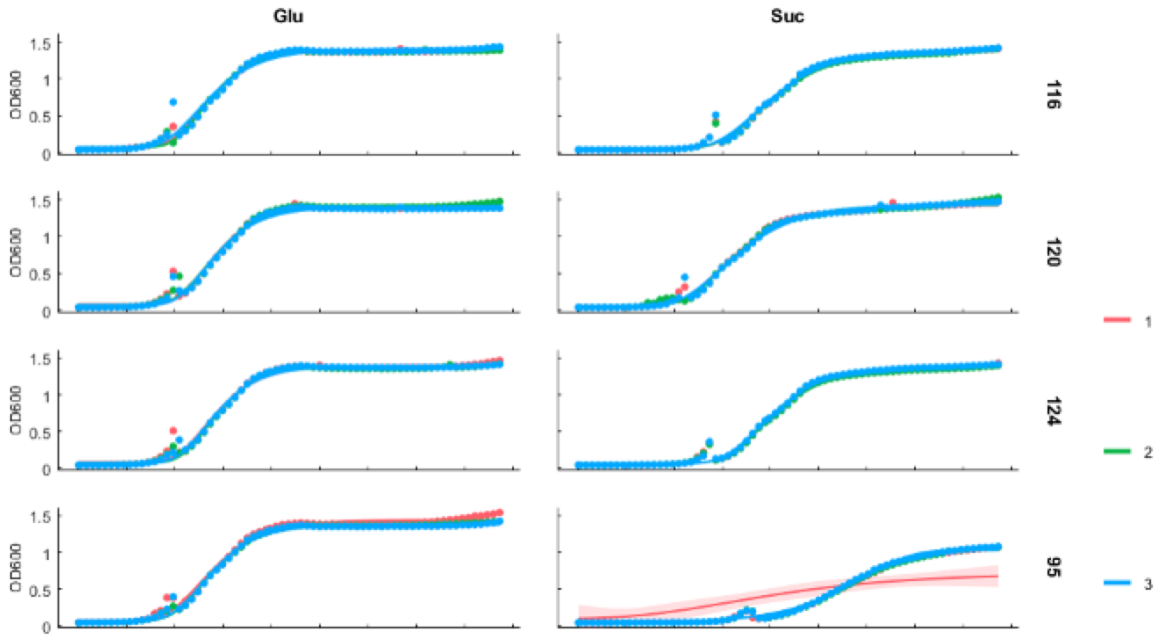

Supplemental Figure 2.
Additional growth curves display additional cooperators do not differ from the pSUC2 cooperator (116) and a poor fit of the Gompertz equation for cheaters

Growth curves of additional cooperators used in cooperator versus cooperator competitions to measure composition after seven days. The data points represent the three replicates and the Gompertz fitted

curve for each of those replicates. The very slow, non-typical growth of the cheater (95) is likely a contributor to the poor fit of the Gompertz model.

Table 1.
Yeast Strains

Strain alias	Genotype	Strain	Referred in Chapter
yNM72	MATalpha his3Δ1 leu2Δ0 lys2Δ0 suc2Δ::KanMX ura3Δ0::pNM52(ura3 5'/3' homology, URA3, pRL18B-Cry/CIB, pTEF-Venus-tADH1)	BY4742	yNM72
yNM73	MATalpha his3Δ1 leu2Δ0 lys2Δ0 suc2Δ::KanMX ura3Δ0::pMM458(ura3 5'/3' homology, URA3, pRL18B-Cry/CIB,EMPTY)	BY4742	yNM73
yNMM82	MATalpha his3Δ1 leu2Δ0 lys2Δ0 ura3Δ0 suc2Δ::KanMX , , pSuc-mCherry-tADH1	BY4742	
yNMM85	MATalpha his3Δ1 leu2Δ0 lys2Δ0 ura3Δ0 suc2Δ::KanMX, integrated pNM46, pSuc-mCherry-tADH1	BY4742	
yNMM 95	MATalpha his3Δ1 leu2Δ0 lys2Δ0 ura3Δ0 suc2Δ::KanMX integrated pNM50 #2,Leu2 5'/3' homology, LEU2, pPGK1-mTurq-tADH1	BY4742	Cheater
yNMM 96	MATalpha his3Δ1 leu2Δ0 lys2Δ0 ura3Δ0 suc2Δ::KanMX integrated pNM 50 #2,Leu2 5'/3' homology, LEU2, pPGK1-mTurq-tADH1	BY4742	
yNMM 98	MATalpha his3Δ1 leu2Δ0 lys2Δ0 ura3Δ0 suc2Δ::KanMX, integrated pMM494 #9	BY4742	
yNMM 114	MATalpha his3Δ1 leu2Δ0 lys2Δ0 ura3Δ0 suc2Δ::KanMX, integrated plasmid: pNM 79 pSuc-SUC-ERBV1	BY4742	
yNMM 116	MATalpha his3Δ1 leu2Δ0 lys2Δ0 ura3Δ0 suc2Δ::KanMX integrated plasmid: pNM 79 pSuc-SUC-ERBV1-mCherry,	BY4742	pSUC2
yNMM 120	MATalpha his3Δ1 leu2Δ0 lys2Δ0 ura3Δ0 suc2Δ::KanMX integrated plasmid: pNM 74 pPGK1-SUC-ERBV1-mCherry	BY4742	*pPGK1
yNMM 124	MATalpha his3Δ1 leu2Δ0 lys2Δ0 ura3Δ0 suc2Δ::KanMX integrated plasmid: pNM80 pREV-suc-ERBV1-mCherry,	BY4742	*pREV
yNMM 128	MATalpha his3Δ1 leu2Δ0 lys2Δ0 ura3Δ0 suc2Δ::KanMX, integrated plasmid: pNM80 pREV-SUC-ERBV1-mCherry,	BY4742	pREV
yNMM 135	MATalpha his3Δ1 leu2Δ0 lys2Δ0 ura3Δ0 suc2Δ::KanMX, integrated plasmid: pNM74 pPGK1-SUC-ERBV1-mcherry	BY4742	pPGK1

Table 2.
Plasmids

Plasmid name	Selection marker	Yeast genes
pNM7	carb	contains the 2A plasmid pSuc-TAV-mcherry-tADH1 and selection with LEU

pNM8	carb	contains the 2A plasmid pSuc-ERBV1FAIL --mCherry-tADH1 and selection with LEU
pNM11	carb	pSuc-mCherry-tADH1 reporter plasmid. LEU selection
pNM12	carb	pZif-mCherry-tADH1 reporter plasmid. LEU selection
pNM13	carb	pZif-SUC-PTV-mCherry-tADH1. LEU selection
pNM14	carb	pZif-SUC-ERBV1-mCherry-tADH1. LEU selection
pNM15	carb	pZif-SUC-TAV-mCherry-tADH1. LEU selection
pNM16	carb	pZif-SUC-ERBV1FAIL-mCherry-tADH1. LEU selection
pNM23	Kan	pZif-SUC-ERBV1-mCherry-tADH1. LEU integration selection. Leu2 5' homology-ConLS-sfGFP dropout-Con1-LEU2-Leu2 3' homology
pNM33	Kan	pSuc-suc-ERBV1-mCherry-tADH1.
pNM45	Kan	pSuc-mCherry-tADH1. Backbone pMM494. #1
pNM50	Kan	Leu2 5'/3' homology, LEU2, pPGK1-mTurq-tADH1
pNM74	Kan	pNM23 w/ promoter pPGK1
pNM80	Kan	pREV w/ pnm23
pNM57	Kan	pREV-suc-tadh1
pNM59	Kan	pREV1-SUC-ERBV1-mCherry-tADH1
pNM60	Kan	pPGK1-SUC-ERBV1-mCherry-tADH1
pNM61	Kan	pPGK1-SUC-ERBV1-mCherry-tADH1
pNM62	Kan	pPGK1-SUC-ERBV1-mCherry-tADH1
pNM63	Kan	pREV-mCherry-tADH1
pNM64	Kan	pPGK1-mCherry-tADH1

Table 2.
Plasmids

Oligo name	Sequence	Function
oMM1607	GCCAATTTCAACAAAGAAAAATTAGTAGCACCACCAGATTTTACTTCCCTTACTTGGAAC	Invertase gene and part of

		the ERBV1 2A peptide sequence
oMM1608	TGTTGAAATTGGCTGGTGATGTTGAATTGAATCCAGGTCCAatggtgagcaagggcgagg	mCherry and part of the ERBV1 2A peptide sequence
oMM1609	gctctagaactagtggatcccccgggctgcaggaattccggtagaggtgtggtcaataag	The ADH1 promoter and pMM8 backbone
oMM1610	TCACCAGCTTGTTTCAACAAAGAAAAATTAGTAGCTTTTACTTCCCTTACTTGGAACTTG	Invertase gene and part of the PTV 2A peptide sequence
oMM1611	TTGAAACAAGCTGGTGATGTTGAAGAAAATCCAGGTCCAatggtgagcaagggcgaggag	mCherry and part of the PTV 2A peptide sequence
oMM1612	TCAACATCACCACAAGTCAACAAAGAACCTCTACCTTCTTTTACTTCCCTTACTTGGAAC	Invertase gene and part of the TAV 2A peptide sequence
oMM1613	CTTTGTTGACTTGTGGTGATGTTGAAGAAAATCCAGGTCCAatggtgagcaagggcgagg	mCherry and part of the TAV 2A peptide sequence

oMM1614	GCCAATTTCAACAAAGAAAAATTAGTAGCACCACCAGATTTTACTTCCCTTACTTGGAAC	Invertase gene and part of the ERBV1 2A peptide sequence (with the consensus NPG-P deleted). So that this 2A peptide sequence does not work
oMM1615	AATTTTTCTTTGTTGAAATTGGCTGGTGATGTTGAATTGatggtgagcaagggcgaggag	mCherry and part of the ERBV1 2A peptide sequence (with the consensus NPG-P deleted). So that this 2A peptide sequence does not work.

Chapter 6: Conclusions and Future directions

Neydis Moreno Morales wrote the chapter.

Introduction

The primary focus of my thesis was to examine the role of invertase regulation in the public goods community of *Saccharomyces cerevisiae*. Despite the popularity of this model system for investigating microbial cooperation and public goods utilization the role of invertase regulation had remained unexplored. I hypothesized that regulation could be an important factor to consider when studying cooperation in this model system. There were clues from cell physiology research [1], and biofuels production from industrial yeast strains [2] that regulation was likely. I suspected that there could be consequences to oversimplifying the activity of a wildtype cell (driven by pSUC2 promoter) to that of a constant "cooperator" within a mixed community including cheaters.

Before I was able to explore the role of invertase regulation I addressed the need for tools to study cooperation. I first focused on developing tools that would allow me to control cooperation in the public goods community in space and in time. This was largely the focus for Chapters 2 and 3. I developed tools to achieve spatiotemporal control of cooperation through optogenetics. With these tools I was able to control cooperation in a light dependent manner, demonstrating that I could control where and when cooperation in a community occurred. Experiments in this chapter led to a serendipitous observation of the "bullseye" pattern that I hypothesized might be due to the unique properties of a spatial environment such as diffusion of limiting nutrients, and cellular organization. In chapter 4, I continued to explore this patterning and how different factors might affect the evolution of the pattern by developing a model. The model was able to recapitulate and predict the patterning I observed in different experiments involving growth throughout a week, different leucine concentrations, and starting densities of cheaters, or total cells. There was a clear disagreement between experiment and model in the case of varying sucrose concentrations, with a notable absence of the ring in concentrations below 40% sucrose (chapter 4, Figure 11). This prompted me to once again take a closer look at control of cooperation, in this case how wildtype cells might regulate invertase production. As the cooperator strains in yeast public goods models are

wildtype cells with an intact invertase gene (SUC2) and an intact promoter (pSUC2), [3]–[7] (see Chapter 1, Table 1 for more detail). In chapter 5 I demonstrated that invertase regulation was indeed taking place in a pSUC2 regulated population of *Saccharomyces cerevisiae* by tracking expression of a fluorescent reporter mCherry (Chapter 5, Figure 5). I also presented data that highlighted differences between cooperators that were constitutively expressing invertase and cooperation from regulated invertase. Specifically, that regulation was advantageous to limiting nearby cheater growth when competing in a spatially structured environment (Chapter 5). This chapter will provide a summary of the powerful tools and key results from my work, as well as, contextualize my work within the field. I will also discuss the potential applications and limitations of my work and future directions.

Spatiotemporal control of cooperation with optogenetics

In chapter 2, I described the development of a new method to calibrate Light Plate Arrays (LPAs) to ensure reproducibility of accurate light doses delivered between individual wells of the LPA and the delivered light doses across LPAs. The method was successful in reducing the coefficient of variation (CV) from 12.6% (of an uncalibrated plate) to a CV of 0.82% for a calibrated plate. The method also generated a standard curve, which allows the user to correlate Iris values to irradiance values. Optogenetics has some extremely attractive characteristics as a method for control of gene expression over traditional chemical induction mainly: reduced cost, instantaneous addition and removal of inducer, and accessibility (just need an appropriate light source). Our method to calibrate an optogenetic tool follows a good trend to make light addition more standardized (irradiance measurements), higher throughput, and reproducible across conditions and experiments. The reproducibility and comparability between light illumination methods will be extremely important as the use of optogenetics continues to boom. There is consistent addition of new optogenetic tools [8] [9] [10] to meet the needs of an increasing array of optogenetics applications to engineer microbes [11].

In chapter 3, I continue developing optogenetic tools. This time, focusing on incorporation of the genetic elements to control public goods production in *Saccharomyces cerevisiae* with light. I report a method for assembling a light activated control of a gene of interest. I demonstrated that by placing invertase under light control I had the ability to control where and when cells were cooperating. When provided a sufficient light dose (~5.7 uW/cm^2) yeast were able to grow and saturate at similar levels as the levels observed for the wildtype control strain (pSUC2) after 24 and 48 hours during growth on sucrose. Even with smaller doses of light the optogenetic strain could reach saturation given a longer time (48 hours). The properties of the light inducible promoter (pZF(3BS)) also resulted in some growth in the dark which we attributed to leakiness of the promoter.

I was also able to pattern the growth of the optogenetic yeast strain in a light-dependent way. Cells spread on a plate were only able to grow where light was patterned, and because of the diffusive properties of the public good, growth was supported at a distance from the light. This patterning also resulted in an unexpected observation of the growth which I described as a "bullseye". While there was light-localized growth on the plate, there also appeared to be a denser ring of growth at a distance from the spot. The pattern became more apparent in nutrient limited conditions, which caused me to consider how spatial organization of cooperators and nutrient competition could be responsible for the growth pattern. Exploring this patterning and developing a model became the focus of the following chapter.

In the future incorporation of the optogenetic strain (pZF(3BS)) in competition experiments presented in chapter 5 would provide an additional opportunity to understand the role of regulation on growth dynamics, community composition, and patterning. The optogenetic strain is able to be dynamically regulated by the researcher which would allow for the design and implementation of different regulation regimes . One option is to test the effect of different light duty cycles (1 min of light, 1 min off etc.) on the community properties discussed (composition, patterning).

Biotechnology applications of optogenetic control of cooperation

Our system could also be useful in the development of microbial consortia control, as the pZF(3BS) strain could be used to develop a feedback regulated system to drive a more complex microbial consortia. There is preliminary work that supports the incorporation of optogenetics for microbial consortia control [12]. One potential microbial consortia for our particular public goods yeast is the kombucha community where bacteria are dependent on yeast to breakdown sucrose in the media [13] [14].

This will require a more intensive quantification of the invertase expression from this strain, and would likely necessitate a model to inform the light regime protocol to achieve desired or optimal dynamic regulated expression with light. This was outside the scope of the work in chapter 5 but is nonetheless an interesting project for a future researcher to incorporate.

Indeed there seems to be a rapidly increasing interest in the use of optogenetics to control complex functions like flocculation [15] , creation of living materials [16](which is discussed in more detail in Appendix 1), and biofilm production [17].

The ability to control interactions within a microbial community with spatial and temporal precision is an extremely powerful and covetous quality. My work has clear applications to developing the framework for optogenetic control of microbial consortia or to study similar cooperative behaviors by adding tunable control (an example of similar cooperative behaviors is discussed in Appendix 2).

Model development for long range patterning effects in nutrient limiting environments

As described in the previous section for optogenetic tool development I encountered an interesting bullseye pattern that appeared to be the result of the co-localization of cooperators in space and the nutrient limitations that the cells were encountering. The pattern formation was interesting due to the length scales over which microbial interactions seemed to have an effect on their environment (mm scale). As discussed in chapter 4, interactions at the short-range (cellular distances) are often thought to be the relevant scales over which interactions have effects [18] [19], [20].

In chapter 4 I sought to develop a model that could help explain the factors were responsible for the pattern formation. The model described our system with four equations: the growth of cheater cells, the growth of cooperator cells, and the diffusion of the limiting nutrients in our system, sucrose, glucose and leucine. The model was able to nicely capture the patterning observed in experiments and make some good predictions, for example, the effect of varying cheater density on patterning (there was none). The model also allowed me to tune properties of the system *in silico* which would not be easily achieved with empirical methods, these are, the ability to tune growth rate or the sucrose conversion rate of the cells in the community.

There were some cases where the model was not as tractable, for example, when sucrose concentrations were varied. Some strengths of the model were the simplicity of the four equations that were able to recapitulate and predict some situations well. Perhaps, as was hypothesized in chapter 4, the model could be improved upon by incorporating equations that represented invertase regulation as a variable that impacts growth. This would allow us to greatly expand on the work done in chapter 5 to compare and contrast how regulation changed the growth and composition of a public goods community when compared to constitutive invertase expression.

the model is not unique in the incorporation of invertase expression as constant. The existing work that treats the public goods model in *Saccharomyces cerevisiae* does not often incorporate spatial organization if a model is proposed and further does not consider invertase regulation (see Chapter 1 Table 1). It is important that the field keep developing models that incorporate both spatial organization and regulatory properties of the system, as there is increasing evidence that where and when public goods are made is important for maintaining cooperativity and community stability in biological systems [20]. My work is a valuable contribution to the field as it combines an experimental model, with the genetic tractability to engineer its functions and the computational power of a model, which provides a useful framework for approaching similar biological systems.

Future work on the role of regulation in well-mixed and spatially organized environments

In chapter 5 I found some unexpected effects on growth dynamics and composition resulting from the constitutive cooperator strains. I hypothesized that changing the invertase regulation in cooperators had unexpected consequences on other properties of the cell such as glucose capture efficiency. It would be informative and important to measure this and other properties such as changes to density-dependent growth (described as the allee effect). These properties could affect the way that the data generated by competitions is interpreted as well as, may influence the methodology of these experiments to control for potentially confounding factors.

For example, pPGK1 had shorter lag times, and reached higher fractions when competing with other cells (both cheaters and cooperators) it appeared that high constitutive expression was incredibly beneficial, this was in well-mixed conditions where the generation of glucose would be easily diffused away, and so perhaps in this case having more invertase per cell changed the glucose capture efficiency that had been previously described for a wildtype cooperator as ~1% [4]. Benefits for high constitutive expression disappeared in the spot assays. Both pPGK1 and pREV supported more cheater growth when compared to regulated pSUC2. It was clear that spatially organized environments suited the regulated strain but what factors explain the results in well-mixed competitions

If it is due to the interplay of changes in capture efficiencies and the properties of a spatial environment, how can we compare the capture efficiencies between well-mixed environments and spatially organized environments? These are measurable in glucose, but perhaps more difficult to measure on a plate. As discussed previously the model developed in chapter 4 allows for the exploration of otherwise difficult to tune variables. Perhaps an adaptation of the model to include invertase regulation as a parameter and glucose capture efficiencies could greatly inform our understanding of properties not previously considered to affect cooperativity.

Conclusions

The work presented here provides a sophisticated approach to controlling interactions in microbial communities and visualizing their interactions. One lesson from my work is to re-visit the frameworks used to study a model system carefully. With time more advanced tools and technology become available. For microbial systems, including the one studied here, new tools to measure, control or visualize the interactions between microbes. My work contributed significantly to the development of tools for this particular model system that can utilized by future researchers. I created a tool that allowed for precise spatiotemporal control of invertase expression, this meant that my tool could be used to directly drive cooperation in a community. I also created a model that was able to predict pattern formation for most of the conditions I tested, and that could be improved and adapted by others. Lastly, I found that pSUC2 was regulated during growth in sucrose, and demonstrated when regulation could be beneficial. It will be exciting to see how much more we uncover about regulation of invertase in the near future due to new tools and new questions.

References

[1] C. I. S. Rodrigues, A. Wahl, and A. K. Gombert, "Aerobic growth physiology of Saccharomyces cerevisiae on sucrose is strain-dependent," *FEMS Yeast Res.*, vol. 21, no. 3, p. foab021, Apr. 2021, doi: 10.1093/femsyr/foab021.

[2] C. Herwig, C. Doerries, I. Marison, and U. von Stockar, "Quantitative analysis of the regulation scheme of invertase expression in Saccharomyces cerevisiae," *Biotechnol. Bioeng.*, vol. 76, no. 3, pp. 247–258, Nov. 2001.

[3] D. Greig and M. Travisano, "The Prisoner's Dilemma and polymorphism in yeast SUC genes.," *Proc. R. Soc. B Biol. Sci.*, vol. 271, no. Suppl 3, pp. S25–S26, Feb. 2004.

[4] J. Gore, H. Youk, and A. van Oudenaarden, "Snowdrift game dynamics and facultative cheating in yeast," *Nature*, vol. 459, no. 7244, pp. 253–256, May 2009, doi: 10.1038/nature07921.

[5] J. H. Koschwanez, K. R. Foster, and A. W. Murray, "Improved use of a public good selects for the evolution of undifferentiated multicellularity," *eLife*, vol. 2, p. e00367, Apr. 2013, doi: 10.7554/eLife.00367.

[6] R. C. Maclean and C. Brandon, "Stable public goods cooperation and dynamic social interactions in yeast," *J. Evol. Biol.*, vol. 21, no. 6, pp. 1836–1843, doi: 10.1111/j.1420-9101.2008.01579.x.

[7] R. C. MacLean, A. Fuentes-Hernandez, D. Greig, L. D. Hurst, and I. Gudelj, "A Mixture of 'Cheats' and 'Co-Operators' Can Enable Maximal Group Benefit," *PLOS Biol.*, vol. 8, no. 9, p. e1000486, Sep. 2010, doi: 10.1371/journal.pbio.1000486.

[8] T. C. Höhener, A. E. Landolt, C. Dessauges, L. Hinderling, P. A. Gagliardi, and O. Pertz, "LITOS: a versatile LED illumination tool for optogenetic stimulation," *Sci. Rep.*, vol. 12, no. 1, p. 13139, Jul. 2022, doi: 10.1038/s41598-022-17312-x.

[9] L. J. Bugaj and W. A. Lim, “High-throughput multicolor optogenetics in microwell plates,” *Nat. Protoc.*, vol. 14, no. 7, Art. no. 7, Jul. 2019, doi: 10.1038/s41596-019-0178-y.
[10] M. Rullan, D. Benzinger, G. W. Schmidt, A. Milias-Argeitis, and M. Khammash, “An Optogenetic Platform for Real-Time, Single-Cell Interrogation of Stochastic Transcriptional Regulation,” *Mol. Cell*, vol. 70, no. 4, pp. 745-756.e6, May 2018, doi: 10.1016/j.molcel.2018.04.012.
[11] S. M. Hoffman, A. Y. Tang, and J. L. Avalos, “Optogenetics Illuminates Applications in Microbial Engineering,” *Annu. Rev. Chem. Biomol. Eng.*, vol. 13, no. 1, pp. 373–403, 2022, doi: 10.1146/annurev-chembioeng-092120-092340.
[12] M. A. Lalwani, H. Kawabe, R. L. Mays, S. M. Hoffman, and J. L. Avalos, “Optogenetic Control of Microbial Consortia Populations for Chemical Production,” *ACS Synth. Biol.*, vol. 10, no. 8, pp. 2015–2029, Aug. 2021, doi: 10.1021/acssynbio.1c00182.
[13] A. May, S. Narayanan, J. Alcock, A. Varsani, C. Maley, and A. Aktipis, “Kombucha: a novel model system for cooperation and conflict in a complex multi-species microbial ecosystem,” *PeerJ*, vol. 7, Sep. 2019, doi: 10.7717/peerj.7565.
[14] C. Gilbert *et al.*, “Living materials with programmable functionalities grown from engineered microbial co-cultures,” *Nat. Mater.*, vol. 20, no. 5, pp. 691–700, May 2021, doi: 10.1038/s41563-020-00857-5.
[15] F. Salinas, V. Rojas, V. Delgado, J. López, E. Agosin, and L. F. Larrondo, “Fungal Light-Oxygen-Voltage Domains for Optogenetic Control of Gene Expression and Flocculation in Yeast,” *mBio*, vol. 9, no. 4, pp. e00626-18, Jul. 2018, doi: 10.1128/mBio.00626-18.
[16] Y. Cao *et al.*, “Programmable assembly of pressure sensors using pattern-forming bacteria,” *Nat. Biotechnol.*, vol. 35, no. 11, Art. no. 11, Nov. 2017, doi: 10.1038/nbt.3978.
[17] A. Pirhanov *et al.*, “Optogenetics in Sinorhizobium meliloti Enables Spatial Control of Exopolysaccharide Production and Biofilm Structure,” *ACS Synth. Biol.*, vol. 10, no. 2, Art. no. 2, Feb. 2021, doi: 10.1021/acssynbio.0c00498.
[18] A. Dal Co, S. van Vliet, D. J. Kiviet, S. Schlegel, and M. Ackermann, “Short-range interactions govern the dynamics and functions of microbial communities,” *Nat. Ecol. Evol.*, vol. 4, no. 3, Art. no. 3, Mar. 2020, doi: 10.1038/s41559-019-1080-2.
[19] M. J. I. Müller, B. I. Neugeboren, D. R. Nelson, and A. W. Murray, “Genetic drift opposes mutualism during spatial population expansion,” *Proc. Natl. Acad. Sci.*, vol. 111, no. 3, pp. 1037–1042, Jan. 2014, doi: 10.1073/pnas.1313285111.
[20] B. Momeni, A. J. Waite, and W. Shou, “Spatial self-organization favors heterotypic cooperation over cheating,” *eLife*, Nov. 12, 2013. https://elifesciences.org/articles/00960 (accessed Jul. 27, 2018).

Appendix 1: Engineered bacteria self-organize to sense pressure

This was previously published here, and adapted for this thesis:

N. M. Morales and M. N. McClean, “Engineered bacteria self-organize to sense pressure,” *Nat Biotechnol*, vol. 35, no. 11, pp. 1045–1047, Nov. 2017, doi: 10.1038/nbt.3992.

Neydis Moreno Morales and Megan N. McClean wrote this news & views article. Neydis Moreno Morales wrote the introduction. Neydis Moreno Morales designed figure schematics and the editors adapted the figure.

Introduction:

My thesis work utilizes bioengineering approaches, through the combination of synthetic biology tools and hardware to study biological questions. As was discussed in the *Conclusions and future directions* chapter a possible application of the powerful tools I developed could be useful to the development of living biomaterials. Which combine desirable properties from living organisms with the desirable properties of inorganic materials. My tools allowed for exquisite spatiotemporal control of cellular functions that could be used to pattern cells on a surface, or to drive and visualize interactions within a material. Thanks in part to my thesis work I developed a broad knowledge of topics including the intersection of synthetic biology and biomaterials which made my opinions about current work valuable. Here, I present a communications piece I wrote to highlight the work by Cao et al. and share my insights about their work and their contribution to engineering biomaterials. Cao et al. improved upon an existing circuit for the production of curli fibrils. Through the combination of the curli fibril circuit with a Lac circuit the researchers produced self-assembled, 3D patterned “buttons”. The self-organized biological materials could then be combined with inorganic materials to create complete electric circuits that sense pressure with tunable characteristics. I inform the broader community of the contributions of this work within the existing work and look to what the future holds for living materials.

Bacteria are engineered with pattern-generating circuits to produce self-organized materials that can function as pressure sensors.

Natural systems use self-assembly of organic and inorganic materials to generate sophisticated structures. For example, *Shewanella* bacteria can form extracellular networks of arsenic-sulfide nanotubes with

unique electrical and photoconductive properties[1. Synthetic biology approaches can mimic these processes to engineer nano- and macro-structures, but thus far haven't achieved the self-patterning available in nature. In this issue, Cao *et al.*[2] engineer self-assembling dome-structures from *E. coli* by coupling production of a protein containing an inorganic interface with a pattern-forming circuit. When gold nanoparticles are bound to these inorganic interfaces, the composite domes can be integrated into simple electrical circuits and function as pressure sensors.

Design of genetic circuits to produce specific cellular behaviors, such as oscillations in protein concentration or toggling between genetic states [3], [4] was achieved almost twenty years ago. More recently, circuits that can specify population-level behaviors have been engineered by manipulating secretion of signaling molecules to produce synchronous oscillations or spatial patterning in multicellular communities [5],[6],[7]. Genetic circuits that enable production of materials, including self-assembling structures such as curli fibrils, have also been reported[8]. By regulating the timing and distribution of inputs to these circuits, material properties can be tuned. When appropriate domains such as a polyhistidine tag are incorporated into these organic materials, the engineered materials can be bound with inorganic materials to create composite materials with desirable properties, such as the ability to conduct electricity. Patterning of these materials can be achieved by spatial manipulation of inducers, but thus far self-patterning has not been described.

To generate three-dimensional self-patterning structures , Cao, *et al. [2]* combine a circuit they previously described that enables 2-D patterns[6] with expression of a modified curli protein[8]. The circuit[6] consists of a positive feedback loop (a mutant T7 RNA polymerase that activates its own expression) and a negative feedback loop based on production of the diffusible quorum-sensing molecule acyl-homoserine lactone (AHL) (Figure 1). High levels of AHL drive expression of the curli protein, an extracellular amyloid material that forms fibrils based on self-assembly of the major secreted curli subunit CsgA and an additional subunit CsgB. Patterning is enabled by the interplay between temporal accumulation of AHL (which induces curli

expression) and gene expression capacity, which is highest towards the edge of the colony allowing mCherry and curli expression. By engineering curli to contain a polyhistidine tag (6XHis) inorganic materials, for example, gold nanoparticles conjugated with Ni-Nitrilotriacetic acid $(NTA)_8$ can be bound to the fibrils.

Using inkjet printing, Cao *et al. [2]* place cells onto membranes to form single colonies of *E. coli* that contain a synthetic curli-producing circuit. Expression of the spatial patterning circuit causes curli to be produced only in the exterior of the colony, forming domed structures after 32 hours. In contrast, cells that constitutively express curli but lack the patterning circuit form solid cap structures, with curli protein distributed throughout. The height and diameter of the curli domes can be controlled by altering the hydrophobicity and pore size of the membrane. The authors hypothesize that membrane properties may affect nutrient transport and motility of the bacterial cells. A differential-equations model developed by the authors was able to predict the size of domes and the distribution of curli based on the underlying membrane properties.

Once structures had assembled, the bacterial colonies were fixed and labelled with gold nanoparticles to create a composite organic/inorganic material. Due to the distribution of the expressed curli proteins, gold particles were concentrated in the exterior layers of the dome. This allowed the domes, which are elastic, to function as pressure sensors. When two domes are pressed together distances between gold particles decrease allowing current to flow in a pressure-dependent manner. In contrast, caps formed using bacteria without the pattern-forming circuit are unable to sense pressure because the uniform distribution of gold particles caused a high baseline current. By varying the size of the domes, the authors constructed pressure sensors with varying responses. Integrating dome structures with different sensitivities into current-canceling or current-adding circuits created sensors that only responded to high pressures, or circuits that amplified low pressure signals. Finally, spatial distribution of domes enabled the creation of location sensors.

The bacterial-enabled electric circuits of Cao et al.[2] are not the first time that curli fibrils have been used for this purpose. An earlier study[8] used a small-molecule inducible circuit to regulate expression of CsgA-6xHis in *E. coli*, with spatial patterning governed by an external gradient of inducer. It is also plausible that spatial and temporal patterning could be achieved using three-dimensional printing[9] to control cell placement, or light-patterning [10], [11]to control the induction of optogenetic synthetic circuits. Instead, Cao, *et al.* utilized external cues generated by membrane properties to control colony growth and intrinsic curli patterning making the process of self-assembly innate. An advantage of the Cao, *et al.* approach is that the information required to grow in the final structure is contained in each individual *E. coli* cell. Though the *E. coli* colonies were fixed, and therefore killed, this suggests the ability to use living organisms to pattern structures in response to environmental cues and growth properties of microbial cells. This is exciting given that a longer term aim for the biomaterials community is to produce synthetic, live materials with the ability to pattern, self-heal and remodel.

Cao, *et al.[2]* report an important next step toward harnessing the potential of biomaterials. Building on this work, self-assembling complex biomaterials might comprise consortia of multiple species that contain different synthetic circuits. Some organisms already have specific material-generating properties (e.g., *Shewanella* or *Geobacter sulfurreducens*), which can produce electrically conductive pili[12]. Engineering these less genetically tractable organisms is difficult, owing to a lack of genetic tools. It is conceivable that consortia of less tractable organisms with easily engineered model organisms such as *E. coli* or *S. cerevisiae* could enable the engineering of more complex composite biomaterials.

Creating complex hybrid living biomaterials and interfacing them with traditional electromechanical systems will require interdisciplinary collaborations between microbiologists, physicists, material scientists, biochemists and electrical engineers. The future beckons for biomaterials research.

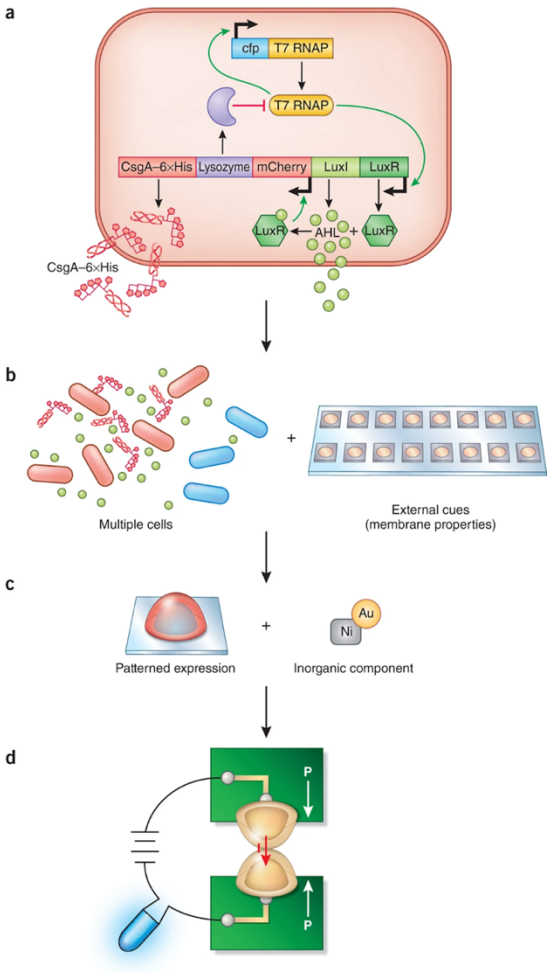
a
cfp
T7 RNAP
T7 RNAP
CsgA–6×His
Lysozyme
mCherry
LuxI
LuxR
LuxR
AHL
LuxR
CsgA–6×His
b
Multiple cells
External cues
(membrane properties)
c
Patterned expression
Au
Ni
Inorganic component
d
P
P

Figure 1.

Strategy for creating composite materials using engineered bacteria. **(A)** A synthetic gene circuit controls secretion of a modified organic material (CsgA-6xHis). CsgA is one component (along with CsgB) of the curli protein produced in the extracellular matrix of many bacteria. A mutant T7 RNA polymerase activates its own expression and expression of LuxI and LuxR. LuxI synthesizes AHL (A, green spheres) which is a membrane-diffusible chemical that activates LuxR. Once activated, LuxR induces expression of T7 lysozyme, which inhibits T7RNAP. **(B)** Diffusion of AHL results in spatially patterned secretion of CsgA-6xHis coincident with mCherry expressing cells. Curli fibrils are formed from the modified CsgA-6xHis and constitutively expressed CsgB (not shown). Cells are grown on membranes placed onto a nutrient reservoir. Colony formation and patterning of curli can be controlled by altering membrane properties such as hydrophobicity and pore size. **(C)** Patterned colonies are fixed and labelled with gold nanoparticles conjugated with a Ni-NTA group, which forms a bond with the 6x-His tag. This produces a composite material comprising organic (curli) and inorganic (gold) components. **(D)** Patterned bacterial "domes" function as pressure sensors. Pressure applied to the domes reduces the distance between gold particles, allowing electric current to flow.

References

[1] J.-H. Lee, *et al*, "Biogenic formation of photoactive arsenic-sulfide nanotubes by *Shewanella sp*. strain HN-41," *Proceedings of the National Academy of Sciences*, vol. 104, no. 51, pp. 20410–20415, 2007.
[2] Cao, *et al* "Programmable assembly of pressure sensors using pattern-forming bacteria," *Nature Biotechnology*, 2017.
[3] M. Elowitz and S. Leibler, "A synthetic oscillatory network of transcriptional regulators," *Nature*, vol. 403, pp. 335–338, 2000.
[4] T. S. Gardner, C. R. Cantor, and J. J. Collins, "Construction of a genetic toggle switch in *Escherichia coli*," *Nature*, vol. 403, no. 6767, pp. 339–342, 2000.
[5] S. Basu, Y. Gerchman, C. H. Collins, F. H. Arnold, and R. Weiss, "A synthetic multicellular system for programmed pattern formation," *Nature*, vol. 434, no. 7037, pp. 1130–1134, 2005.
[6] S. Payne, B. Li, Y. Cao, D. Schaeffer, M. D. Ryser, and L. You, "Temporal control of self-organized pattern formation without morphogen gradients in bacteria," *Molecular systems biology*, vol. 9, no. 697, 2013.

[7] A. Prindle, P. Samayoa, I. Razinkov, T. Danino, L. S. Tsimring, and J. Hasty, “A sensing array of radically coupled genetic ’biopixels’.” *Nature*, vol. 481, no. 7379, pp. 39–44, 2012.
[8] A. Y. Chen, Z. Deng, A. N. Billings, U. O. Seker, M. Y. Lu, R. J. Citorik, B. Zakeri, and T. K. Lu, “Synthesis and patterning of tunable multiscale materials with engineered cells,” *Nature materials*, vol. 13, no. 5, pp. 515–523, 2014.
[9] B. A. Lehner, D. T. Schmieden, and A. S. Meyer, “A straightforward approach for 3d bacterial printing,” *ACS Synthetic Biology*, vol. 6, no. 7, pp. 1124–1130, 2017.
[10] J. J. Tabor, *et al* “A synthetic genetic edge detection program.” *Cell*, vol. 137, no. 7, pp. 1272–1281, Jun 2009.
[11] J. Melendez, M. Patel, B. L. Oakes, P. Xu, P. Morton, and M. N. McClean, “Real-time optogenetic control of intracellular protein concentration in microbial cell cultures.” *Integr Biol (Camb)*, vol. 6, no. 3, pp. 366–372, 2014
[12] R.Y. Adhikari, N.S. Malvankar, M.T. Tuominen, D.R. Lovley, “Conductivity of individual *Geobacter* pili” RSC Advances, vol. 6, pp. 8354-8357, 2016

Appendix 2: Secrete to beat the heat

This was previously published here, and adapted for this thesis:

K. R. Lauterjung, N. M. Morales, and M. N. McClean, “Secrete to beat the heat,” *Nat Microbiol*, vol. 5, no. 7, pp. 883–884, Jul. 2020, doi: 10.1038/s41564-020-0748-3.

Neydis Moreno Morales, Kevin Stindt, and Megan N. McClean wrote this news & views article. Neydis Moreno Morales wrote the introduction. Neydis Moreno Morales designed figure schematics and the editors adapted the figure.

Introduction:

My thesis work highlighted the use of a model system in *Saccharomyces cerevisiae* to study the cooperative use of a carbon source; sucrose. As was alluded to in the *Conclusions and future directions* chapter, there are other systems with similar secretion-diffusion characteristics for which my work's findings could be extrapolated to. One example of such a system may be the cooperative approach of *S. cerevisiae* to combating higher temperatures. In this comment piece, I report on another cooperative mechanism in yeast, the cooperative survival and growth of yeast in higher temperatures. The secretion of a protective molecule (glutathione) increases the habitable temperature range for the yeast community. Youk and Laman present a cooperative behavior whereby cells can combat the stressors of life in an unfriendly environment, by secretion and accumulation of glutathione. This extends the habitable temperature range of yeast to temperatures previously considered inhospitable. There are clear parallels to the model public goods system such as, the cell density dependent effects as well as the way that yeast continuously craft their environment throughout growth. These parallels suggest that the lessons learned from my thesis work could have broader implications for understanding the cooperative behavior of microbial communities and may help to provide a framework for studying other cooperative microbial systems.

The textbook picture of microbial temperature response is this: as temperatures increase, cells autonomously remedy heat-induced damage in order to survive. Here, in contrast to the conventional view, a cooperative phenomenon is identified that allows denser populations of yeast cells to work together to survive high temperatures.

Temperature is a key variable controlling microbial life. It affects growth rate, metabolism, morphology, and reproduction. At optimal temperatures microbes grow and reproduce happily but as temperature increases reactive oxygen species are produced and proteins denature leading to stress response, growth cessation, and death. A microbe's relationship with temperature is characterized by

cardinal numbers: upper and lower limits for growth and an optimum temperature at some point between these two extremes. Eons of domesticating the microbe *Saccharomyces cerevisiae* for food and beverage production, and work with this yeast as a model organism, have revealed that budding yeast grows optimally around 35°C, and above 40°C growth ceases. Yet in this issue of *Nature Microbiology,* Trip and Youk[1] discovered something unexpected. When they inoculated yeast cultures at 39°C, a transition temperature between habitable (~38°C) and uninhabitable (~40°C) temperatures, growth was dependent on the initial population density.

Trip and Youk pushed this finding further, experimentally mapping out an entire phase diagram for population-level yeast growth (deterministic, random, or none) as a function of temperature and initial density (Fig. 1). The phase diagram indicated a key population tipping point: beyond 40.3°C all yeast populations go extinct. What happens leading up to the tipping point warrants attention. As the critical temperature is approached, dense yeast populations can still grow to their carrying capacity. However, less dense populations sometimes grow to carrying capacity and sometimes don't (deemed random growth). More-diluted populations never grow. Transitions between these growth regimes delineate the boundaries of the phase diagram and are sensitive to additional stress on the yeast; yeast forced to constitutively overexpress a fluorescent protein have a similarly shaped phase diagram but with the phase boundaries and tipping point shifted to lower temperatures. The authors ruled out the appearance of heat-tolerant mutants or persister cells as explanations for these growth phenomena; subcultured survivors do not display additional heat tolerance and initial population decay rates are inconsistent with persisters.

The phase diagram conflicts with the traditional autonomous view of microbial response to stress, where survival is decided based on each individual microbe's response and fitness. Tripp and Youk's results clearly show that yeast are better equipped to survive high temperatures when surrounded by more neighbors; the transition between habitable and uninhabitable temperature conditions is

exquisitely sensitive to density. This kind of behavior has been observed in many ecological systems that demonstrate cooperativity, and the various features of the phase diagram are well described in the dynamical systems and ecology literature[2]. Cooperation leads to an Allee effect, that is, at low densities population growth rate increases with population density[3]. This effect further leads to the catastrophic tipping point seen at 40.3°C (called a fold bifurcation) where a stable state of the system (the carrying capacity) merges with the unstable state indicated by the random growth region (the upper boundary of the no-growth phase). Once past this tipping point, the only stable state available to the system is extinction. Similar behavior is seen in many ecological systems[4], including microbial populations that demonstrate cooperativity[5,6]. A particularly relevant example is budding yeast populations growing on sucrose, which they cooperatively metabolize by secreting invertase. When dilution is used to introduce a mortality rate, a very similar phase diagram is evident, including density dependent growth and a catastrophic tipping point at high dilution rates[7].

Damaging reactive oxygen species increase at high temperatures, leading Trip and Youk to hypothesize that glutathione, an important yeast antioxidant[8,9], might be the factor responsible for cooperative protection. They found that glutathione accumulated in growing yeast cultures at high temperature. Furthermore, spent media from these cultures or high concentrations of pure glutathione enabled growth when added to cultures that were otherwise too dilute to grow. Analysis of genetic mutants in genes involved in glutathione transport and production further demonstrated that production and export of glutathione are essential to maintain growth at high temperatures, whereas import is not. This suggests that the mechanism of protection takes place in the extracellular space. A stochastic mathematical model of yeast growth, where the probability of replication is nonlinearly dependent on extracellular glutathione concentration, predicts population growth for different initial densities and temperatures and fully recapitulates the experimental phase diagram.

The authors' results spur a number of questions that could be examined in future research. While the data suggests that glutathione accumulation is necessary and sufficient for growth at high temperatures, it would be interesting to examine if other unidentified cooperative interactions also play a role. The mechanisms that allow some populations to grow in the random growth phase, but not others, could also be examined in the context of cell age, expression capacity, and other factors. This also might be an interesting model system for examining early warning signals of population collapse[10], particularly in the context of global warming and climate change.

On the surface, this report primarily serves to update the conventional view of how yeast combat heat stress. But more broadly this research challenges a view of microbial biology based on autonomous actors, instead adopting a systems biology frame--on par with the dynamical systems of macro ecology--for even the simplest and most well understood features. In the simple intraspecies system examined here, intercellular interactions give rise to emergent population-level phenotypes. In more complex communities, including monospecies communities with metabolic specialization or multispecies communities, even more complicated interactions are possible with correspondingly difficult-to-predict population-level behaviors. Further experimental and theoretical research connecting measurable interactions with the ecology of microbial populations represents an important frontier in microbiology and carries myriad implications for human and environmental health.

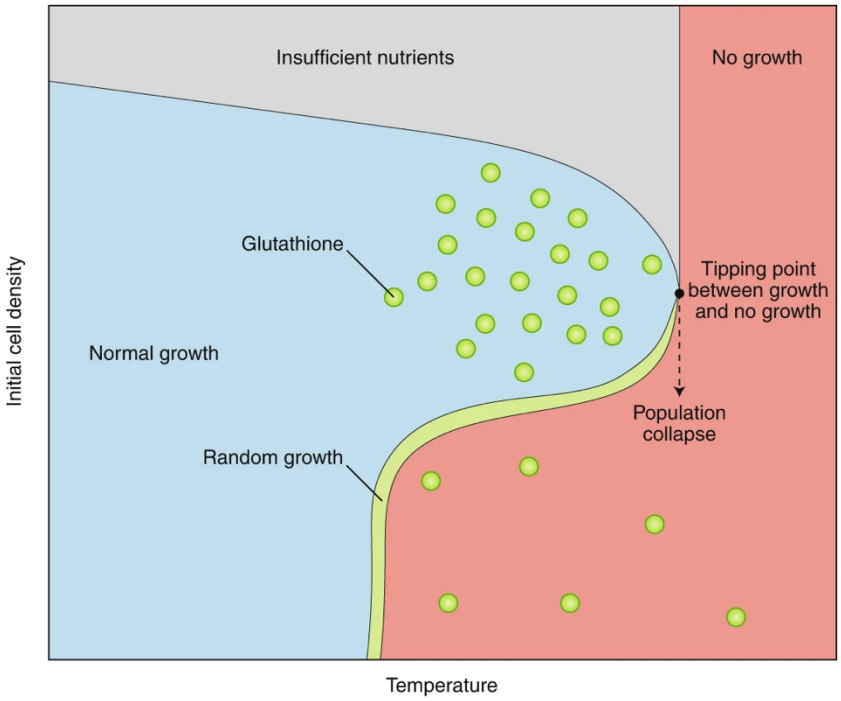
Insufficient nutrients
No growth
Glutathione
Tipping point between growth and no growth
Normal growth
Population collapse
Random growth
Initial cell density
Temperature

Figure 1:

The growth of yeast populations was measured by Trip and Youk[1] as a function of initial cell density and temperature. These conditions result in deterministic growth (blue region), random growth (green region), no growth (red) or no growth due to nutrient depletion (gray regions). Past a critical temperature, indicated by a fold-bifurcation where the stable fixed point (boundary between deterministic and nutrient-limited regions) and unstable fixed point (random growth region) collide, no growth is possible. Secretion of glutathione (green) by yeast (blue) leads to density-dependent growth at intermediate temperatures. Glutathione acts as an antioxidant protecting yeast from cellular damage by reactive oxygen species (ROS). Too few cells results in insufficient amounts of glutathione produced and cells thus failing to divide (no growth/collapse). At higher cell densities the cooperative production of glutathione protects yeast from heat damage and extends the habitable temperature range resulting in deterministic growth

References

1. Laman Trip, D. S. & Youk, H. Yeasts collectively extend the limits of habitable temperatures by secreting glutathione. *Nat. Microbiol.* (2020).
2. Clements, C. F. & Ozgul, A. Indicators of transitions in biological systems. *Ecology Letters* (2018).
3. W.C. Allee, A.E. Emerson, O. Park, T. Park, K. P. S. *Principles of Animal Ecology*. (W.B. Saunders, Philadelphia, 1949).
4. Scheffer, M., Carpenter, S., Foley, J. A., Folke, C. & Walker, B. Catastrophic shifts in ecosystems. *Nature* (2001).
5. Artemova, T., Gerardin, Y., Dudley, C., Vega, N. M. & Gore, J. Isolated cell behavior drives the evolution of antibiotic resistance. *Mol. Syst. Biol.* (2015).
6. Veraart, A. J. *et al.* Recovery rates reflect distance to a tipping point in a living system. *Nature* (2012).
7. Dai, L., Vorselen, D., Korolev, K. S. & Gore, J. Generic indicators for loss of resilience before a tipping point leading to population collapse. *Science* **336**, 1175–1177 (2012).
8. Thorsen, M. *et al.* Glutathione serves an extracellular defence function to decrease arsenite accumulation and toxicity in yeast. *Mol. Microbiol.* **84**, 1177–1188 (2012).
9. Grant, C. M. Role of the glutathione/glutaredoxin and thioredoxin systems in yeast growth and response to stress conditions. *Molecular Microbiology* (2001).
10. Scheffer, M. *et al.* Early-warning signals for critical transitions. *Nature* (2009).

Appendix 3: Easy calibration of the light plate apparatus for optogenetic experiments

Supplementary methods

Table 1.
Saccharomyces cerevisiae strain information

Lab Catalog No.	Strain	Genotype
yMM1462	S288C	Matα trp1Δ63 leu2Δ1 ura3-52 ura3::pRPL18B-SV40NLS_VP16_CIB1-tENO1-pRPL18B-SV40NLS_Zif268Cry2PHR-tSSA1-Scar2-pGAL1(3Zif268BS)-mRuby2-ScarRE-URA3

Yeast Growth and Media
For the flow cytometry experiments, we grew yeast to mid log-phase in low fluorescence media [10] in a shaking incubator at 30°C and 275 RPM. We aliquoted 1ml of the mid-log culture into two 24-well plates, which had a sterile glass bead loaded in each well to improve mixing and water loaded in the spaces between wells to reduce thermal isolation and evaporation. We covered each 24-well plate with a Breathe-Easy membrane and loaded the plates onto two LPAs mounted in a shaking incubator. We incubated the samples for four hours at 30°C under the described light conditions, then prepared them for flow cytometry.

Flow cytometry
All cell concentration and mRuby fluorescence data shown was acquired with an Attune NxT flow cytometer. The mRuby data was acquired using a 602/15 nm filter and excitation at 561 nm. All yeast samples were prepared for flow cytometry by adding 50 uL yeast culture to 150 uL PBS + 0.1% Tween over ice. All flow cytometry acquisitions included at least 20,000 initial events that were gated to remove debris and isolate single cells. Mean mRuby fluorescence for each gated sample was calculated in FlowJo.

Power sensor adaptor
We designed the power sensor adaptor in 3D Studio Max and had it 3D printed in PC-ABS using a Stratasys F370. The .STL file for the power meter can be found in our supplementary materials.

Supplementary results

Consistency of calibration among multiple users
In order for our method to be useful, it should perform consistently between different users. Four different users calibrated the same LPA and each generated a slightly different standard curve (**Fig. S4**). The users then programmed the LPA with the Iris values needed to achieve the target irradiances of 25, 50, 100, 200 and 300 μW/cm^2, as predicted from each user's standard curve. Though each user predicted slightly different Iris values, they were always able to generate light doses within 5.4% of the intended irradiance. This demonstrates that the calibration process is straightforward and yields consistent results for different users.

Edge effects

We encountered strong edge effects when initially using the LPA for long (18 hour) gene induction experiments (**Fig. S5**). After mapping our flow cytometry results back onto the LPA wells from which they came, it was clear that mRuby expression was consistently lower in the central wells versus the peripheral wells. We did not see a systematic difference between central and peripheral wells in endpoint cell concentration measurements (**Fig. S5A**), which were acquired via flow cytometry when measuring mRuby expression. We hypothesized that a temperature difference between wells could be causing the edge effects or that oxygen deficits in the central wells were preventing mRuby from folding correctly. To test the effect of temperature differences, we induced mRuby expression by incubating yeast at 30°C for 18 hours over two LPAs, each configured to produce a light dose of 200 $\mu W/cm^2$ in every well. One of the LPAs had a 24-well plate in which water had been loaded in the space between wells to reduce thermal isolation between wells, while the other LPA had a 24-well plate with no water between the wells (**Fig. S5B**). We simultaneously tested the potential effect of an oxygen deficit between wells by sampling our yeast after the 18-hour light induction and splitting the samples into two groups. One group was simply added to PBS + 0.1% Tween, refrigerated at 4°C for 1 hour, and measured by flow cytometry. To the other sample we added 27.4 ng/uL cycloheximide in media to arrest protein translation, then aerated the samples by pipetting repeatedly before allowing the samples to incubate at room temperature for one hour, such that immature mRuby produced during the experiment would have time to fold in an oxygen rich environment. We then added these samples to PBS + 0.1% Tween and measured mRuby fluorescence by flow cytometry. The samples that were treated with cycloheximide and allowed to mature for an extra hour had no observable difference in mRuby fluorescence. While there is still a pronounced difference in mRuby expression between the central and peripheral wells, the inclusion of water between wells more than halved the coefficient of variation in mRuby fluorescence across the plate (**Fig. S5C**). While we were unable to identify the cause of these edge effects, they largely disappear when performing a shorter (4-hour) experiment with water loaded between the wells (**Fig. S5D**). We caution others to check for the presence of edge effects with their experimental conditions.

Effects of light dose on cell growth

When comparing mRuby expression between a calibrated and uncalibrated LPA, we also acquired endpoint cell concentration measurements after four hours of blue light induction at a range of light doses (**Fig. S6A**). For these conditions, there appears to be no obvious systematic effect of light dose on the mean endpoint cell concentration (**Fig. S6B**).

Supplementary figures

Figure S1

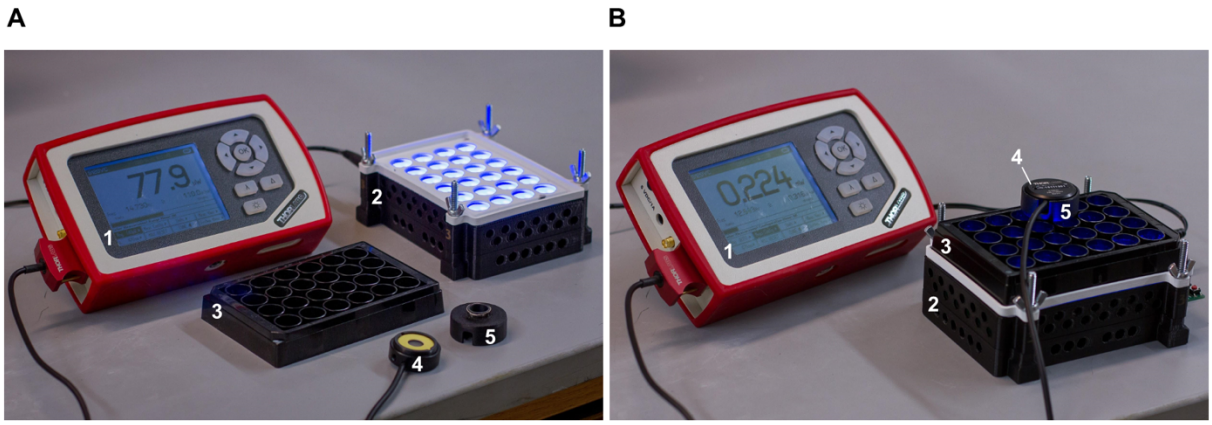

Figure S1.
LPA calibration equipment both (A) unassembled and (B) in use. Depicted components include 1) a Thorlabs power meter, 2) an assembled LPA with diffuser sheets, 3) an Arctic White 24-well plate with a flat, transparent bottom, 4) a Thorlabs S120VC optical power sensor, and 5) a power sensor adapter.

Figure S2

A

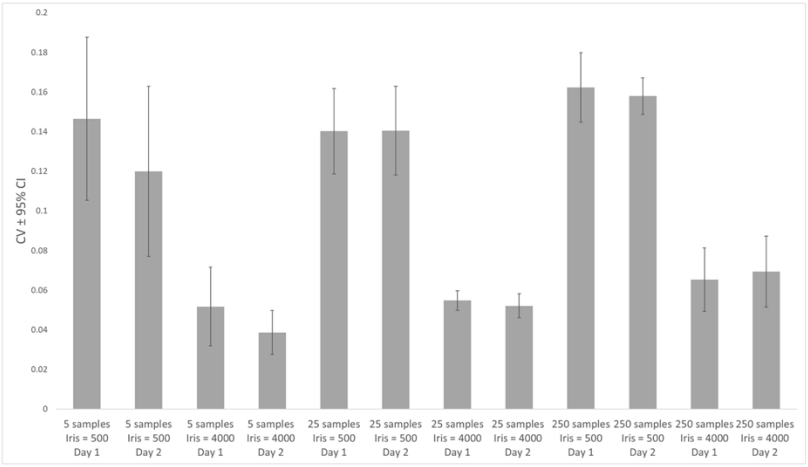

B

Illuminated well irradiance (uW/cm^2)	Neighboring well irradiance (nW/cm^2)
35	2.2 ± 24.2
150	62.1 ± 16.6
270	110 ± 25.5

Figure S2.

(A) Repeated measurements of the same LED show that the intrinsic variability of the measurement system is low. We acquired these measurements over two days at Iris values of 500 and 4000 while keeping dc and gcal constant. Each bar represents the average CV for 5, 25 or 250 samples per measurement. The measurements were repeated five times and the error bar represents the 95% confidence interval. The average CV did not exceed 0.19%. Increasing the number of samples did not consistently cause the CV to decrease. (B) Measurements of an illuminated well and an unlit, adjacent well indicate there is very little crosstalk in well irradiance measurements. Even when the illuminated well is set to output a high light dose, the irradiance in the neighboring well is in the nW/cm^2 range.

Figure S3

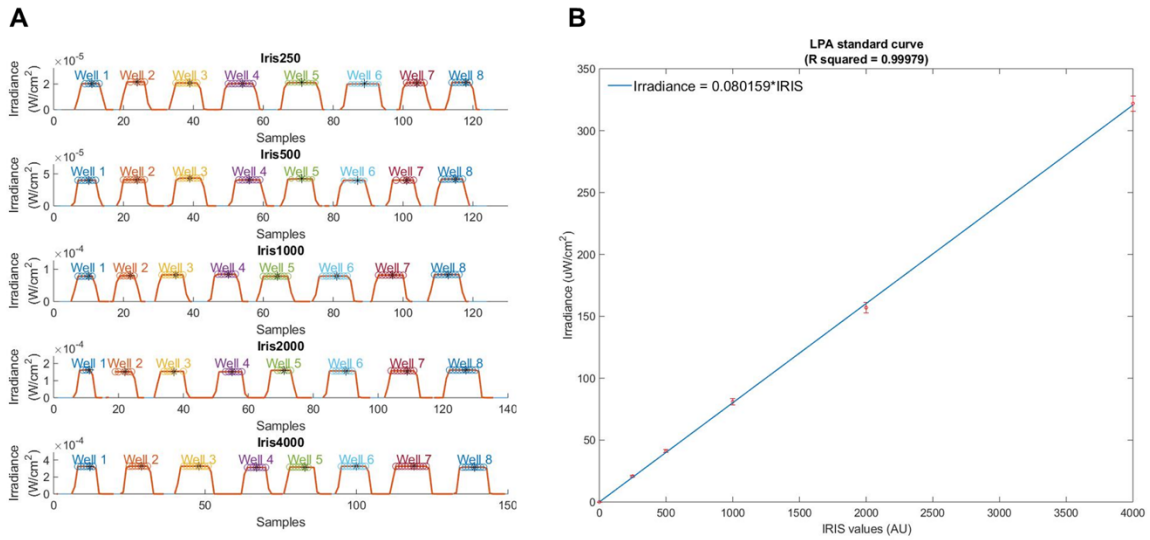

Figure S3.

Figures output by "LPA_standardCurve.m". (A) Representative standard curve image for five irradiance measurements at Iris values of 25, 250, 500, 1000,2000, and 4000 with the fitted line displayed. (B) Representative well irradiance measurements.

Figure S4

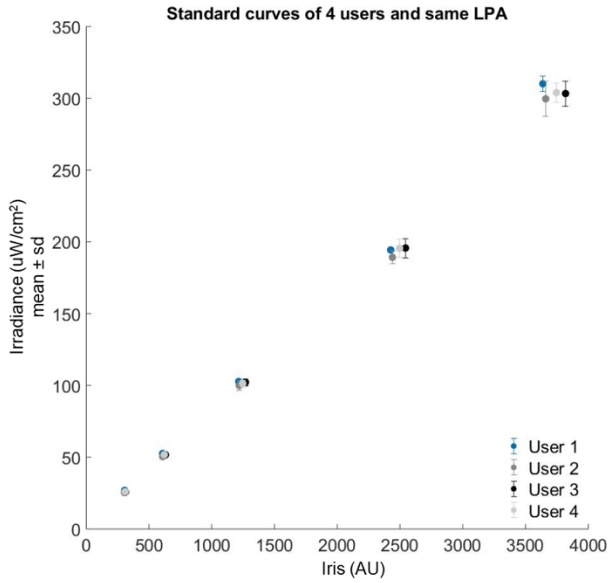
Standard curves of 4 users and same LPA
Irradiance (uW/cm²)
mean ± sd
Iris (AU)
User 1
User 2
User 3
User 4
0
50
100
150
200
250
300
350
0
500
1000
1500
2000
2500
3000
3500
4000

Figure S4.

Four individuals calibrated a single LPA from default settings and generated a standard curve for their calibration. The individuals then measured at specific Iris values to obtain a desired target irradiance (circular markers). All measured irradiances were within 5.4% of the targeted irradiance.

Figure S5

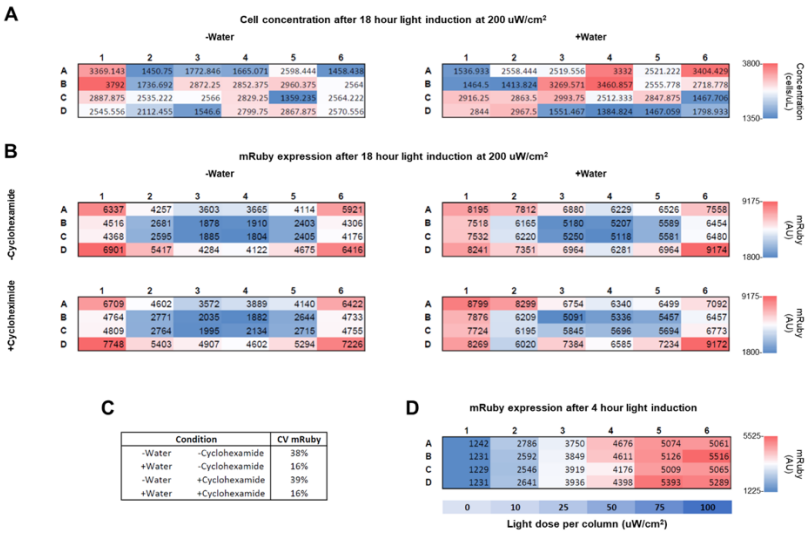

Figure S5.

(A) Mean cell concentration versus LPA well location following an 18-hour light induction experiment during which the administered irradiance in all wells was set to 200 µW/cm^2. Data is shown for 24 well plates with and without water loaded in the spaces between the wells. (B) Mean mRuby fluorescence versus LPA well location following the same light induction experiment shows a strong edge effect. Data is shown for cells with and without cycloheximide treatment prior to measurement by flow cytometry. (C) Effect of water and cycloheximide treatments on the coefficient of variation of mRuby fluorescence over a plate with uniform illumination conditions. (D) Mean mRuby expression versus LPA well location following a 4-hour light induction experiment over a range of light doses and with water loaded in the spaces between the wells of the 24-well plate. No edge effects are evident under these conditions.

Figure S6

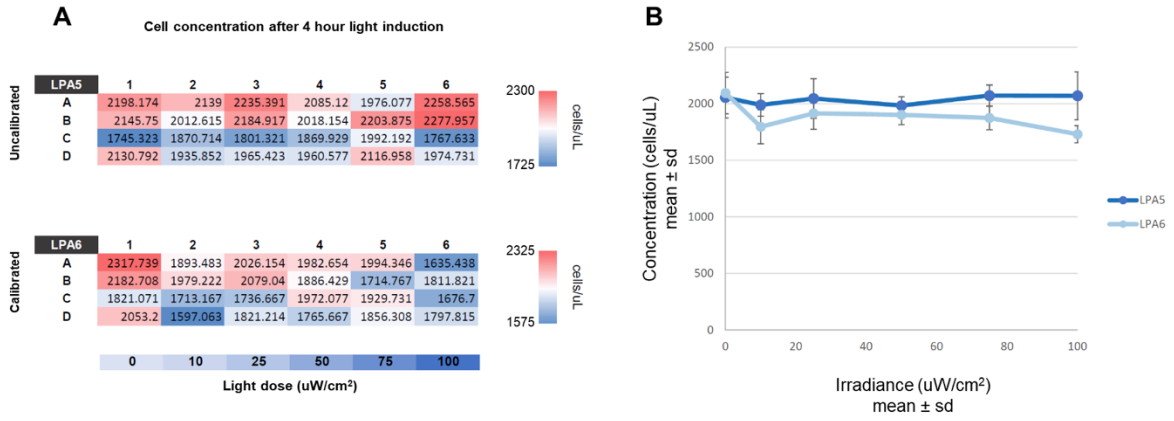

Figure S6.
(A) Mean cell concentration versus LPA well location following a 4-hour light induction experiment over a range of light doses and with water loaded in the spaces between the wells of the 24-well plate. Data is shown for the uncalibrated LPA5 and the calibrated LPA6. (B) Plot of mean cell concentration versus light dose for the same experiment. There is no observable relationship between endpoint cell concentration and light dose; the difference between mean concentrations was not significant ($p>0.05$ in a one-way ANOVA). This suggests these light conditions are not causing a growth defect, because all wells started with equally concentrated aliquots of yeast culture.

Figure S7

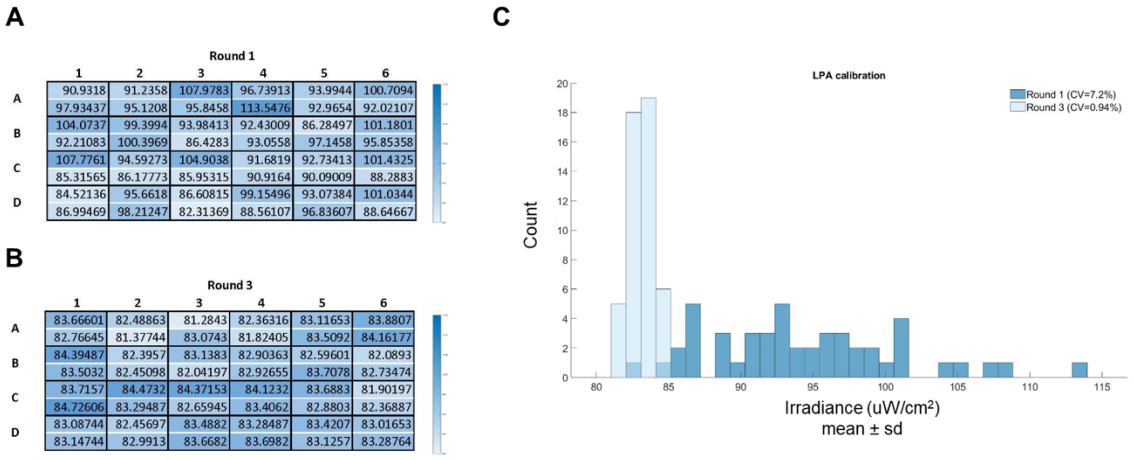

Figure S7.

Representative results for the calibration of another LPA (different from that of Fig. 2). (A) Heatmap of the irradiance measurements for each LED prior to calibration, where the mean plate irradiance was 94.4 µW/cm^2 and the CV of the LED irradiances was 7.2%. (B) Heatmap showing the irradiances of each LED after three rounds of calibration, which resulted in a mean plate irradiance of 83.1 µW/cm^2 and a CV of LED irradiances of 0.94%. (C) Histogram depicts the data represented in the heatmaps in (A) and (B). Following calibration, the irradiance values converge to the irradiance of the dimmest LED of the uncalibrated plate.

Figure S8

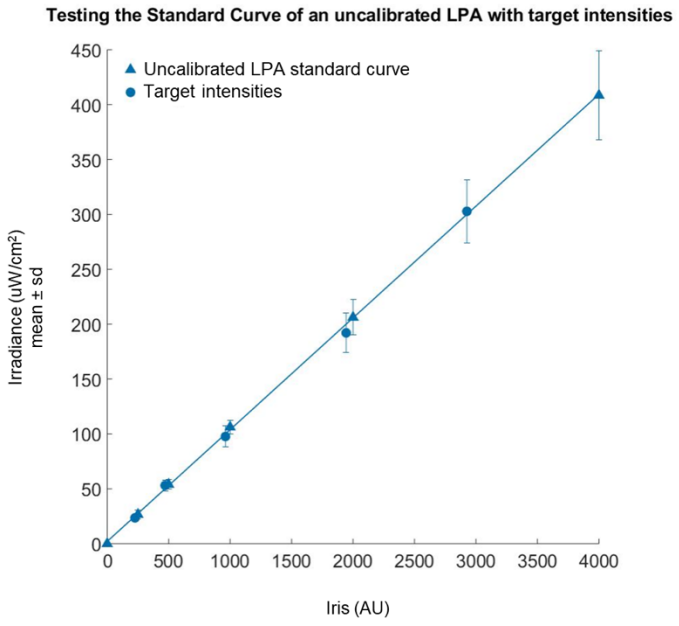

Figure S8.

A standard curve for an uncalibrated LPA (triangles and line) and attempts to achieve targeted irradiance values based on Iris values predicted from the standard curve. All plot markers represent the mean and standard deviation of eight irradiance measurements. The Iris values calculated from the standard curve of the uncalibrated LPA resulted in irradiance measurements (circles) that missed their target irradiance values by up to 23.1%.

Figure S9

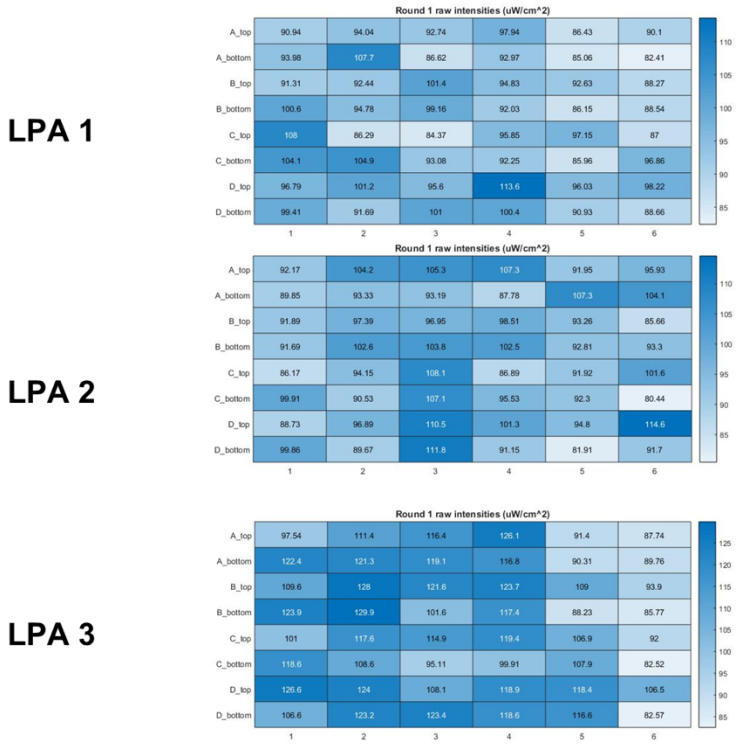

Figure S9.
Irradiance measurements (μW/cm^2) for three LPAs before calibration. Comparison of these measurements with those of the uncalibrated LPA in Fig. 1C show that differences in LED brightness prior to calibration does not have an obvious underlying structure related to the configuration of the LPA. In either case, calibration greatly reduces inter-well irradiance variability.

Appendix 4 : Optogenetic tools for control of public goods in *Saccharomyces cerevisiae*

Supplemental Methods

Plasmid Construction

The plasmid carrying GAL4DBD-CRY2 loxP-KIURA3-loxP CIB1-VP16 (pMM335) was created using yeast homologous recombination into pMM7. The GAL4AD-CIB1 cassette was PCR amplified using primers oMM628 and oMM629. The primer oMM628 contains (from 5' to 3') homology to pMM7, an added XmaI site, and forward priming to pMM159. The primer oMM629 contains (5' to 3') homology to loxP-KLURA3-loxP cassette and reverse priming to pMM159. The loxP-KLURA3-loxP cassette was PCR amplified from pMM326 with primers oMM250 and oMM251. The GAL4BD-CRY2 cassette was PCR amplified with primers oMM630 and oMM631. The primer oMM630 consists of homology to the downstream region of loxP-KLURA3-loxP and forward priming to pMM160. The primer oMM631 consists of homology to pMM7, an added PacI site, and reverse priming to pMM160. The ADH1 promoters and terminators were preserved for both CIB1 and CRY2 amplifications. XmaI and PacI restriction sites are not present in the final construct except for where they were included by PCR. For yeast homologous recombination, pMM7 was digested to completion at its unique SacI site and cotransformed with the three PCR products listed above into yMM1146 and plated on SC –URA-LEU for selection. Colonies were picked and plasmid recovered with the Zymo Yeast Plasmid Miniprep Kit. Plasmid verified by digest with HindIII and sequencing. To generate an integrating version (pMM337), the cassette from pMM335 containing GAL4DBD-CRY2 loxP-KIURA3-loxP VP16-CIB1 was cloned into pMM327 between the XmaI and PacI cassettes.

The plasmid containing ZDBD-CRY2PHR loxP-KIURA3-loxP CIB1-VP16 was generated using the same scheme as for pMM335 with the following exceptions: oMM653 replaced oMM630 to amplify the ZDBD-CRY2PHR construct, oMM664 replaced oMM628 and contains a PacI site instead of XmaI, and oMM665

replaces oMM631 and contains an AscI site instead of PacI. To increase the spacing between the ZDBD-CRY2PHR and CIB1-VP16 the resulting plasmid was linearized using BsiWI and a fragment containing the tetR sequence from pBR322 (amplified with oMM681/682) was ligated between CIB1-VP16 and the loxP-URA3-loxP cassette. The ZDBD-CRY2 loxP-KIURA3-loxP Spacer CIB1-VP16 cassette from the resulting plasmid (pMM364) was liberated using PacI/AscI and ligated into pMM327 to generate a plasmid capable of integration at the HO locus. The plasmid (pMM359) containing Gal4AD-CIB1 loxP-KIURA3-loxP ZDBD-CRY2PHR was generated using the same scheme as for pMM364. This plasmid was then cut and ligated into pMM327 as described for pMM364 and integrated into yMM1146 to make yMM1355 which was used with pMM369 (yMM1377) and pMM6 (yMM1378) to demonstrate light-induced drug resistance in **Supplemental Figure 2.**

The pGAL1-yEVENUS episomal reporter on a scTRP1 backbone (pMM336) was constructed by cutting pMM301 with PvuII and ligating into the corresponding site on pMM6.

The pZF(3BS)-yEVENUS scTRP1 CEN reporter plasmid (pMM365) was created using yeast homologous recombination. The plasmid pMM287 (pZF(3BS)-yEVENUS scURA3 CEN) was digested with ApaI and co-transformed with TRP1 amplified from pMM6 using oMM611/612 into yMM1146, selected on SC-TRP and recovered by plasmid prep and transformation into *E. coli* competent cells.

The pZF(3BS)-NatMX construct was constructed using yeast recombinational cloning by amplifying the NatMX cassette from pMM129 with oMM687/688 and co-transforming with pMM365 cut with EcoIR and AscI into yMM1146 and selecting for TRP+ yeast. Plasmids were prepped from yeast, transformed into *E. coli*, and verified by sequencing.

STRAIN CONSTRUCTION

The integrated pZF(3BS)-mRUBY2 strain was generated by transforming the unrecycled optogenetic strain (yMM1367 Matα trp1Δ63 leu2Δ1 ura3-52 HO::SV40NLS-VP16-CIB1 loxP-KLURA3-loxP SV40NLS-Zif268DBD-CRY2PHR) with pMM553 linearized at NotI to generate yMM1427.

The pZF(4BS)-HIS3 strain was created by swapping pGAL1-HIS3 with pZF(4BS)-HIS3 in a common yeast two-hybrid strain [3] using primers oMM575/576 to amplify KanMX4-pZF(4BS) from pMM299 and transform into yMM770. Strains were selected for G418 resistance and checked with oMM624, 625.

The pZF(4BS)-yVENUS reporter was created by yeast recombinational cloning by digesting pMM299 with EcoRI, amplifying yEVENUS from pMM289 with oMM191/626 and co-transforming into yMM1146. Plasmids were recovered from yeast and sequenced before using with pMM159/pMM284 to assess expression from the pZF(4BS) promoter.

The pZF(3BS)-yEVENUS strain was created by linearizing pMM287 at URA, removing the CEN/ARS and integrating into yMM1146 and selecting for URA+ transformants.

Initial tests of the system were performed using strains (yMM1332, 1351) with integrated version of the GAL4DBD-CRY2/Gal4AD-CIB1 split transcription factor. Strain yMM1351 (Matα trp1Δ63 leu2Δ1 ura3-52 pADH1-GAL4AD-CIB1-tADH2 loxP-KIURA3-loxP pADH1-GAL4BD-CRY2-tADH2) was generated by integrated pMM337 at the HO and loxing out the KIURA3 marker using pMM296 as described in the main text to generate yMM1332 (Matα trp1Δ63 leu2Δ1 ura3-52 pADH1-GAL4AD-CIB1-tADH2 loxP pADH1-GAL4BD-CRY2-tADH2).

Strain yMM1367 (Matα trp1Δ63 leu2Δ1 ura3-52 HO::SV40NLS-VP16-CIB1 loxP-kKlURA30loxP SV40NLS-Zif268DBD-CRY2PHR) was constructed by ligating the SV40NLS-VP16-CIB1 loxP-KlURA3-loxP SV40NLS-Zif268DBD-CRY2PHR cassette from pMM364 into pMM327, linearizing the resulting plasmid with AatII and integrating at the HO locus. Appropriate integration was checked by colony PCR and by the ability of the resulting strain to induce blue-light expression of yEVENUS when transformed with pMM365 (pZF(3BS)-yEVENUS). To generate yMM1390 (Matα trp1Δ63 leu2Δ1 ura3-52 HO::SV40NLS-VP16-CIB1 loxP SV40NLS-Zif268DBD-CRY2PHR) we used Cre-recombinase mediated recycling to remove the KlURA3 marker following the protocol described in the main text. The light inducible SUC2 strain (yMM1406) was constructed by transforming yMM1390 with the PCR product of pMM353 and oMM768/769

consisting of the KanMX4-pZF(3BS) cassette amplified with appropriate homology to replace the pSUC2 promoter with pZF(3BS). Transformants were checked by colony PCR and the ability to grow on YP-Sucrose only in blue-light.

Supplemental Table 1:

Yeast Strains

ID	Alias	Genotype	Notes	Source/ Reference
yMM0770	Yeast2Hybrid	MATa trp1-901 leu2-3,112 ura3-52 his3-200 gal4Δ gal80Δ LYS2::GAL1-HIS3 GAL2-ADE2 met2::GAL7-lacZ	Yeast two-hybrid strain (HIS3 expression)	James , et al 1996 [3]
yMM1146	DBY8750, KSY1284	Matα trp1Δ63 leu2Δ1 ura3-52		Botstein lab
yMM1295	pZF(4BS)-scHIS3	MATa trp1-901 leu2-3,112 ura3-52 his3-200 gal4Δ gal80Δ LYS2::KanMX4-pZF(4BS)-HIS3 GAL2-ADE2 met2::GAL7-lacZ	HIS3 expression under pZF(4BS)	This Study
yMM1332	GAL4AD-CIB1 GAL4BD-CRY2	Matα trp1Δ63 leu2Δ1 ura3-52 pADH1-GAL4AD-CIB1-tADH2 loxP pADH1-GAL4BD-CRY2-tADH2	Strain with integrated GAL4DBD - CRY2/CIB1-AD optogenetic system. Marker (KIURA3) has been lox'd out.	This Study
yMM1351	yMM1146 CIB1-KLURA3-CRY2	Matα trp1Δ63 leu2Δ1 ura3-52 pADH1-GAL4AD-CIB1-tADH2 loxP-KIURA3-loxP pADH1-GAL4BD-CRY2-tADH2	Strain with integrated GAL4DBD - CRY2/CIB1-AD optogenetic system. Marker (KIURA3) has not been lox'd out.	This Study
yMM1353	yMM1146_pMM287	Matα trp1Δ63 leu2Δ1 URA3::pZF(3BS)-yEVenus	pZF(3BS)-yEVENUS integrated	This Study
yMM1355		Matα trp1Δ63 leu2Δ1 ura3-52 HO::GAL4AD-CIB1 loxP-KLURA3-loxP		This Study

		FLAG(3X)-SV40NLS-Zif268DBD -CRYPHR		
yMM1367	yMM1146_pMM364atHO	Matα trp1Δ63 leu2Δ1 ura3-52 HO::SV40NLS-VP16-CIB1 loxP-KLURA3-loxP SV40NLS-Zif268DBD-CRY2PHR	Strain with integrated optogenetic system, to allow for induction of GOI using KanMXREV-pZF promoter	An-Adirekkun, et al 2020 [3]
yMM1377	yMM1377+pMM369	Matα trp1Δ63 leu2Δ1 ura3-52 HO::GAL4AD-CIB1 loxP-KLURA3-loxP FLAG(3X)-SV40NLS-Zif268DBD -CRYPHR [pMM369]		This Study
yMM1378	yMM1377+pMM6	Matα trp1Δ63 leu2Δ1 ura3-52 HO::GAL4AD-CIB1 loxP-KLURA3-loxP FLAG(3X)-SV40NLS-Zif268DBD -CRYPHR [pMM6]		This Study
yMM1390	yCS16	Matα trp1Δ63 leu2Δ1 ura3-52 HO::SV40NLS-VP16-CIB1 loxP SV40NLS-Zif268DBD-CRY2PHR	Strain with integrated optogenetic system (HO::VP16CIB1/ZFCRY2PHR) with marker (KLURA3) excised. To allow for induction of GOI using KanMXRev-pZF promoter.	This Study
yMM1406	pZF-SUC2, yCS22	Matα trp1Δ63 leu2Δ1 ura3-52 HO::SV40NLS-VP16-CIB1 loxP SV40NLS-Zif268DBD-CRY2PHR KanMX-pZF(3BS)-SUC2	Blue-light inducible SUC2 strain	This Study
yMM1427	pZF-mRUBY2	Matα trp1Δ63 leu2Δ1 ura3-52 HO::SV40NLS-VP16-CIB1 loxP-KLURA3-loxP SV40NLS-Zif268DBD-CRY2PHR		This Study

Supplemental Table 2:

Oligos used in this study

oMM	**Alias**	**Sequence**	**Target**	**Purpose (Brief)**

oMM 0166	rev_pGal4AD-CIB1_check	aagtgaacttgcggggtttt	CIB1	Colony PCR
oMM 0191	Forward_pGAL1	GCGAAGCGATGATTTTTGAT		
oMM 0250	Lox_General_for	cgtacgctgcaggtcgac	loxP cassette	Amplification
oMM 0251	Lox_General_rev	cactatagggagaccggcag	loxP cassette	Amplification
oMM 0575	revKanMX_pGAL_4xZif_reverse_YRC	GTCGACGGTATCGATAAGCTTGATATCGAATTCCTGCAGCatagtttttctccttgacg	KanMX	Amplification & Transformation
oMM 0576	revKANMX_LYS2_forward	TTCAGGTGCTGGTGCTCGTGGAAGCTCCGCAGCAGCTTAAcgcacttaacttcgcatctg	KanMX	Amplification & Transformation
oMM 0611	pRS_markerswap_for	CTTAACTATGCGGCATCAGA	pRS marker	Yeast recombinational cloning
oMM 0612	pRS_markerwap_rev	CCTGATGCGGTATTTTCTCC	pRS marker	Yeast recombinational cloning
oMM 0624	LYS2_forward	CTAGTTGCTTCAGGTGCTGG	LYS2	Colony PCR/checking
oMM 0625	HIS3_reverse	GCCTGTTCTGCTACTGCTTC	HIS3	Colony PCR/checking
oMM 0626	Venus_reverse	CCAGTGAGCGCGCGTAATACGACTCACTATAGGGCGAATTaggaaacagctatgaccatg	Venus	Yeast recombinational cloning
oMM 0628	pRS_XmaI_CIB1_forward	GTCGACGGTATCGATAAGCTTGATATCGAATTCCcccggggatggtggtacataacgaac	pRS vector	Yeast recombinational cloning
oMM 0629	loxP_CIB1_reverse	ACGAAGTTATATTAAGGGTTGTCGACCTGCAGCGTACGtggaatatgttcatagggtagg	CIB1/loxP cassette	Yeast recombinational cloning
oMM 0630	loxP_CRY2_forward	AGTTATTAGGTGATATCAGATCCACTAGTGGCCTATGCGGtccctaacatgtaggtggcg	loxP cassete/CRy2	Yeast recombina

				tional cloning
oMM 0631	CRY2_pRS_PacI_reverse	GATTACGCCAAGCGCGCAATTAACCCTCACTATTAATTAAcatgccggtagaggtgtggt	CRY2	Yeast recombinational cloning
oMM 0646	HO-L forward_check	GGGAGAACGAGTACCTGTAG	HO	Colony PCR
oMM 0647	CIB1 reverse_check	CTTTGCAAAGCTTGGAGTTG	CIB1	Colony PCR
oMM 0650	tADH2_downstream_forward_seq	CAGGTATAGCATGAGGTCGC	tADH1	Sequencing/Colony PCR
oMM 0651	pMM160_upstream_reverse_seq	CCACCATCAATGAGGCAGTG	pADH1	Sequencing/Colony PCR
oMM 0652	CIB1_downstream_for_seq	GGCCATGTAACCTCTGATCT	CIB1	Sequencing/Colony PCR
oMM 0653	loxP_ZCRY2_forward	AGTTATTAGGTGATATCAGATCCACTAGTGGCCTATGCGGcgatttagagcttgacgggg	ZCRY2	Yeast Recombinational Cloning
oMM 0664	pRS_PacI_CIB1_Forward	GTCGACGGTATCGATAAGCTTGATATCGAATTTTAATTAAgatggtggtacataacgaac	CIB1	Yeast Recombinational Cloning
oMM 0665	CRY2-AscI-pRS Reverse	GATTACGCCAAGCGCGCAATTAACCCTCACTAGGCGCGCCcatgccggtagaggtgtggt	CRY2	Yeast Recombinational Cloning
oMM 0673	ZF(3BS)_for	CTAGACGCCCACGCTCGCCCACGCTCGCCCACGCGC	pMM347 ZFBS	Anneal and ligate
oMM 0674	ZF(3BS)_rev	GGCCGCGCGTGGGCGAGCGTGGGCGAGCGTGGGCGT	pMM347 ZFBS	Anneal and ligate
oMM 0675	ZF(2BS)_for	CTAGACGCCCACGCCGCCCACGCCCACGCGC	pMM347 ZFBS	Anneal and ligate
oMM 0676	ZF(2BS)_rev	GGCCGCGCGTGGGCGTGGGCGGCGTGGGCGT	pMM347 ZFBS	Anneal and ligate
oMM 0681	BsiWI_tetR_for	ggtcgtacgGCGCTCATCGTCATCCTCGG	tetR	Cloning
oMM 0682	BsiWI_tetR_rev	cctcgtacgCTAGCCGGGTCCTCAACGAC	tetR	Cloning
oMM 0684	KLURA3_rev	GAATCAGCGCTCCCCATTAA	KIURA3	Sequencing/Colony PCR

oMM0687	NatMX_for	cctctatactttaacgtcaaggagaaaaaactataaccactcttgacgacacggcttacc	NatMX	Yeast recombinational cloning
oMM0688	NatMX_rev	atcataaatcataagaaattcgcttatttagaagtggggcaggcatgctcatgtagagc	NatMX	Yeast recombinational cloning
oMM0745	Lox_check_for	GTCATGCTTCAACAATGGCGA	loxP	Checking/colony PCR
oMM0746	Lox_check_rev	TAAGCTCATCCGAGCGAGAAA	loxP	Checking/colony PCR
oMM0768	scSUC2_pZF_forward	CTCAGAGAAACAAGCAAAACAAAAAGCTTTTCTTTTCACTaacaaaagctggagctgcat	SUC2 promoter	Amplification & Transformation
oMM0769	scSUC2_pZF_rev	CAAAAGGAAAAGGAAAGCTTGCAAAAGCATCATATACGTTattgggacaacaccagtgaa	SUC2 promoter	Amplification & Transformation

Supplemental Table 3:

Plasmids used in this study

ID	Alias	Gene(s) or Insert Name	Yeast Marker	Bacterial Resistance	Source/ Reference
pBR322	pBR322	N/A	N/A	Ampicillin	Gift from Rose/Gammie Lab
pMM0006	pRS414	scTRP1 CEN6 ARS4	scTRP1	Ampicillin	Sikorski and Hieter, 1989 [4]
pMM0007	pRS415	scLEU2 CEN6 ARS4	scLEU2	Ampicillin	Sikorski and Hieter, 1989 [4]
pMM0008	pRS416	scURA3 CEN6 ARS4	scURA3	Ampicillin	Sikorski and Hieter, 1989 [4]
pMM0129	NatMX	Nat1	Nat1	Ampicillin	Goldstein and McCusker, 1999 [5]
pMM0159	pGal4AD-CIB1	pscADH1-GAL4AD-CIB1-tscADH1	scLEU2	Ampicillin	Kennedy, et al 2010 [7]
pMM0160	pGal4DBD-CRY2	pscADH1-GAL4DBD-CRY2-tscADH1	scTRP1	Ampicillin	Kennedy, et al 2010 [7]

pMM0284	FLAG(3X)-NLSZIF26 8DBD- CRY2 (L3)	pscADH1-pFLAG(3X)-NLS-ZIF268DBD-CRY2 (L3)-tscADH1 TRP1	scTRP1	Ampicillin	An-Adirekkun, et al 2020 [3]
pMM0287	pZF(3BS) URA	pZF(3BS)-yEVENUS CEN scURA3	scURA3	Ampicillin	An-Adirekkun, et al 2020 [3]
pMM0289	pZF(4BS) URA	pZF(4BS)-yEVENUS CEN scURA3	scURA3	Ampicillin	An-Adirekkun, et al 2020 [3]
pMM0296	pSH65	pGAL1-CRE PheloR	PHLEO	Ampicillin	Botstein Lab; Gueldener, et al 2002 [5]
pMM0299	KanMXrev-pZF(4BS)	KanMXrev-pZF(4BS) in pIDTBlue	KanMX	Ampicillin	This Study
pMM0301	pGAL1-yEVENUS	pGAL1-yEVENUS scURA3 CEN	scURA3	Ampicillin	An-Adirekkun, et al 2020 [3]
pMM0326	pUG72	loxP-KIURA3-loxP	NA	Ampicillin	Gueldener, *et al* 2002 [5]
pMM0327	HO-Polylinker-HO	HO-Polylinker-HO	NA	Ampicillin	Voth, et al 2001 [6]
pMM0335	GAL4ADCIB1/GAL4DBDCRY2	GAL4AD-CIB1 loxP-KIURA3-loxP GAL4DBD-CRY2 LEU2 Cen/ARS	scLEU2	Ampicillin	This Study
pMM0336	pGAL1-YFP	pGAL1-yEVENUS CEN scTRP1	scTRP1	Ampicillin	This Study
pMM0337	HO GAL4 split	HO-GAL4AD-CIB1 loxP-KIURA3-loxP GAL4DBD-CRY2-HO	klURA3	Ampicillin	This Study
pMM0347	pMM299-VENUS	KanMXrev-pZF(4BS)-VENUS in pIDTBlue	KanMX	Ampicillin	This Study
pMM0353	KanMXrev-pZF(3BS)	KanMXrev-pZF(3BS)-VENUS in pIDTBlue	KanMX	Ampicillin	This Study
pMM0354	KanMXrev-pZF(2BS)	KanMXrev-pZF(2BS)-VENUS in pIDTBlue	KanMX	Ampicillin	This Study
pMM0359	Gal4AD-CIB1/ZCRY2-PHR HO	GAL4AD-CIB1 loxP-KLURA3-loxP FLAG(3X)-SV40NLS-	LEU2	Ampicillin	This Study

		Zif-ZCRYPHR LEU2 CEN/ARS			
pMM0364	CIB1/CRY2PHR loxURA CEN	SV40NLS-VP16-CIB1 loxP-KLURA3-loxP SV40NLS-ZIF268DBDCRY2PHR LEU2 CEN/ARS	LEU2	Ampicillin	This Study
pMM0365	pZF(3BS) TRP1	pZF(3BS)-yEVENUS CEN scTRP1	TRP1	Ampicillin	This Study
pMM0369	pZF(3BS)-NatMX	pZF(3BS)-NatMX scTRP1 CEN	scTRP1	Ampicillin	This Study
pMM0553	pZF(mRUBY2) @LEU2	Leu2 5' homology-pZF(3BS)-mRUBY2-tADH1-Con1-LEU2-Leu2 3' homology	scLEU2	Kanamycin	An-Adirekkun, et al 2020 [3]

References

[1] E. Andersen, "tPCR-Directed In Vivo Plasmid Construction Using Homologous Recombination in Baker's Yeast," Molecular Methods for Evolutionary Genetics. Methods in Molecular Biology , vol. 772, pp. 409-421, 8 7 2011.

[2] R. McIsaac, S. Silverman, M. McClean, P. Gibney, J. Macinskas, M. Hickman, A. Petti and a. D. Botstein, "Fast-acting and nearly gratuitous induction of gene expression and protein depletion in Saccharomyces cerevisiae.," Molecular Biology of the Cell, vol. 22, pp. 4447-4459, 2011.

[3] J. An-Adirekkun, C. Stewart, S. Geller, M. Patel, J. Melendez, B. Oakes, M. Noyes and M. McClean, "A yeast optogenetic toolkit (yOTK) for gene expression control in Saccharomyces cerevisiae," Biotechnology and Bioengineering, vol. 117, no. 3, pp. 886-893, 2020.

[4] R. Sikorski and P. Hieter, "A system of shuttle vectors and yeast host strains designed for efficient manipulation of DNA in Saccharomyces cerevisiae," Genetics, vol. 122, no. 1, pp. 19-27, 1989.

[5] U. Gueldener, J. Heinisch, G. Koehler, D. Voss and J. Hegemann, "A second set of loxP marker cassettes for Cre-mediated multiple gene knockouts in budding yeast," Nucleic acids research, vol. 30, no. 6, 2002.

[6] W. Voth, J. Richards, J. Shaw and D. Stillman, "Yeast vectors for integration at the HO locus," Nucleic Acids Research, vol. 29, no. 12, p. e59, 2001.

A

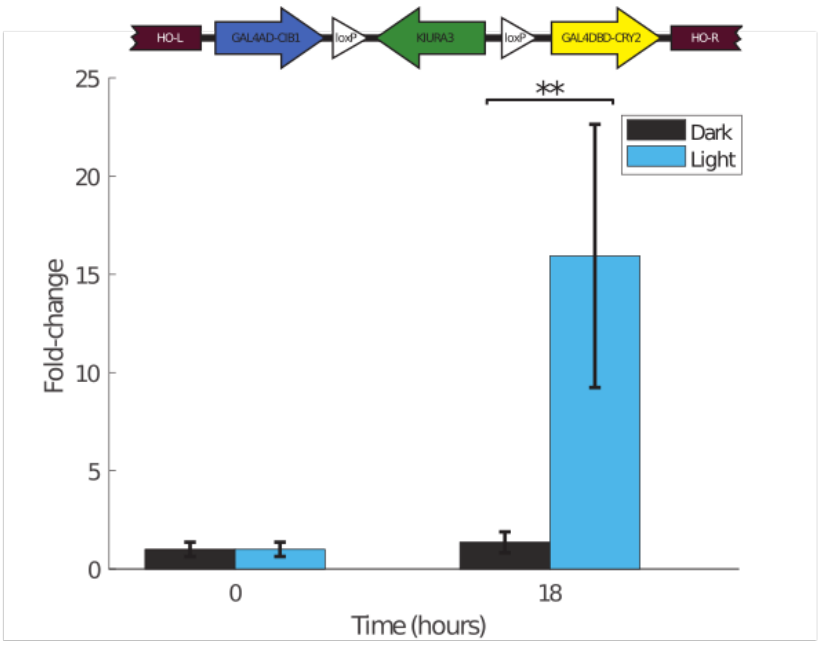
HO-L
GAL4AD-CIB1
loxP
KlURA3
loxP
GAL4DBD-CRY2
HO-R
**
Dark
Light
Fold-change
25
20
15
10
5
0
0
18
Time (hours)

B

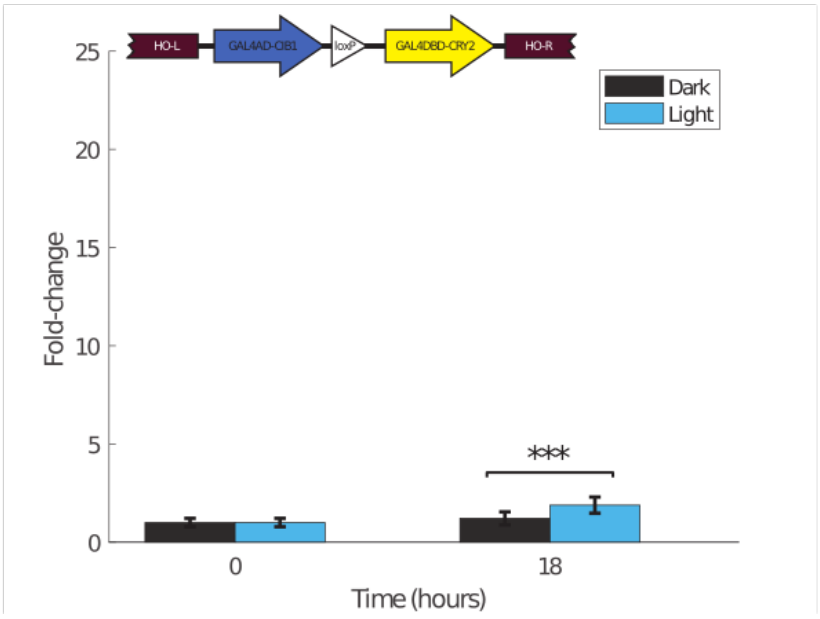
HO-L
GAL4AD-CIB1
loxP
GAL4DBD-CRY2
HO-R
Dark
Light
Fold-change
25
20
15
10
5
0
***
0
18
Time (hours)

Supplemental Figure 1:

Characterization of vectors to integrate the blue light inducible split transcription factor (GAL4DBD-CRY2PHR/CIB1-GAL4AD) into yeast with marker recovery. (A) Yeast cells carrying an integrated copy of a light activatable split GAL4 transcription factor (GAL4DBD-CRY2/VP16-CIB1) integrated at the HO locus without subsequent excision of the KlURA3 marker (inset) and a reporter plasmid (pGAL1-yEVENUS) were exposed to ~ 25 µW/cm^2 light for 18 hours. This resulted in a 15-fold induction in yEVENUS (p-value <0.005; Welch's t-test). (B) In contrast, when Cre-recombinase is used to excise the KIURA3 marker (inset), only 2-fold induction in yEVENUS occurs after 18 hours of growth in ~ 25 µW/cm^2 blue light (p-value<0.0005; Welch's t-test). Error bars are the standard error of the mean from 3 replicates.

Supplemental Figure 2

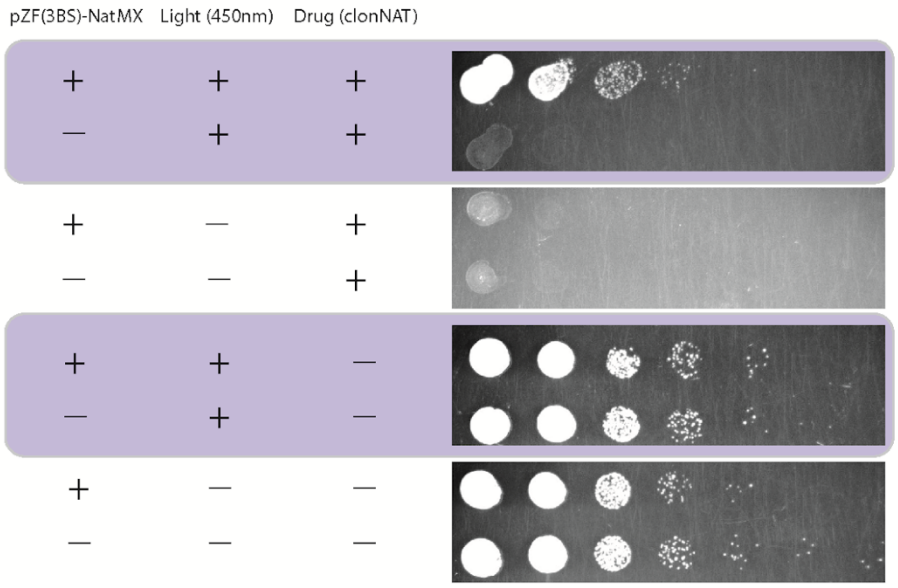

Supplemental Figure 2: Recovery of clonNAT resistance with light-inducible NatMX. Yeast strains with the integrated optogenetic system and either a plasmid containing pZF(3BS)-NatMX or the empty vector control were grown in the presence of clonNAT (nourseothricin, 50 µg/ml) in either 450nm blue light (50 µW/cm^2) or the dark (1:10 dilution series). Induction of the NatMX resistance marker (nat1 gene) by blue-light confers the ability to grow on nourseothricin.

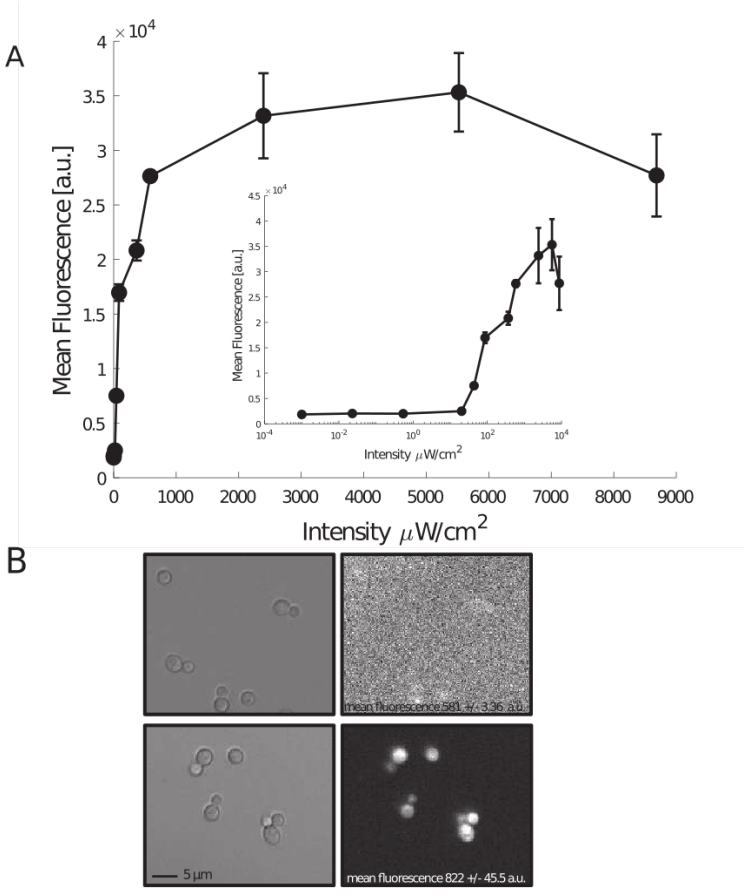

Supplemental Figure 3:
Expression from the pZF(3BS) promoter in blue light (A) The marker recycled strain (HO::SV40NLS-VP16-CIB1 loxP SV40NLS-Zif268DBD-CRY2PHR [pZF(3BS)-yEVENUS]) was grown for 18 hours in 460nm blue light over a range of intensities (0 μW/cm^2-8000 µW/cm^2). At least 20 μW/cm^2 of light is required to induce significant expression from the pZF(3BS) promoter (see inset) under these conditions. Error bars are the mean absolute deviation. (B) Integration of a pZF(3BS)-mRUBY2 reporter at the LEU2 locus in the unrecycled strain (HO::SV40NLS-VP16-CIB1 loxP-KlURA3-loxP SV40NLS-Zif268DBD-CRY2PHR) confers blue-light dependent expression on mRUBY2 (50 μW/cm^2 460nm blue light, 18 hours, bottom row. Dark control-top row).

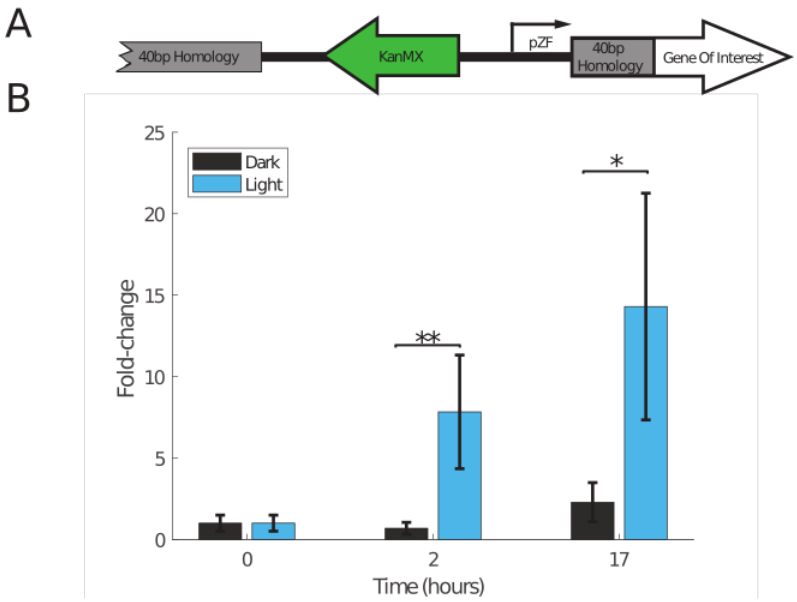

Supplemental Figure 4:
Characterization of KanMX-pZF cassette. (A) Integration of the pZF promoter in front of a gene of interest using homologous recombination in yeast confers light-regulation. (B) Expression of a yEVENUS reporter from the pZF promoter under 25 μW/cm^2 460nm illumination shown as fold-change relative to the T=0 dark sample. There is significant induction as early as T=2hrs of blue light (**p-value<0.005, * p-value<0.05; Welch's t-test). Error bars indicate standard error of the mean fold-change.

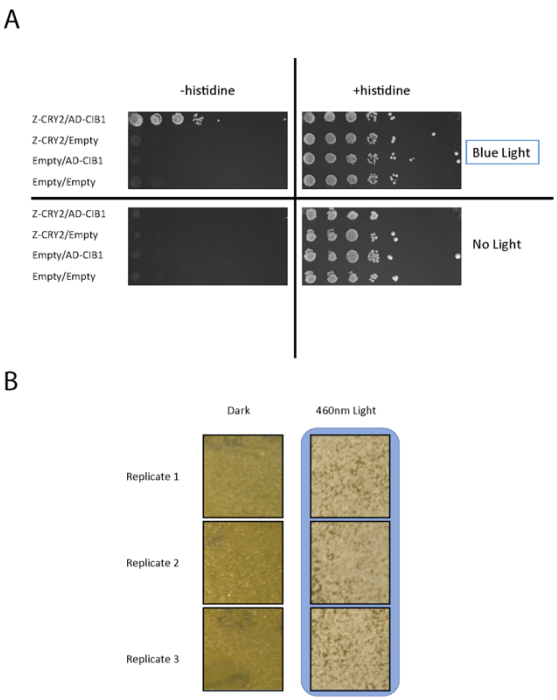

Supplemental Figure 5:

Light control of auxotrophy and drug resistance. (A) Light inducible expression of HIS3 recovers histidine auxotrophy. A yeast strain expressing imidazoleglycerol-phosphate dehydratase under the pZF promoter (pZF-HIS3) transformed with appropriate combinations of ZDBD-CRY2 (pMM284), AD-CIB1(pMM159) and/or empty vector controls (pMM6, pMM7) was frogged onto media without or with histidine at 1:10 dilutions either in the presence or absence of 57 µW/cm^2 460 nm blue light. In the dark the pZF-HIS3 strain is a histidine auxotroph, while growth on media lacking histidine is conferred in blue-light only in the strain that also contains the ZDBD-CRY2/AD-CIB1 light-activated split transcription factor. **(B)** pZF-SUC2 allows light-dependent growth on sucrose. The pZF-SUC2 yeast strain yMM1406 (Matα trp1Δ63 leu2Δ1 ura3-52 HO::SV40NLS-VP16-CIB1 loxP SV40NLS-Zif268DBD-CRY2PHR KanMX-pZF(3BS)-SUC2) was plated at a density of 0.119 and grown on YP-Sucrose in either 0 µW/cm^2 or 57 µW/cm^2 460 nm blue light for 7 days (n=3 technical replicates per condition). Blue-light confers the ability to grow on YP-Sucrose, while the replicates grown in the dark show no discernable growth.

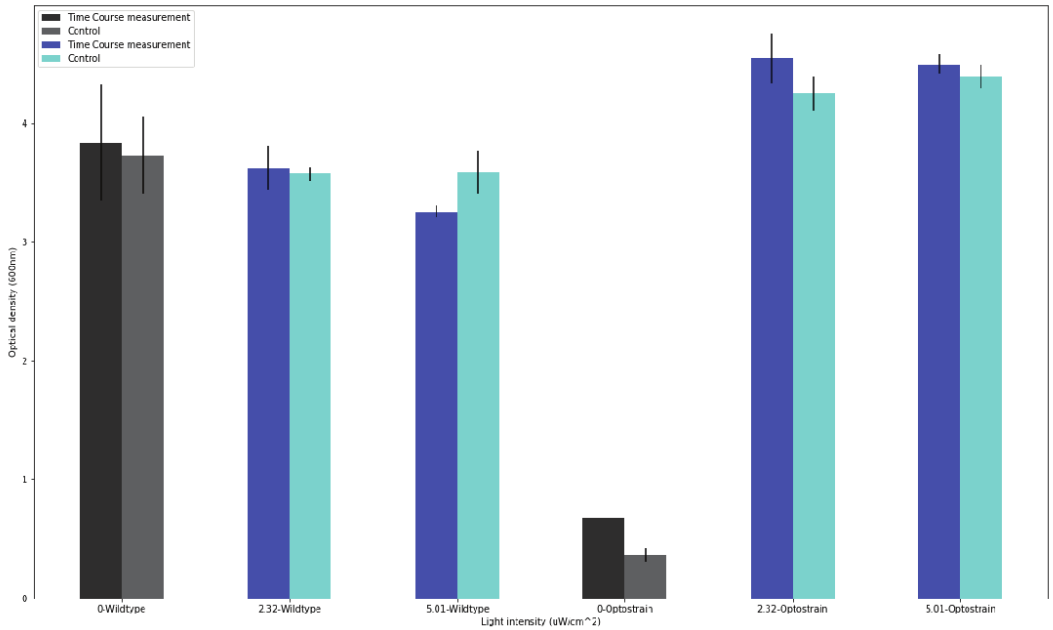

Supplemental Figure 6:
Endpoint measurements to identify unintended light induction during sampling. Endpoint densities are compared between the time course sampled wells (black and blue bars) and control wells (gray and cyan bars) to determine whether there were any effects on the cultures due to the unintended addition of light during sampling for the time course experiment (**Figure 3**). The bars represent the mean density of the cultures at 52 hours for two technical replicates. The error bars represent the standard deviation from the population mean. Where there is no error bar (0, pZF-SUC2) the two measurements of density were the same value. A two-way ANOVA identified significant differences between the effect of strain and light intensity on density of the cultures ($F_{(3,6)} = 46.72$, $p = 0$). However, a multiple comparisons test did not identify any significant differences between the density reached for the control measurement and the time course measurement pairs for each intensity.

A

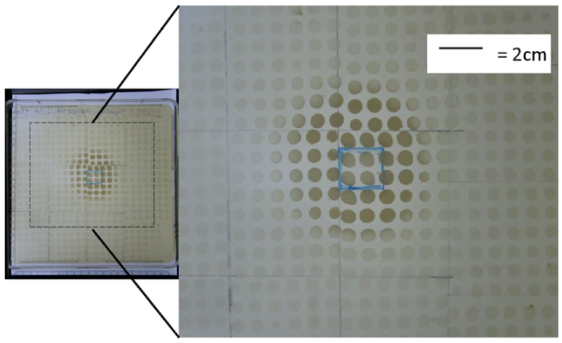
= 2cm

B

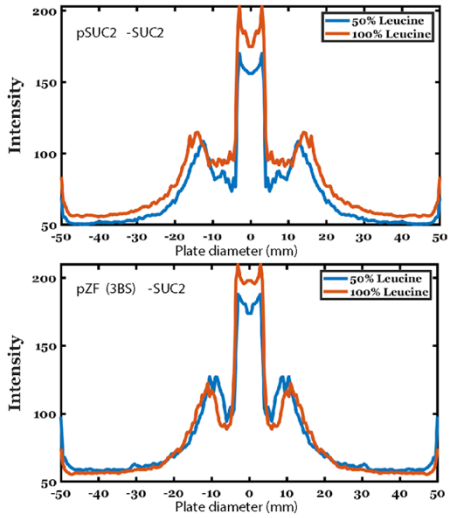
pSUC2 -SUC2
50% Leucine
100% Leucine
Intensity
Plate diameter (mm)
pZF (3BS) -SUC2
50% Leucine
100% Leucine
Intensity
Plate diameter (mm)

Supplemental Figure 7:

Spatial control of the optogenetic strain (yMM1406, Matα trp1Δ63 leu2Δ1 ura3-52 HO::SV40NLS-VP16-CIB1 loxP SV40NLS-Zif268DBD-CRY2PHR KanMX-pZF(3BS)-SUC2). (A) The optogenetic strain was stamped on the surface of a 224 mm^2 square petri dish, and only a small, 20 mm^2 region (blue square) of the petri dish surface area was illuminated during incubation. The area around the illuminated portion of the plate (dashed outline) is magnified. A large number of colonies outside the illuminated region were able to grow. (B) Quantification of radial patterning. Plots represent an averaged radial intensity profile of the spotted plates across the diameter of the plate. The wild-type pSUC2-SUC2 (top) and pZF-SUC2 (bottom) are separately plotted and the two concentrations of leucine are distinguished by color (blue, 50% leucine; orange, 100% leucine). The wild-type pSUC2-SUC2 has a larger region of inhibited growth than pZF-SUC2 in both growth conditions.

A

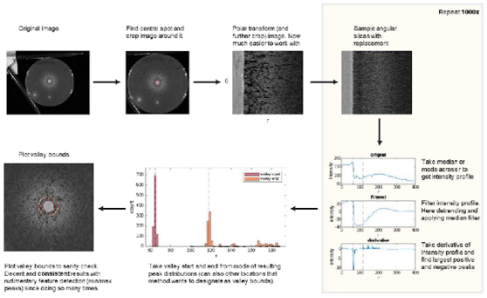

C

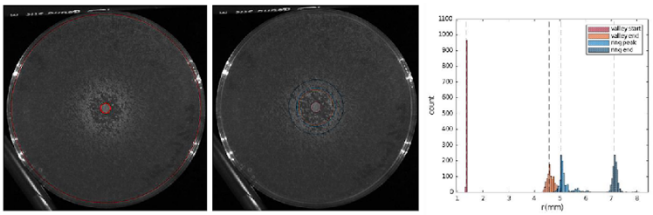

B

Spot strain	suc2Δ	pZF(3BS)-SUC2	pZF(3BS)-SUC2	pSUC2-SUC2*	pSUC2-SUC2
Leucine concentration	50% & 100%	50%	100%	50%	100%
Valley length (mm)	N/A	**1.34** (1.32,1.37)	**2.30** (2.24,2.36)	**3.76**	**3.65** (3.39,3.96, 3.61)
Ring length (mm)	N/A	**3.69** (3.54,3.83)	**3.37** (3.34,3.41)	**2.79**	**3.89** (4.20,3.49, 3.98)
Valley intensity	N/A	**89.66** (101.32,78)	**112.31** (130.07, 94.56)	**71.31**	**104.24** (115.45, 97.32, 99.96)
Ring intensity	N/A	**106.72** (112.48, 100.97)	**122.2** (127.64, 116.77)	**93.88**	**113.25** (113.07,110.02,116.66)

Supplemental Figure 8:
Image processing and identification of patterning features. (A) Determination of pattern features and growth from plate images using a custom Matlab script. (B) Plate features of the emergent pattern between strains and between leucine concentration. Mean values are in bold, followed by both replicate measurements (*, n=1). (C) Representative image of a patterned plate. Inset highlights pattern regions, the spot (red), valley (orange) and ring (blue) quantified by the Matlab script.